
***INTER AND INTRAMOLECULAR INTERACTIONS
BETWEEN DIVALENT SELENIUM CENTERS***

INAUGURAL-DISSERTATION

**ALBERTH LARI
HEIDELBERG 2008**

INAUGURAL-DISSERTATION

zur Erlangung der Doktorwürde
der Naturwissenschaftlich-Mathematischen Gesamtfakultät
der
Ruprecht-Karls-Universität
Heidelberg

vorgelegt von
Alberth Lari (M.Sc.)
aus Fagaras, Rumänien

Tag der Disputation:
31.10.2008

INTER AND INTRAMOLECULAR INTERACTIONS
BETWEEN DIVALENT SELENIUM CENTERS

Referees:

Prof. Dr. Dr. h.c. Rolf Gleiter

Prof. Dr. A. Stephen K. Hashmi

This research was carried out under the scientific supervision of Prof. Dr. Dr. h.c. Rolf Gleiter at the Institute of Organic Chemistry, Ruprecht-Karls-University Heidelberg.

Prof. Rolf Gleiter's interest in my scientific endeavours, his generous support and open-mindedness towards my research – let alone his never ending patience, as well as the confidence he placed in me and the academic freedom he granted me significantly contributed to the success of this thesis.

**Science at its best provides us
with better questions, not absolute answers.**

Norman Cousins, 1976

Contents

1. ABSTRACT	1
2. INTRODUCTION	9
2.1 GENERAL REMARKS ON MOLECULAR SELF-ASSEMBLY	9
2.2 STRUCTURAL TYPES OF TUBULAR MOTIVES.....	14
2.2.1 Tubular structures based on pure covalent bonding	14
2.2.2 Tubular structures based on pure non-covalent bonding	16
2.2.3 Tubular structures based on both non-covalent and covalent bonding ...	17
2.2.3.1 Hydrogen bonding	18
2.2.3.2 π - π stackings	21
2.2.3.3 Van der Waals forces	23
2.2.3.4 Chalcogen-chalcogen interactions.....	24
3. EXPERIMENTAL PART	27
3.1 MOTIVATIONS	27
3.2 SYNTHESIS AND STRUCTURE OF NEW TETRASELENADIYNE CYCLOPHANES.....	31
3.2.1 Introduction.....	31
3.2.2 Synthesis of new cyclophanes	34
3.2.3 Structural investigations.....	41
3.2.3.1 Solid state structures	41
3.2.3.2 2,5,14,17-Tetraselena[6,6]- <i>ortho</i> -cyclophan-3,15-diyne (18a)	41
3.2.3.3 2,5,14,17-Tetraselena[6,6]- <i>meta</i> -cyclophan-3,15-diyne (18b)	44
3.2.3.4 2,5,14,17-Tetraselena[6,6]- <i>para</i> -cyclophan-3,15-diyne (18c).....	46
3.2.3.5 NMR investigations of compounds 18 a - c	50
3.3 EXPERIMENTAL AND THEORETICAL INVESTIGATIONS OF NEW MODEL COMPOUNDS ...	53
3.3.1 Introduction.....	53
3.3.2 Synthesis of model compounds	55
3.3.3 Structural investigations of model compounds.....	61
3.3.3.1 Solid state structures	61
3.3.3.1.1 Crystal structure of 2-(methylselenyl)-benzylselenocyanate (29) . .	61
3.3.3.1.2 Crystal structure of 1,6-bis(2'-methylselenylbenzene)-2,5-diselena-	
3-hexyne (48).....	65
3.3.3.1.3 Crystal structure of 2-(methylselenyl)-benzyl-alcohol (46)	66
3.3.3.1.4 Crystal structure of 2,2'-diselenobis(benzyl alcohol) (51).....	68
3.3.3.1.5 Comparison of the crystal structures of 2,2'-diselenobis(benzyl	
bromide) (52) vs. bis(2-bromo)benzyl selenide (42).....	69

3.3.3.2	NMR chemical shifts	71
3.3.3.3	Couplings between selenium atoms	75
3.3.3.4	NMR relaxation times.....	78
3.3.4	Theoretical investigations	79
3.3.4.1	Theoretical aspects of calculations of NMR parameters.....	80
3.3.4.2	Conformational analysis of model compounds.....	83
3.3.4.3	Calculations of ⁷⁷ Se NMR chemical shifts	89
4.	OUTLOOK.....	97
4.1	SYNTHESES	97
4.1.1	Selenium containing cycles with larger inner cavities	97
4.1.2	Cage molecules	98
4.2	NMR INVESTIGATIONS	99
4.3	THEORETICAL CALCULATIONS OF NMR PARAMETERS	99
5.	PREPARATIVE PROCEDURES.....	101
5.1	GENERAL CONSIDERATIONS	101
5.2	PREPARATION OF TETRASELENADIYNES CYCLOPHANES	104
5.2.1	General procedure for preparation of the bis(seleno-cyanatomethyl)-benzenes.....	104
5.2.1.1	1,2-bis(selenocyanatomethyl)-benzene (15a)	104
5.2.1.2	1,3-bis(selenocyanatomethyl)-benzene (15b)	105
5.2.1.3	1,4-bis(selenocyanatomethyl)-benzene (15c).....	107
5.2.2	General procedure for preparation of the bis(trimethylsilyl) diselenaalkadiynes	108
5.2.2.1	1,2-bis(((trimethylsilyl)ethynyl-selenyl)methyl)benzene (16a)	108
5.2.2.2	1,3-bis(((trimethylsilyl)ethynyl-selenyl)methyl)benzene (16b)	110
5.2.2.3	1,4-bis(((trimethylsilyl)ethynyl-selenyl)methyl)benzene (16c)	111
5.2.3	General procedure for preparation of the diselenaalkadiynes.....	113
5.2.3.1	1,2-bis(ethynylselenylmethyl)-benzene (17a)	113
5.2.3.2	1,3-bis(ethynylselenylmethyl)-benzene (17b)	115
5.2.3.3	1,4-bis(ethynylselenylmethyl)-benzene (17c)	116
5.2.4	General procedure the preparation of the tetraselena-cyclodiynes	118
5.2.4.1	2,5,14,17-tetraselena[6.6]- <i>ortho</i> -cyclophan-3,15-diyne (18a)	118
5.2.4.2	2,5,14,17-tetraselena[6,6]- <i>meta</i> -cyclophan-3,15-diyne (18b)	120
5.2.4.3	2,5,14,17-tetraselena[6,6]- <i>para</i> -cyclophan-3,15-diyne (18c).....	121
5.3	EXPERIMENTAL PROCEDURES FOR SYNTHESIS OF SMALL MODEL COMPOUNDS	122
5.3.1	General preparation procedure for synthesis of lithium methyl selenide	122
5.3.2	Model compounds containing one selenium center	123
5.3.2.1	Phenyl methyl selenide (22).....	123
5.3.2.2	Benzyl methyl selenide (23).....	124

5.3.2.3	Phenyl selenocyanate (27)	126
5.3.2.4	Benzyl selenocyanate (28)	127
5.3.2.5	Phenyl-2-(trimethylsilyl)-ethynyl selenide (38)	129
5.3.2.6	Benzyl-2-(trimethylsilyl)-ethynyl selenide (39)	131
5.3.2.7	Phenyl ethynyl selenide (31)	133
5.3.2.8	Benzyl ethynyl selenide (32)	134
5.3.3	Model compounds with two selenium centers	136
5.3.3.1	2-(methylselenyl) benzyl-methyl-selenide (24)	136
5.3.3.2	3-(methylselenyl) benzyl-methyl-selenide (25)	138
5.3.3.3	4-(methylselenyl) benzyl-methyl-selenide (26)	139
5.3.3.4	2-bromobenzyl methyl selenide (41)	141
5.3.3.5	Bis-(2-bromobenzyl) selenide (42)	142
5.3.3.6	2-bromobenzyl- <i>t</i> -butyldimethylsilyl ether (44)	144
5.3.3.7	2-(methylselenyl)-benzyl- <i>t</i> -butyldimethylsilyl ether (45)	145
5.3.3.8	2-(methylselenyl)-benzyl alcohol (46)	147
5.3.3.9	2-(methylselenyl)-benzyl selenocyanate (29)	149
5.3.3.10	2-(methylselenyl)-benzyl-2-(trimethylsilyl)-ethynyl selenide (47)	151
5.3.3.11	1,6-bis(2'-methylselenylbenzene)-2,5-diselena-3-hexyne (48)	152
5.3.3.12	2-(methylselenyl)-benzyl ethynyl selenide (33)	154
5.3.3.13	Methyl 2-selenocyanatobenzoate (50)	156
5.3.3.14	2,2'- diselenobis(benzyl alcohol) (51)	157
5.3.3.15	2,2'- diselenobis(benzyl bromide) (52)	159
5.3.3.16	2-(bromoselenyl)-benzyl bromide (55)	161
5.3.3.17	2-(cyanoselenyl)-benzyl bromide (56)	162
5.3.3.18	2-(cyanoselenyl)-benzyl selenocyanate (57)	164

6. X-RAY STRUCTURES 167

6.1	2,5,14,17-TETRASELENA[6,6]- <i>ORTHO</i> -CYCLOPHAN-3,15-DIYNE (18 A)	167
6.2	2,5,14,17-TETRASELENA[6,6]- <i>META</i> -CYCLOPHAN-3,15-DIYNE (18 B)	170
6.3	2,5,14,17-TETRASELENA[6,6]- <i>PARA</i> -CYCLOPHAN-3,15-DIYNE (18 C)	172
6.4	1,4-BIS(SELENOCYANATOMETHYL)-BENZENE (15c)	174
6.5	1,4-BIS(ETHYNYLSELENYLMETHYL)-BENZENE (17c)	177
6.6	BIS-(2-BROMOBENZYL) SELENIDE (42)	179
6.7	2-(METHYLSELENYL)-BENZYL ALCOHOL (46)	182
6.8	2-(METHYLSELENYL)-BENZYL SELENOCYANATE (29)	184
6.9	2,2'- DISELENOBIS(BENZYL ALCOHOL) (51)	186
6.10	2,2'- DISELENOBIS(BENZYL BROMIDE) (52)	189
6.11	1,6-BIS-(2'-METHYLSELENYLBENZENE)-2,5-DISELENA-3-HEXYNE (48)	192

7. LITERATURE 195

INDEX OF ABBREVIATIONS

A. General abbreviations

ACHC	2-aminocyclohexylcarboxylic acid
BETS	<i>bis</i> (ethylenedithio)tetraselenafulvalene
BuLi	Butyllithium
<i>t</i> -Bu	<i>tert</i> -Butyl
Bz	Benzyl
CCDB	Cambridge Crystallographic Database
CI	<i>chemical ionization</i>
COSY	<i>correlation spectroscopy</i>
CSA	<i>chemical shift anisotropy</i>
CT	charge transfer
DE	Diethyl ether
DEPT	<i>distortionless enhancement by polarization transfer</i>
DMF	Dimethyl formamide
DMSO	Dimethyl sulfoxide
EI	<i>electron impact</i>
Et	Ethyl
eq	equivalents
FAB	<i>fast atom bombardement</i>
FD	<i>field desorption</i>
GC	gas-chromatography
GPX	glutathione peroxidase
HMBC	heteronuclear multiple bond correlation
HMQC	heteronuclear multiple quantum correlation
HOESY	<i>heteronuclear Overhauser effect spectroscopy</i>
HR	high resolution
IR	infrared
LIFDI	<i>liquid injection field desorption ionization</i>
MALDI	<i>matrix assisted liquid desorption / ionization</i>
Me	methyl
MeSeLi	lithium methyl selenide
MS	<i>mass spectrometry</i>
m.p.	melting point
NMR	<i>nuclear magnetic resonance</i>
NOE	<i>nuclear Overhauser effect</i>
ORTEP	<i>oak ridge thermal ellipsoid plot</i>
PDB	Brookhaven National Laboratory (BNL) Protein Data Bank
PE	petroleum ether
Ph	phenyl
RDC	<i>residual dipolar coupling</i>
R _f	<i>ratio of front</i>
R _t	retention time
RT	room temperature
TBDMS	<i>t</i> -butyldimethylsilyl
TES	transmission electron microscopy
THF	tetrahydrofuran
TLC	thin layer chromatography
TMS	trimethylsilyl

TMSA	trimethylsilyl acetylene
TMSCN	trimethylsilyl cyanide
TMTSF	tetramethyl tetraselenafulvalene
TSF	tetraselenafulvalene
TTF	tetrathiafulvalene
UV	ultraviolet spectrum

B. Abbreviations on theoretical calculations

AO	atomic orbital
B3LYP	Becke's three-parameter hybrid functional combined with the Lee-Yang-Parr correlation functional
B98	Becke's 1998 revision of a three parameter hybrid functional
cc-pVTZ	<i>correlation consistent polarized valence triple zeta</i>
CCSD	coupled cluster with double substitution operator
CSGT	<i>continuous set of gauge transformations</i>
DFT	Density Functional Theory
ECP	electron core potentials
GIAO	<i>gauge-invariant atomic orbitals</i>
HF	Hartree-Fock formalism
HOMO	highest occupied molecular orbital
IGAIM	<i>individual gauges for atoms in molecules</i>
IGLO	<i>individual gauge for localized orbitals</i>
KT3	<i>Keal and Tozer's</i> generalized gradient approximation functional
LORG	localized orbitals/localized origins
LUMO	lowest unoccupied molecular orbital
MO	molecular orbital
MP	Møller-Plesset perturbation theory
NAO	natural atomic orbital
NBO	<i>natural bond orbital</i>
PBE	Perdew, Burke and Enzerhof 1997 functional
SCF	self consistent field

C. Abbreviations referring to spectroscopic methods

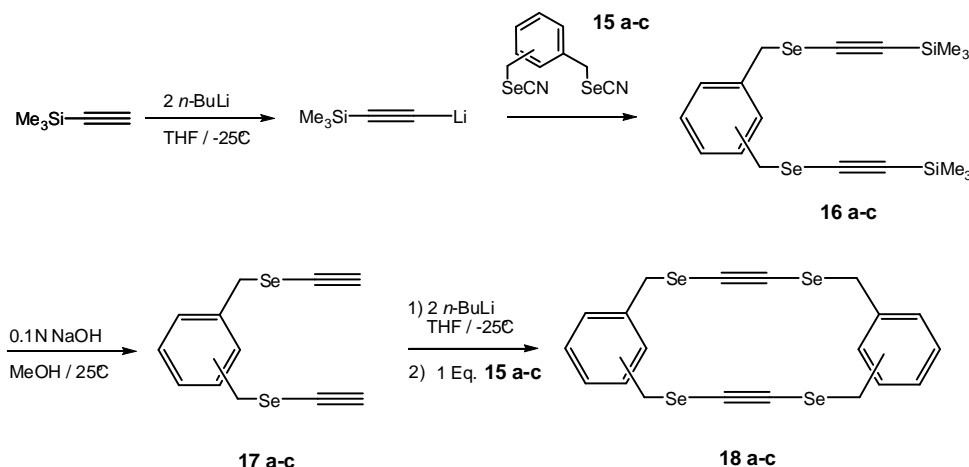
a, b, c	unit cell length dimensions [\AA]
α, β, γ	angles of the unit cell [$^\circ$]
δ	chemical shift [ppm]
ϵ	extinction coefficient [$1000 \text{ cm}^2 \cdot \text{mol}^{-1}$]
J	coupling constant [Hz]
λ	absorption maximum
m/z	mass-to-charge ratio
R	final R factor
R_w	weighted R factor
V	volume of the unit cells [\AA^3]
Z	number of molecular formula fragments in the unit cell

1. Abstract

The main topic of this thesis is the comparative investigation of divalent selenium centers interactions in solids and solution. Therefore we decided to combine experimental and theoretical results in order to gather more insight into selenium – selenium interactions.

The idea of using the chalcogen–chalcogen interactions as directional forces to obtain tubular structures was validated during recent experimental studies in which cyclic aliphatic diynes and dienes containing chalcogen atoms organized themselves in columnar structures¹. Moreover, theoretical investigations confirmed the description of divalent selenium interactions as a secondary interaction between an occupied p-type orbital of one chalcogen center (X) and the empty X-C σ^* orbital of the other (see Figure 3.19.), together with induction and dispersion forces².

The first part of this work deals with the synthesis of three isomeric cyclophanes and their solid-state structures in comparison with previously synthesized similar cyclic compounds. The cycles investigated so far consisted of rigid units (e.g. X-C \equiv C-X, where X= S, Se, Te) and methylene chains as flexible parts. The inclusion of benzene rings into the methylene chains is expected to add more rigidity and also to open the possibility of π - π stacking. To investigate the results of this idea we synthesized three isomeric cyclic tetraselenadiynes containing the building blocks mentioned. We analyzed their solid-state structure characteristics in our larger effort to understand the nature of chalcogen–chalcogen non-bonding interactions. The synthesis of the three isomeric tetraselena-[6.6]cyclophanes **18 a-c** was achieved using a stepwise approach, as shown in Scheme 1.1.



Scheme 1.1. Multi-step synthesis of isomeric tetraselena [6.6]cyclophanes **18 a-c**.

Remarkable features of the solid-state structure of **18 a-c** were analyzed and compared with other structural features of compounds that involved Se centers in $\text{Se}\cdots\text{Se}$ interactions.

Se...Se intermolecular interactions with distances between 348 pm and 397 pm have been detected in all three isomers, generating columnar-like structures in all three cases (see Figure 1.1. and figures in Chapter 3.2.3.). These values are significantly smaller or close to the sum of the Van-der-Waals radii for Se, indicating strong interactions. Besides the intermolecular selenium-selenium interactions, in the stacked structures other intramolecular and intermolecular interactions involving selenium centers can be observed, like significant inter- and intramolecular Se...H hydrogen bonding or offset aligned π - π interactions (see Figure 2.14.)

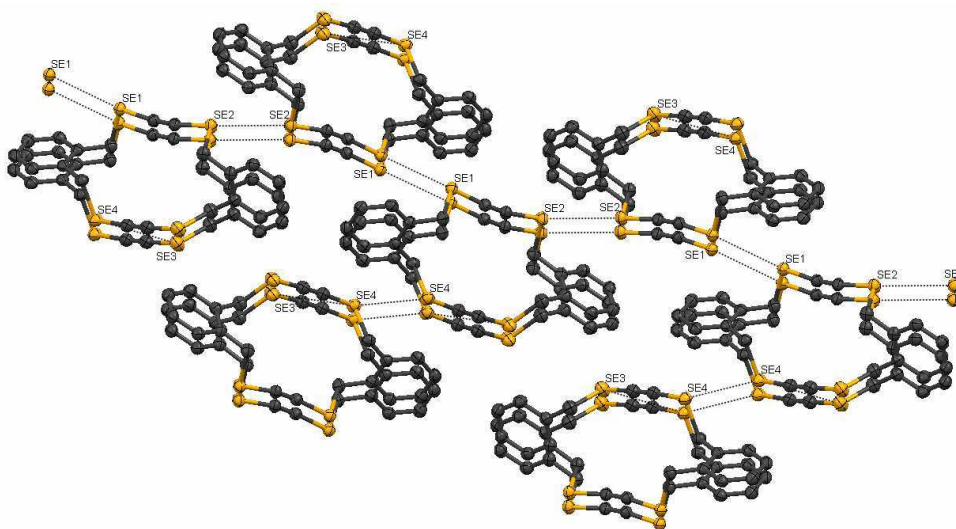
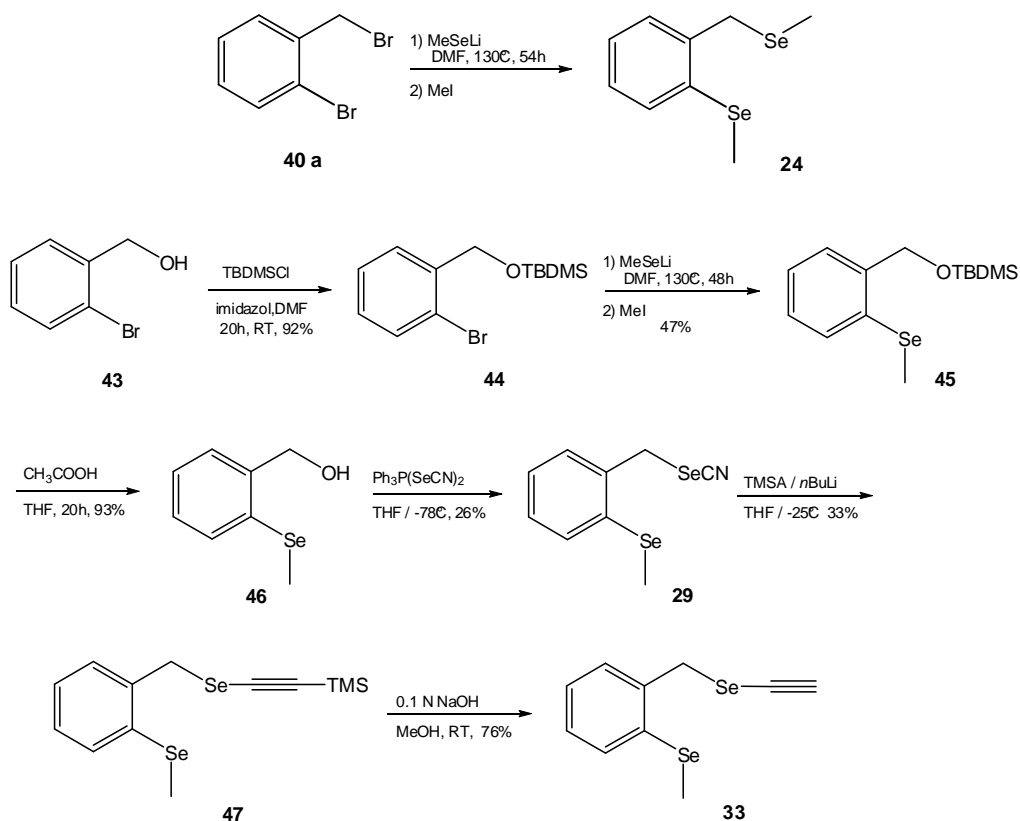


Figure 1.1. Threaded arrangement in the solid state structure of compound **18a**.

The second part of this work investigates the presence and the strength of the Se...Se interaction in solution. A series of model systems containing two selenium centers situated at a convenient distance, but also with significant internal motion ability, were synthesized. The NMR spectroscopy was the method of choice to investigate the interaction in solution. ^{77}Se NMR chemical shifts (δ_{Se}) are sensitive to the electronic environment around the Se atom, therefore their behaviour can be used as gauge for evaluating the strength of nonbonding interactions involving Se centers.

The synthesis of the desired model compounds was performed using a less direct synthetic pathway, mainly due to the difficulties encountered in introducing the second Se center. Due to the ambivalent character (electrophile/nucleophile) of the first Se atom, the synthetic pathways available for introducing the second Se atom are severely reduced. The synthetic approach used for obtaining three of the desired model compounds is depicted in Scheme 1.2.



Scheme 1.2. Synthetic pathway for obtaining the desired model compounds **24**, **29** and **33**.

A comparison of the experimental values for the ⁷⁷Se chemical shifts for the synthesized compounds **24**, **29** and **33** with simpler compounds such as **22** and **61** (see page 71) revealed a high field shift for the ⁷⁷Se NMR signal of the SeCH₃ group, implying an increased electron density around the Se atom. The same trend was observed when comparing the chemical shift of the second Se atom in comparison with the respective simpler fragments **23**, **28** and **32**, indicating an increased electron density, despite the electron withdrawing character of the C≡CH and CN groups. Taken together, this leads to the conclusion of increased electron density around both Se atoms, due to a non-bonding interaction between them in which the SeCH₃ group plays the electron donor role, while the second group is the acceptor, the interaction being slightly stronger starting from Se-CH₃ to SeCN.

A comparison of the observed ⁷⁷Se NMR signal shifts in our compounds with the literature data³ for 2-methyl-selenobenzylhalogenides (**62–64**) leads us to assume that the Se···Se interactions are slightly stronger than the Se···halogen interactions.

Investigation of the coupling constants (*J* coupling) between the ⁷⁷Se nuclei for the compounds **24**, **29** and **33** confirmed our assumption of increasing interaction strength. The values of the *J* coupling are increasing in the order **24** < **33** < **29**. Additionally NMR

methods for determining the relaxation time of the ^{77}Se nuclei involved in the interactions were used and confirmed the observation based on chemical shifts and coupling constants. Variable temperature NMR experiments revealed the existence of several conformers for each of the model compounds, but also showed that there is only a very small energy barrier between them.

In order to get some more insight in the behaviour of our model compounds and the predominant interactions in their conformers, we performed a conformational analysis for all three model compounds. Theoretical calculations at the MP2/6-311+g(d)//B98/6-311+g(d) level revealed the existence of four conformers for each of the investigated compounds, in which the Se...Se interaction or the competing Se...H bonding is the predominant force. A comparison of the theoretical results against the solid-state structure of compound **29** showed that in the solid-state the Se...Se interaction can become predominant. Theoretical calculated nuclear shieldings and chemical shifts were compared with the experimental values. Based on this comparisons we assume that in solution, the Se...Se interactions are less favoured in comparison with Se-H bonding. In the solid-state, the Se...Se interaction becomes the predominant stabilization force for the model compounds.

In conclusion, our investigation of the nature of the Se...Se interactions show that the ^{77}Se chemical shifts represent an useful tool in qualitatively assessing the strength of the interaction. The strength in the order $\text{MeSe}\cdots\text{SeMe} < \text{MeSe}\cdots\text{SeC}\equiv\text{CH} < \text{MeSe}\cdots\text{SeCN}$ qualitatively revealed from the NMR chemical shifts is consistent with the $n_{\text{Se}}-\sigma^*_{\text{Se-C}}$ orbital interaction model. It proves furthermore that electron correlation and dispersion forces play an intimately interconnected role in these interactions, that influence each other, therefore being difficult to analyze separately.

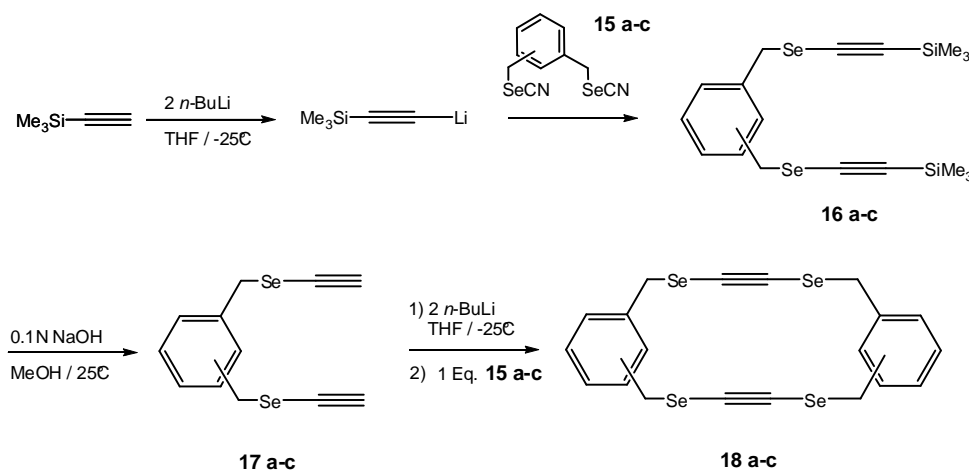
Zusammenfassung

Der Schwerpunkt der vorliegenden Arbeit liegt auf der Untersuchung von Wechselwirkungen divalenter Selenzentren in Festkörpern und Flüssigkeiten. Hierzu werden Ergebnisse experimenteller und theoretischer Untersuchungen kombiniert, um mehr Licht in die Natur dieser Selen-Selen-Wechselwirkungen zu bringen.

Das Konzept, gerichtete Chalkogen-Chalkogen-Wechselwirkungen zur Erzeugung röhrenförmiger Strukturen zu nutzen, wurde jüngst durch experimentelle Arbeiten bestätigt, in denen chalkogenhaltige cyclische aliphatische Diene und Diene sich in säulenartigen Strukturen organisierten¹. Des Weiteren bestätigen theoretische Untersuchungen die

Beschreibung von divalenten Selen-Selen Wechselwirkungen als sekundäre Wechselwirkung zwischen einem besetzten p-Orbital des einen und dem leeren X-C σ^* -Orbital des anderen Chalkogen-Zentrums (siehe Abbildung 3.19.) in Verbindung mit Induktions- und Dispersionskräften².

Im ersten Teil dieser Arbeit werden die Synthesen dreier isomerer Cyclophane und deren Festkörperstrukturen behandelt und mit ähnlichen, bereits dargestellten, cyclischen Verbindungen verglichen. Die bisher synthetisierten Cyclen bestanden aus starren Untereinheiten (z.B.: X-C \equiv C-X mit X=S, Se, Te) und flexiblen Alkylketten. Die Einführung von Phenyleinheiten in diese Ketten sollte die Rigidität erhöhen und darüber hinaus die Möglichkeit von π - π -Wechselwirkungen eröffnen. Um die Gültigkeit dieser Gedanken zu überprüfen, wurden drei isomere cyclische Tetra[6.6]selenadiine dargestellt, die eben solche Phenyleinheiten enthalten, und ihre Festkörperstrukturen untersucht, um mehr Aufschluss über die nichtbindenden Chalkogen-Chalkogen-Wechselwirkungen zu erhalten. Die Synthese dieser Cyclophane erfolgte über einen mehrstufigen Ansatz (Schema 1.1.).



Schema 1.1. Synthese der isomeren Tetraselen[6.6]cyclophane

Signifikante Strukturdaten von **18 a-c** wurden mit den Daten vergleichbarer Verbindungen mit Selen-Selen-Wechselwirkungen verglichen. Hierbei wurden in allen drei isomeren Verbindungen Selen-Selen-Wechselwirkungen mit Abständen zwischen 348 und 397 pm gefunden, die zu röhrenartigen Strukturen führten. Diese Abstände sind bedeutend kleiner bzw. nahe der Summe der Van-der-Waals-Radien zweier Selenatome, was auf starke Wechselwirkungen hinweist. Neben den eben erwähnten (intermolekularen) Wechselwirkungen können weitere intra- und intermolekulare Wechselwirkungen von Selenzentren beobachtet werden wie z.B. inter- und intramolekulare Selen-Wasserstoffbrücken und versetzt angeordnete π - π -Wechselwirkungen (siehe Abbildung 2.14.).

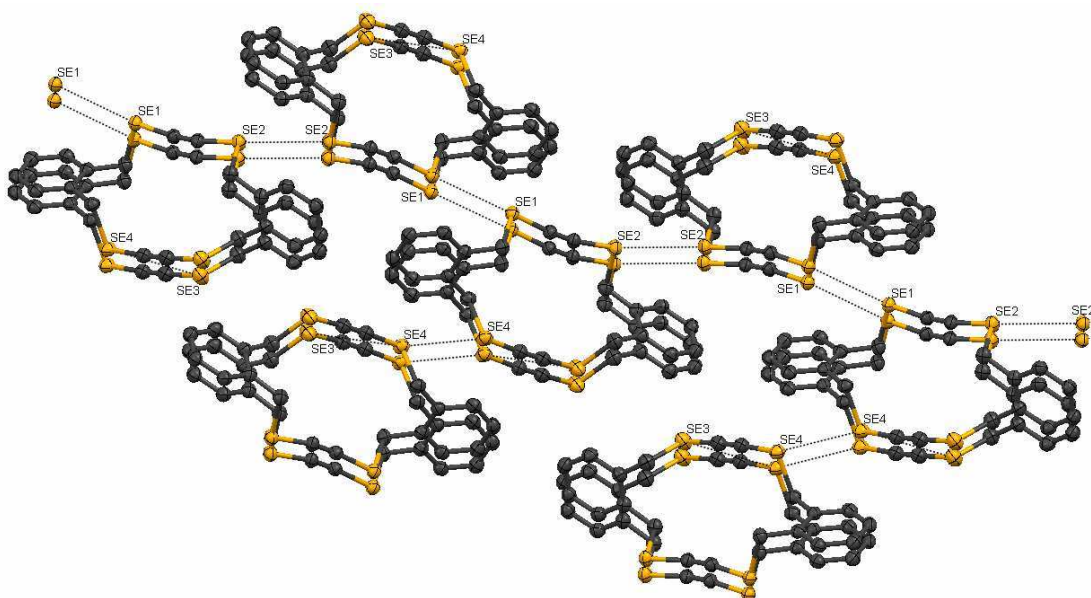
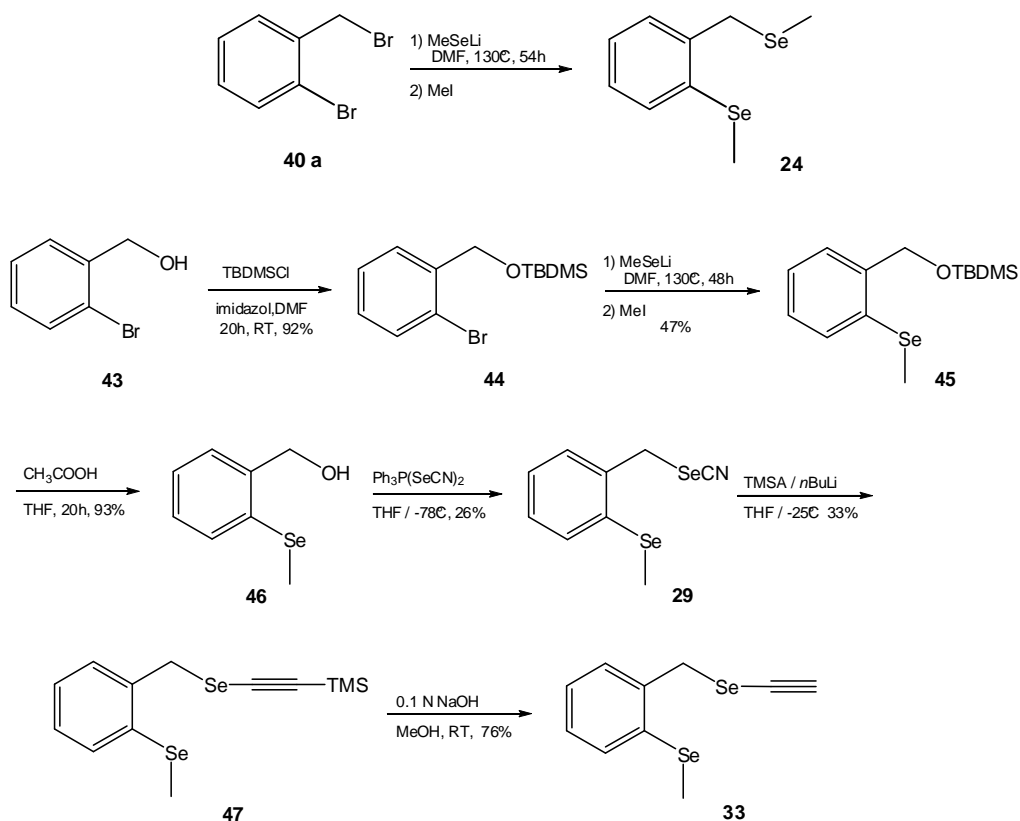


Abbildung 1.1. Anordnung im Kristallstruktur von Verbindung **18 a**.

Der zweite Teil dieser Arbeit konzentriert sich auf das Vorhandensein und die Beschaffenheit von Selen-Selen-Wechselwirkungen in Lösung. Eine Reihe von Modellsystemen, die zwei Selenatome in geeignetem Abstand enthalten, aber trotzdem flexibel sind, wurden hierfür dargestellt. Da die Verschiebungen in den ^{77}Se -NMR-Spektren von der elektronischen Umgebung der Selenatome beeinflusst werden, stellen NMR-Experimente eine geeignete Methode zur Untersuchung der Selen-Selen-Wechselwirkungen in Lösung dar.

Da die Einführung des zweiten Selenzentrums synthetisch schwer durchführbar war, musste die Darstellung der für die NMR-Untersuchungen genutzten Modellverbindungen über einen komplizierten Weg erfolgen (siehe Schema 1.2.).



Scheme 1.2. Syntheseweg zur Darstellung der Modelverbindungen **24**, **29** und **33**.

Ein Vergleich der experimentellen Werte der Verschiebungen der synthetisierten Verbindungen **24**, **29** und **33** mit den einfacheren Verbindungen **22** und **61** zeigt in den ^{77}Se -NMR-Spektren eine Hochfeldverschiebung der Signale für das methylsubstituierte Selenatom, was auf eine erhöhte Elektronendichte hindeutet.

Der gleiche Trend konnte beim Vergleich der Verschiebungen des zweiten Selenatoms mit den einfacheren Verbindungen **23**, **28** und **32** festgestellt werden, trotz des elektronenziehenden Effektes der Alkin- und Nitrilfunktionen. Zusammengenommen deuten diese Befunden auf eine nichtbindende Wechselwirkung zwischen den Selenzentren hin, wobei das methylsubstituierte Selenatom die Rolle des Elektronendonors übernimmt, während das Zweite als Elektronenakzeptor fungiert.

Vergleicht man die von uns beobachteten Verschiebungen in den ^{77}Se -NMR-Spektren mit den Daten von *Iwaoka*³ für 2-Methyl-selenbenzylhalogenide (**62–64**), liegt der Schluss nahe, dass die Selen-Selen-Wechselwirkungen leicht stärker sind als die Selen-Halogen-Wechselwirkungen.

Eine nähere Betrachtung der Se-Se-Kopplungskonstanten der Verbindungen **24**, **29** und **33** bestätigt die Vermutung zunehmender Wechselwirkungsstärke in der Reihenfolge **24** < **33** < **29**. Eine zusätzliche Bestimmung der Relaxationszeiten der ^{77}Se -Kerne, die in die Se-Se-Wechselwirkungen involviert sind, bestätigt die auf Grundlage von Verschiebungen und Kopplungskonstanten gemachten Annahmen. Tieftemperatur- ^{77}Se -NMR-Spektren zeigen das Vorhandensein mehrerer Konformere für jede Modellverbindung an, allerdings mit äußerst geringen Energiedifferenzen zwischen den Konformeren.

Um das Verhalten der Modellverbindungen und die bevorzugten Wechselwirkungen in ihren Konformeren besser verstehen zu können, wurden Konformationsanalysen für sämtliche Modellverbindungen durchgeführt. Theoretische Berechnungen auf dem MP2/6-311+g(d)//B98/6-311+g(d) Niveau ergeben vier Konformere für jede der untersuchten Verbindungen in denen entweder die Se-Se-Wechselwirkung oder die konkurrierende Se-H-Bindung die vorherrschende Kraft ist. Ein Vergleich der berechneten Struktur mit der Kristallstruktur von Verbindung **29** lässt erkennen, dass im Kristall die Se-Se-Wechselwirkung überwiegen kann. Es wurden theoretische Berechnungen in Bezug auf die Abschirmung und magnetischen Verschiebungen mit experimentellen Befunden verglichen. Daraus kann man schliessen, dass in Lösung die Se-Se-Wechselwirkung weniger stark ausgeprägt ist als die Se-H Bindung. Hingegen dominiert im Festkörper die Se-Se-Wechselwirkung für die gegebenen Modellverbindungen.

Diese Arbeit zeigt, dass die chemische Verschiebung in ^{77}Se -NMR-Spektren eine nützliche Sonde bei der quantitativen Untersuchung von Se-Se-Wechselwirkungen darstellt. Die gefundene Zunahme in der Reihenfolge von $\text{MeSe}\cdots\text{SeMe}$ < $\text{MeSe}\cdots\text{SeC}\equiv\text{CH}$ < $\text{MeSe}\cdots\text{SeCN}$ stimmt mit dem $n_{\text{Se}}-\sigma^*_{\text{Se-C}}$ -MO-Wechselwirkungsschema überein und zeigt, dass Elektronenkorrelation und dispersion eng verknüpfte Rollen bei diesen Wechselwirkungen spielen, die sich gegenseitig beeinflussen und somit schwer von einander zu trennen sind.

2. Introduction

2.1 General remarks on molecular self-assembly

Intermolecular interactions have always fascinated scientists, as they are essential⁴ forces for any form of life. They enable molecules to interact with each other, control how they relate to their environment, they even “hold” us, human beings, together. Intermolecular interactions are also pivotal for all conveniences of modern living, such as building constructions, the printing and binding of books, LED and touch screens of laptops and mobile phones and countless other advantages of nowadays comfortable living. Therefore, it is essential that scientists understand the way molecules are bound to each other.

There are numerous types of intermolecular interactions comprising an extended range of attractive and repulsive forces. The simplest could be considered for example the *cation-anion* interaction. With strength comparable to covalent bonding (bond energy = 100–350 kJ/mol)⁴ ion–ion interactions are long-ranged and directional, and they induce a well-organized complementary pattern of cations and anions in crystal lattices. Even if not involved in pure electrostatic (Coulomb) interactions, electronically neutral molecules do take part in similar interactions, as they can be influenced by the electrostatic field of surrounding molecules. The bonding of an ion with a polar molecule is another type of interaction, the *ion-dipole* interaction. A slightly weaker interaction (50–200 kJ/mol bond energies)⁴, can be observed in solid and liquid states, a typical example being that of complexes of alkali metal cations with large macrocyclic ethers, also known as crown ethers, in which the oxygen lone pairs of the ethers are attracted to the cation positive charge, stabilizing it. Coordinative (dative) bonds can also be included in the ion-dipole interaction category, although in this case, the border between non-bonding and bonding is relatively difficult to pinpoint. Interactions of metal and organic cations with molecules containing π systems is a much more noncovalent “weak” interaction (5–80 kJ/mol interaction energy)⁴, but the *cation- π* interactions play an important role in biological systems⁵ and lately have been used in organic synthesis for controlling molecular conformations⁶.

If neutral molecules have a dipole moment, they can interact with each other due to the *dipole-dipole* interaction. Relatively weak (5–50 kJ/mol interaction energy)⁴, this attractive interaction results from matching either one pair of poles from adjacent molecules (Type I) or opposing arrangements of one dipole of one molecule with one dipole from another

molecule (Type II). The typical example is observed in solid state arrangements of organic carbonyl compounds (Figure 2.1.), but in solution the interactions are even weaker⁴.

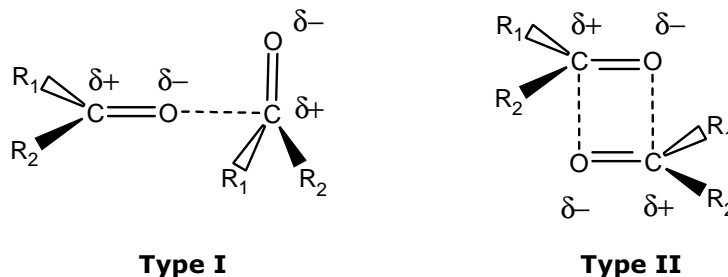


Figure 2.1. Types of dipole-dipole interactions in carbonyls

One particular type of dipole-dipole interaction could be considered as the ubiquitous *hydrogen bonding* (4-120 kJ/mol interaction energy)⁴. A hydrogen bond is formed when a hydrogen atom covalently bonded to an electron withdrawing group is attracted to a neighboring dipole or functional group (be it from an adjacent molecule or even from the same molecule in the case of larger cyclic molecules). Hydrogen bonds have an amazingly large range of strengths, lengths and geometries⁷. As little as one strong hydrogen bond may be sufficient to determine the solid-state structure of organic compounds and influence behaviors in solution or gas phase. On the other hand, weaker hydrogen bonds play an important role in structural stabilization in various chemical and biological systems⁸. Given its significant strength, highly directional nature and omnipresence, there is no argument why hydrogen bonding has been labelled as the "masterkey interaction in supramolecular chemistry"⁴.

π - π *stacking* is another type of weak electrostatic interaction (1-50 kJ/mol interaction energy)⁴ that occurs between aromatic rings, usually in the situation where one is relatively electron poor and the other electron rich.

Even weaker are interactions based on *Van der Waals forces* (less than 5 kJ/mol), arising from the polarization of an electron cloud due to the proximity of a neighboring group, resulting in a weak temporary electrostatic interaction. Van der Waals interactions provide a general attractive interaction for most polarizable species. They can be divided into a dispersion (London) term and an exchange-repulsion term. The dispersion interaction is attractive and results from interactions between fluctuating dipoles, it also includes *induced dipole-to-induced dipole* interactions. This interactions decrease with the distance, while the exchange-repulsion term dictates the molecular shape and compensates the dispersion effect. Usually non-directional, Van der Waals forces are considered to have only a minor importance, but lately specific cases of directional interactions of this type surfaced and generated new interest in understanding and using them in organic synthesis.

All these types of interactions can be found as building blocks of a whole range of supramolecular structures in natural as well as artificial systems. These nanoscale supramolecular structures have been generating a lot of interest in the last quarter of a century as they are the logical candidates for filling the gap between molecular (chemical) and macromolecular (biological) structures.

The field of electronics pushed the limits and forced stepwise the realization that the so-called "engineering down" approaches may find their limit in the following decade. The current lithographic techniques can still be improved, but the practical limit of these methods seems to lie at a microscale unit. In semiconductor devices with dimensions lower than 0.2 to 1 μm , the difficulties of isolating the silicon components, due to the electronic cross-talk between devices as a direct consequence of electron tunneling or poor heat dissipation, would increase the difficulty of fabrication and sky-rocket the costs of production. These factors make it an economically unfeasible technology. Therefore, an increased interest is manifested in understanding of supramolecular biological structures and the forces behind their self-organization and extension of this understanding to chemical or less-complicated biological systems. Biological systems consisting of nanoscale structures and devices provide a lot of valuable information about the rules of self-organization or self-assembly of molecular structures, interacting chemically and physically in certain defined ways. One can even claim that the phenomenon of self-organization is responsible for life itself. Chemists are seeking to understand, imitate and even surpass the functions of biological systems in building nanoscale structures, with the ultimate goal of being able to control the assembly and function of these structures with the same precision displayed by nature.

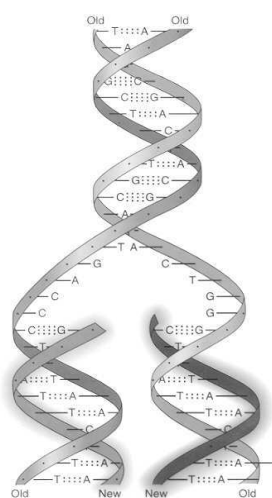


Figure 2.2. Nucleation and propagation in nucleic acid self-assembly.

Probably the most well-known and extensively studied example of self-assembly in biological structures is the reproduction through self-assembly of the DNA double helix from two complementary oligonucleotides (Figure 2.2). Simply explained, the assembly results after the contact and recognition of one nucleotide strand by another, which is followed by the propagation of the growing helix based on matching of complementary base pairs. Successive dynamic assembling and disassembling allow for correction of errors due to mismatching base pairs, ultimately leading to correct connections between the two strands.

Another typical example that helps to illustrate many features present in the self-organization of biological systems is the tobacco mosaic virus (TMV), a helical virus particle, 300 nm in length and 18 nm in diameter (Figure 2.3), composed of 2130 identical units (each comprising 158 aminoacids), which form a helical ribbon around a single strand of 6390 base pairs of RNA.

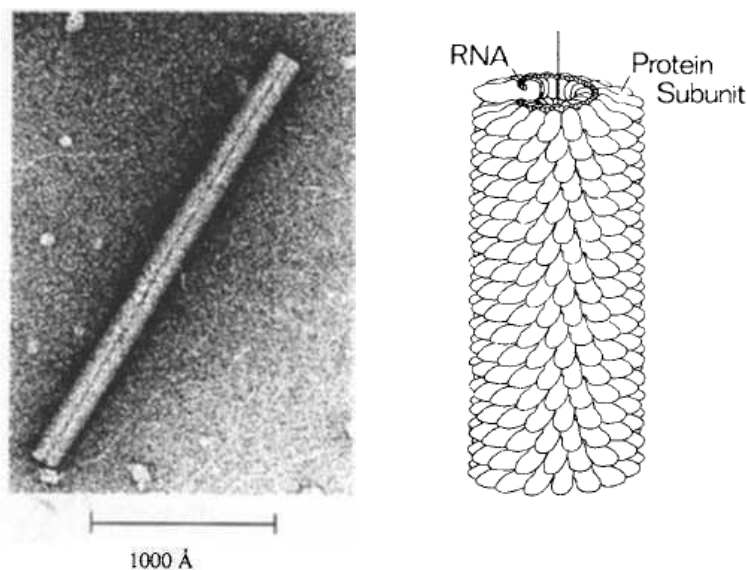


Figure 2.3. Electron micrograph image (left, from lit.⁹) of the tobacco mosaic virus and schematic representation (right, from lit.¹⁰).

Each protein subunit forms a disk-shaped building unit (Figure 2.4.a), which grows together into a helical form supported by the insertion of a loop of RNA into the central cavity of the disk (Figure 2.4.b). Additional protein subunits associate with the growing structure through non-covalent interactions (Figure 2.4.c and d).

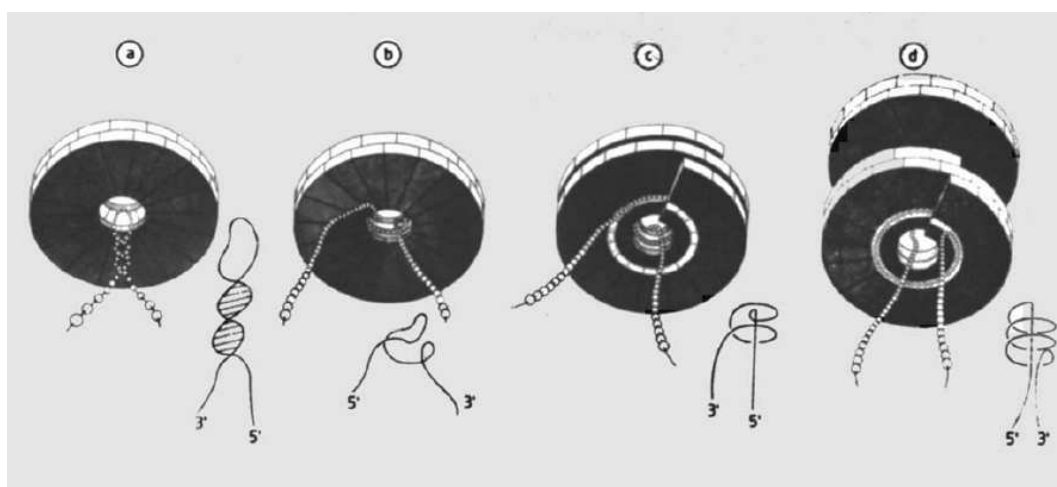


Figure 2.4. Self-assembling process of the tobacco mosaic virus (from lit.¹¹).

The self-assembling process of TMV demonstrates the ability of biological systems to construct large-size ordered supramolecular structures from relatively simple subunits.

Further examples can be found easily in the literature, but the most common feature of all these biological self-assembling processes is the ability to use many weak so called nonbonding interactions between subunits in order to construct a supramolecular structure as well as to stabilize the final construct¹².

Tubular structures resulting from a self-assembling process have received a particular interest from chemists due to their occurrence in biological systems where they act as chemical information carriers. Transmembrane ion channels¹³ are natural nanotubes made of protein molecules in cell membranes that link the out- and in-solutions of cells, allowing the transfer of ions (like Na^+ , K^+ , Ca^{2+} or Cl^-) through their cylindrical cavity. The transfer is controlled not only based on electrodiffusion (controlled by the charge of the cavity), but also by the size of the opening. An illustrative example is the membrane protein aquaporin, which selectively allows only the transport of water molecules through its central channel¹⁴.

Natural nanotubes are not only transport channels, but also "miniature reactors" as proven by protein degrading enzymes or protein-folding chaperonins. The cylindrical inside surfaces of these tubes contain the specific chemical functional groups enhancing the enzyme/protein activity based on functional group complementarity and/or chemical catalysis¹⁵. Many other biological systems which rely on self-assembling inspired much research in the construction of smaller chemically synthesized tubes used as tiny molecular reaction chambers, molecular sieves or ion detection devices. Biologically derived principles for construction of supramolecular structures have been used in synthesizing materials that

don't necessarily have a biological action. The best example would be liquid crystal display components¹⁶, birefringent materials with optical applications¹⁷ or anti-misting additives for safer jet fuels¹⁸.

2.2 Structural types of tubular motives

The approaches for generating tubular structures could be classified according to the different proportions of intratubular covalent and non-covalent bonding involved in assembling ("encoding") the chemical information (shape, connecting groups, local charges, recognition sites) contained in the small molecular building blocks.

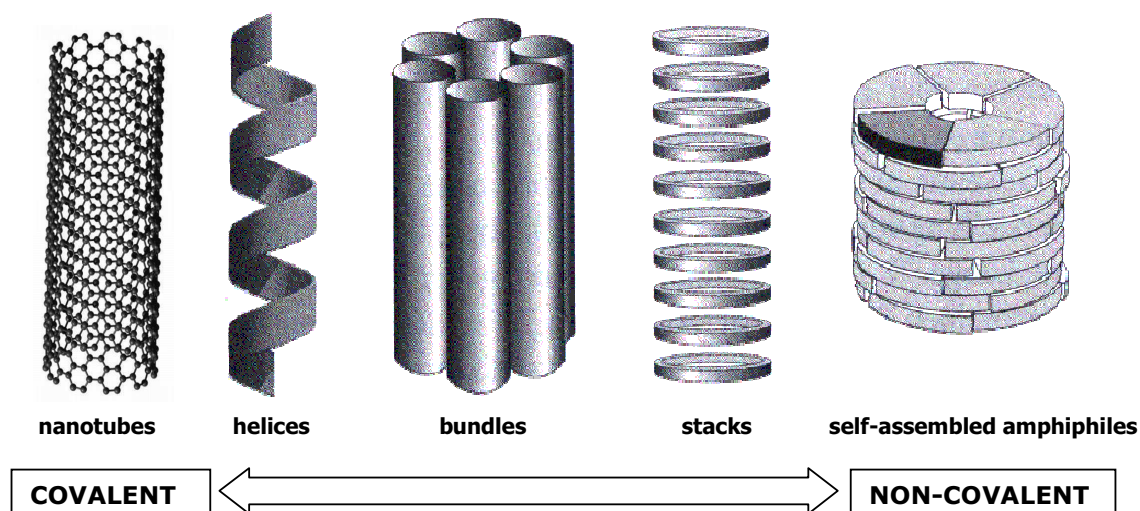


Figure 2.5. Possibilities for molecular assembling of tubular structures, based on pure covalent (left) to pure non-covalent (right) bonding

Both extremes (pure covalent, left side of Figure 2.5. and pure non-covalent bonding, right side) can be used for generating open-ended tubular objects, with a lot of mixing possibilities in between.

2.2.1 Tubular structures based on pure covalent bonding

Chemical bonding in building the tubular structure increases the stability of the molecule as well as offering synthetic control of the conformations, but has the disadvantage of being (at the moment) a tedious approach, with significant drawbacks due to purification issues¹⁹. The highest covalent bond containing nanotubes are represented by the carbon nanotubes,

already commercially available. Carbon nanotubes are some of the most promising candidates for the future of nanomaterials. It should be mentioned that research on different electronic properties of single-walled carbon nanotubes proved that they are related to the direction in which a starting graphene sheet is to be folded in order to form the tubular structure. Therefore, research in the field of carbon nanotubes is bound to continue and be enlarged due to the multiple preparation and synthesis strategies available²⁰. Carbon nanosheets and tubes are predicted as a new revolutionary material that will replace silicon in the search for manufacturing super-fast computer chips²¹. But, in the not-so-distant future, carbon could lose its monopoly in the nanoengineering world, as recently synthesized boron nanotubes²² might even outperform carbon nanotubes for certain electronic applications according to published theoretical calculations²³.

Another approach in generating tubular nanostructures based on covalent bonding is based on generating an inherently stiff helical structure containing an internal void channel²⁴. The classical examples are α -helices from nucleic acids (DNA), peptides from α - and β -amino acids or Vollhart's [n]phenylenes, synthesized by the insertion of cyclobutadienes into *meta*-annulated benzene ring systems through two- or threefold intramolecular Co-catalyzed [2+2+2] cyclotrimerization reactions²⁵. Figure 2.6. shows schematically a top view and a side view of [8]phenylene, the stiff and helical backbone induced due to the ring annelation being easily recognizable.

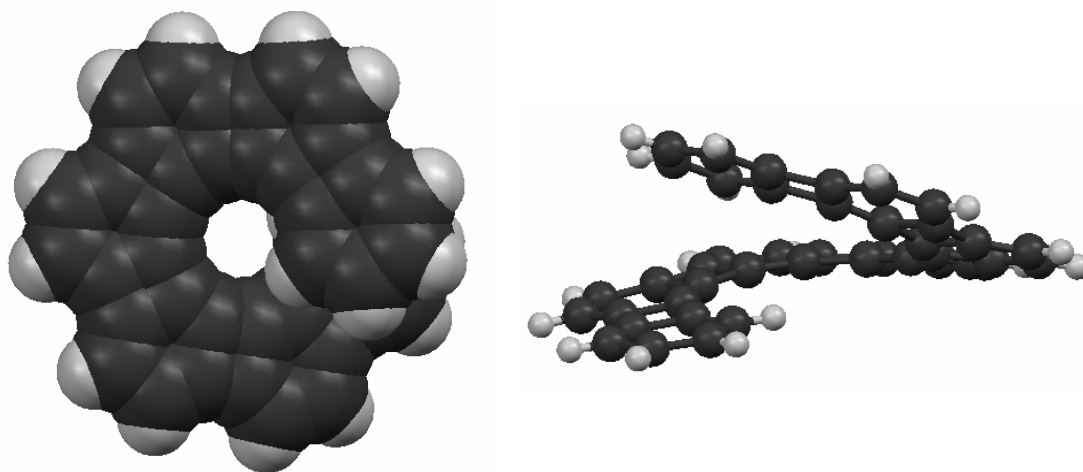


Figure 2.6. Top view (left, spacefilling representation) and side-view (right, ball and stick representation) of [8]phenylene (CCDC ref. no: 180984).

2.2.2 Tubular structures based on pure non-covalent bonding

The other extreme of the scale, where the predominant driving forces of the self-assembly are non-covalent interactions, consists of sector or wedge-like molecules that due to non-bonding interactions assemble themselves into discs and furthermore, as a result of face-to-face interactions, stack to form continuous cylinders similar to macrocycles. The typical examples are biological amphiphiles, lipids composed of long hydrocarbon tails and polar head groups as depicted in Figure 2.7. The aspect of the self-assembled structure is dependant on the volume difference between head and tail, the bigger the tail proportion the easier cyclic structures are realized. Typical amphiphile structures include a large class of compounds like: nucleic acid derivatives²⁷, N-acylated amino acids²⁸, double chain amonium salts²⁹, unsaturated double-chain phosphatidylethanolamines³⁰ and aldonamides or gluconamides³¹. Polar or ionic heads, usually an ionized or esterified carboxylic group, will form the inner part of the cylinders, filled with polar solvent molecules and the disordered non-polar tails will form the outer part and isolate the tubes from each other.

Different type of shapes can be used, and through covalent stabilization using cross-linking, more complicated structures with induced features can be obtained. Considering the simple and easily preparation, this type of self-assembling nanotubes has become interesting for potential applications in life and material sciences³².

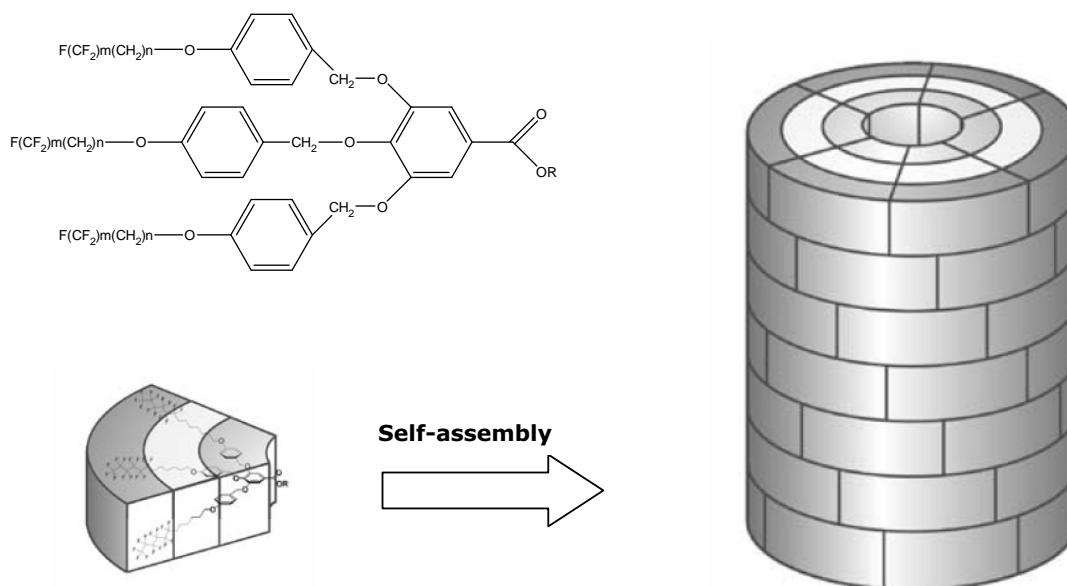


Figure 2.7. Flat-shaped dendritic amphiphile, based on gallic acid, self-assembly into layered tubes, based on polar inner core and crosslinkable tails (from lit.³³).

2.2.3 Tubular structures based on both non-covalent and covalent bonding

In between these two extremes, the process of generating tubular structures is a compromise of using both covalent and non-covalent bonding in order to obtain the desired structural features. When the starting molecular building block is already prone to form a helical backbone or sheet, non-covalent interaction is used to manipulate the secondary structure, like in the chains of alternating non-cyclic D,L- α -peptides which, due to stabilization through hydrogen bonding, adopt a beta-helical conformation. The amino acid side chains point outward, generating an inner cylindrical cavity with a diameter of up to 5 Å according to early computational studies, strongly influenced by the helix periodicity and the number of residues per turn³⁴. Alternatively, hydrogen bonding can be used to constrain the backbone into a continuously forced kinked conformation that given enough length would afford a helical structure, as in aromatic and heteroaromatic amides³⁵. These in turn will generate a tubular structure, especially if the H-bonding interaction would manifest its influence on the external side of the backbone, rather than in the interior part³⁶.

Furthermore, helical structures with small cavities can be interconnected through non-bonding interactions to form stacking helices³⁷ or helical bundles with inner cavities having either hydrophilic or hydrophobic characteristics³⁸ (see Figure 2.5.). Most of the known examples are based on peptides, so a rational design of the amino acid sequence allows for controlling the electrostatic properties and dimension of the inner void size, with examples known to vary from only 1.5 Å³⁹ up to even 1 nm⁴⁰.

Probably the largest class of tubular structures is based on cyclic molecules which take advantage of a mixture of bonding and directional non-bonding interactions self-assembling or stacking on top of each other. This type of architecture is the most balanced between bonding and non-bonding design, as the covalent structure of the molecule contains information regarding the inner and outer dimensions of the tubes, while the non-covalent interactions direct the length, strength and direction for the structure. The hydrogen bond proved to be the most prominent non-covalent directional force involved in the self-assembly of biological systems, so it is logically the first candidate considered when designing a stacked molecular association. But other intermolecular interactions responsible for this type of structure must include π - π interactions, ion dipole interactions, short interactions between halogen centers and also chalcogen-chalcogen interactions. Strangely enough, the macrocycle stacking motif is not very common in biological systems, but it has been used extensively to design artificial tubular systems.

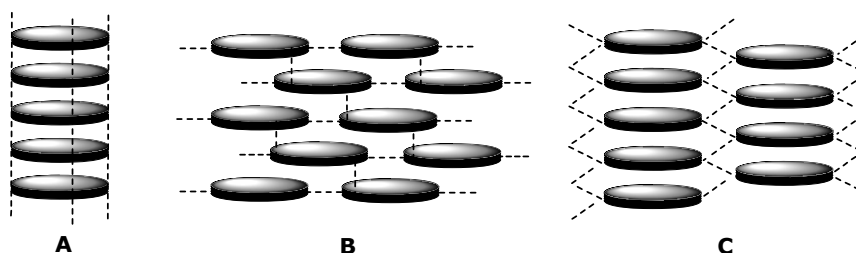


Figure 2.8. Strategies for interconnecting molecular rings to form tubular structures

Possible strategies to connect molecular rings to form tubular structures include the connection with each other based on strong interaction forces only in the stacking direction (Figure 2.8 A); strong in-plane connections and weaker inter-planar interactions (Figure 2.8 B) or connections based on zig-zag and ladder-type weak forces in between the rings (Figure 2.8 C) generating stacked structures as well.

Several types of non-bonding interaction are involved in generating tubular or columnar structures and the most important ones of them are discussed in the following paragraphs.

2.2.3.1 Hydrogen bonding

The first strategy generates a densely packed aggregation of rods as in the case of cyclic peptides. After the original recognition of *De Santis*³⁴ that peptides have the potential to generate hollow cylinders through H-bonding if the amino acid sequence is carefully selected, *Ghadiri et al.*⁴¹ proved the validity of the concept designing and synthesizing alternating cyclic peptides with an even number of amino acids, that later aggregated to form a tubular structure (Figure 2.9.).

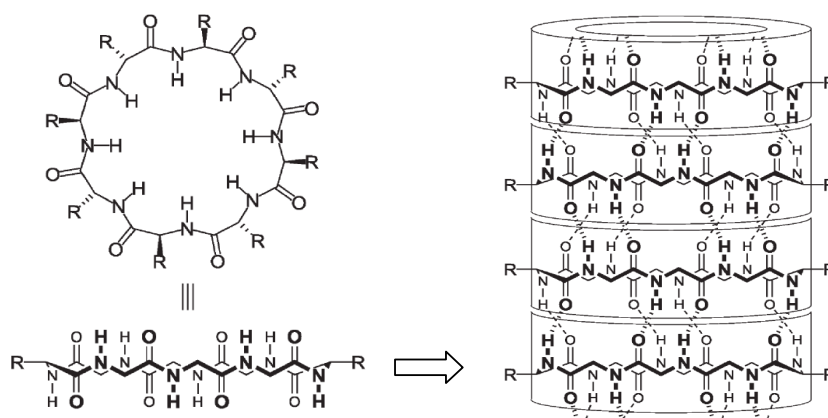


Figure 2.9. *Ghadiri's* self-assembling columnar structures using a cyclic α -peptide with an even number of alternating D- and L-amino acids as building blocks.

The approach is extremely versatile, the internal diameter (to a certain extent) and the properties of the internal as well as external surface can be easily modified by carefully adjusting the number of amino acids in the ring⁴². When the outside chains are kept hydrophobic, the tubular structures can be used to create ionic channels with transport activity for potassium and sodium ions close to that of natural systems. The inside of the tube was also made hydrophobic by incorporating triazole-containing ϵ -amino acids⁴³.

Similarly, a H-bonding-based tubular organizational behaviour has been observed by *Seebach's* group in the case of cyclic tetramers of 3-aminobutanoic acid⁴⁴ and by *Ranganathan et al.* for cystinospirobicyclic peptides⁴⁵. Based on the work of *Seebach, Kimura et al.* constructed through self-assembly a stacked column of cyclic peptides. Three *trans*-2-aminocyclohexylcarboxylic acid (ACHC) units linked in a ring yielded a cyclic tri- β -peptide. The computationally predicted stacking was confirmed through electron crystallography. Rod-shaped crystals were observed using transmission electron microscopy (TEM) (Figure 2.10.). Interestingly, all amide groups in the peptide are in the *trans* positions and thus oriented in the same direction in the generated tubes, resulting in a macrodipole moment of the nanostructure. This property has been suggested as one mechanism by which electron transfer might occur in molecules. Therefore, this type of dipolar nanotubes could find a role in future molecular electronic devices, like a molecular diode⁴⁶.

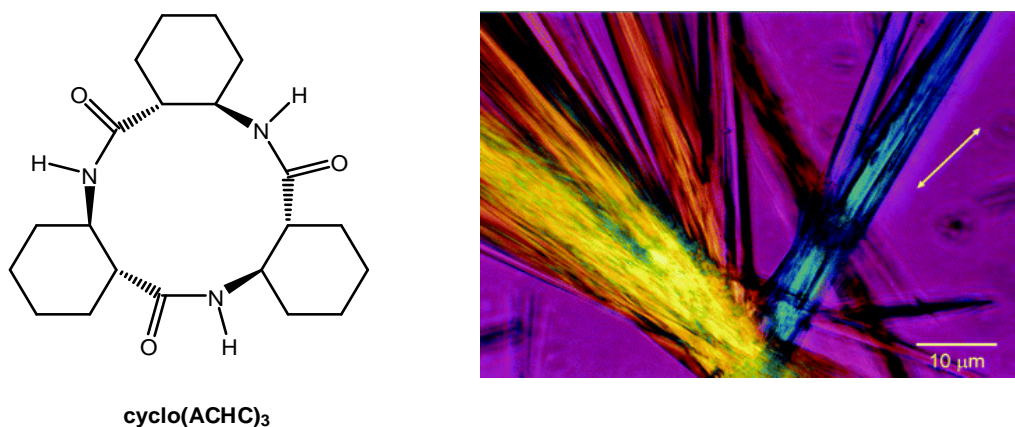


Figure 2.10. *Kimura's* cyclic tri- β -peptide chemical formula (left) and optical microscopic image (right) of crystal nanotubes.

Similar channel-like structures have been obtained from cyclic oligosaccharides. Cyclodextrines (CDs) consist of six or more α -1,4-linked D-glucopyranose rings, resulting in a rigid, well defined bucket-shaped structure (Figure 2.11.).

Cyclodextrines can form inclusion complexes with a wide variety of substrates⁴⁷, the precise nature of the binding interaction has been a subject of debate for a long time, most likely consisting of a sum of several relatively weak forces, like Van der Waals interactions, hydrophobic binding⁴⁸ and even CH/ π hydrogen bonds^{8,49}.

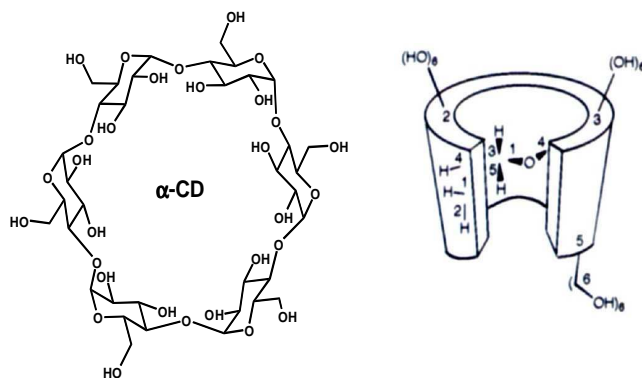


Figure 2.11. Chemical formula (left) and schematic representation of the structure (right, from lit.⁹) of α -CD.

Through self-assembly cyclodextrines generate tubes, in most of the cases including solvent molecules in the inner channel (Figure 2.12.). *Stoddart et al.* described similar tubular channels obtained from 1,4-linked α -D- and α -L-rhamnopyranose residues⁵⁰. The cycles stack in a head-to-tail pattern generating tubular channels with diameters of around 10 Å. An interesting feature of the tubes is that intermolecular H-bonds are not involved in stabilizing individual stacks, but mainly in connecting the adjacent columns.

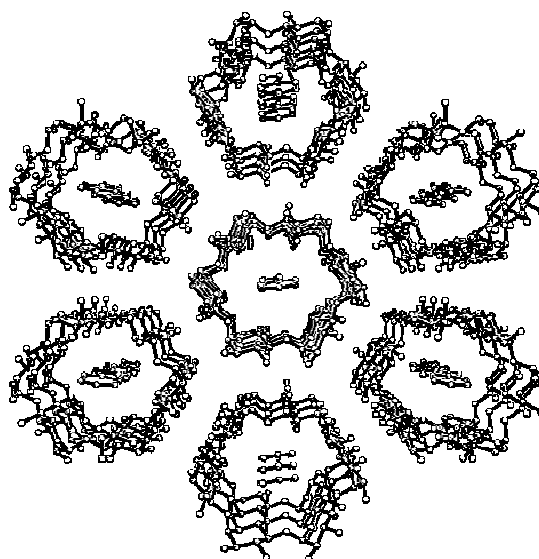


Figure 2.12. Columnar structures based on α -cyclodextrines (from lit.⁵¹)

Furthermore, the ability to form inclusion complexes with guest molecules has been used by researchers for constructing polyrotaxanes. *Harada et al.* synthesized a 20 nm long polyrotaxane and following a cross-linking reaction involving OH groups of adjacent cyclodextrin with epichlorohydrin and then removal of the polymeric thread, obtained a cyclodextrin-based-nanotube⁵² (Figure 2.13.).

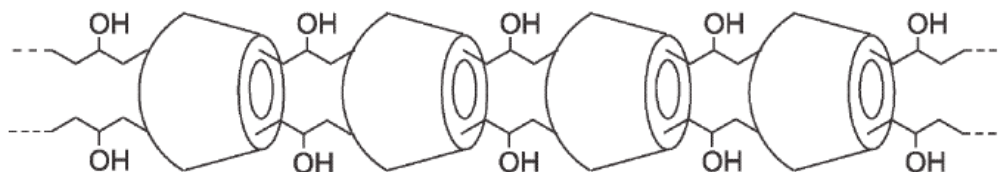


Figure 2.13. *Harada's* α -cyclodextrin-based nanotube.

Similarly, *Liu et al.* prepared tubular dimers from β -cyclodextrine derivatives linked by selenium and platinum complexes⁵³.

2.2.3.2 π - π stackings

Another commonly found interaction that is responsible for channel-like molecular aggregations is the π - π interaction. π - π stacking is certainly a weaker force compared to H-bonding, but nevertheless an important one, especially in systems where H-bonding based structural stabilization is not favourable. There are two types of π - π stacking: *face-to-face* and *edge-to-face* (as pictured in Figure 2.14.), but a wide range of intermediate geometries have been observed, especially in the solid state.

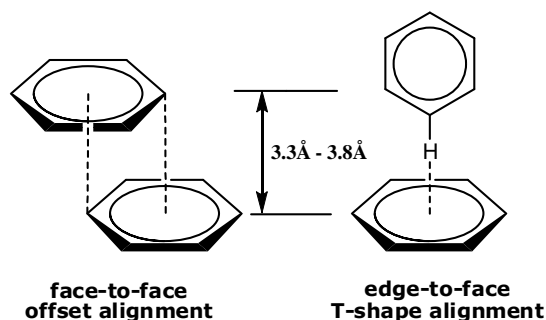


Figure 2.14. The two limiting cases of alignments in π - π stacking interactions.

The *edge-to-face* alignment can be regarded as a weak hydrogen bond between the aromatic ring electron cloud and the slightly electron deficient H atom perpendicular

to it^{54,55}. The *face-to-face* alignment is representative of stacked structures with strong in-plane connectivity and a weak inter-stack connection (see Figure 2.8.B), in molecules containing an aromatic building block. Largely conjugated π -systems like [8]annulene, kekulene or porphyrins show in the solid state a cofacial arrangement with offset centers. Due to the π - π repulsion of the aromatic moieties, the planes tend to shift sidewise. *Sanders* rationalized this behavior through a competitive process⁵⁶. The repulsion between the π electrons forces the planes to slip sideways, but the attraction forces between the electronically poor σ -frame and the electronically rich π -system just barely outweigh the repulsion ones, enough though to generate a channel-like arrangement in solid-state. This model stresses the importance of interactions between individual pairs of atoms, rather than whole molecules. According to this model, extended π -systems like kekulenes are not suited to generate tubular structures, but additional directional non-bonding interactions could easily influence the competitive process, stabilizing the stacking.

The debate on the nature of π - π stacking is far from being finished, with suggestions that London dispersion forces might play a more important role than the electrostatic interactions⁵⁴. However, the electrostatic principle was advantageously used by *Moore* and others⁵⁷ to create not only a foldamer family²⁴, but also a variety of macrocycles and dendritic architectures which generate channels between the macrocycles (Figure 2.15.).

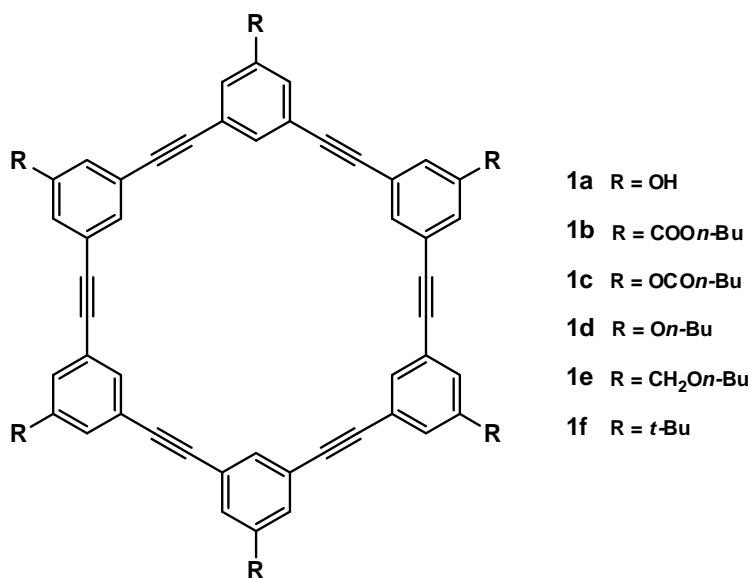


Figure 2.15. Several members of *Moore's* shape-persistent phenylacetylenes⁵⁸

Based on *meta*-connected phenylacetylenes containing peripheral phenolic groups, two-dimensional H-bonded closely packed sheets are formed with two types of holes of about 9 Å in diameter, one due to the macrocycle itself, the other due to the hydrogen bonds. The sheets are aligned in such a way that they build columnar structures, being only slightly

shifted from a symmetrical alignment. Presumably, the concentrated electron-withdrawing effects of the triple bonds and aromatic ring substituents reduce the repulsive π - π interaction, allowing the stacking to be maintained (Figure 2.16.).

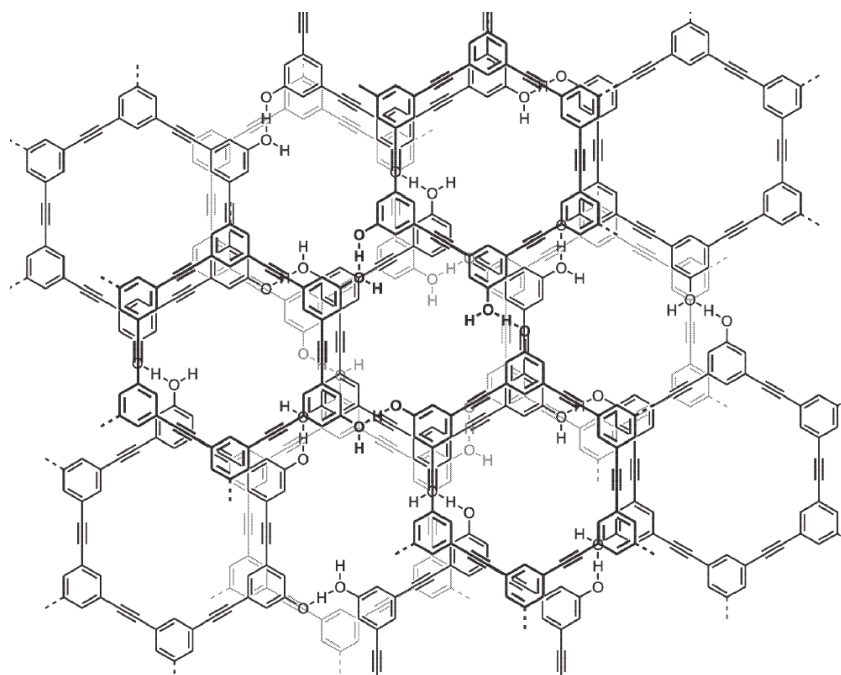


Figure 2.16. Arrangement of **1a** in crystalline lattice forming a mesoporous material⁵⁹.

Solvent-induced conformational changes were observed for similar macrocycles⁶⁰. Recrystallization from a polar solvent resulted in conformations with the interior cavity occupied, leaving only external channels of about 5 Å, while recrystallization from a less polar solvent forced the side chains outwards, generating therefore channels with larger oval inner pores of up to 8 x 12 Å.

2.2.3.3 Van der Waals forces

Further self-assembling directional forces are short interactions between halogen centers⁶¹ and between chalcogen centers⁶². These interactions generate intermolecular X...X contacts slightly shorter (0.1 to 0.4 Å) than the sum of the Van der Waals radii. These interactions have been described as Van der Waals type forces, which usually do not show much directionality, resulting in two- and three-dimensional networks, but no helical or tubular structures were reported until recently.

Desiraju analyzed halogen–halogen interactions in the solid state. Although previously considered as a predominantly non-directional interaction, he revealed that it could be subdivided in two types (I and II) with preferred directionalities (Figure 2.17.)⁶¹. Furthermore, it was shown that for the Cl···Cl interaction a realistic anisotropic model including repulsion, dispersion and electrostatic forces has to be used in order to reasonably describe the non-covalent interactions⁶³.

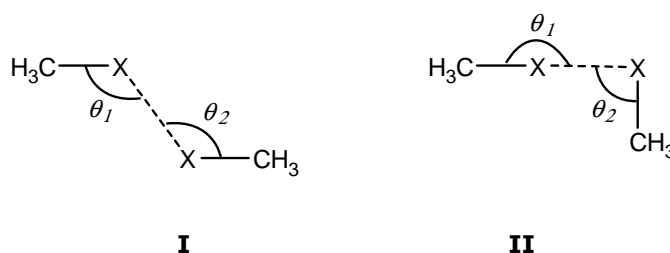


Figure 2.17. *Desiraju's* definition of two types (**I** and **II**) of halogen–halogen interactions based on θ_1 and θ_2 angles.

The directional concept of halogen–halogen interactions was experimentally confirmed by *Morita et al.*⁶⁴ who obtained stacked molecular structures based on interactions between iodide atoms .

2.2.3.4 Chalcogen - chalcogen interactions

The discovery of the superconducting properties of complexes of tetrathiafulvalene (TTF)⁶², revived the interest in investigating solid state structures of chalcogen containing molecules.

Gleiter and coworkers¹ previous studies of cyclic tetrachalcogenadiynes revealed a series of tubular structures in which the rings associate in such a way that one chalcogen center of one ring is involved in a short contact with other chalcogen centers from rings belonging to the neighboring stacks (Figure 2.18.). This type of interaction leads to tubes like the ones shown schematically in Figure 2.8.C, based on a zig-zag arrangement of the chalcogen centers.

Studies demonstrate that the chalcogen–chalcogen interactions are mostly responsible for the build-up of the networks in the solid state. Beside them others interactions such as C-H···S, C-H··· π and π - π stacking contribute to the organized assemblies⁶⁵.

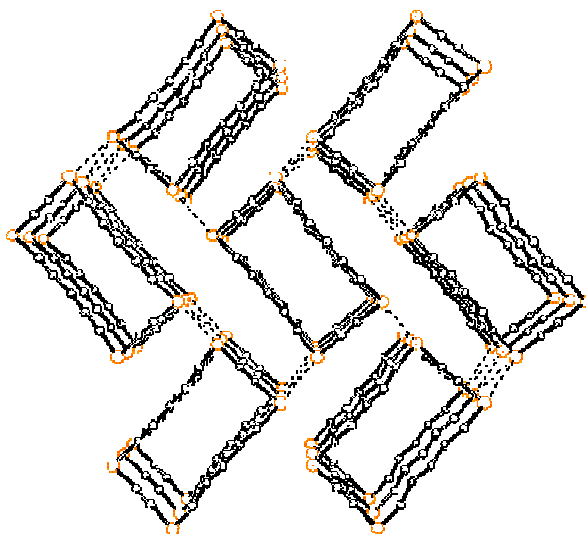


Figure 2.18. Plot of a typical columnar structure generated as a result of self-assembly of cyclic tetraselenadiyne molecules.

Interestingly enough, larger cyclic building blocks containing chalcogen atoms allow the formation of columnar structures with included guests in the inner cavities of the generated tubes⁶⁶. Flexible enough, the rings allow the conformation to be alternated in such a way that even larger solvent molecules can be specifically hosted inside (Figure 2.19.).

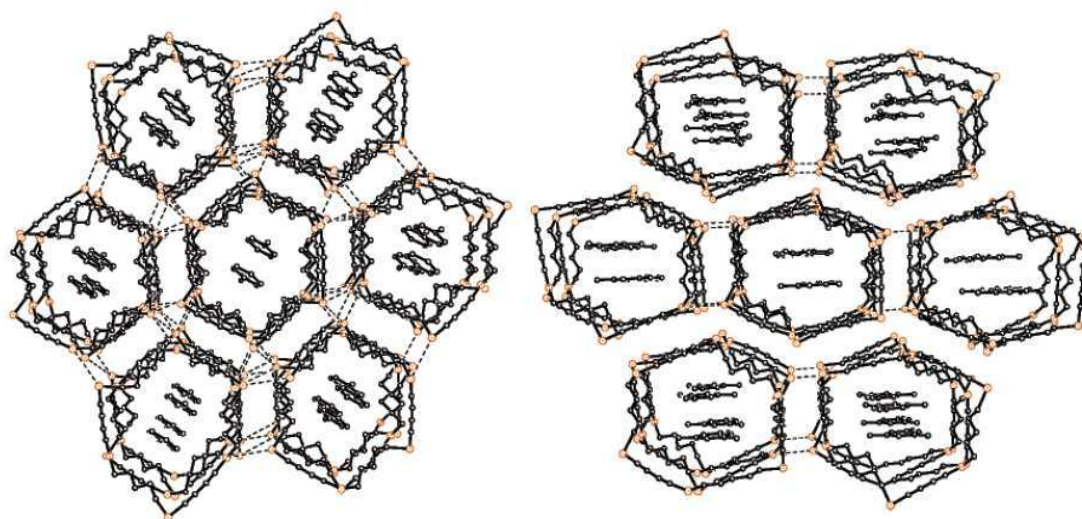


Figure 2.19. Top view of columnar arrangements of a hexaselenacyclohexayne based self-assembling tube with inclusion of toluene (left) and mesitylene (right).

Two main contributions to the chalcogen–chalcogen interactions have been revealed: the isotropic dispersion forces and the interaction between an occupied p-orbital at one chalcogen center (the nucleophilic unit) and an unoccupied X-C(sp) σ^* -orbital of another chalcogen center (the electrophilic unit). The p- σ^* interaction determines the directionality of this type of non-bonding interaction. The concept has been confirmed through recent quantum chemical calculations² and statistical analysis of crystal structures of dimethyldichalcogenides⁶⁷.

Continuing previous interest, the present work is focused on widening the knowledge about chalcogen–chalcogen interactions, especially selenium–selenium interactions with a special interest in predicting and manipulating the non-bonding contacts. This would provide a major impact on material sciences.

3. Experimental part

3.1 Motivations

Following experimental and theoretical interest in chalcogen-chalcogen interactions in our group, we decided to focus our research on selenium containing molecules. We intended to investigate chalcogen-chalcogen interactions in solution using NMR spectroscopy. For this purpose selenium containing molecules were the most suitable, as from all chalcogen elements (O, S, Se, Te), Se has the more advantageous spectral properties (higher magnetic susceptibility, greater magnetically active isotope abundance) in comparison with the known synthetic difficulties (odor, solubility, air and humidity sensitivity).

Selenium has valences 2, 4 and 6 like sulfur and is a third row element in the periodic table. Since selenium can be substituted for sulfur even in biological systems, it is logical to assume that some of the important electronic and chemical properties are similar.

Although selenium is not as common in biological processes as sulfur, it is still an important component of several biological macromolecules such as formate dehydrogenase, glycine reductase, nicotinic acid hydroxylase and glutathione peroxidase (GPX)⁶⁸. Unfortunately, appreciation of the bad odor and toxicity of selenium and selenium containing compounds is more widespread than the appreciation of the essential nature of selenium in many functional proteins. However, it is becoming increasingly evident that there are many enzymes that are selenium dependent and also that selenium is able to substitute sulfur in many biological molecules. For instance, when organisms receive more than micromolar concentrations of selenium, some enzymes begin to substitute sulfur with selenium in many cellular constituents.

Very recent research reported the first case of a naturally occurring Se-Se bond⁶⁹, formed by two selenocysteine residues within the same protein, with an unusual high occurrence in diverse aquatic organisms, including fish, invertebrates, and marine bacteria. The low redox potential of the Se-Se bond suggests that it might play a role in regulation of redox levels in cells, based on similarity with thioredoxins (with known bioactivity, using a reversible disulfide bond to reduce cellular substrates), both having the (seleno)cysteine residues in the active site. Other known selenocysteine-containing proteins tend also to have a cysteine residue, the two amino-acids forming a reversible selenium-sulfur bond.

The mechanism for formation and reduction of the diselenide bond *in vivo* is not completely clear, but chalcogen – chalcogen interactions are thought to have significant importance.

The ability to get involved in non-bonding interactions is considered to be essential for the biological activity of selenium and selenium containing compounds. It was reported that the molecular structure and biological activity of selenazofurin (**2** in Figure 3.1.) and its 5-amino derivative are controlled by intermolecular interactions involving the Se atom^{70,71}. Taking advantage of the Se preference to build intramolecular interactions with oxygen and/or nitrogen atoms in several types of diselenide, several compounds with enzyme-like activity have been synthesized (**3–5** in Figure 3.1.)⁷².

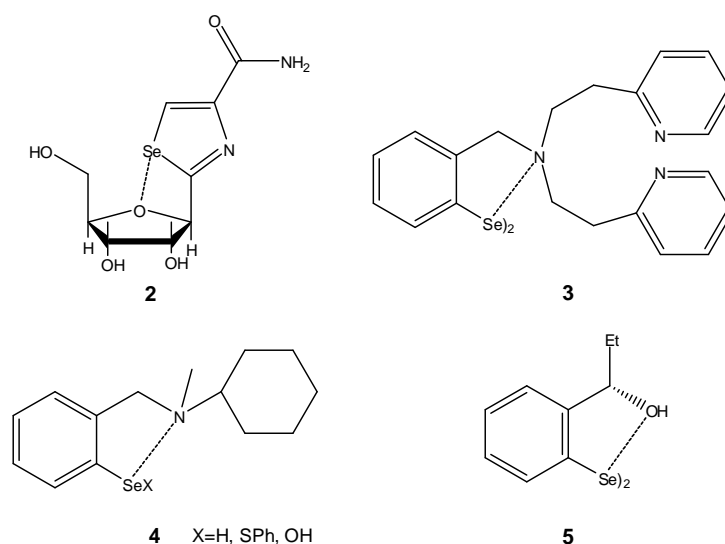


Figure 3.1. Different applications of organoselenium compounds with non-bonding Se centers in biologically active compounds (**2**), enzyme-mimetic compounds (**3**) and in catalysis (**4, 5**).

Not only the biological activity of selenium containing compounds, but also their application in organic synthesis has been proved useful during several decades⁷³. Based on their ambivalence of being able to function as either electrophiles or nucleophiles organoselenium substances have been inserted in other organic molecules, producing compounds which are very useful intermediates in organic synthesis. Preparation of novel optically active organoselenium compounds and their application as chiral ligands to some transition metal catalyzed reactions is a research domain of current interest⁷⁴. Diselenides and selenides having internal tertiary amine groups (**3** and **4** in Figure 3.1.), with significant intramolecular Se...N interactions have been used for catalytic conversion of alkenes into allylic ethers and esters⁷⁵. *Wirth et al.*⁷⁶ demonstrated that high asymmetric induction is

achieved in the oxyselenation reaction of alkenes by use of asymmetric selenium reagents that possess strong intramolecular Se \cdots O interactions.

Furthermore, there has been an increasing interest in Se interactions with the new developments in organic superconducting materials. A full understanding of the type and/or strength of the intermolecular interactions involved is a prerequisite for the intelligent design of superconducting crystals, the final goal of the crystal engineering of molecular materials⁷⁷.

Since the original synthesis of tetrathiafulvalene (TTF) (Figure 3.2.) and its selenium analogue tetraselenafulvalene (TSF) (Figure 3.2.), more than three decades ago⁷⁸ these type of compounds have been at the center of extensive research of electrically conducting materials on account of their unique π -electron-donor properties. With the discovery of the first metallic charge-transfer (CT) TTF complex⁷⁹ and later the discovery of the first organic superconductor, tetramethyltetraselenafulvalene (TMTSF) (Figure 3.2.)⁸⁰, a considerable attention was devoted to finding new TTF/TSF type molecules with superconducting properties. The most advantageous feature of TTF/TSF-type π donor molecules in the design of the organic conductors is in fact that the HOMO (highest occupied molecular orbital) from which the conduction band is formed has a large amplitude and the same sign on every chalcogen atom. Because of the large electron cloud at the S (or Se) atom, intermolecular HOMO-HOMO overlap becomes large. Furthermore, because of the same sign of HOMO on every S (or Se) atom, every intermolecular S \cdots S contact can contribute additively to enhance the intermolecular interaction. According to *Novoa et al.*⁸¹, the S \cdots S interaction is moderately attractive (in the range of -0.35 to -0.60 kcal/mol) and plays an important role in the packing of ionic crystals showing metallic and superconducting properties.

These interactions have been used as a crystal engineering tool for the design of new π -electron donor molecules, combining both Se and S atoms to synthesize bis(ethylene-dithio)tetraselenafulvalene (BETS) (Figure 3.2.) and generating a whole new class of organic metals and superconducting materials with more than 60 organic compounds⁸².

With all the interesting applications where weak interacting selenium centers are of obvious importance, our scope was to try to understand the origin and characteristics of the selenium-selenium interactions. This would allow for controlled design and development of selenium containing reagents for organic and bioorganic synthesis, as well as new materials.

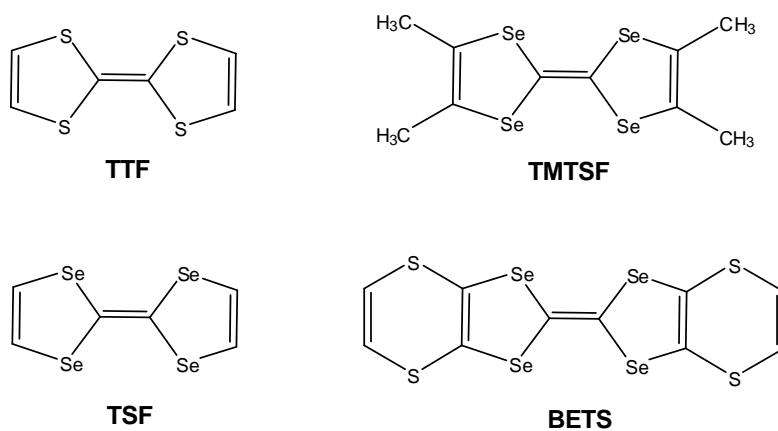


Figure 3.2. Different chalcogen containing compounds with important applications in organic superconducting materials.

In the current work, we approached the understanding of the selenium–selenium interaction both from an experimental point of view and from a theoretical one. Experimentally, we were interested in synthesizing new cyclophane-type compounds containing Se centers and analyzed their structural organization features. For the theoretical scope of this work, firstly a series of model compounds were synthesized, then their properties were compared with results of theoretical studies referring to NMR chemical shifts and conformational analysis.

3.2 Synthesis and structure of new tetraselenadiyne cyclophanes

3.2.1 Introduction

The weak interactions between chalcogen centers are influenced by a combination of factors including steric and electrostatic effects, as well as attractive and repulsive orbital interactions. The stabilizing contributions are stronger for the heavier chalcogens, especially when bonded to electron-withdrawing groups.

Theoretical and experimental studies of the chalcogen-based weak interactions indicate that their binding energies are comparable to those of some hydrogen bonds, therefore it is possible to build supramolecular entities based on organo-chalcogen molecules⁸³.

Although weakly bonding interactions of the chalcogens are observed frequently as intramolecular contacts as described before, there are important examples in the literature of intermolecular association. It was shown that the electric conductivity of sulfur and selenium organic compounds in the solid state is favored by the formation of chalcogen-chalcogen networks, as in the cases of TTF and TSF-like compounds.

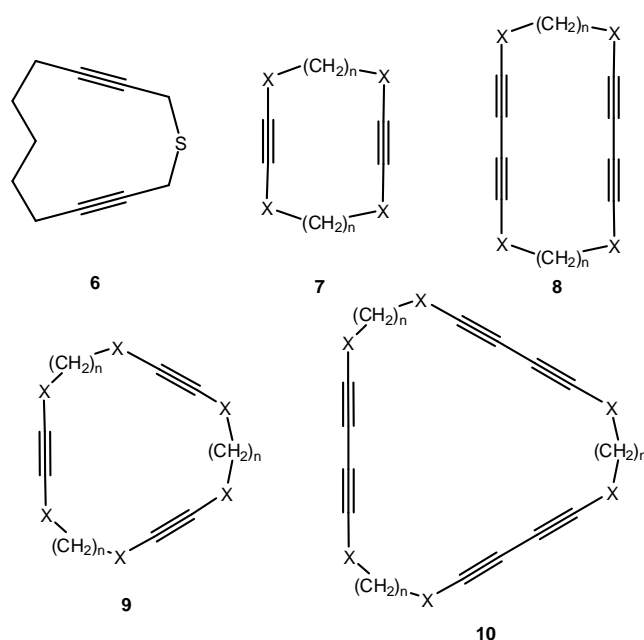
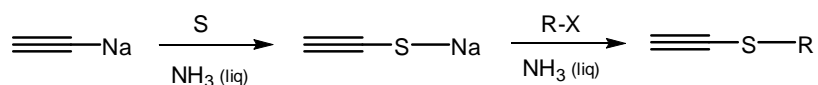


Figure 3.3. Several chalcogen containing cycles (**6** - **10**) with mono- and dialkyne bridges as building blocks.

Previous work in our group on synthesizing electron-rich cyclic polyynes which contain chalcogen atoms generated a series of cyclic polyynes (Figure 3.3.), whose columnar-type solid-state structures are based on short chalcogen–chalcogen contacts. These type of molecules differentiate themselves from the many other cases previously discussed in Chapter 2, as being constructed from flexible (aliphatic) and rigid (alkyne) units. Due to the flexibility of the aliphatic chain, the inside cavity could even modify its shape in order to accommodate guest molecules, such as solvent molecules.

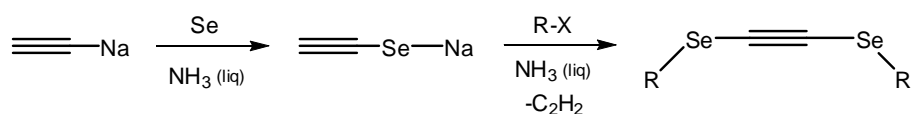
Our goal was to extend the series of electron-rich polyynes studies to systems containing some rather rigid units, like benzene rings and to observe the influence in the solid-state organization of new interactions. We decided to focus on selenium containing cyclic compounds, as the ^{77}Se isotope offered the most favorable NMR properties⁸⁴ in the chalcogene series (natural abundance and receptivity relative to ^{13}C) in our attempt to study the existence of chalcogen-chalcogen interactions also in solutions. Moreover, selenium-containing molecules were considered as early theoretical calculations^{85,86} suggested that the interactions would be stronger than in the case of analogous sulfur containing compounds.

Although sulfur containing alkynes have been already synthesized as early as the 20's⁸⁷ through dehydrohalogenation of convenient dithioethers, analogous compounds containing selenium attracted interest only in the 60's⁸⁸. Based on already developed methods for synthesis of sulfur acetylenes, *Brandsma* tried to synthesize analogous compounds containing selenium instead of sulfur. He used sodium ethynyl, which reacts in liquid ammonia with elemental sulfur to obtain the thiol anion. This nucleophilic agent was reacted with halogenated compounds to obtain substituted thiol acetylene species (Scheme 3.1.).



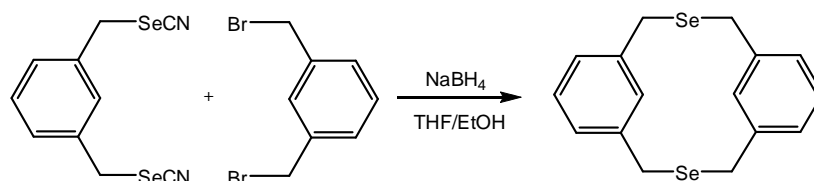
Scheme 3.1. *Brandsma's* synthesis of terminal alkynes containing sulfur atoms.

While using the same procedure with elemental selenium, the desired selena-acetylene could only be observed in small traces. Unexpectedly, the terminal alkyne containing selenium suffered a disproportionation reaction, eliminating acetylene and obtaining for the first time an acetylenediselenaether (Scheme 3.2.).



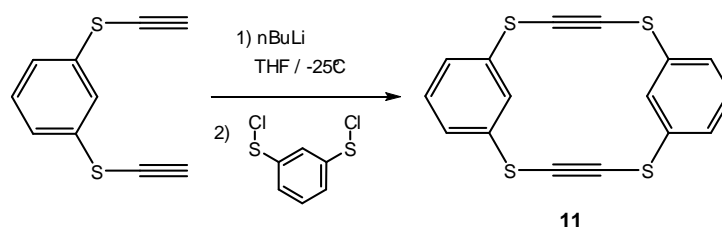
Scheme 3.2. Brandsma's synthesis of the first acetylenediselenoether.

Cyclophanes, as cyclic hosts made by linking aromatic rings, with their rigid geometry and interesting conformational characteristics, are important building blocks in supramolecular chemistry and belong to one of the most interesting and used macrocyclic ligands. Heteraphanes containing nitrogen, oxygen and sulfur have been widely studied⁸⁹. Not so many reports can be found on heteraphanes containing selenium atoms⁹⁰. The first unsubstituted 1,13-diselena[3.3]phane was obtained through coupling of dihalogenides with sodium selenide⁹¹ and the synthesis was later improved by *Misumi*⁹² using a coupling of bis(selenocyanate) with the respective dibromide in the presence of NaBH₄ in a solvent mixture of ethanol and THF (Scheme 3.3.)



Scheme 3.3. Misumi's synthesis of 1,11-diselena[3.3]phane.

In the previously synthesized selenium containing cyclic dialkynes shown in Figure 3.3. the conjugation between the diselenaalkynes units is interrupted through the alkylic chains, therefore the idea to introduce aromatic building blocks was considered as a chance to obtain a possible electronic conjugation.



Scheme 3.4. Synthesis of tetrasulfuridyne [5.5]cyclophane **11**.

Previous attempts to introduce an aromatic building block between the dichalcogenaalkyne bridges as in Scheme 3.4. resulted, however in very low yields of the desired cyclophane and unexpected products, like dibenzotetrathiofulvalene (**12**) and a tris-disulfide bridged cyclophane (**13**)⁸⁵.

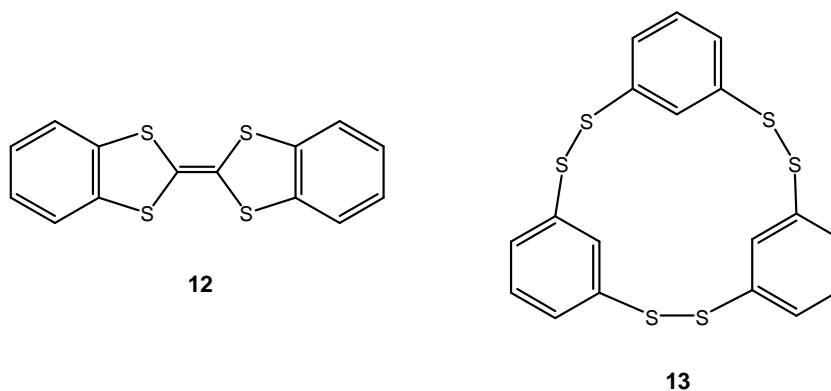
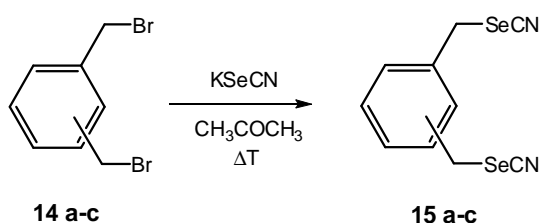


Figure 3.4. Unexpected products obtained at the attempted synthesis of cyclophane **11**.

3.2.2 Synthesis of new cyclophanes

Considering previous attempts of obtaining chalcogen containing cyclophanes, we decided to replace only one part of the methylene chains with benzene rings. Therefore we used xylene derivatives instead of pure aliphatic fragments, for inducing more rigidity in the cycles and also opening the possibility of further stabilization through π - π stackings.

The synthesis of cyclic tetraselenadiynes containing benzene rings as building blocks was based on *Brandsma's* synthesis of acetylenedithioethers⁹³ and protocols already developed in *Gleiter's* group for the synthesis of cyclic tetrathiadiynes by *Benisch*⁹⁴ and *Werz*⁸⁵.

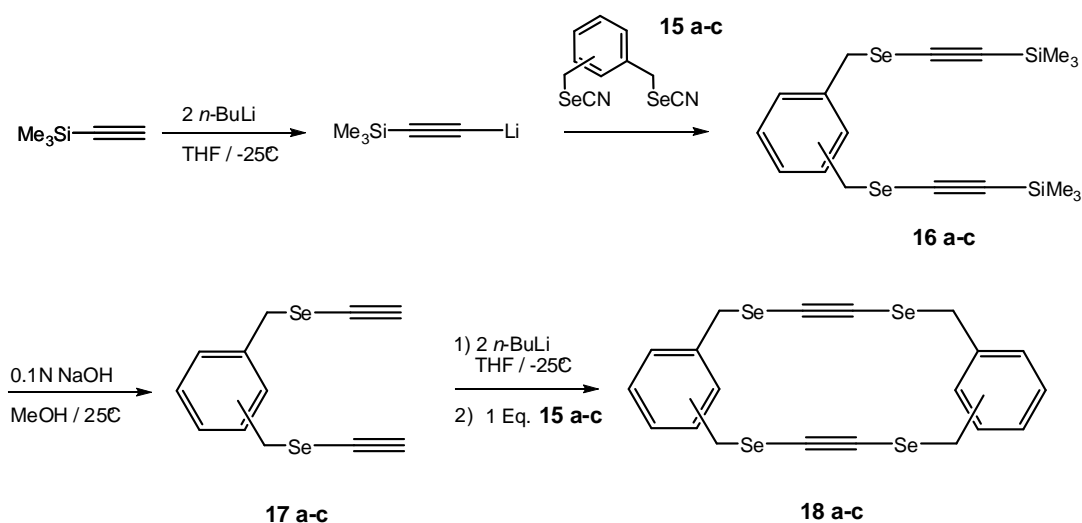


Scheme 3.5. Synthesis of isomeric bis-selenocyanatomethyl benzenes

The alkyne-selenium bond resulted from a reaction between lithiated acetylene derivatives as nucleophilic reagents and positively polarized selenium containing

compounds. Due to their enhanced stability we preferred selenocyanato compounds over selenochlorides or selenobromides. The bis-selenocyanatomethyl-benzenes were synthesized from the respective bis-bromides and potassium selenocyanate reacted in degassed acetone at reflux⁹⁵ (Scheme 3.5).

The reaction of the terminal bis-selenocyanates **15 (a-c)** with lithiated trimethylsilylacetylene in dry THF at -25°C , afforded the protected bis-selenadiynes **16 a-c** with yields between 45 and 66% (Scheme 3.6.).



Scheme 3.6. Step-wise synthesis of cyclic tetraselenadiynes.

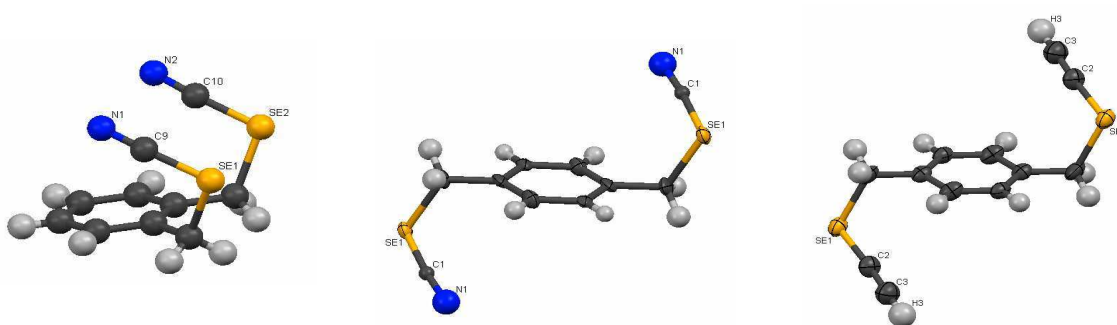
The protecting TMS groups were removed easily using 0.1N solution NaOH in a mixture of solvents consisting of methanol and THF at room temperature, under vigorous stirring for ca. 2 hours⁹⁶. After purification by silica gel column-chromatography the terminal bis-selenadiynes **17 (a-c)** were reacted with 2 equivalents of *n*-butyllithium and then with an equivalent of the corresponding bis-selenocyanato compound **15**. During the coupling reactions low concentration conditions were maintained, in order to avoid unwanted side-reactions. The cyclic tetraselenadiynes **18 (a-c)** were obtained in low yields after purification as pale-yellowish solids, usually crystallizing as tiny needles.

The low yields (see Table 3.1.) in comparison with the methylene chains bridged congeners can be explained by the much lower solubility of the compounds containing aromatic rings. Similar results were obtained in the case of the synthesis of cyclic tetraselenatetraynes containing aromatic rings⁹⁷. Furthermore, usage of long aliphatic chain substituted benzene derivatives, which have better solubility in solvents, led to the orientation of the aliphatic chain towards the interior of the cycle, therefore blocking the formation of the columnar structures.

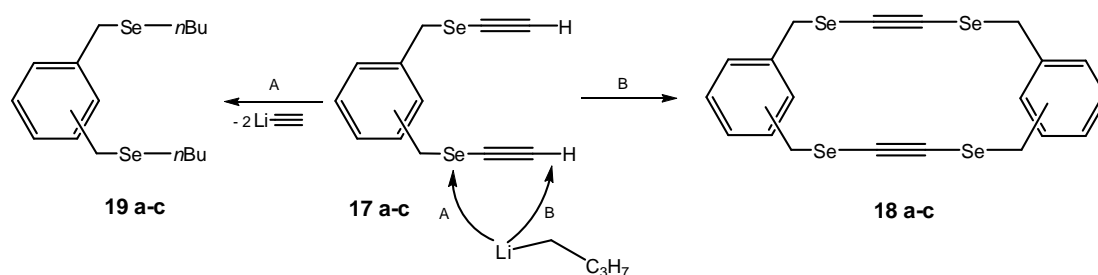
Table 3.1. Overview of reaction conditions and yields for synthesis of cyclic tetraselenadiynophanes **18 (a-c)**.

Compound	Coupling reaction Time	Coupling reaction Temperature [°C]	Concentration [mmol/l]	Yield [%]
18 a	5h	-40	9	3,6
18 b	6h	-45	1.9	< 0.5
18 b	7h	-50	1.8	7,4
18 c	6h	-40	5	< 0.5
18 c	6h	-50	1.25	1,8

Preliminary DFT calculations suggested the *para* isomer as the most stable; therefore we expected better yields for this isomer in comparison with the other two isomers. Surprisingly, the yields for synthesis of the *para* isomer were extremely low, even at the lowest concentrations. A possible explanation followed after the investigation of the precursor compounds' geometries. The solid-state structures for 1,2-bis-(selenocyanatomethyl)-benzene (**15a**) could be obtained from the Cambridge Crystallographic Database (CCDB ref. code: NARBIR)⁹⁸ and it shows that both SeCN groups are on the same side of the benzene rings (see Figure 3.5. left side). We successfully crystallized both 1,4-bis-(selenocyanatomethyl) benzene (**15c**), as well as 1,4-bis-(ethynyl-selenylmethyl) benzene (**17c**) and we observed that in their case the SeCN and SeCCH groups are on opposite sides of the benzene ring (Figure 3.5. middle and right), thus reducing drastically the probability of a simultaneous coupling reaction. Therefore, we assume that this geometrical restrains play an important role in the synthesis of the *para*-isomeric cyclophane.

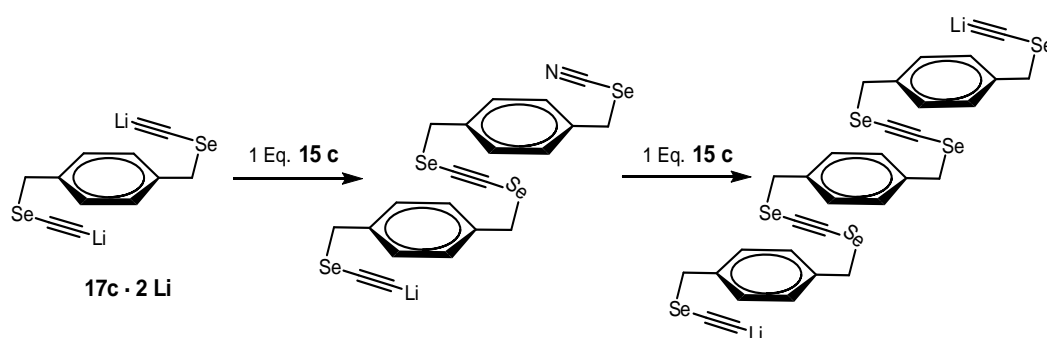
**Figure 3.5.** Solid-state structures of intermediates for the synthesis of the cyclic tetraselenadiynes: left 1,2-bis(selenocyanatomethyl)-benzene (**15a**) from CCDB; middle 1,4-bis-(selenocyanatomethyl)benzene (**15c**); right 1,4-bis-(ethynylselenylmethyl)-benzene (**17c**) (50% ellipsoid probabilities).

Furthermore, the overall low yields are also due to several possible side- and/or secondary reactions. For example, the base *n*-butyllithium present in the reaction flask can attack the precursor terminal alkyne in two ways: A) at the Se center, partially positively polarized and having two pairs of non-bonding electrons or B) at the terminal H, leading to the desired deprotected terminal alkynes (Scheme 3.7.).



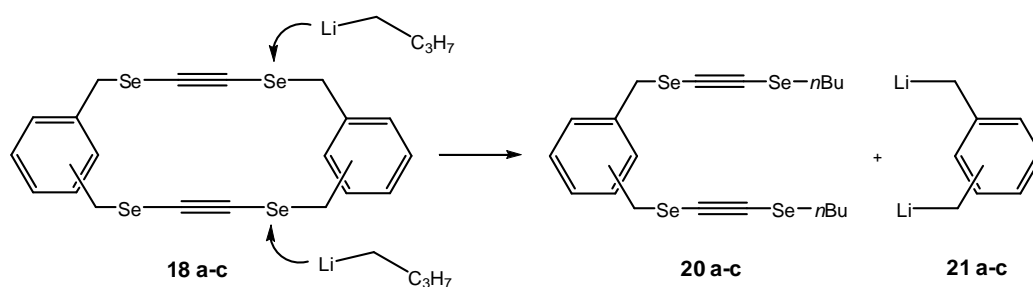
Scheme 3.7. Pathways of attack of the deprotonating agent *n*-BuLi generating the desired product (path B), or unwanted by-products (path A).

Another difficulty in the synthesis is due to the fact that the deprotonated alkynes have to react with only one selenocyanide in order to obtain the desired cycle. If this is not the case, oligomerisation products (Scheme 3.8.) can easily be formed, reducing the yields.



Scheme 3.8. Oligomerization possibilities for the case of coupling reaction generating the *para* isomer **18 c**.

Even worse, traces of unreacted *n*-butyllithium could also attack molecules of the desired product, reducing even more the yields (Scheme 3.9.).



Scheme 3.9. Possible secondary reaction involving the desired tetraselenacyclophanes.

The existence of some of the possible by-products could be confirmed either through mass spectrometric evidence, or through NMR spectroscopic data. In conclusion, the coupling reaction generating the desired cyclic tetraselenides is dependant essentially on the concentrations of the coupling partners and the *n*-butyllithium base. The desired products being themselves only one favored product in a multitude of other possibilities.

Complete spectroscopic characterization of the three desired tetraseleno cyclophanes (**18 a-c**) was possible, although all three isomers are highly sensitive to air, light and humidity. Melting points could not be determined as the compounds **18 a-c** decomposed upon heating in a temperature range from 68 to 78°C. The usual ionization methods for obtaining a high-resolution mass spectrum (Electron Ionization, Fast Atom Bombardment and even the very mild Matrix Assisted Liquid Desorption / Ionization) proved not to be suitable for these type of compounds, only decomposition and fragment peaks could be determined. Only using the Field Desorption Ionization procedure we managed to observe the molecular peaks of the three isomeric compounds and also some of the fragment peaks which differ from one isomer to the others. In Figure 3.6. all three Liquid Injection Field Desorption Ionization (LIFDI) mass spectra of the target compounds are depicted. In Figure 3.7., a comparison of the theoretically calculated isotopic pattern for the molecular formula C₁₆H₂₀Se₄ versus the experimentally observed isotopic distribution patterns is depicted. Based on this comparison and taking in consideration the results of other analytical investigation methods (NMR spectra and X-ray diffraction) we can assume with certitude that we did obtain all the three isomers of the tetraselena-cyclophanes in pure form.

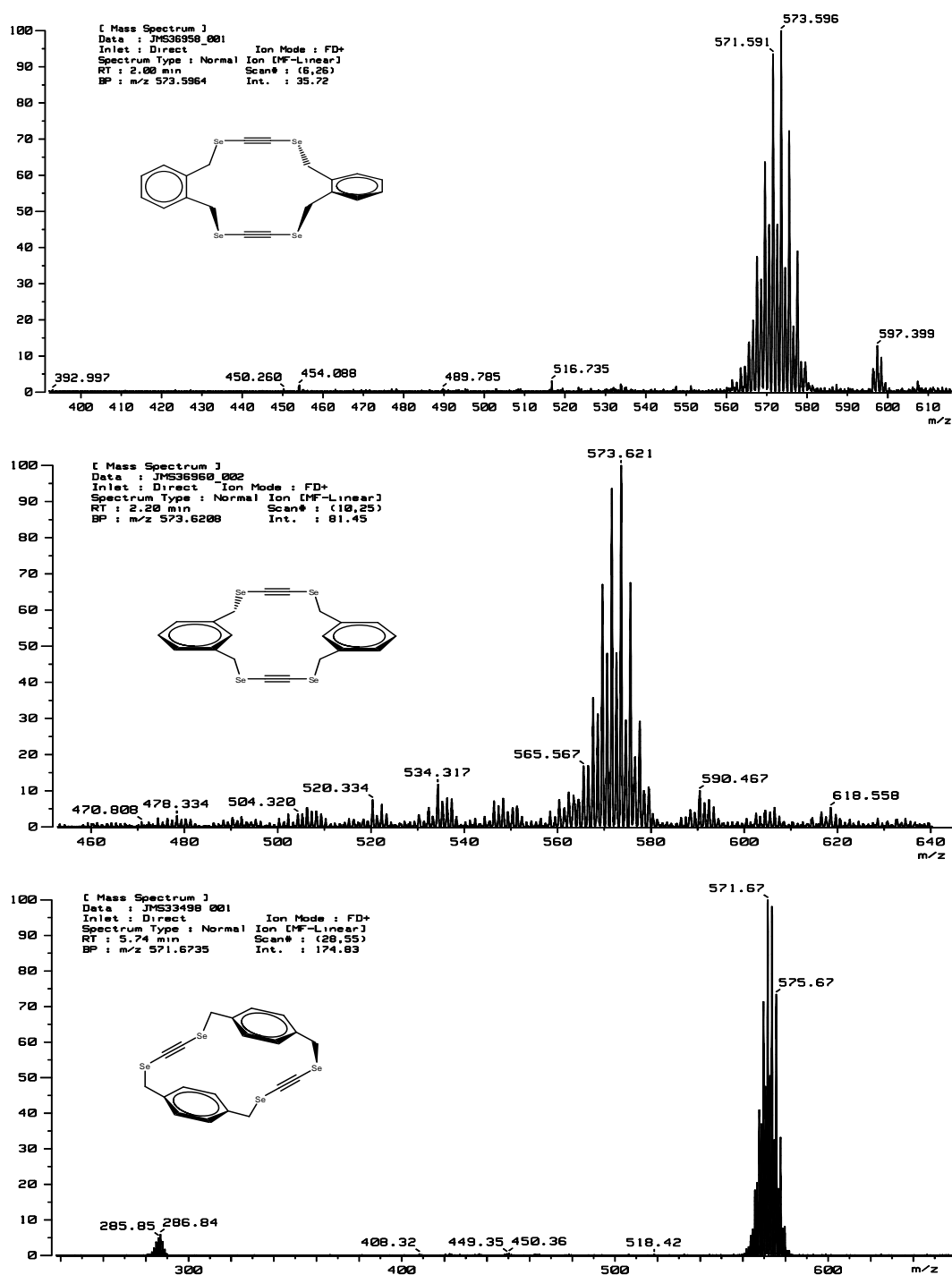


Figure 3.6. Mass spectra (LIFDI ionization method) of the three isomeric selenium containing cyclophanes (**18a** – top; **18b** –middle; **18c**– bottom).

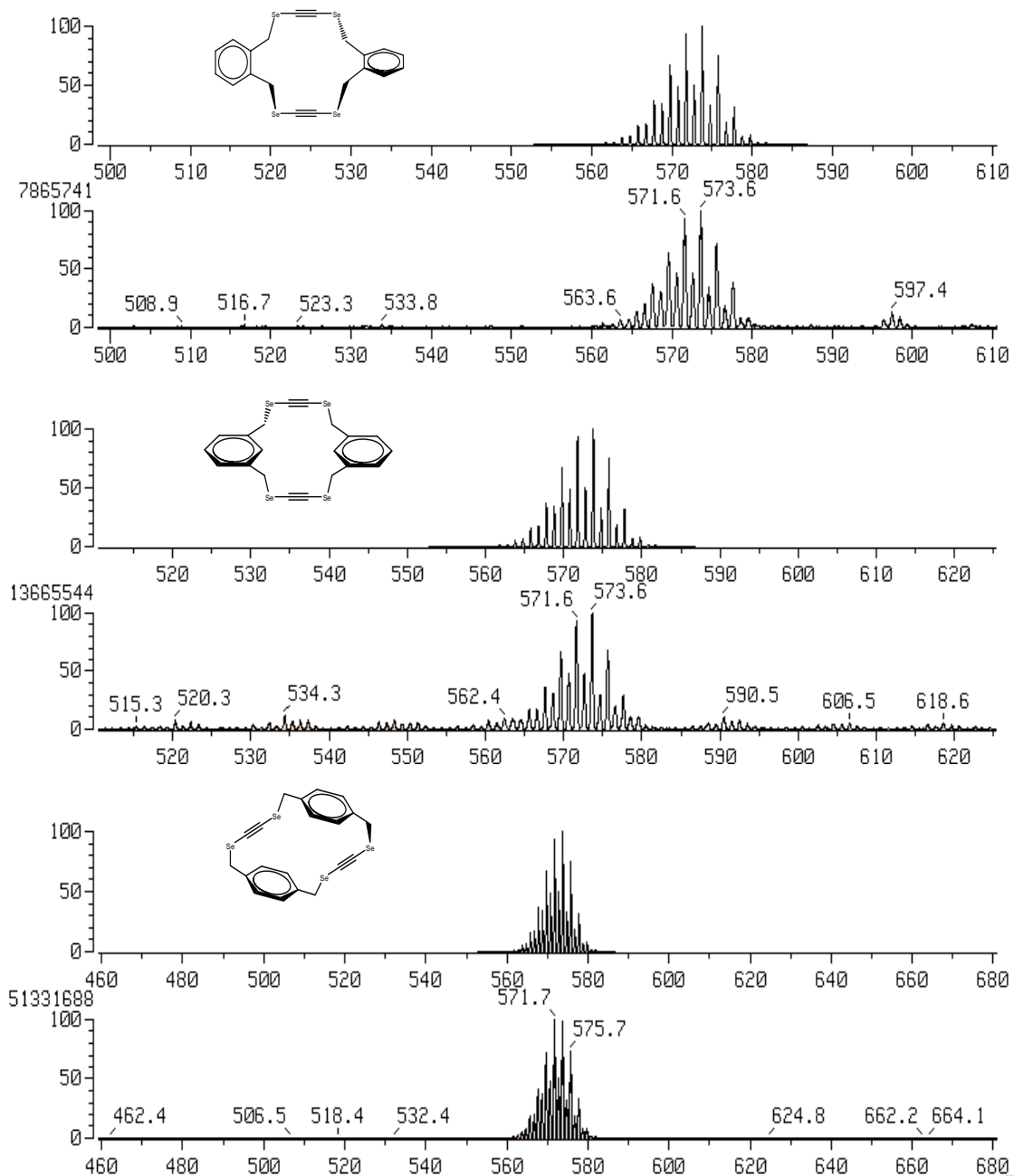


Figure 3.7. Comparison of theoretically calculated (upper) and experimentally observed (lower) isotopic distribution patterns for the three isomeric selenium containing cyclophanes (**18a** – top; **18b** –middle; **18c** - bottom).

3.2.3 Structural investigations

3.2.3.1 Solid state structures

All isomeric cyclic tetraselenadiynes were crystallized from a mixture of *n*-hexane / dichloromethane at room temperature. Usually needle-like single crystals were obtained. In Figure 3.8., the most important bonding angles and torsional angles for the following discussion are defined.

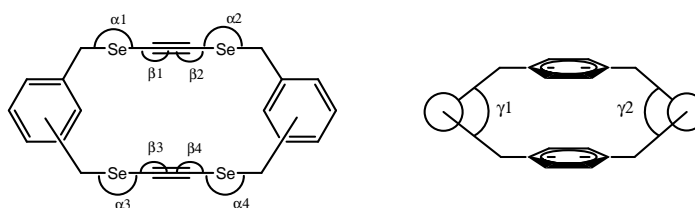


Figure 3.8. Definition of the bonding angles α_1 - α_4 at selenium and the bonding angles at the *sp*-type C atoms β_1 - β_4 , as well as torsion angles γ_1 and γ_2

3.2.3.2 2,5,14,17-Tetraselena[6.6]-*ortho*-cyclophan-3,15-diyne (**18a**)

Single crystals suitable for X-ray diffraction studies of **18a** were obtained from a solution of *n*-hexane / dichloromethane at 20°C. The most striking features of the molecular structure of **18a** (Figure 3.9.) are the twisting of the planes of the two benzene rings by 87° along the common axis and the differences in the bending of the two Se-C≡C-Se units.

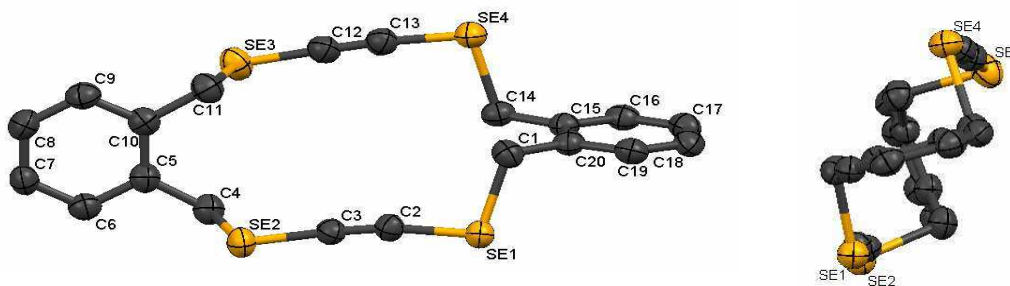


Figure 3.9. Molecular structure of compound **18a** in the solid state (50% ellipsoid probability, hydrogen atoms are not displayed)

The twisting of the two benzene rings we ascribe to the fact that the torsion angles γ of the two $\text{CH}_2\text{-Se}$ bonds⁹⁹ of each $\text{CH}_2\text{-Se-C}\equiv\text{C-Se-CH}_2$ unit in a cyclic system tries to adopt values between 60° and 90° , depending on the size of the ring⁹⁹. In the case of **18a**, γ amounts to 75° (C1-Se1-Se2-C4) and 92° (C11-Se3-Se4-C14).

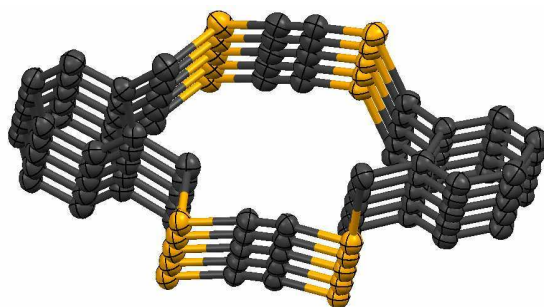


Figure 3.10. Plot of a columnar structure of **18a** in the solid state.

Figure 3.10. presents a section of the columnar structure, which arises in the solid state by stacking the rings on top of each other. A remarkable feature of the structure of **18a** is that only one $\text{Se-C}\equiv\text{C-Se}$ unit of each ring is involved in the stronger intermolecular bonding. This gives the impression that the various rings are threaded like pearls on a string made of $\cdots\text{Se-C}\equiv\text{C-Se}\cdots\text{Se-C}\equiv\text{C-Se}\cdots$ units (Figure 3.11.).

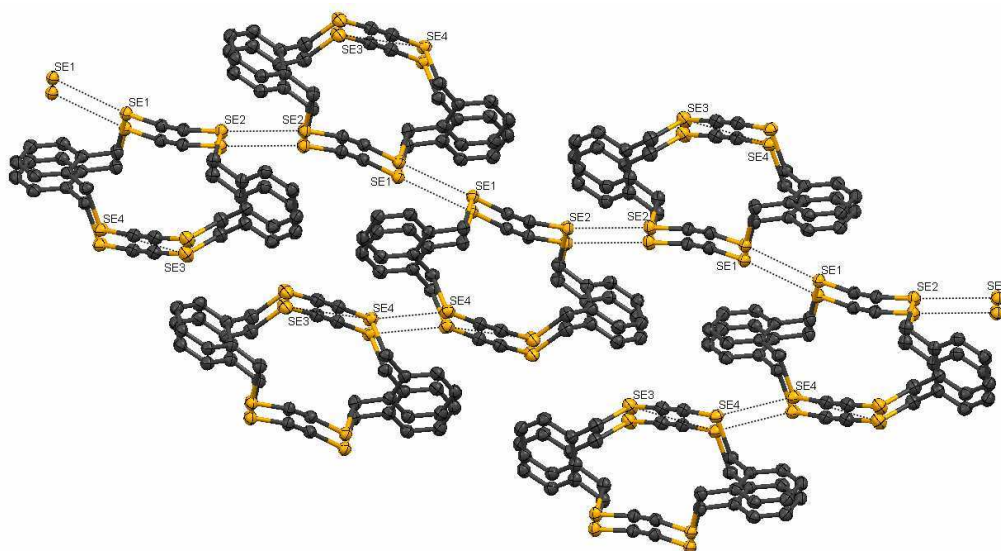


Figure 3.11. Threaded arrangement in the solid state structure of compound **18a** (50% ellipsoid probability; hydrogen atoms not displayed). Dotted lines represent different Se-Se interactions (Se1-Se1= 3.476 Å, Se2-Se2= 3.523 Å, Se4-Se4=3.934 Å).

To optimize the Se...Se interaction, the angles at the *sp* centers have been altered. Those units that are involved in the string formation show a stronger bending (167.1° and 168.7°) than those angles of the *sp* centers of the Se-C≡C-Se units which are not a member of the intermolecular thread (176.2° and 178.2°). The inter-ring distances between the Se atoms are 348 pm and 352 pm, both values being considerably smaller than the sum of the Van-der-Waals radii for Se (380 pm)¹⁰⁰. Parallel strings are interconnected through weaker Se...Se interactions (Se4-Se4=393 pm) in the crystallographic *a*-direction. It is remarkable that the C(*sp*³)-Se-C(*sp*) angles amount to 102.1° (Se1) and 102.6° (Se2) for the selenium atoms involved into the short Se...Se contacts, whereas this angle for the selenium atoms with the weaker interaction is much smaller, 99.1° (Se3) and 98.1° (Se4) respectively.

Selenium-selenium interactions are not the sole interactions responsible for the solid state characteristics of **18a**. All four Se atoms are involved also in selenium-hydrogen intra- and intermolecular interactions. Interestingly enough, when analyzing intramolecular Se-H interactions (see Table 3.2.), it can be observed that the two longest interactions (Se1-H14A=305 pm and Se2-H11A=306 pm) involve the Se atoms that build the strongest Se...Se interaction, while the shortest two interactions (Se3-H4A=283 pm and Se4-H1A=296 pm) relate to Se centers involved in the weakest Se...Se interaction. This behavior can be seen as an added proof of the competition between selenium-selenium and selenium-hydrogen interactions, as it will be discussed later in Chapter 3.3.4.

Table 3.2. Most relevant short intra- and intermolecular selenium-hydrogen contacts (in pm) of **18a** (Se_x-H_z).

	Intramolecular	Intermolecular	
Se _x	H _z (distance)	H _z (distance)	
Se ₁	H14A (305)	H'1B (330)	H'19 (328)
Se ₂	H11A (306)	H''4B (318)	H''6 (310)
Se ₃	H4A (296)	-	-
Se ₄	H1A (283)	-	-

Furthermore, intermolecular Se-H interactions also help in stabilizing the columnar structure, as Se centers are involved in weak bonding with H atoms belonging to molecules situated either under or on top in the molecular column (see Table 3.2.).

3.2.3.3 2,5,14,17-Tetraselena[6,6]-meta-cyclophan-3,15-diyne (**18b**)

In Figure 3.12. the solid-state structure of compound **18b** is depicted and it can be observed that the molecule shows an anti-chair conformation with C_{2h} symmetry.

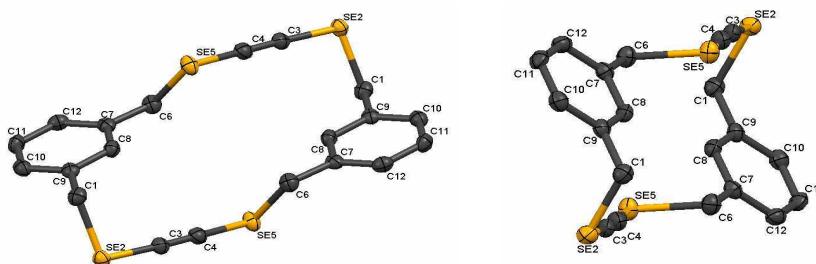


Figure 3.12. Molecular structure of compound **18b** in the solid state (50% ellipsoid probability, hydrogen atoms are not displayed)

Both aromatic rings are parallel and the torsion angle γ of the two $\text{CH}_2\text{-Se}$ bonds along the $\text{CH}_2\text{-Se-C}\equiv\text{C-Se-CH}_2$ unit amounts to -58.2° , while the $\text{C}(sp^3)\text{-Se-C}(sp)$ angles amount to 98° . We notice in the crystal a stacking of the rings on top of each other in the crystallographic b -direction. The $\text{Se}\cdots\text{Se}$ interactions within one stack are rather long (> 436 pm), but inter-stacks Se-Se contacts are relatively strong, amounting for about 397 pm (Figure 3.13.). This value is similar to those found in related systems⁹⁹ and close to

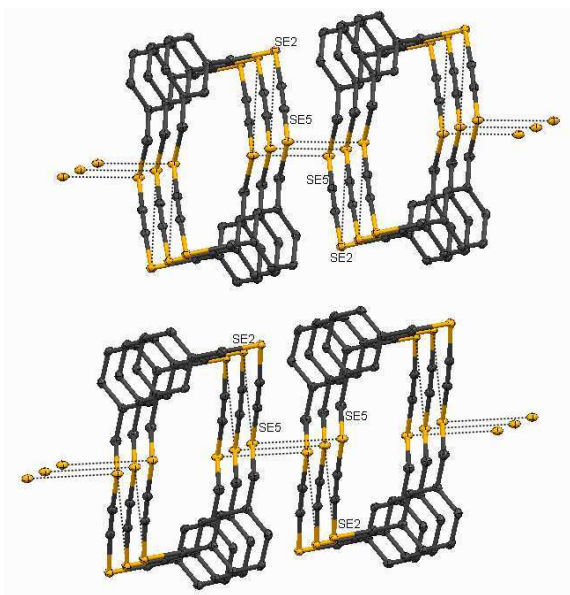


Figure 3.13. Columnar structure of compound **18b** in the solid state (50% ellipsoid probability, hydrogen atoms are not displayed for sake of clarity). Dotted lines represent selenium-selenium interactions in the structure ($\text{Se5-Se5}=3.975$ Å; $\text{Se5-Se2}=4.363$ Å)

close to the values computed for a Van-der-Waals dimer consisting of two dimethylselenide units².

Therefore, it was reasonable to assume that the columnar structure is based on a mixture of Se-Se interactions, weak Se-H as well as CH/ π interactions. A closer look at the crystal structure of **18b**, revealed a network of Se-H interactions varying from 295 pm (intramolecular) to up to 320 pm (intermolecular), representing the so called weak hydrogen bonds^{7,8} (see Figure 3.14.).

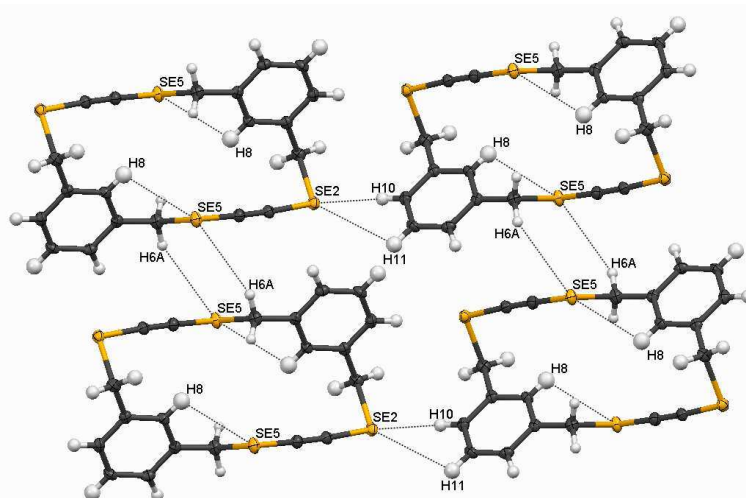


Figure 3.14. Plot of inter- and intramolecular Se-H interactions in the solid state structure of compound **18b** (50% ellipsoid probability). Dotted lines illustrate the Se-H interactions (SE5-H8=2.948 Å; SE5-H6A=3.200 Å; SE2-H10=3.194 Å, SE2-H11=3.161 Å).

Furthermore, CH/ π interactions between the benzylic proton and the C(sp)-C(sp) unit from a molecule situated in the same stacks, with distances of 274 pm are also involved in generating the stacks. Similar interactions have been observed in the case of **18a**, with even smaller distances of around 264 pm. π - π stacking contributes, although to a smaller extent, to the stabilization of the stacked structure. The distance between two benzene planes amounts to 352 nm, (comparable with the 350 nm distances between planes in graphite and pyrene¹⁰¹) with the benzene rings in an offset arrangement (as in Figure 2.14.) in which the benzylic CH₂ is situated right under one benzene ring from the upper molecule in stack. These interactions illustrate both the competitive relation between non-bonding weak interactions and also their complementary action that helps keep up a supramolecular structure.

3.2.3.4 2,5,14,17-Tetraselena[6,6]-*para*-cyclophan-3,15-diyne (**18c**)

The *para* isomer, compound **18c**, also adopts a chair conformation (non-crystallographic C_{2h}) in the solid state as does **18b**. The planes of the two aromatic rings are symmetry imposed parallel. The torsion angles between the $\text{CH}_2\text{-Se}$ bonds along the $\text{CH}_2\text{-Se-C}\equiv\text{C-Se-CH}_2$ unit axes amount to 116.7° (Figure 3.15.).

This value is considerably larger than those values found for **18a** and **18b** indicating some strain energy due to the *para*-connection. The $\text{C}(sp^3)\text{-Se-C}(sp)$ angles in **18c** were recorded to be 97.1° and 99.7° , respectively.

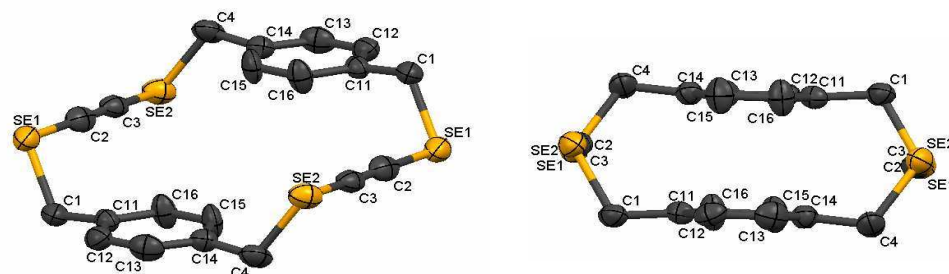


Figure 3.15. Molecular structure of compound **18c** in the solid state (50% ellipsoid probability, hydrogen atoms are not displayed).

In the solid state each selenium atom of **18c** is involved in three short contacts (379, 380 and 381 pm) with selenium atoms of three different neighboring molecules, giving rise to a structure with two-dimensional Se regions showing multiply linked selenium networks. The smallest $\text{Se}\cdots\text{Se}$ interactions (379 pm) are the main forces that generate a sheet-like arrangement in the crystallographic *c*-direction, consisting of intercalating stair-arrangements as depicted in Figure 3.16.A. The sheets have a thickness of about 530 pm and they are closely packed one with the others due to the marginally larger $\text{Se}\cdots\text{Se}$ interactions (see Figure 3.16.D).

Once again, the selenium-selenium interactions are not strong enough to be the sole forces involved in the solid-state structure of **18c**. Selenium – hydrogen weak bondings, along with $\pi\text{-}\pi$ interactions provide a significant contribution to the supramolecular structure. Like in the case of **18b**, the distances between two benzene ring planes in the solid structure of **18c**, amount to 359 pm, also with an offset arrangement of the benzene rings. The selenium atoms do not have identical behavior as far as the weak selenium-hydrogen interaction is concerned. One selenium center (Se1) has only one weak Se-H

interaction amounting to 315 pm with an aromatic proton, while the other (Se2) has two weak Se-H interactions with benzylic protons from neighboring molecules, amounting to 314 and 320 pm, respectively.

Another interesting observation is that in **18a**, the -Se-C_{sp}-C_{sp}-Se- unit is the most compact, with slightly smaller Se-C and C≡C bond lengths than the respective averages and also the -Se-C_{sp}-C_{sp}-Se- unit with the strongest intermolecular Se-Se contacts.

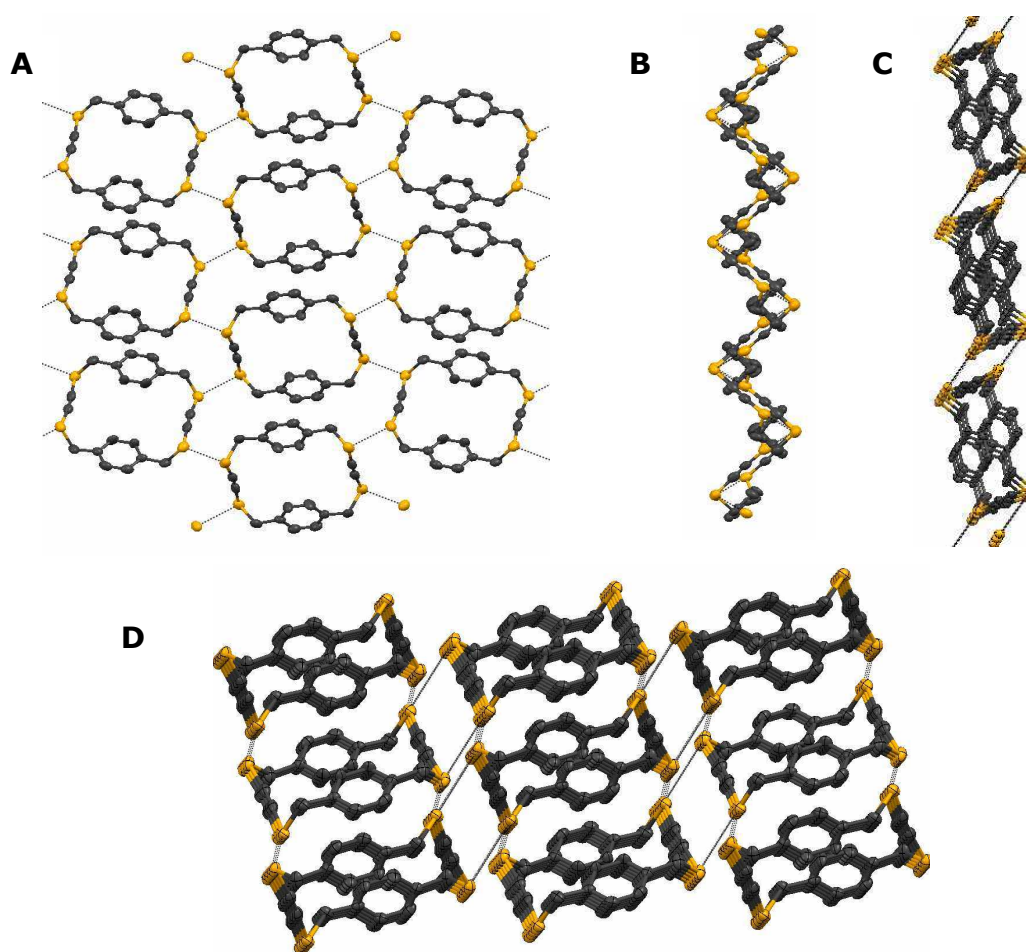


Figure 3.16. Sheet-like arrangement of compound **18c** in the solid state structure (50% ellipsoid probability, H atoms are not displayed). **A.** Front view of the sheet. Dotted lines represent the smallest observed Se-Se contacts (3.79 Å); **B.** Side view; **C.** Top view of one sheet with the internal Se-Se contacts; **D.** Top view of several sheets closely packed together. Dotted lines represent the larger Se-Se contacts (3.80 and 3.81 Å).

In order to establish if there is a preference of orientation in the Se...Se interactions, the interatomic contacts were analyzed using the spherical polar coordinates, θ and ψ , where θ

is the azimuthal angle and ψ , the elevation angle, specifying the direction of the Se...Se contact with reference to the selenide plane C(sp³)-Se-C(sp), as depicted in Figure 3.17.

Early studies on the directionality of interactions involving chalcogenes had been done already before the Cambridge Crystallographic Database¹⁰² was generally available, suggesting that functional groups involved in non-bonding contacts with sulfur atoms, show a preference of their location depending on their (partial) charges¹⁰³.

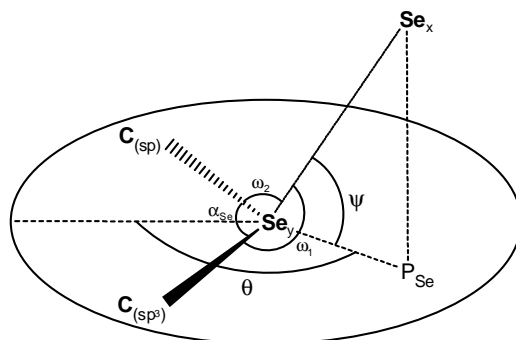


Figure 3.17. Definition of azimuthal (θ) and elevation (ψ) angles

Electrophiles tend to approach in a direction of elevation angle ψ between 50° to 90° to the sulfide plane (the X-S-Y plane, when usually X and Y are carbon atoms), while nucleophiles approach the sulfur within 30° of the sulfide plane. The study was further extended to S...S contacts¹⁰⁴ and the analysis showed that if one sulfur atom acts as an electrophile, it approaches the other which behaves as a nucleophile. Another study of protein structures in the Protein Data Bank (PDB) database¹⁰⁵ showed that metal ions approach the sulfur of methionine fragments at around 62° to the C-S-C group¹⁰⁶ a value very similar to small-molecule crystal structures, where electrophiles are presumed to interact with the sulfur lone-pair orbital.

Furthermore, an extension of the study on selenium interactions observed similarity in the directionality preference of electrophiles and nucleophiles approach at divalent selenium centers, with average ψ values of 68° for electrophiles and 11° for nucleophiles, respectively¹⁰⁷. Also, evidence of incipient formation of attractive electrophile-nucleophile interaction in Se-Se contacts are presented. Although, Se...Se interactions closely resemble S...S interactions in crystals, the complementary electrophile nucleophile pairing for Se...Se interactions is much more pronounced than for S...S.

Frontier orbital theory¹⁰⁸ suggests that the electrophiles (electron acceptors) are interacting with the highest occupied molecular orbital (HOMO) of the chalcogen atom, this being a lone-pair orbital nearly perpendicular to the chalcogenide plane. On the other hand, nucleophiles (electron donors) approach the chalcogen atom closely to the chalcogenide

plane, and have the tendency to lie along the extension of one of the C-X (X=S,Se,Te) bonds, the direction predicted for the lowest unoccupied molecular orbital (LUMO).

Table 3.3. Selected intermolecular Se–Se distances, measured and calculated angles for determining directionality of Se⋯Se interactions.

	Contact Se _x -Se _y	Dist. Se⋯Se [Å]	ω_1 [°]	ω_2 [°]	α_{Se} [°]	θ [°]	ψ [°]
ORTHO (18 a)	Se ₁ -Se _{1A}	3.476	99.22	150.05	102.08	150.92	20.90
	Se ₂ -Se _{2A}	3.523	100.51	152.48	102.59	152.17	14.80
	Se ₄ -Se _{4A}	3.934	95.61	158.51	98.12	144.91	16.49
	Se ₃ -Se _{4A}	4.28	130.4	67.91	98.12	72.97	44.85
	Se ₄ -Se _{3A}	4.28	70.84	140.68	99.15	115.39	36.77
META (18 b)	Se ₅ -Se _{5A}	3.975	76.17	76.17	97.95	180.00	68.64
	Se ₅ -Se _{5A}	4.505	120.38	111.39	97.95	188.02	47.96
	Se ₂ -Se _{5A}	4.363	161.69	64.63	97.95	66.51	5.34
	Se ₅ -Se _{2A}	4.363	70.68	59.1	98.02	169.35	49.08
PARA (18 c)	Se ₁ -Se _{2A}	3.792	102.43	149.83	99.66	153.09	20.18
	Se ₂ -Se _{1A}	3.792	78.82	74.38	97.14	171.83	69.29
	Se ₁ -Se _{2A}	3.805	142.79	72.53	99.66	61.81	35.49
	Se ₂ -Se _{1A}	3.805	77.55	153.83	97.14	124.77	25.36
	Se ₁ -Se _{2A}	3.812	77.15	82.47	99.66	192.31	73.72
	Se ₂ -Se _{1A}	3.812	160.84	99.29	97.14	212.00	9.76

We calculated the corresponding azimuthal θ and elevation angles ψ as defined in Figure 3.17. for all intermolecular selenium – selenium contacts observed in the solid-state structures of the three isomeric cyclic tetraselenadiynes. In Table 3.3., the measured distances and the corresponding angles are presented. Contacts that are longer than the sum of the Van der Waals radii were also included, since theoretical calculations of the interaction energy of the Se⋯Se interactions showed that the potential energy curve is a very flat one, with 50% of the maximum stabilization energy still being observed at 4.5 Å². In Figure 3.18., a correlation between the elevation angle ψ and the distance of Se–Se

contact is presented and one can observe that the Se...Se interactions tend to cluster themselves in three regions. The ones involving long contact distances display mostly a preference of interacting at a 45° elevation angle (red circles), while the contacts with significantly short distances, separate in two groups, around $\psi=20^\circ$ (dark blue squares) and $\psi=70^\circ$ (green triangles) showing that the Se...Se interactions have a preferential directionality.

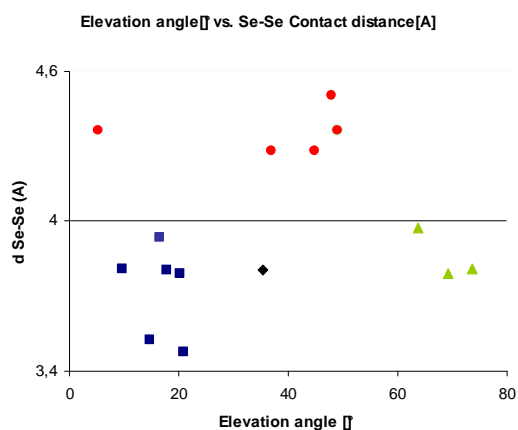


Figure 3.18. Plot of elevation angles against distances of the Se–Se contacts.

These observations confirm the non-spherical shape of the Se atom¹⁰⁹ and that Se–Se contacts are more than just simple Van der Waals forces, which do not show much directionality, as already theoretically predicted by previous investigations².

3.2.3.5 NMR investigations of compounds **18 a - c**

A single signal was observed for ⁷⁷Se chemical shifts in all three cyclophanes, indicating the equivalency of the selenium atoms in the compounds when in solution. An interesting phenomenon was observed for the chemical shifts of the selenium atoms. The chemical shifts move downfield in the series *ortho* < *meta* < *para* indicating an increase in the cavity of the cycle, or at least a less crowded one. This is evident in comparing the *meta* and the *para* compounds, where the cavity size is not significantly different, but due to the two aromatic protons the cavity is more crowded in the case of the *meta* isomer.

Table 3.4. ⁷⁷Se chemical shifts of the isomeric tetraselenacyclophanes

	ORTHO (18a)	META (18b)	PARA (18c)
⁷⁷ Se (δ, ppm)	235.0	288.5	299.8

The same pattern could be observed not only in the three cyclophanes, but also in the precursor compounds **16 a-c** and **17 a-c**. These findings seem to confirm the observations made for the solid-state for compounds **15a** and **15c**. It can be assumed that in solution, in the *ortho* type compounds the SeCN or SeCCH groups are on the same side of the aromatic plane, whereas in the case of the *para* type compounds, they find themselves on opposite sides. For the *meta* type compounds, the ^{77}Se chemical shifts suggest that the distance between the selenium containing groups is significantly larger than for the *ortho* type compounds and more similar to the *para* type compounds.

The NMR spectra of **18 a** in deuterated dichloromethane show only one signal for the four selenium atoms, one for the four CH_2 carbon atoms and even a broad singlet for the four aromatic protons instead of the expected AA'BB' pattern specific of *ortho* identically bis-substituted benzene rings. The spectra are almost unchanged during a variable temperature NMR measurement between -80°C and room temperature indicating C_2 symmetry due to very rapid motion.

Table 3.5. Selected ^1H , ^{13}C , ^{77}Se chemical shifts (ppm), $^2J_{\text{Se,H}}$ coupling constants (Hz) and some $^1J_{\text{Se,C}}$ coupling constants (in brackets) (Spectra were measured in CD_2Cl_2 unless otherwise stated).

Compound	$^1\text{H CH}_2$	$^2J_{\text{Se,H (CH}_2)}$	$^{13}\text{C} - \text{SeCH}_2$	$^{13}\text{C} - \text{SeC}_{\text{sp}}$	^{77}Se
15 a	4.63	15.0 Hz	29.89 (48.5 Hz)	101.52	302.30 ^a
15 b	4.29	16.2 Hz	32.56 (48.9 Hz)	101.83	294.55
15 c	4.44	16.3 Hz	32.53	101.81	307.10 ^a
16 a	4.21	13.9 Hz	30.30 (53.4 Hz)	86.40	255.00
16 b	4.00	15.4 Hz	32.97	86.60	267.64
16 c	4.01	15.4 Hz	32.83 (52.9 Hz)	86.73	269.13
17 a	4.21	13.1 Hz	29.90 (51.8 Hz)	90.40 (37.9 Hz)	232.12
17 b	4.04	14.9 Hz	32.14 (52.9 Hz)	90.02 (37.9 Hz)	246.44
17 c	4.04	14.2 Hz	32.34	90.22	247.79
18 a	4.47	7.9 Hz	33.05	85.92	235.04
18 b	3.93	17.4 Hz	33.92	85.66	288.52
18 c	3.89	20.3 Hz	33.32	84.37	299.81

^a - due to solubility issues the spectra were measured in deuterated acetone.

The chemical shifts of the methylene carbons and protons are almost not influenced by formation of the cyclophanes in the cases of **18 b** and **18 c**, a small deshielding (less than 1 ppm for ^{13}C and 0.15 ppm for ^1H) being observed in comparison with the corresponding terminal alkynes (**17 b** and **c**). In the case of **18 a**, the deshielding of the ^{13}C chemical shift in comparison with **17 a** is more significant, accounting to about 3 ppm, while in the case of benzylic protons a shielding effect of about 0.24 ppm is observed.

The values of $^2J_{\text{Se,H}}$ are in the range of 13 to 20 Hz, again with the exception of the CH_2 protons of compound **18 a**, with a lower value of about 8 Hz. Due to solubility and sensitivity reasons, only a few $^1J_{\text{Se,c}}$ could be determined, ranging from 48 to 53 Hz, without determining the sign of the coupling constant. According to *McFarlane et al.* $^1J_{\text{Se,c}}$ values larger than 45 Hz are indicative of a direct $\text{C}(sp^3)\text{-Se}$ bond¹¹⁰. Surprisingly small $^1J_{\text{Se,c}}$ values (around 38 Hz) were observed in the case of the $\text{C}(sp)$ atoms in **17 a** and **17 b**, usually $^1J_{\text{Csp-Se}}$ being known to be in the -184 to -193 Hz range^{111,112}. More detailed interpretations of the values for $^2J_{\text{Se,H}}$ or $^1J_{\text{Se,c}}$ are difficult.

In conclusion, we observed that by using benzene rings helps in stabilizing the bridge between the diselenaalkyne units, but doesn't necessary reduce the internal motion of the molecules in the solution state, as it could be observed from low temperature NMR experiments of **18 a**. Nevertheless, the aromatic ring induces an extra stabilizing effect, in the solid-state structures of **18 b** and **18 c**, which prefer a chair-type conformation, based mainly on $\pi\text{-}\pi$ interactions and also on CH/π interactions. Solid-state structures are preponderantly based on the selenium – selenium interactions, but additional stabilizing forces are involved. The internal cavities of the cycles are not big enough to allow trapping of even small guest solvent molecules and due to a reduced solubility, a three- or four-component coupling, which would have generated cycles with a larger internal cavity, could not be observed.

3.3 Experimental and theoretical investigations of new model compounds

3.3.1 Introduction

Despite an already large interest and an abundance of mechanistic studies on interactions between chalcogens and other donating heteroatoms (halogens, nitrogen, oxygen) and also between different chalcogen centers, it doesn't seem that the discussion on the nature of these interactions is likely to reach a point of agreement soon. The physical mechanism of these interactions is not yet completely clear.

The nature of these interactions was already explained either as a pure electrostatic phenomena⁷⁰ or as a pure second order orbital interaction phenomena¹¹³. In the literature, explanations in between these two extreme cases can be found, especially as they actually do not exclude each other. The latest theoretical calculations² illustrate, based on NBO population analysis, that the electrostatic nature of the mechanism can not be completely ignored, concluding that the real nature of the interaction mechanism can not be simplified to only one of the already mentioned extremes. The situation is even more complicated as many different terms are used in order to describe the heteronuclear-chalcogen and/or chalcogen-chalcogen interaction, ranging from "non-bonded"¹², "secondary bonding"¹¹⁴, "fractional bonding"¹¹⁵, "specific non-covalent contacts"¹¹⁶ to "premature hypervalent bonds"¹¹⁷ or "three center - four electron interactions"¹¹⁸.

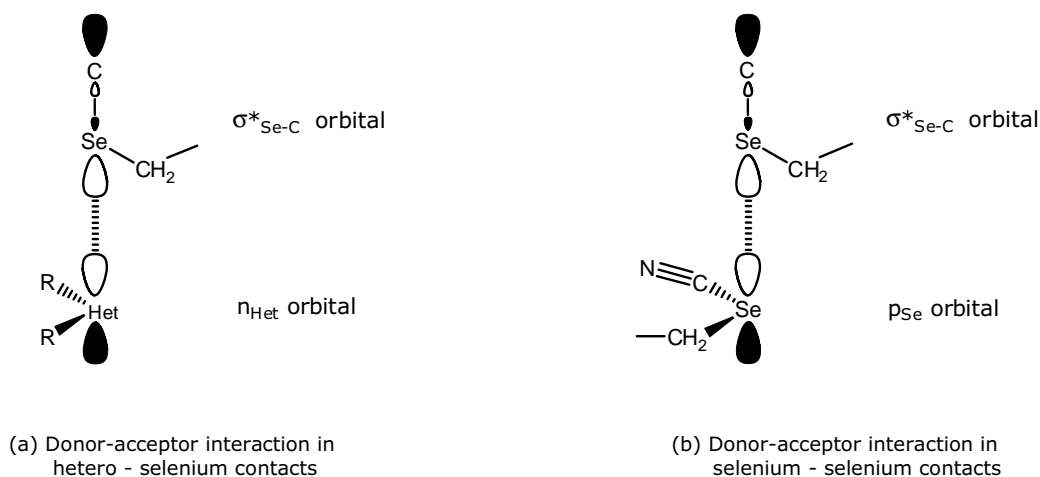


Figure 3.19. Orbital interaction models for contacts involving selenium centers.

Our group was interested in the chemistry involving the interactions of lone-pair electrons of chalcogen atoms and in order to elucidate the nature of the interaction. In the particular case of selenium, we decided to study a series of model compounds containing

divalent selenium at suitable distances. Benzylselenide compounds with different seleno containing groups in the 2 position (Figure 3.20.) are expected to provide a good system to study such non-bonded interactions, as the distances between two selenium centers is favorable, while the mobility of the second selenide group is not strongly hindered, thus not forcefully inducing the Se atom in an interacting alignment. The model compounds are not very large molecules so we also intended to compare experimental results (from X-ray crystallography and NMR spectroscopy) with theoretically calculated properties at the highest level that was available.

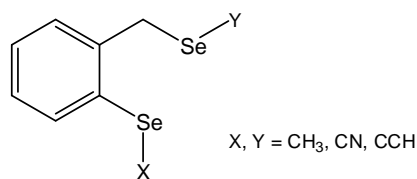
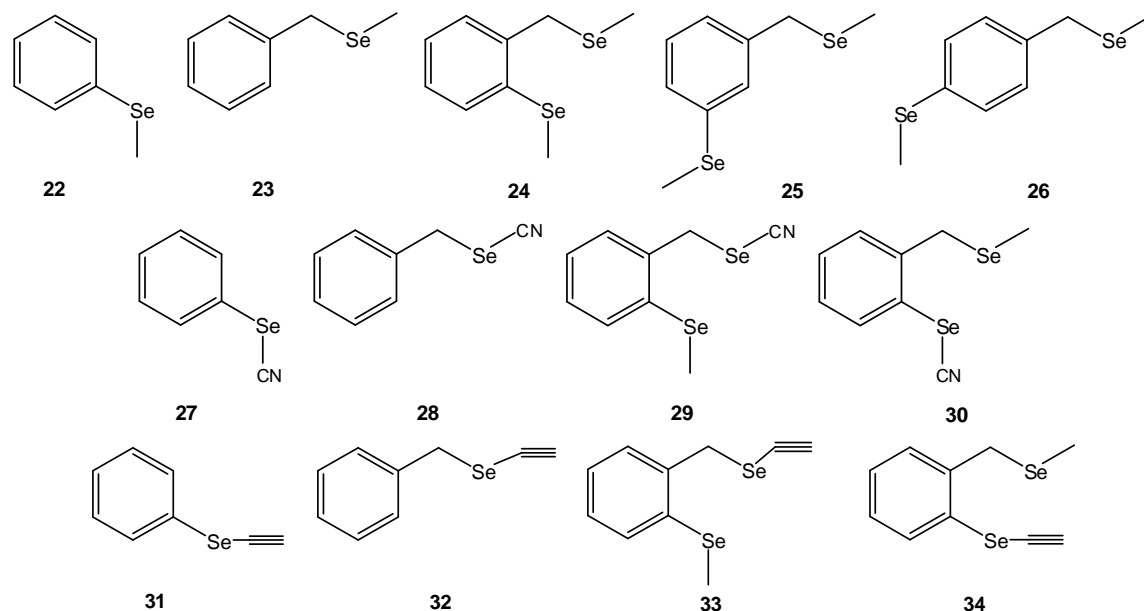


Figure 3.20. Scheme of model compounds to be synthesized for investigation of intramolecular Se...Se interactions.

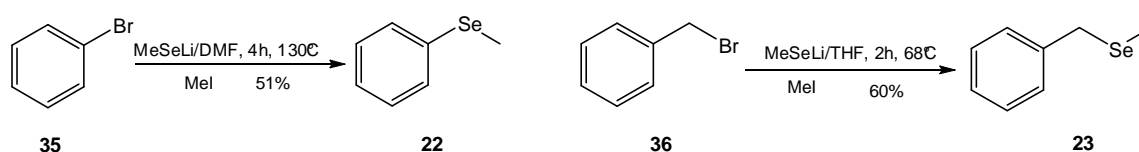
In order to assess either qualitatively or quantitatively the strength of the Se...Se interaction in solution, we decided to compare the NMR parameters of newly synthesized model compounds with those of already known ones. The comparison series are depicted in Scheme 3.10.



Scheme 3.10. Series of model compounds to be synthesized and investigated.

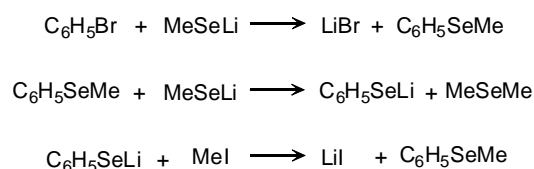
3.3.2 Synthesis of model compounds

We intended to compare experimental values of NMR chemical shifts in the mentioned series to test if the chemical shifts could be a good probe for interaction between selenium atoms in solution. Since it is known that ^{77}Se chemical shifts are quite sensitive to solvent and temperature effects, we had also to synthesize model compounds with only one Se center., so that our comparison would be meaningful.



Scheme 3.11. Synthesis of phenyl methyl selenide (**22**) and benzyl methyl selenide (**23**).

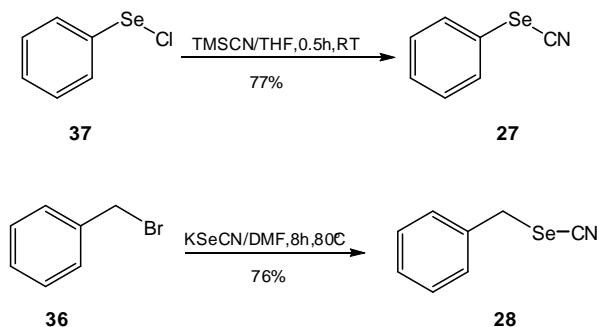
Phenyl methyl selenide (**22**) and benzyl methyl selenide (**23**) were prepared (Scheme 3.11.) according to literature procedures¹¹⁹, by reacting the corresponding bromide with *in-situ* generated MeSeLi¹²⁰. For the more reactive benzylic bromide the reaction gives good yields in refluxing THF. In the case of the unreactive aryl bromide, the reaction is successful in DMF, whereas in THF the yields are poor (less than 5%). *Tiecco et al.*¹²¹ demonstrated that MeSeLi in DMF seems to be the most effective reagent for carrying out $\text{S}_{\text{N}}2$ type cleavage reactions. The addition of methyl iodide is absolutely necessary to obtain a yield of over 50%. This is due to the fact that two consecutive reactions are taking place: a nucleophilic aromatic substitution on the unreactive bromobenzene by the strongly nucleophilic methylselenide anion, followed by a nucleophilic aliphatic substitution on the phenyl methyl selenide. This yields the demethylated product, with the latter reaction being much faster than the $\text{S}_{\text{N}}\text{Ar}$ reaction¹¹⁹. Therefore, by adding methyl iodide, the product of the $\text{S}_{\text{N}}2$ reaction is transformed back into the desired phenyl methyl selenide (see Scheme 3.12.).



Scheme 3.12. Competing substitution reactions during the synthesis of phenyl methyl selenide (**22**).

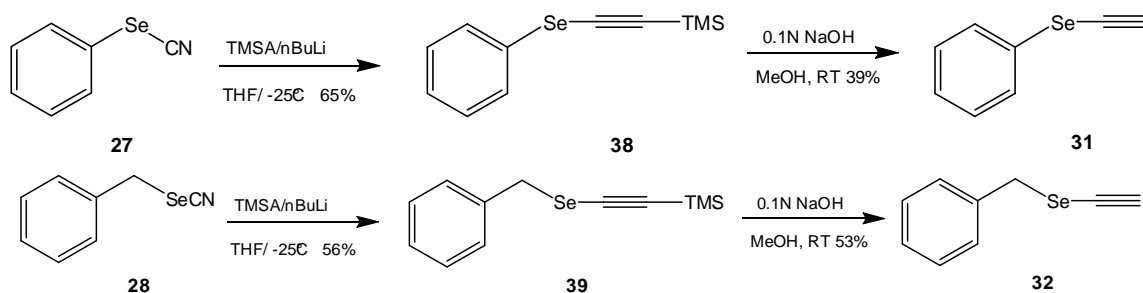
To obtain phenyl selenocyanate (**27**) and benzyl selenocyanate (**28**) (see Scheme 3.13.), we used standard methods given in the literature. For the synthesis of phenyl

selenocyanate, we reacted commercially available phenyl selenylchloride (PhSeCl) (**37**) with trimethylsilylcyanide (TMSCN) in dry THF¹²², while the reaction of the benzylbromide (**36**) with potassium selenocyanate (KSeCN) in hot DMF⁹⁵, generated benzyl selenocyanate.



Scheme 3.13. Synthesis of phenyl selenocyanate (**27**) and benzyl selenocyanate (**28**).

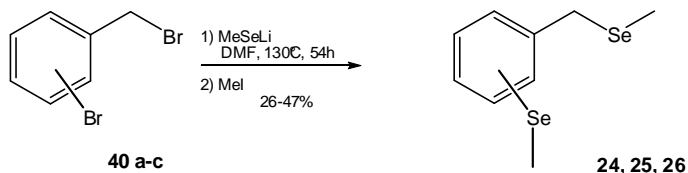
Aryl and alkyl selenocyanates possess reactive groups, which tend to be hydrolyzed rapidly to selenols and further generate their respective di-aryl and di-alkyl diselenides¹²³. This drawback makes them difficult to purify and to be manipulated. However, based on their reactivity, selenocyanates are very good precursors for the synthesis of terminal selenoalkynes. The reaction of the lithiated salt of TMSA with selenocyanates generates by means of a nucleophilic substitution the TMS protected terminal selenoalkynes (Scheme 3.14.). The protecting TMS groups were removed easily using a 0.1N solution of NaOH in a mixture of solvents consisting of methanol and THF at room temperature, under vigorous stirring for ca. 2 hours⁹⁶. As a result, the desired phenyl ethynyl selenide (**31**) and benzyl ethynyl selenide (**32**) were generated in relatively good yields of up to 53%.



Scheme 3.14. Synthesis of phenyl ethynyl selenide (**31**) and benzyl ethynyl selenide (**32**).

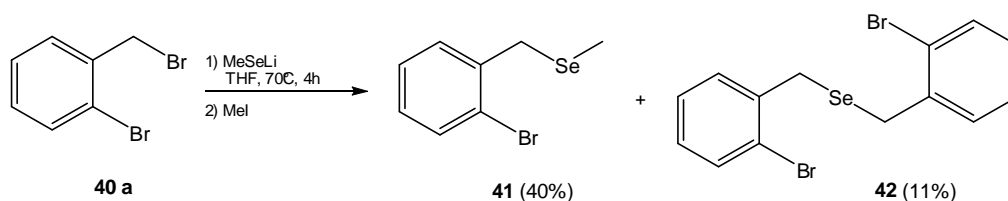
The preparation of the three isomers **24**, **25** and **26** was achieved in an one pot reaction starting from the corresponding *o*-, *m*- and *p*-bromo-benzylbromide (**40 a-c**). Treatment of

the bromides with *in-situ* generated lithium methyl selenide (MeSeLi) followed by methylation yielded the desired (methylselenyl)-benzylmethyl selenides (Scheme 3.15.).



Scheme 3.15. One-pot reaction for synthesis of isomeric 2-, 3-, and 4-(methylselenyl) benzyl methyl selenide (**24**, **25**, **26**).

During our initial trials of synthesizing 2-(methylselenyl)-benzyl methyl selenide (**24**), we attempted the synthesis in THF as solvent. We observed that we could only achieve methylselenation of the benzylic bromine center. Although methyl iodide was used to prevent demethylation, this could not be completely avoided. As a by-product, probably due to the reaction between a demethylated **41** and one equivalent of **40 a**, compound **42** was obtained. Its solid state structure, which is discussed in Chapter 3.2.3.1.5., revealed some interesting features about interactions between the Se and Br atoms.



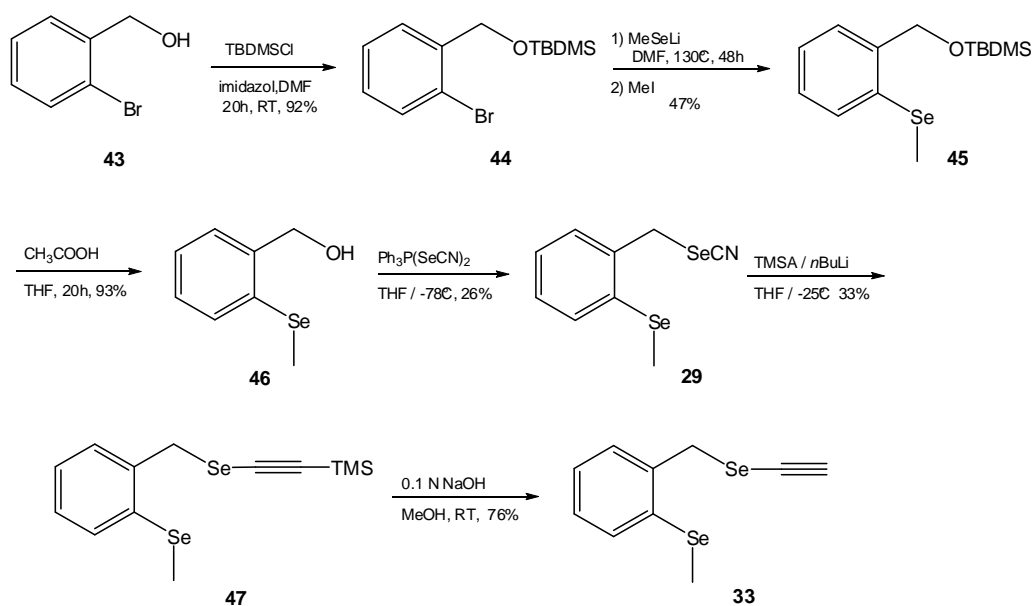
Scheme 3.16. Products obtained by reacting MeSeLi with **40a** in THF.

The aryl-bromide position is unreactive, therefore the bromo-benzylbromides dissolved in DMF were added over the THF solution containing MeSeLi and, after removal of the THF, the reaction mixture was stirred at reflux for long periods of time of up to 3 days. After methylation with methyl iodide, the equilibrium of the competing substitution reactions (see Scheme 3.12) can be manipulated to obtain the desired (methylselenyl)benzyl methyl selenide isomers with acceptable yields in the range of 25 to 50%.

Several synthetic approaches were considered in our attempt to synthesize model compounds containing different substituents at the selenium centers. Due to the ambivalence of selenium, behaving either as a nucleophile or as an electrophile depending on reaction conditions, we had to consider alternative methods to what was available in the literature.

The syntheses of **29** and **33** were finally successful using a rather less direct synthetic procedure, summarized in Scheme 3.17. The synthesis commenced with commercially available 2-bromobenzylalcohol (**43**) which, after protection with *t*-butyldimethylsilyl (TBDMS) chloride, was reacted with MeSeLi followed by methylation to yield **45**. The TBDMS protection group is relatively stable under mild basic conditions as compared to their trimethylsilyl (TMS) equivalents¹²⁴. There are also literature reports¹²⁵ of metallation reactions in the presence of *t*-BuLi, during which TBDMS protected ethers were unaffected, thus making TBDMS the protection group of choice for our synthetic method.

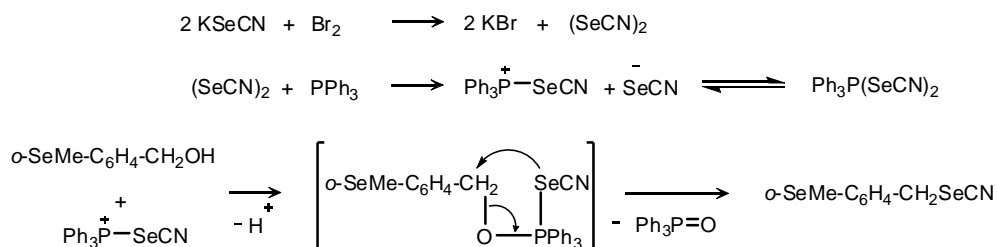
The TBDMS group was not removed using the classical fluoride reagents like HF in MeCN¹²⁶, HF-pyridine complexes in MeOH¹²⁷ or tetra-*n*-butylammonium fluoride (TBAF) in THF¹²⁸, as a fluoride attack at the already introduced selenium center was to be expected. We preferred the rather mild conditions of deprotection using diluted acetic acid in THF at room temperature¹²⁸ to afford the corresponding 2-(methylselenyl)-benzyl alcohol (**46**).



Scheme 3.17. Reaction scheme for the synthesis of 2-(methylselenyl)-benzylseleno cyanate (**29**) and 2-(methylselenyl)-benzyl-ethynyl selenide (**33**)

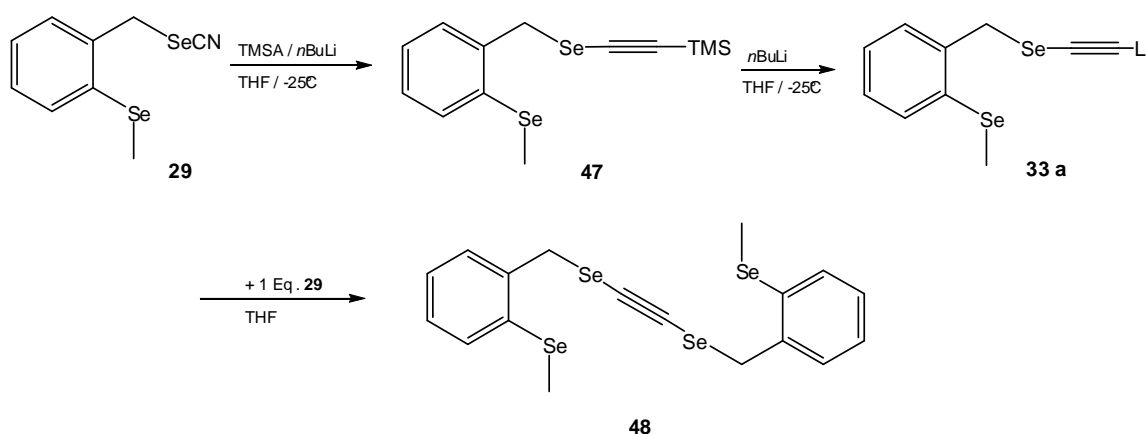
The introduction of the SeCN-group was successfully achieved using a selenocyanation reagent (Ph₃P(SeCN)₂), according to the literature¹²⁹ affording 2-(methylselenyl)benzyl selenocyanate (**29**) with a yield of 26%. Similar to halogenation of alcohols using tertiary phosphine dihalides¹³⁰, the Ph₃P(SeCN)₂ reagent, easily prepared by addition of an equimolar amount of triphenylphosphine to a freshly prepared selenocyanogen¹³¹ solution in dichloromethane and THF, reacts at temperatures below -60°C with primary alcohols to

yield the corresponding selenocyanates, according to the following mechanism (Scheme 3.18):



Scheme 3.18. Mechanism of selenocyanation of benzylic alcohols¹²⁹.

The selenocyanate **29** was reacted with the lithium salt of trimethylsilylacetylene (TMSA) to afford **47**, which was deprotected with a 0.1 N solution of NaOH in MeOH⁹⁶ to give the terminal alkyne **33** (see Scheme 3.17.).

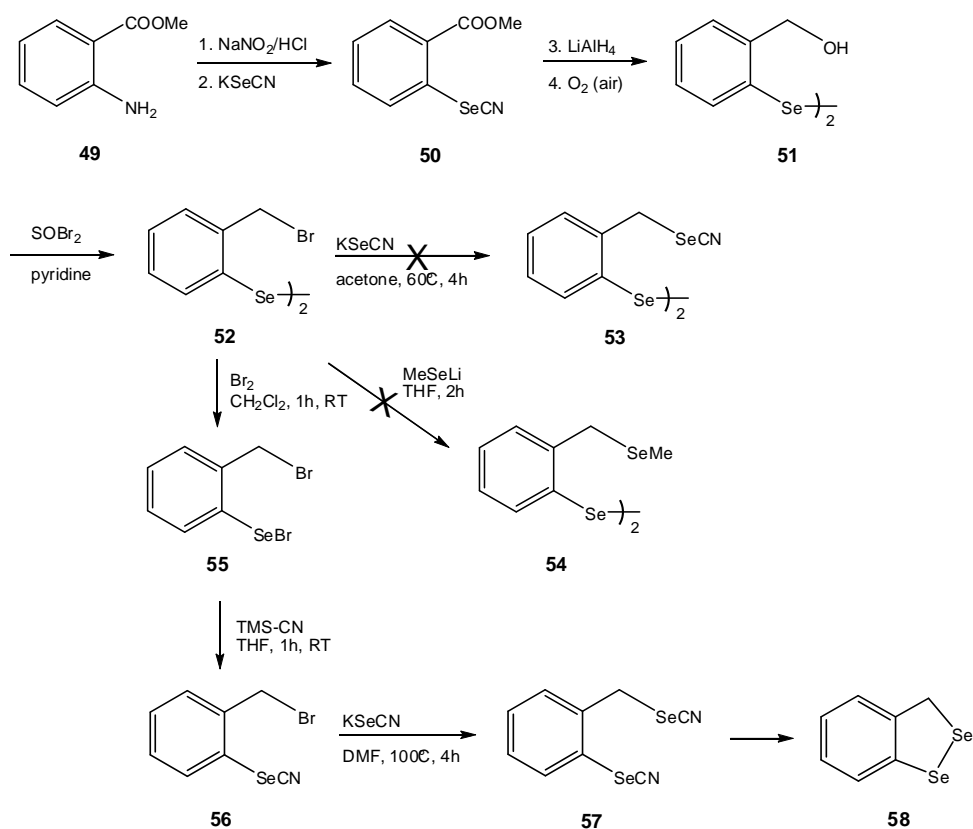


Scheme 3.19. Possible side reactions generating compound **48**.

The use of *n*-BuLi as deprotonating agent for TMSA (see Scheme 3.17.), can also cause side reactions, either by an attack at the selenylmethyl group, thus reducing the yields of the desired product, or as depicted in Scheme 3.19., by removing the TMS group of the terminal alkyne and allowing another SeCN moiety from a separate molecule of **29** to react. This later possibility affords the di-selena di-substituted alkyne **48**, which turns out to be a very interesting compound for our investigations of selenium-selenium interactions. Its solid-state structure will be discussed in Chapter 3.3.3.1.2.

After the series with a SeMe group in the 2-position on the aromatic ring was completed, we attempted to synthesize other model compounds with other groups in that position. A

promising reaction pathway focused on synthesizing a diselenide type compound. Diselenide bonds can be cleaved using different methods, therefore it looked as a promising approach. Following a procedure of *Iwaoka and Tomoda*¹³² we synthesized 2,2'-diselenobis(benzyl alcohol) (**51**) starting from commercially available methyl anthranilate (**49**) as depicted in Scheme 3.20. We isolated crystals of the bis-alcohol, and using thionyl bromide (SOBr₂) and pyridine we obtained 2,2'-diselenobis(benzyl bromide) (**52**). To our surprise, no crystal structure of **52** was yet reported in the literature, although a similar compound, based on naphthene rings, bis[3-(bromomethyl)-2-naphthyl] diselenide was reported having a short Se...Br contact. A discussion of the solid-state structure of **52** is presented in Chapter 3.2.3.1.5.



Scheme 3.20. Synthesis attempts for some other model compounds.

Attempts to synthesize 2,2'-diselenobis(benzyl selenocyanate) (**53**) or 2,2'-diselenobis(benzyl methylselenide) (**54**) using the usual procedures failed, although in the case of **54** traces of the compound have been observed in a FD mass spectra and also a benzylic proton signal in a ¹H-NMR spectrum displays the typical ²J_{Se,H} coupling pattern. In the ⁷⁷Se NMR spectrum two signals could be detected in the region characteristic for diaryldiselenide (381 and 410 ppm)^{111,112}. Considering the reactive nature of selenocyanate groups and their

ability to transform themselves into diselenides¹²³, one can assume that unwanted reactions of this sort take place. Therefore, products like oligomeric or macrocyclic compounds containing diselenide bridges are to be expected, but none of these could be isolated and characterized. Reaction of 2,2'-diselenobis(benzyl bromide) (**52**) with bromine¹³² afforded 2-(bromoselenyl)-benzyl bromide (**55**) as a purple solid. Despite its reactive nature, **55** could be characterized through mass spectrometry and complete NMR spectroscopy analysis, before being reacted with TMSCN to afford 2-(cyanoselenyl)-benzyl bromide (**56**). Attempts of using MeSeLi to replace the benzylic bromide of **56** failed, as the attack was also taking place at the Se atom of the selenocyanate group. As a result the main product obtained was 2-(methylselenyl) benzyl methyl selenide (**24**). Upon reacting **56** with KSeCN in DMF, 2-(selenocyanato) benzyl selenocyanate (**57**) was obtained and although, due to the reactivity of the SeCN, it quickly decomposed, but we were able to obtain a NMR spectroscopic characterization of the compound. As illustrated from the mass spectra, one of the possible decomposition products could be 3*H*-1,2-benzodiselenole (**58**), whose molecular mass peak was detected in a mass spectrum (EI) of the raw reaction product. The anticipated 2-(selenocyanato) benzyl selenocyanate (**57**) could not be isolated and fully characterized.

3.3.3 Structural investigations of model compounds

3.3.3.1 Solid state structures

3.3.3.1.1 Crystal structure of 2-(methylselenyl)-benzyl-selenocyanate (**29**).

We were able to grow single crystals of 2-(methylselenyl)-benzyl-selenocyanate (**29**) from a *n*-hexane / dichloromethane solvent mixture, which allowed a detailed structural investigation by means of a X-ray diffraction analysis. A closer look at the solid-state structure of **29** reveals strong intra- and intermolecular interactions involving both selenium centers. Competing intramolecular Se...Se interactions, weak Se...H bonding (Figure 3.21.), strong intermolecular Se...Se interactions in between pairs of diastereoisomers of **29** (Figure 3.22.) and some strong intermolecular interactions between nitrogen atoms and selenium atoms of the SeCN groups are all involved in the packing of the crystal of 2-(methylselenyl)-benzyl-selenocyanate (**29**).

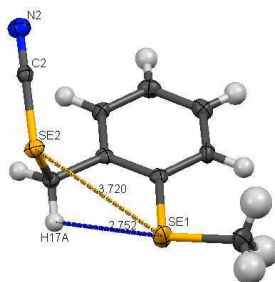


Figure 3.21. Molecular structure of 2-(methylselenyl)-benzyl-selenocyanate (**29**) in the solid-state (ellipsoid probability 50%).

Figure 3.21. depicts the molecular structure of **29** in the solid-state and the significant intramolecular interactions. A short Se...Se distance between the SeCH₃ and the SeCN moieties of 372 pm and a small (275 pm) distance between Se1 and H17a indicating weak hydrogen bonding, competing with the intermolecular Se...Se interaction. These observations confirm the competing character of these interactions. An evaluation of which interaction has a stronger effect in the solid-state structure of **29** can only be speculative. Interestingly enough, in order to favour these interactions, the C(*sp*²)-Se1-C(*sp*³) angle is larger than the usual divalent selenium angle (around 95°), having a value of 102.1°. The methyl group bonded to Se1 lies almost in the same plane with the aromatic ring, with a deviation of only 9.7°.

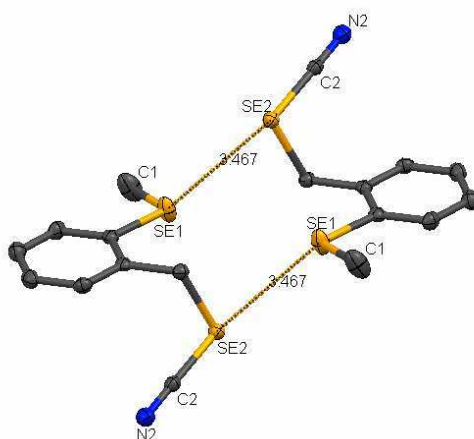


Figure 3.22. Diastereoisomeric pairs in the solid-state structure of **29** showing Se...Se intermolecular contacts (50% ellipsoid probability, H atoms are not displayed).

The intermolecular interactions between the selenium centers of (**29**) (Figure 3.22) are short (347 pm) and are among the shortest reported in the literature. Only 15 compounds, out of 227 compounds reporting intermolecular Se–Se contacts below 380 pm in the Cambridge Crystallographic Database (CCDC)¹⁰², show Se–Se distances equal or below 347 pm. Furthermore, the spatial orientation between the selenocyanate group and the selenium atom of the methylselenyl group of the pairing molecule displays nearly a linear configuration (163.4°), which does provide favorable geometrical conditions for an attractive interaction between a lone-electron-pair of Se1 and the σ^* -orbital of the Se2-C2 bond as depicted in Figure 3.19. The favored alignment explains the shorter intermolecular Se–Se contact, in comparison with the intramolecular one, thus offering more support for the orbital interaction theory of chalcogen-chalcogen interactions.

To verify whether these short intermolecular Se...Se interactions would not be only a result of crystal packing effects¹³³, we decided to investigate the pairing of the diastereoisomers also on a theoretical level. By freezing the internal coordinates of the two molecules and only varying the distance between them, we obtain an energy profile of the two interacting molecules corresponding to Se–Se contact distances in the range of 335 pm to 531 pm. The energy calculations of the diastereoisomeric pair were carried out at DFT level of theory, using the B3LYP functional of Becke¹³⁴, Lee, Yang and Parr functional¹³⁵ in combination with a large basis set, 6-311++g(2d), containing both polarization and diffusion functions. The necessity of these additional functions for relatively accurate theoretical calculations of chalcogen – chalcogen interactions was already illustrated in previous theoretical investigations of these types of interaction² and confirmed in our theoretical investigations of the model compounds (see Chapter 3.3.4.).

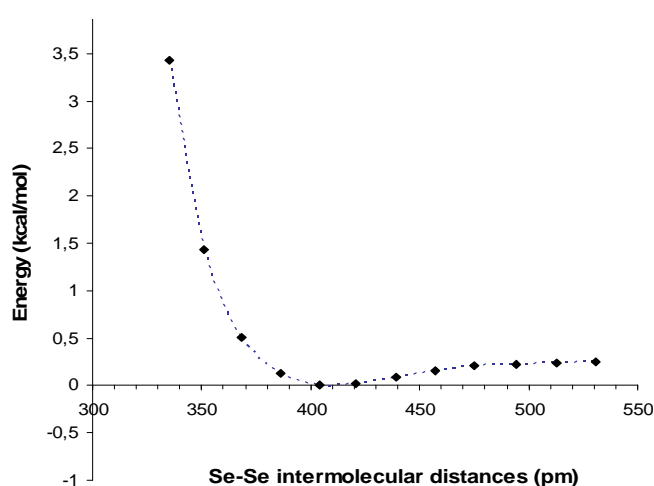


Figure 3.23. Energy profile for a diastereoisomeric pair of compound (**29**) relative to the Se–Se contact distances.

Some additional intermolecular interactions can be observed in the X-ray structure of compound **29** (see Figure 3.24.). The distance between a nitrogen atom (N2) of a cyano group and a selenium atom (Se2) of a methylene selenocyanate group from another neighboring molecule is relatively short at 313 pm (compared to the sum of the Van der Waals radii of 345 pm) and represents a further strong attractive interaction. Its geometric characteristics support again the orbital theory of interactions (as in Figure 3.19.a), as the N-Se-C(sp^3) angle amounts to 166.7° , again close to a linear alignment.

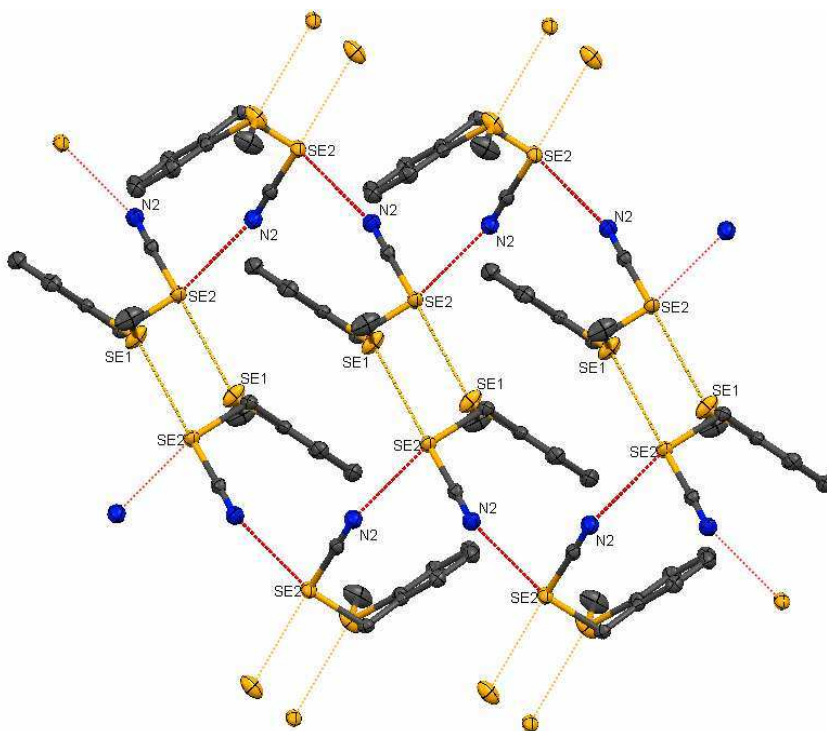


Figure 3.24. Top view of a “layer” of diastereoisomeric pairs of **29**, connected through Se...Se (dark orange dotted lines) and Se...N (red dotted lines) interactions (50% ellipsoid probability, H atoms are not displayed)

These interactions between heavy atoms of molecules in the crystal structure build up to a sort of a crystal layer construction based on the interactions between selenium centers on one hand and between nitrogen and selenium on the other (Figure 3.24.). Thus, Se...Se interactions are responsible for pairing of the diastereoisomers, while Se...N interactions are the driving force that is linking the diastereoisomeric pairs with each other.

3.3.3.1.2 Crystal structure of 1,6-bis(2'-methylselenylbenzene)-2,5-diseleno-3-hexyne (**48**)

We obtained compound **48** as a by-product in the synthesis of **47**, most probably based on the side-reaction illustrated in Scheme 3.19. That could have occurred due to unreacted *n*-BuLi present in the reaction mixture, or even in the initial phase, when TMSA might have been deprotected besides being deprotonated, resulting in the dilithiated salt of acetylene (LiCCLi), which in turn could have been reacting with 2 equivalents of **29**, leading to the by-product **48**. Although not a target compound for our studies, **48** received our attention, especially after discovering that, contrary to our expectations, the terminal alkyne **33** cannot be recrystallized. We managed to recrystallize **48** out of a solvent mixture of *n*-hexane/dichloromethane, thus allowing us to investigate its solid-state structure.

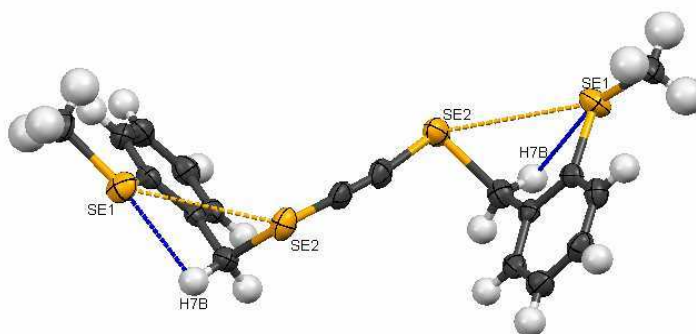


Figure 3.25. Molecular structure of compound **48**. Dotted lines represent strong intramolecular interactions: Se...Se (dark orange, 364 pm) and Se...H (blue, 277 pm) (50% ellipsoid probability)

Interestingly enough, significantly strong intermolecular interactions could be detected. Figure 3.25. depicts the molecular structure of **48** and the observed interactions. The strong Se...Se interaction, with a distance of 364 pm is surprising, because a short distance was not expected when replacing the SeCN group with a SeCCH group, considering that they are isoelectronic. Also, a surprisingly short Se...H contact could be observed between Se1 and one of the benzylic protons (H7B). Its value of 277 pm is well below the sum of the Van der Waals radii, and also shorter than the first reported C-H...Se bond by Tomoda *et al.*¹³⁶

It is interesting to observe that the strength of the intramolecular Se...Se (364 pm in **48** vs. 372 pm in **28**) interaction increased, while the Se...H (277 pm in **48** vs. 275 pm in **29**) interaction is almost unchanged with the disappearance of the N center from **29** and its ability to get also involved with one Se center in an interaction.

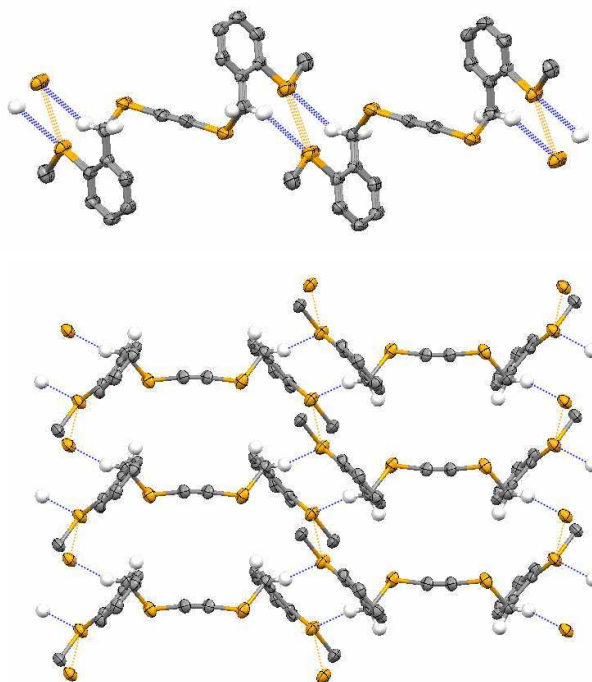


Figure 3.26. Solid state structure of **48**. The column like arrangement of the molecules is presented in a top view (top) and in a side-view (bottom). (50% ellipsoid probability, only selected H are displayed). Thin dotted lines represent the significant intermolecular contacts: dark orange for Se...Se (383 pm) and blue for Se...H (297 pm)

The intramolecular interactions are the strongest in the case of **48**. Similar to the case of compound **29**, the driving forces in building a column-like structure are weak Se...Se interactions, with lengths of 383 pm and Se...H interactions with lengths of 297 pm. It can be observed that because of the strong intramolecular Se...Se interactions, the expected zig-zag arrangement of the Se-Se contacts is not anymore alone responsible for the column-like arrangement, such as in the case of the selenium containing cyclic compounds (see Chapter 3.1.). In this case, one could speak of a collaborative effect of Se...H bonding that "keeps together" molecules in the same plane, and weak Se...Se contacts that build the "connection" between the planes.

3.3.3.1.3 Crystal structure of 2-(methylselenyl)-benzyl-alcohol (**46**)

The preparation of the alcohol **46** was already described by *Tomoda et al.*¹³⁷ However, we were able to grow crystals of **46** for the first time. Recrystallization of the raw material

was successful only at -20°C , from dichloromethane, in the presence of traces of *n*-hexane as co-solvent. Even if not a main focus for our investigations of Se \cdots Se interactions, the solid-state structure of **46** brings some additional insights regarding the interaction of selenium with other chalcogen atoms.

A relatively strong interaction between the oxygen and the selenium center was to be expected, as theoretically calculated values¹³⁸ indicated an interaction energy of 2.5 to 4 kcal/mol. This was explained by a $n_{\text{O}} \rightarrow \sigma^*_{\text{Se-C}}$ orbital overlap (as depicted in Figure 3.19.a). Tomoda *et. al.*¹³⁷ reported that the ^{17}O -NMR chemical shift of **46** ($\delta_{\text{O}}=10.6$ ppm), shows a significant downfield shift as compared to that of reference compound benzyl alcohol ($\text{C}_6\text{H}_5\text{-CH}_2\text{OH}$, $\delta_{\text{O}}=0.7$ ppm)¹³⁹. Recent investigations of Singh *et. al.*¹⁴⁰ also assigned a downfield shift of ca. 54.5 ppm in this case in the ^{77}Se -NMR spectrum of *o*- $\text{CH}_2(\text{OH})\text{-C}_6\text{H}_4\text{-SeH}$ ($\delta_{\text{Se}}=199$ ppm) in comparison with benzeneselenol ($\text{C}_6\text{H}_5\text{-SeH}$, $\delta_{\text{Se}}=152$ ppm)¹⁴¹ to a strong intramolecular interaction between Se and O atoms.

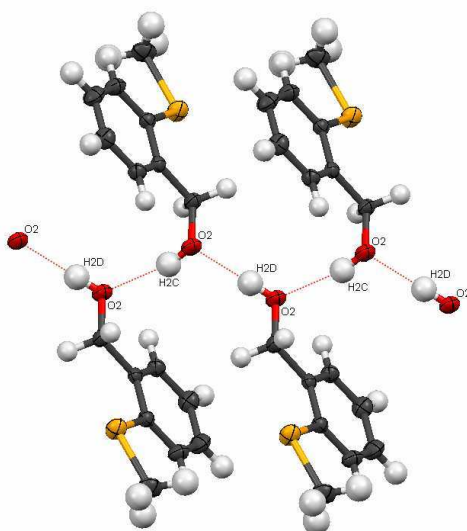


Figure 3.27. Crystal packing at -20°C , for **46** (ellipsoid probabilities 50%). Red thin dotted lines represent O-H \cdots O bonding.

The most stable conformer of **46** based on DFT calculations (B3LYP/631H//B3LYP/631H level), reported in the already mentioned publications of Tomoda *et al.*, displays the Se and O atoms being situated at a distance of 300 pm (42 pm less than the sum of Van der Waals radii) and the O atom is almost linearly aligned with the Se-CH₃. In the measured solid-state structure, however, the most important force behind the crystal packing is classical hydrogen bonding. Even if a short contact of 278 pm between Se and one of the benzylic protons can be detected and also some weak Se \cdots Se contacts, the predominant interaction

observed is the strong O-H...O bonding, with distances of 272 and 276 pm in between the O atoms. In Figure 3.27. it can be seen that the O atom in the molecules are pointing away from the Se atom, in such a way that the O-H...O contact is favored.

These observations illustrate once again that, even if the Se...O interaction is considered one of the strongest Se...heteroatom interactions (*Tomoda et al.*¹³⁸ reported a decrease in strength of Se...heteroatom interactions in the following series: Se...N > Se...O > Se...F > Se...Cl ≥ Se...Br), it can not compete with the "classical" hydrogen bonding.

3.3.3.1.4 Crystal structure of 2,2'-diselenobis(benzyl alcohol) (**51**).

Obtained as an intermediate product in the synthesis of some of the model compounds, 2,2'-diselenobis(benzyl alcohol) (**51**), was easily recrystallized from a solvent mixture of light-petroleum and dichloromethane.

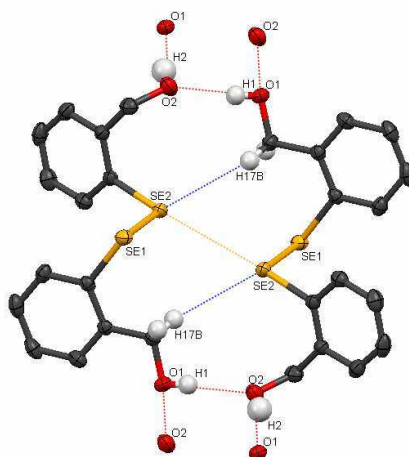


Figure 3.28. Intermolecular interactions observed in the solid-state structure of 2,2'-diselenobis(benzyl alcohol) (**51**): O-H...O bonding – thin red dotted lines; Se...Se interactions – thin dark orange dotted line; Se...H contacts – thin blue dotted lines (50 % ellipsoid probabilities, only selected H atoms displayed).

After comparison with the already reported solid-state structure of **51** available in the Cambridge Crystallographic Database reported by *Singh et al.* (CCDC ref. no: 292678)¹⁴⁰, we were surprised to observe significant differences between our findings and that reported by *Singh*. While in the reported structure a strong Se...O contact (301 pm) was to be observed and the two aromatic rings being almost perpendicular to each other, in our case, there is no significant interaction between Se and O atoms, the intramolecular Se...O distances amounting to 368 and 459 pm and the two benzene rings are situated in planes almost parallel to each other. The interesting features of our solid-state structure are not only the strong classical O-H...O bonds, with O...O distances amounting to 275 and 279 pm.

A short intermolecular Se...Se contact (376.5 pm) and two Se...H contacts (309 pm) between Se atoms from the diselenide bond with benzylic protons from another molecule are generating a "pairing" of molecules in the crystal structure (Figure 3.28.).

Another structural feature that attracted our attention was a short distance from one Se atom to a benzene ring from a neighboring molecule. A closer look revealed the arrangement depicted in Figure 3.29., where pairs of molecules are kept together in the crystal based on short (342 pm) offset-type π - π interactions (see also Figure 2.14.) that involve also the Se atoms.

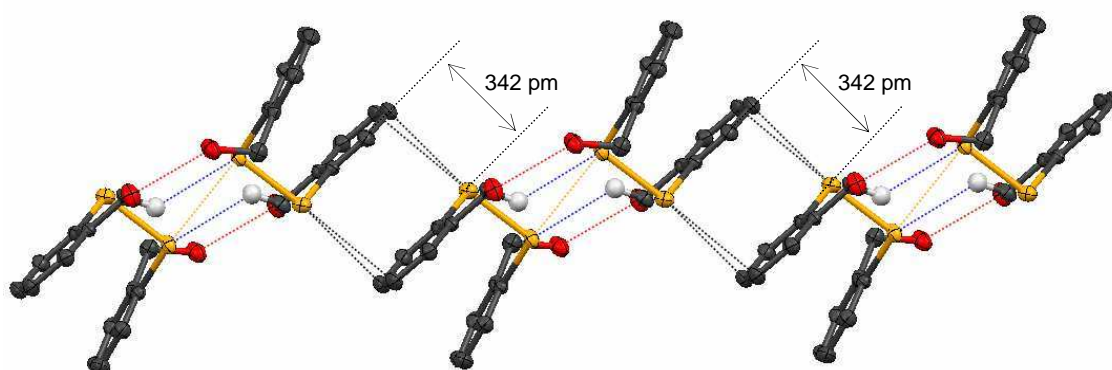


Figure 3.29. π - π interactions in the solid-state structure of 2,2'-diselenobis(benzyl alcohol) (**51**) (50% ellipsoid probabilities, H atoms are not displayed, except the benzylic protons interacting with Se atoms).

These significant differences in between the solid-state structures of the same molecule (**51**) can be explained by the difference of solvents used in the crystallization (toluene vs. light petroleum / dichlormethane mixture) and illustrate that even small changes in the conditions can influence strongly whether the selenium atoms are involved in selenium-selenium or selenium-heteroatom interactions.

3.3.3.1.5 Comparison of the crystal structures of 2,2'-diselenobis(benzyl bromide) (**52**) vs. bis(2-bromo)benzyl selenide (**42**).

Further insight into the chalcogen interactions with different heteroatoms can also be gained from investigating the molecular structures of 2,2'-diselenobis(benzyl bromide) (**52**) and bis(2-bromo)benzyl selenide (**42**).

Both were obtained during the synthetic attempts of our desired model compounds, either as a intermediate, as in the case of **52** or as an unwanted by-product, as in the case

of **42**. Molecular structures in the solid-state of both of them could be measured by means of X-ray crystallography after recrystallizing them from a solvent mixture of light petroleum / dichloromethane.

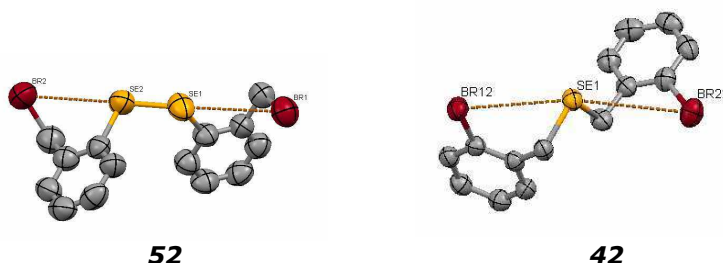


Figure 3.30. Molecular structures of 2,2'-diselenobis(benzyl bromide) (**52**) and bis-(2-bromo)benzyl selenide (**42**). (50% ellipsoid probabilities, H atoms are not displayed). Dotted brown lines represent the weak Se-Br interactions.

Comparing the structural features of the two molecular structures provides a new experimental confirmation of the $n_{\text{Het}} \rightarrow \sigma^*_{\text{Se-C}}$ orbital overlap concept in the case of non-bonding interactions of divalent selenium atoms. In the case of **52**, two rather short bromine – selenium contacts have been observed. The shorter of them, amounting to 367 pm, is smaller than the sum of the Van der Waals radii (375 pm) and it occurs at an angle ($\text{Br2}\cdots\text{Se2}-\text{Se1}$) of 170.1° , almost linearly aligned with the diselenide bond. Another, slightly larger Se \cdots Br contact, with a length of 383 pm is marginally less aligned with the selenide bond, forming an angle ($\text{Br1}\cdots\text{Se1}-\text{Se2}$) of 168° . As a result of these short contacts, the alignment $\text{Br1}\cdots\text{Se1}-\text{Se2}\cdots\text{Br2}$ is almost linear, as shown in Figure 3.30. (left). Similar linear alignments of four interacting centers was reported by *Nakanishi et al.*¹⁴² for bis[8-(phenylselenenyl)naphthyl]-1,1'-diselenide, where four linearly aligned selenium atoms are strongly interacting. This strong interaction was explained based on a four-center six-electron (4c-6e) model constructed with the non-bonded interaction between the two p-type lone pairs of the outer Se atoms and the $\sigma^*_{\text{Se-Se}}$ orbital of the diselenide bond, which results in charge transfer from the outside Se atoms to the inside Se atoms. On the other hand, in the case of **42**, although the three heteroatoms are almost linearly aligned ($\text{Br12}-\text{Se1}-\text{Br22}$ angle amount for 169°), the Se \cdots Br distances are significantly larger than in the case of **52**, amounting for 389 and 406 pm. This supports the interpretation of this interaction on the basis of a Van-der-Waals interaction between Se and Br.

3.3.3.2 NMR chemical shifts

Nuclear magnetic resonance (NMR) is probably the most widely spread spectroscopic technique applied in modern organic chemistry. Highly sensitive and requiring usually mild conditions for measurements, it's the method of choice for structural determination and especially for kinetic measurements. Formerly limited to solution state samples, it has expended its application to solid-state in the latest years, with better results and an accuracy that can even compete with X-ray spectroscopy. A lot of proteins that form disordered aggregates but can not be crystallized, play an important role in diseases such as Alzheimer's disease or in spongiform encephalopathies. They still can be investigated by means of solid-state NMR which provides high-resolution information otherwise unavailable¹⁴³. Several NMR parameters that are very important: *chemical shift*, *direct* and *indirect coupling* and also *relaxation times*.

The *chemical shift* reflects the distribution of electrons surrounding the observed nucleus (bonding and valence electrons, but also non-bonding electron pairs and other electronic influences like the electronegativity of neighbouring groups) and is, in general, a very sensitive probe for the characterization of chemical properties in a molecule.

Although considerable progress has been made towards a refined theory of nuclear shielding, the *ab initio* calculation of chemical shifts is still a difficult problem and a satisfactory correlation with experimental data remains relatively limited. We also attempted a comparison of experimentally acquired ⁷⁷Se chemical shifts vs. theoretically calculated values, but we discuss these results later, in Chapter 3.3.4.3.

In the case of ⁷⁷Se, the large range of around 1000 ppm for the observed chemical shifts of common selenium containing organic compounds makes ⁷⁷Se NMR spectroscopy a powerful tool for organic chemists.

Tomoda et al. reported monitoring Se...F interactions based on ⁷⁷Se,¹⁹F couplings, with *J* values of up to 84 Hz for 2-(fluoromethyl)-benzene selenocynate. Calculations suggested that an $n_F \rightarrow \sigma^*_{Se-X}$ interaction is responsible (X=CN, in 2-(fluoromethyl)-benzene selenocynate). Analogous interactions were reported when F was replaced with Cl, and Br, but the interaction's strength decreased with a lower electronegativity value of the halogen: Se...F > Se...Cl > Se...Br. When the X substituent was a methyl group, the chemical shift of the Se nuclei experienced a shielding, opposing the previously observed trends. This could be an indication that due to the electron donating character of the CH₃ group, the interaction mechanism could be slightly different.

Nakanishi et al. observed a similar inverse substituent effect of X (X=OMe, Me, H, Cl, Br, COOEt and NO₂) on the chemical shift of the ⁷⁷Se nuclei in *peri*-substituted bis(naphthyl) diselenides and could also determine long range ⁷⁷Se,⁷⁷Se coupling constants. A non-bonding interaction involving the p-orbitals of one type of Se atoms and the σ* orbitals of diselenide bond is invoked in what is known as a 4c-6e interaction between four linear Se atoms.

Silks et al. have proven the existence of through-space N-H...Se=C coupling and also C-H...Se=C interactions by recording ¹H,⁷⁷Se HMQC spectra. For compound **59**, a signal splitting of 13 Hz was registered as being much too high for a through-bond ⁵J_{Se,H} coupling constant, while for compound **60**, it was found that the CH proton interacts with selenium, based on a through-space ⁷⁷Se,¹H coupling of 5-7 Hz, rather than the initially expected hydrogen bonding between the OH group and the selenium atom¹⁴⁴.

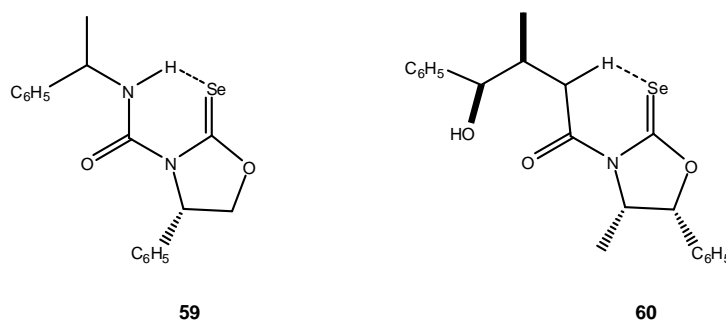


Figure 3.31. N-H...Se=C and C-H...Se=C interactions detected using ¹H,⁷⁷Se HMQC experiments

A surprisingly strong shielding is found for benzene-1,2-bis(selenylchloride) amounting to almost 200 ppm in comparison with phenyl selenylchloride (885.1 ppm vs. 1039 ppm)¹⁴⁵. The reason is not clear; in the absence of an interaction (like N-Se or O-Se interaction), one expects a deshielding γ-gauche effect from one selenium to the other. On the other hand, benzene-1,2-bis(selenylchloride) forms close dimers in the solid-state which results in intermolecular Se...Se distances that are only slightly larger than the intramolecular Se...Se distances so that some interaction may also be expected in solution.

Considering all the aforementioned examples, it can be concluded that ⁷⁷Se NMR chemical shifts (δ_{Se}) are sensitive to the environment around the Se atom, and their shift can be used as probe for the strength of nonbonding interactions of Se with other heteroatoms^{3,113,137}. Extrapolating, δ_{Se} values for model compounds **24**, **29** and **33** (see Figures 3.32. and 3.33.) were analyzed in our aim of a deeper understanding of the nonbonding Se...Se interactions. Although originally considered as a reference, phenyl

methyl selenide (**22**) (δ_{Se} 199 ppm)^{111,112}, which does not have a methyl substituent at the *ortho* position, cannot be used to appreciate the influence of different substituents on the Se...Se interaction. Compound **61** (2-methylphenyl methyl selenide) is better suited for our purpose. The methyl group in the *ortho*- position to the Se-CH₃ leads to a high field shift of around 37 ppm compared to **22**, an anticipated upfield shift if one takes in consideration the γ effect on ⁷⁷Se chemical shifts^{111,112}.

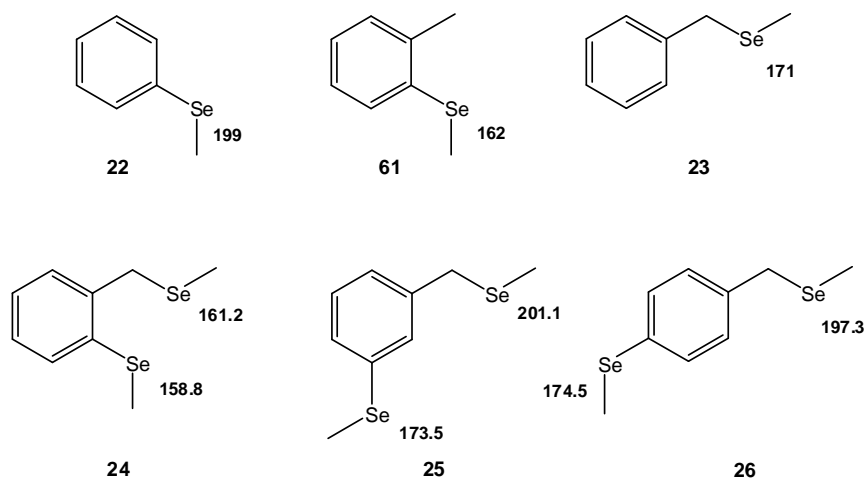


Figure 3.32. ⁷⁷Se – NMR chemical shift comparison of **22–26** and **61**.

We also compared the ⁷⁷Se chemical shift of the three bis-methyl selenide substituted isomers **24**, **25** and **26**, in order to assess if the observed chemical shifts are not simply due to substitution at the different positions of the aromatic ring. As illustrated in Figure 3.32, in comparison with benzyl methyl selenide (**23**), the introduction of another selenium containing substituent at the *meta* (**25**) and *para* (**26**) positions generates the deshielding of the Se nuclei [from **23** (171) to **25** (201), respectively **26** (197) ppm], whereas for the *ortho* position a significant shielding effect was detected. If we compare the δ_{Se} for the SeCH₃ group, we observed a shielding of ca. 25 ppm in comparison with **22**, for the compounds **25** and **26**. An even stronger shielding of 40 ppm is observed in the case of compound **24**, as mentioned before. Therefore, the stronger upfield shifts observed for both Se nuclei of **24** in comparison with the equivalent simpler fragments, compounds **22** and **23** could only be interpreted as a result of a Se...Se interaction, most likely intramolecular.

In Figure 3.33., we have compared the ⁷⁷Se chemical shifts of the **24**, **29** and **33** with those of 2-methylselenobenzylhalogenides **62–64**³ and the simpler compounds **61**, **23**, **32** and **28**. The comparison **61** (162) – **24** (158) – **33** (157) – **29** (157) reveals for the ⁷⁷Se signal of the SeCH₃ group a high field shift, implying an increased electron density around the Se atom bound to the methyl group. The comparisons **23** (171) – **24** (158); **28** (290) –

29 (282); **32** (245) – **33** (238), yield also high field shifts for the ^{77}Se signal of the second Se containing group, indicating an increased electron density on the second Se atom, despite the electron withdrawing character of $\text{C}\equiv\text{CH}$ and CN groups. Taken together, this leads to the conclusion of an increased electron density around both Se atoms, due to a non-bonding interaction between them in which one could consider that the SeMe group plays the electron donor role, while the second Se containing group is the acceptor, the interaction being slightly stronger starting from Se- CH_3 to SeCN. Furthermore, a comparison with literature data for similar compounds **62–64** leads us to assume that the Se \cdots Se interaction is slightly stronger than the known Se \cdots halogen interactions³.

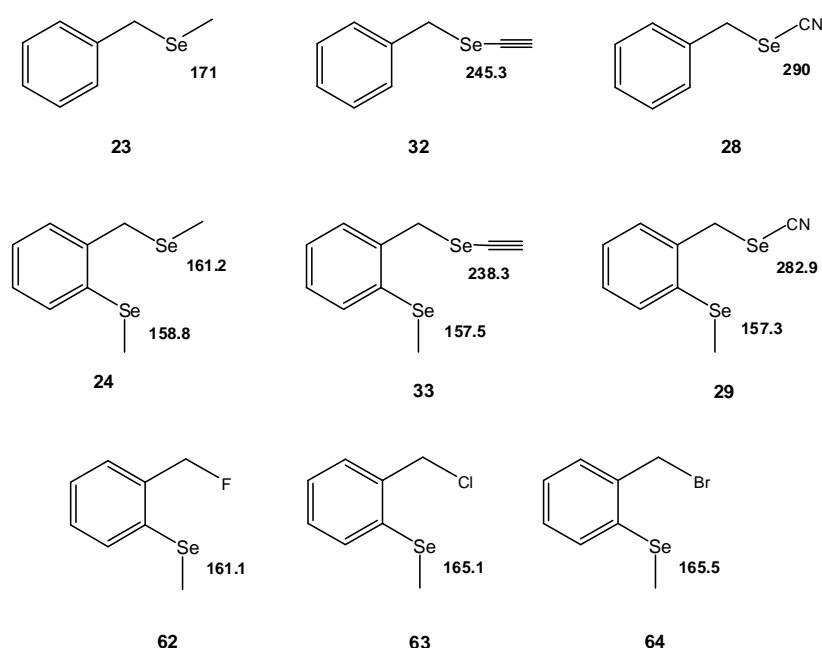


Figure 3.33. ^{77}Se – NMR chemical shift comparison of **23**, **24**, **28**, **29**, **32**, **33** and **62–64**.

Our effort to correlate the ^{77}Se chemical shifts given in Figure 3.33. with the calculated atom charges (Mulliken, ATP and NBO charges) at the Se centers were not convincing, even when we took the conformers of lowest energies ($\Delta E < 2$ kcal/mol) into consideration. Nevertheless, for the NBO charges of the Se center of the Se CH_3 group a trend was observed similar to the chemical shifts. However, our comparison clearly shows that there is a sizeable interaction between the two selenium centers in compounds **24**, **29** and **33** already in solution.

Another interesting observation was made regarding the chemical shifts for the methyl protons and carbons in compounds **24**, **29** and **33**.

Table 3.6. Selected ^1H -, ^{13}C - and ^{77}Se -NMR δ values (in ppm) for **22**, **24**, **29** and **33** in CD_2Cl_2 .

Compound	δ_{H} CH ₃	δ_{C} CH ₃	δ_{Se} SeCH ₃	Se-R
$\text{C}_6\text{H}_5\text{-Se-CH}_3$ (22)	2.30	7.2	199	-
<i>o</i> -(SeCH ₃) -C ₄ H ₄ -CH ₂ -Se-CH ₃ (24)	2.32	7.6	158.8	CH ₃
<i>o</i> -(SeCH ₃) -C ₄ H ₄ -CH ₂ -Se-CCH (33)	2.35	8.3	157.5	C \equiv CH
<i>o</i> -(SeCH ₃) -C ₄ H ₄ -CH ₂ -SeCN (29)	2.37	9.0	157.3	C \equiv N

Comparing δ_{H} and δ_{C} for compounds **22**, **24**, **33** and **29**, we observed that they are shifting downfield in the series, while the Se chemical shifts are shifting upfield, suggesting that electron density is transferred from the CH₃ group to the Se atom. This would confirm our hypothesis that the Se \cdots Se interaction is forcing more electron density towards both Se nuclei.

3.3.3.3 Couplings between selenium atoms

An even more sensitive probe for our investigations was the coupling constant between interacting Se centers. Even in completely isotropic liquids, due to the influence of the bonding electrons on the magnetic fields of the two nuclear spins, they do couple with each other, and this coupling mechanism is called *J-coupling* or *indirect coupling* to illustrate the assistance of the electrons in the coupling mechanism. The *J-coupling* represents the second most important NMR parameter for chemistry. While the chemical shift indicates the local electronic environment, the *J-coupling* provides a direct spectral measurable manifestation of chemical bonding¹⁴⁶. Two nuclear spins have a measurable *J-coupling* only if they are linked together through a small number of chemical bonds; here being included also hydrogen bond types.

Coupling constants between a ^{77}Se nuclei and other nuclei X ($^nJ_{\text{Se},X}$) can be extracted quite easily in the case of first-order spectra, either from the ^{77}Se signals if X has a satisfactory natural abundance (typical for ^1H , ^{19}F and ^{31}P) or from the spectra of X by inspecting the ^{77}Se satellites (typical for ^{13}C and ^{15}N). Several reports of coupling constants of Se nuclei with other nuclei have been already mentioned in relation with the strength of an intramolecular Se \cdots X interaction. The first reported Se \cdots H-C bonding by *Iwaoka and Tomoda*¹³⁶ was confirmed based on a spin-spin coupling between Se and the proton involved in the bonding with values between 25 to 34 Hz. Furthermore, the strength of

Se...N and Se...F interactions was qualitatively and quantitatively evaluated based on long-range ^{77}Se - ^{19}F ^{3,113,147} and ^{77}Se - ^{15}N couplings¹⁴⁸.

Generally, Se-Se coupling did not receive much attention, as it usually requires the observation of Se satellites in ^{77}Se -NMR spectra, with relatively low intensities (2-4 %). One bond $^1J_{\text{Se,Se}}$ couplings have been measured for many compounds, with values varying from -66.5 Hz up to 361 Hz for a diselenide bridged cyclic compound¹⁴⁹. The large variety of values for one-bond couplings makes the understanding of the influence of structure and substitution far from being understood in the case of Se,Se couplings. Two-bond couplings ($^2J_{\text{Se,Se}}$) can adopt large values between 20 and 55 Hz^{111,112}. $^3J_{\text{Se,Se}}$ values have been successfully used for stereochemical differentiation of Se centers in tetraselenafulvalene type compounds¹⁵⁰.

Four-bond couplings received significantly less interest, with values ranging from 0 to 16 Hz mentioned in some sulfur-selenium cycles¹⁵¹. More recently, *Nakanishi's* investigations¹⁵² on Se ...Se interactions determined four- and five-bond coupling constants between Se nuclei, with values ranging from 294 to 371 Hz for 4J and 11.9 to 16.1 Hz for 5J for some bis[8-(arylselenyl)naphthyl] diselenides and 1-(methylselenyl)-8-(phenylselenyl) naphthalene derivatives. The large values are correlated with the strength of the Se...Se interactions, based on orbital overlapping.

Indeed, a careful examination of the satellites of the ^{77}Se signals in the NMR spectra allowed us to determine long range coupling between the two selenium atoms in the case of compounds **29** and **33**. For compound **24**, the ^{77}Se NMR spectrum showed relatively broad signals for both peaks, suggesting the existence of several conformers in solution, which was later confirmed by theoretical calculations. Even at low temperatures of around -80°C, the peaks were not resolved so that it would allow neither to determine the energy barriers of the conformers' equilibrium, nor to determine the long-range ^{77}Se - ^{77}Se coupling constants. Nevertheless, we were able to determine the coupling constant for compound **24** based on a 2D homonuclear ^{77}Se - ^{77}Se shift correlation experiment with proton decoupling¹⁵³, which is depicted in Figure 3.34.

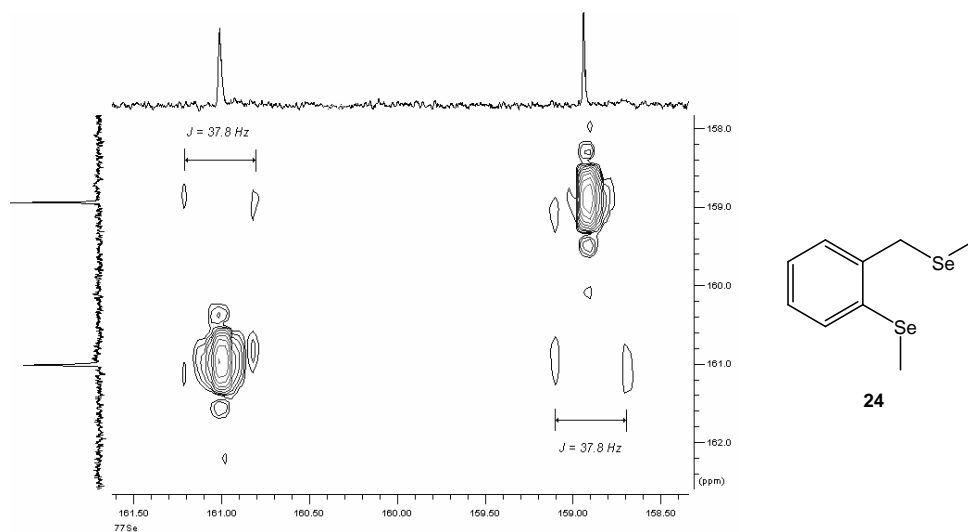


Figure 3.34. ^{77}Se - ^{77}Se correlation spectrum detail for compound **24**. The four bond ^{77}Se - ^{77}Se coupling constant is determined to amount for 37.8 Hz.

The values (see Table 3.7.) ranging from 37.8 to 58.8 Hz are large, therefore we dare to assign them not only to through-bond coupling but also to a direct spin-spin, through-space coupling.

Table 3.7. Chemical shifts (δ_{Se}) and long range couplings ($^4J_{\text{Se,Se}}$) of the Se centers in the model compounds **24**, **29** and **33** (see Figure 3.33.). δ_{Se} measured in ppm, referenced by using the $\bar{\epsilon}$ scale (see experimental part) and $^4J_{\text{Se,Se}}$ is measured in Hz. Only absolute values were determined, the signs of the coupling constants are unknown.

Compound	24	33	29
$\delta_{\text{Se}} - \text{SeX}$	161.0	238.3	282.9
$\delta_{\text{Se}} - \text{SeCH}_3$	158.9	157.5	157.3
$^4J_{\text{Se,Se}}$	37.8	40.9	58.8

The increase in the coupling constant from **24** to **33** to **29**, indicates an increased spin interaction between the two selenium nuclei, which we assign to an increasing intramolecular Se...Se interaction. Confirming these suppositions, the long range $J_{\text{Se,Se}}$ coupling for compound **57** was determined to amount only to 34 Hz, illustrating that in the

case where both substituents (SeCN) are electron withdrawing groups, the Se...Se interaction is less favoured.

3.3.3.4 NMR relaxation times

One of the most important and useful features of NMR spectroscopy is the ability to probe molecular motion, over a wide range of timescales, ranging from picoseconds to several seconds. T_1 – nuclear spin-lattice relaxation, as a physical phenomenon, is an energetic exchange between excited nuclear spins and their environment. The T_1 relaxation values can also provide valuable information concerning molecular dynamics and interactions, molecular structure, conformation and composition.

T_1 relaxation times were determined for compounds **24**, **29** and **33** using an *inverse recovery* method. By definition, time delays in the pulse sequences used for determining the T_1 values should provide enough relaxation of nuclei in each cycle of measurements. In the case of monoexponential nuclear relaxation, it is easy to show that the time delays after acquisitions of FIDs, close to the T_1 values, recover around 63% of an equilibrium nuclear magnetization. In turn, a 99% recovery of the equilibrium magnetization will require time delays equal to or larger than five times the T_1 values. For our experiments, such long relaxation delays were not realistic in terms of NMR spectrometer usage time; therefore we had to do all measurements using relaxation delays of 12 seconds per scan (aprox. three times the T_1 values).

The measurements for non-selective ^{77}Se T_1 relaxation time determination were performed using a proton decoupled inverse recovery pulse program, with a relaxation delay of 12s, using 12 increments for the τ delay between the excitation and recovery pulses and 192 scans for each increment, resulting in experimental times longer than 13 hours. Considering the relatively similarly diluted samples (0.17–0.23 mg/ml) and using the same solvent for all experiments and degassing all samples by *four freeze-pump-thaw cycles*, the errors induced by the smaller relaxation delays should be similar in all samples. Therefore, even if a quantitative evaluation of the obtained values is prone not to be exact, a qualitative evaluation of the observed trends of relaxation should provide us with interesting information about the molecular motions of the Se centers. The T_1 values were calculated from the intensities of the observed peaks using a standard *non-linear three-parameter fitting routine*.

Table 3.8. T_1 relaxation time values (in seconds) for the corresponding ^{77}Se signals of the model compounds (**24**, **29**, **33**) and the smaller molecules **22**, **23**, **28** and **32**.

Compound	$\delta_{\text{Se}} - \text{SeCH}_3$	$T_1(\text{SeCH}_3)$	$\delta_{\text{Se}} - \text{SeX}$ (X=Me, CCH, CN)	$T_1(\text{SeX})$
$\text{C}_6\text{H}_5\text{-Se-CH}_3$ (22)	199	4.86	-	-
$\text{C}_6\text{H}_5\text{-CH}_2\text{-Se-CH}_3$ (23)	-	-	172	5.44
$\text{C}_6\text{H}_5\text{-CH}_2\text{-Se-CCH}$ (32)	-	-	245.3	4.92
$\text{C}_6\text{H}_5\text{-CH}_2\text{-SeCN}$ (28)	-	-	288.9	4.64
$o\text{-(SeCH}_3\text{)-C}_4\text{H}_4\text{-CH}_2\text{-Se-CH}_3$ (24)	158.8	4.52	161.2	3.53
$o\text{-(SeCH}_3\text{)-C}_4\text{H}_4\text{-CH}_2\text{-Se-CCH}$ (33)	157.5	4.91	238.8	4.42
$o\text{-(SeCH}_3\text{)-C}_4\text{H}_4\text{-CH}_2\text{-SeCN}$ (29)	157.3	5.43	282.9	3.83

The T_1 relaxation times for the Se nuclei of the SeCH_3 group are increasing in the series **24** < **33** < **29**. With most factors influencing T_1 relaxation time measurements (temperature, solvent, concentration) being held almost constant the increase in the T_1 relaxation times suggests a restraining of motional freedom at the Se nucleus, as expected from a stronger interaction between the two Se centers. The order of increase of relaxation time is similar to the assumed order of increased strength of the Se-Se interaction.

3.3.4 Theoretical investigations

Following our experimental observations and successful theoretical investigations of chalcogen-chalcogen interactions for very simple systems² we were interested in evaluating the possibility of extending the theoretical investigations to “real-life” systems and furthermore, comparing the theoretical predictions with the experimental results.

As NMR is becoming an increasingly important tool in the study of intermolecular interactions, the *ab initio* calculations of NMR parameters of interacting species are also becoming increasingly more common in the latest years.

Our aim was a comparison between theoretically calculated NMR chemical shifts and experimentally determined values. To reach this goal we had first to determine the level of theory needed to allow a meaningful evaluation of our results. A difficult problem referring to NMR chemical shifts calculations is the choice of method, as well as the basis sets to be

used, especially if theoretical results are to be compared with experimental values. This problem is even more important when investigating weak non-covalent interactions, as it is the case with selenium-selenium interactions. Several of these problems are subsequently discussed and solutions or acceptable approximations that were used in our investigations are presented.

3.3.4.1 Theoretical aspects of calculations of NMR parameters¹⁵⁴

NMR spectroscopy studies energetic levels of the spin eigenstates of chemically bonded nuclei in the presence of a magnetic field and their modifications due to the surrounding electrons. Therefore, the most important parameters of NMR spectra can be satisfactorily accounted for by solving the energy equation of a simpler, effective spin-Hamiltonian in which the electrons do not appear and the nuclei are represented only by their intrinsic spins and their associated magnetic moments. Such a Hamiltonian is described by the Equation 3.1:

$$H = -\sum_i \gamma_i \hbar \cdot \mathbf{B}^T (1 - \sigma_i) \mathbf{I}_i + \frac{1}{2} \sum_{i \neq j} \gamma_i \gamma_j \hbar^2 \mathbf{I}_{ij}^T (\mathbf{D}_{ij} + \mathbf{K}_{ij}) \mathbf{I}_{ij} \quad \text{Eq. 3.1}$$

where γ_i are the nuclear gyromagnetic ratios, σ_i are the *magnetic shielding tensors* of nuclei (describing the magnetic shielding effects of the electrons), \mathbf{D}_{ij} is the classical *dipolar interaction* (describing the direct coupling of the nuclear magnetic dipole moments), \mathbf{K}_{ij} is the *indirect nuclear spin-spin coupling* tensor (which describes the indirect coupling, mediated by the surrounding electrons) and \mathbf{I}_i the *nuclear spin operators*. This is related to the nuclear magnetic dipole moments \mathbf{M}_i as:

$$\mathbf{M}_i = \gamma_i \hbar \mathbf{I}_i \quad \text{Eq. 3.2}$$

For calculating the nuclear shielding and/or the spin-spin coupling tensors, two magnetic fields are of interest: the external field of the magnet and the internal field of the nuclei, therefore they are evaluated *ab initio* as the second derivatives of the electronic energy with respect to the magnetic induction \mathbf{B} and the nuclear magnetic moments \mathbf{M} :

$$\sigma_i = 1 + \left. \frac{d^2 E(\mathbf{M}, \mathbf{B})}{d\mathbf{B} d\mathbf{M}_j} \right|_{\mathbf{B}=0, \mathbf{M}=0} \quad \text{Eq. 3.3}$$

$$\mathbf{K}_{ij} = \left. \frac{d^2 E(\mathbf{M}, \mathbf{B})}{d\mathbf{M}_i d\mathbf{M}_j} \right|_{\mathbf{B}=0, \mathbf{M}=0} - \mathbf{D}_{ij} \quad \text{Eq. 3.4}$$

The equations are rather more complicated because, unlike the electric field, which perturbs the *potential energy* term of the Hamiltonian, the magnetic field perturbs the *kinetic energy* term, as it is the motion of electrons that generates electronic magnetic moments. The nature of the perturbed kinetic energy term in the Hamiltonian is such that an origin must be specified defining a coordinate system for the calculation, this origin being called the "*gauge origin*". The magnetic field itself is independent of the choice of the *gauge origin*, and so the calculated nuclear properties would also be independent if the wave functions used for the calculation would be exact, which is hardly an option. The calculated nuclear shielding values can only be independent of the choice of gauge origin with extremely large basis sets.

Several methods were devised to bypass the gauge origin problem. The older method uses "*Gauge-Invariant Atomic Orbitals*" (GIAO)¹⁵⁵ as basis sets. They incorporate the gauge origin into the basis function, so that all matrix elements involving the basis functions can be arranged to be independent of it. Another version is the "*Individual Gauge for Localized Orbitals*" (IGLO) method¹⁵⁶, where different gauge origins are used for each localized molecular orbital in order to minimize error introduced by having the gauge origin far from any particular molecular orbital. A similar distributed gauge origin method is the "*Localized Orbitals/Localized Origins*" (LORG) method developed by *Bouman and Hansen*¹⁵⁷, in which the local gauge origins are chosen to be at the nucleus for which the shielding is calculated for all orbitals attached to this nucleus, and at the center of electronic charge for the remaining ones. *Bader and Keith* used another approach in their IGAIM method (*Individual Gauges for Atoms In Molecules*)¹⁵⁸: instead of calculating the shieldings from the behaviour of the molecular orbitals, they use the calculation of molecular current density distributions. The induced current density distribution of a molecule is constructed from its constituent current density components accurately determined over each spacially defined atom in the molecule, using their nuclei as origin. A later development, CSGT (*Continuous Set of Gauge Transformations*)¹⁵⁹ uses a continuous shift function, that moves the gauge origin towards the nucleus which is the nearest to the point for which the current density is calculated.

Although the oldest method, after the modern and efficient implementation of *Pulay et. al.*¹⁶⁰ the GIAO method became widespread. For benchmarking our ⁷⁷Se NMR shielding calculations we had to use data from the literature and because the GIAO method is the most widely-used procedure in previous investigations we also decided to use this method. Furthermore, GIAO is free of localization artifacts and appears to be less sensitive to basis set quality¹⁶¹. Adding to this, the method is more robust and also implemented to correlated wave functions in the Gaussian software package. Furthermore, our expectations of not

being able to perform MP2 calculations for the larger compounds being later confirmed (see later) and the good implementation of the GIAO approach with Density Functional Theory (DFT) methods, made the GIAO approach our method of choice.

Interestingly enough, *ab initio* calculations of shieldings are also a very convenient method of testing the “goodness” of newly developed basis sets by performing shielding calculations at various gauge origins. The gauge dependence of the computed shieldings that one sees in these series of calculations can be regarded as an artifact of the basis set used. It is important to note that the convergence observed for calculated shieldings with continuously increasing basis sets is extremely slow. As a result, the effort is on developing methods that would relax the basis sets requirements^{162,163}

Literature reports of benchmarking of NMR calculations mention the use of very large basis sets and recommendations tend to call for at least a triple-zeta basis set with a lot of diffuse and polarization functions. These basis sets are not very practical; nevertheless several basis sets were specially developed for NMR parameter calculations. Although the basis sets developed by *Pople et al.* are not recommended, addition of polarization and diffusion functions improves the results obtained with them. Better results were obtained using the IGLO II-IV basis sets developed by *Schindler and Kutzelnigg*^{156,164}. Also the TZP and QZP sets of *Ahlrichs et al.*¹⁶⁵, which are well suited for larger molecules, although being fairly small basis sets, give only small deviations from the estimated Hartree-Fock limit. The best results were, generally, observed when core-valence correlation consistent basis sets (cc-pVnZ) were used. But these basis sets are even larger and so, they are not an optimal choice for the larger systems that were the aim of our investigations.

Therefore we chose to perform the geometry optimizations and the calculation of vibrational frequencies for the conformational analysis using a more economical basis set and to calculate the NMR parameters using the TZVP basis sets of *Ahlrichs et al.* in the context of a single point calculation.

Recent theoretical calculations² proved that the family of *Dunning’s* correlation consistent basis sets cc-pVnZ¹⁶⁶ with high-quality and large-core effective core potentials (ECPs) representing the core electrons²⁶, are very well suited for quantitatively estimating different chalcogen–chalcogen interactions. However, they are not suited for the calculation of NMR parameters. Not only are they still too large for usage in conformational analysis of our model compounds, but also if the core electrons of a heavy atom are represented by an ECP, it is not possible to correctly predict the nuclear shielding for that nucleus, since the remaining basis functions will have incorrect behaviour at the nuclear position. It is mostly

the “tails” of the valence orbitals at the nucleus that influence the nuclear shielding, not the core orbitals themselves, since they are filled shells¹⁶⁷.

Another issue associated with calculations of NMR chemical shifts of heavier nuclei one has to consider is the influence of relativistic effects¹⁶⁸. In terms of computing absolute nuclear shieldings, the relativistic effects can be very large in heavy elements. It is recommended that for accurate calculations involving atoms beyond the first row of transition metals, relativistic effects have to be considered. Scalar relativistic increase of an average of 300 ppm in the case of ¹²⁵Te nuclear shieldings have been reported¹⁶⁹, but only an average of 63 ppm deviation in the case of ⁷⁷Se nuclear shielding in comparison with the experimental values¹⁷⁰. Since the relativistic effects are primarily associated with core orbitals that do not change much from one chemical environment to the other, the effect is strongly reduced by considering *relative* chemical shifts only. In this case a maximum change in the chemical shift of just 9 ppm was reported¹⁶⁹.

3.3.4.2 Conformational analysis of model compounds

As we intended to analyze the ability to calculate the ⁷⁷Se chemical shifts for the three model compounds (**24**, **29** and **33**) we synthesized, we had to perform a conformational analysis. For all three model compounds considered, we found four conformers. The geometries were optimized first at the density functional theory (DFT) level of the *Becke's* three-parameter hybrid functional¹³⁴ combined with the *Lee-Yang-Parr* correlation functional¹³⁵ using a basis set from *Pople/McLean-Chandler's* 6-311G family of basis sets¹⁷¹, with polarization and diffuse functions, as implemented in the Gaussian 03 software¹⁷². Taking in consideration that using the DFT level with the B3LYP functional is known to over-estimate hydrogen bonding, we refined the preliminary obtained geometries using the B98 hybrid functional¹⁷³. B98 is *Becke's* 1998 revision of one of his previous three parameter hybrid functionals, respectively the B97¹⁷⁴. Using the optimized geometries, the energies were calculated using the MP2 methods¹⁷⁵.

For all three cases, the conformers found have very similar energies, with energy differences less than 2 kcal/mol, between the most stable and the most unstable conformer.

Also, it could be observed that the same types of conformers were obtained in all cases. They are labeled as (*exo/endo*)_{H/X}. The *exo/endo* differentiation is based on the position of the substituents in relationship with the benzene ring (pointing towards or away from the

benzene ring), while the **H/X** labelling refers to the most significant intramolecular interactions observed.

The four conformers obtained for all three model compounds investigated present either predominant selenium-selenium interaction (being labelled with **(exo/endo)_X**) or significant selenium-hydrogen contacts (being labelled with **(exo/endo)_H**). The energy barriers for the equilibrium between the four conformers are very small, as depicted in the Figures 3.35., 3.37. and 3.39.

For compound **24**, considering that both substituents (methyl groups) have an electron donating character, the difference between the two most stable conformers is extremely low. It can also be observed that the two **endo_{X/H}** conformers are the more stable ones in comparison with the **exo_{X/H}** pair.

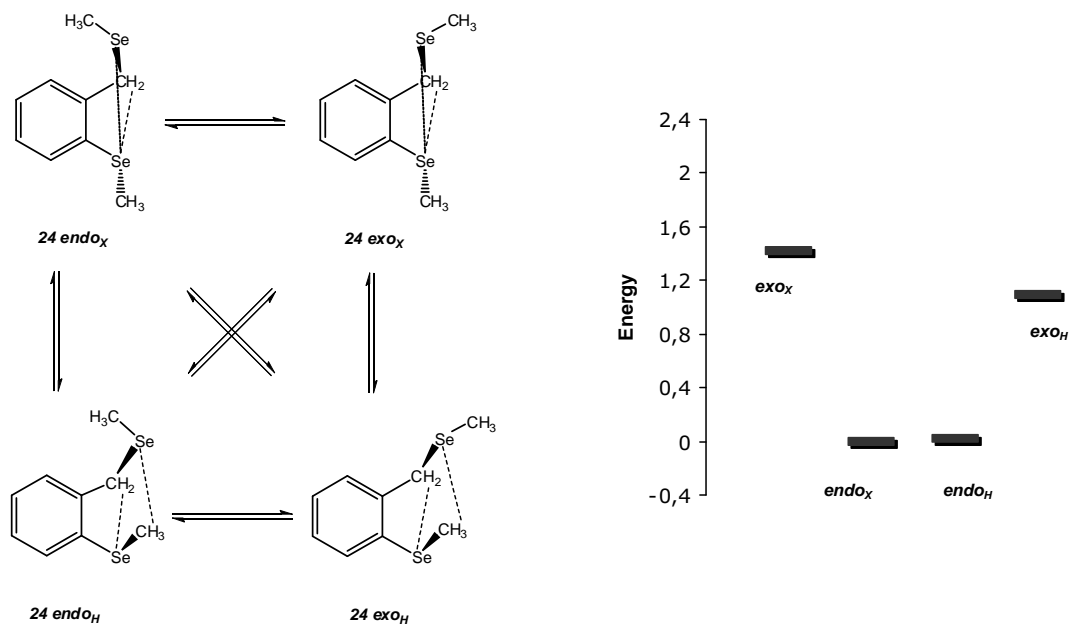


Figure 3.35. Equilibrium diagram for the conformers of compound **24** (left) and energy diagram for the relative energies of the expected conformers. Competing Se...Se (small dotted lines) and Se...H interactions (dashed lines) are depicted for each conformer.

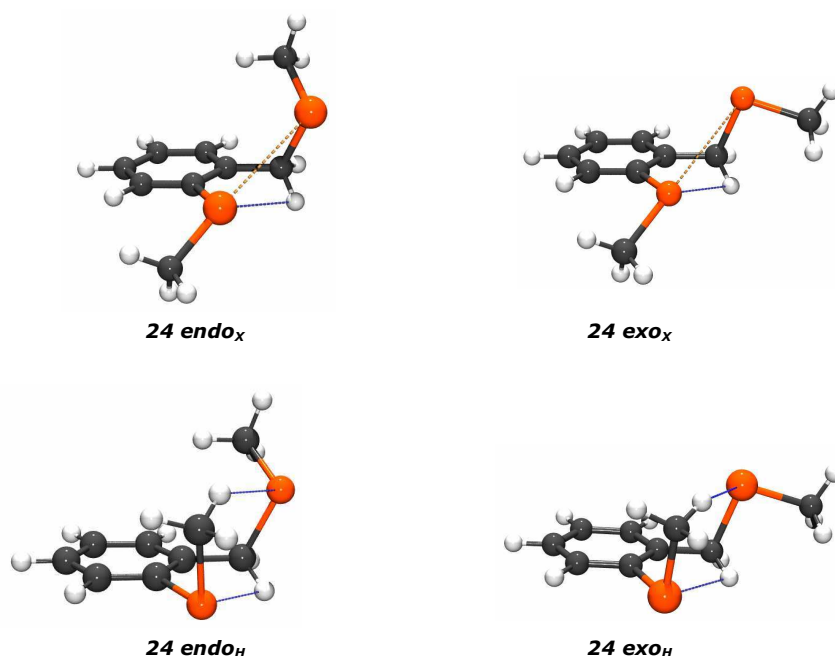


Figure 3.36. Calculated structures of the four conformers of compound **24**.

For the calculated lowest energy conformer (**24 endox**), the calculations predict short Se...Se distance of 371 pm and one weak Se...H bond, between one hydrogen atom of the benzyl fragment and the selenium atom of the methyl group (290 pm). For the **24 endoH** conformer, the one with the next lowest energy, two weak Se...H bonds with lengths of 289 and 317 pm, are the main stabilizing forces, while the Se...Se distance is calculated to be significantly larger than in the previous case amounting to 401 pm. In conformer **24 exox** (having the highest energy) the same two interactions as in **24 endox** were calculated. It is found for **24 endoH** that the Se...Se distance is larger (381 pm), while the Se...H bond with 282 pm in length is shorter, illustrating the competition between the two types of interaction. Similarly, in conformer **24 exoH** the Se...H bonds are shorter (278 pm, respectively 316 pm), while the Se...Se distance is even larger with a length of 434 pm (Figure 3.36.).

For compound **33**, the conformer with the calculated lowest energy **33 endoH** predicts two weak Se...H contacts, amounting for 289 pm and 326 pm. The Se...H bonds are the stabilizing forces for this conformer, but the Se...Se interaction also brings its contribution

to the stabilization. The Se...Se distance amounts to 390 pm, just slightly larger than the sum of the Van der Waals radii. For the **33** *endo_x* conformer, the Se...Se distance is shorter (382 pm), and only one weak Se...H contact, with a length of 288 pm is to be expected.

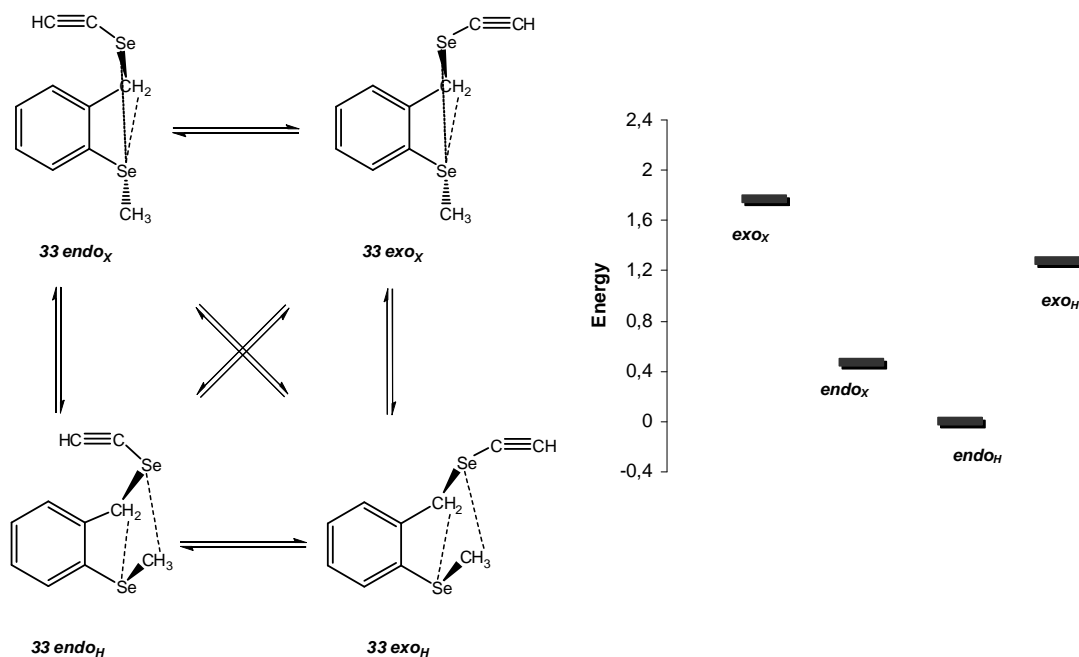


Figure 3.37. Equilibrium diagram for the conformers of compound **33** (left) and energy diagram for the relative energies of the expected conformers. Competing Se...Se (small dotted lines) and Se...H interactions (dashed lines) are depicted for each conformer.

Also in this case, the *exo_{H/X}* types of conformer are the less stable ones. For **33** *exo_H* the predicted two Se...H contacts are stronger than in **33** *endo_H* with lengths of 278 and 316 pm, while the Se...Se contact is weaker, the distance amounting to 433 pm. In the case of conformer **33** *exo_x* the predicted Se...Se distance is 388 pm, while the one weak Se...H contact amounts to 279 pm.

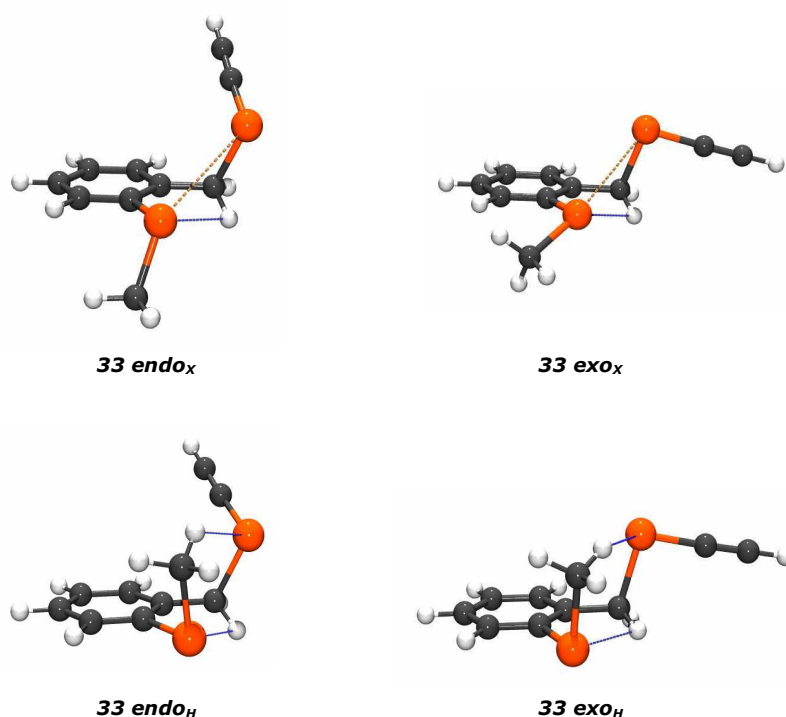


Figure 3.38. The four calculated stable conformers of compound **33**.

The calculated structure of lowest energy (**29 endo_H**), shows a short Se...Se distance (380 pm) and two weak Se...H bonds. One occurs between a hydrogen atom of the benzyl group and the Se atom of the SeCH₃ group (292 pm) and the other between one hydrogen of the methyl group and the Se atom of the SeCN group (336 pm). For structure **29 endox** one close Se...Se bond (386 pm) and one Se...H bond is predicted. The latter is formed between one benzylic hydrogen atom and the CH₃Se- group and amounts to 288 pm. In **29 exox**, the calculated structure with the highest energy, the same interactions as for conformer **29 endox** are expected, although the Se...Se contact is predicted to be slightly larger (389 pm), whereas the Se...H distance slightly smaller (278 pm). For conformer **29 exo_H**, as for **29 endo_H**, two Se...H bonds and one Se...Se weak contact have been predicted, and one can observe that in this case the Se...H bond lengths are smaller than in the case of **29 endo_H** (279 pm and 327 pm, respectively), while the Se...Se contact is very weak, amounting to 430 pm, thus confirming again the competitive nature between the non-bonding Se...Se and Se...H contacts.

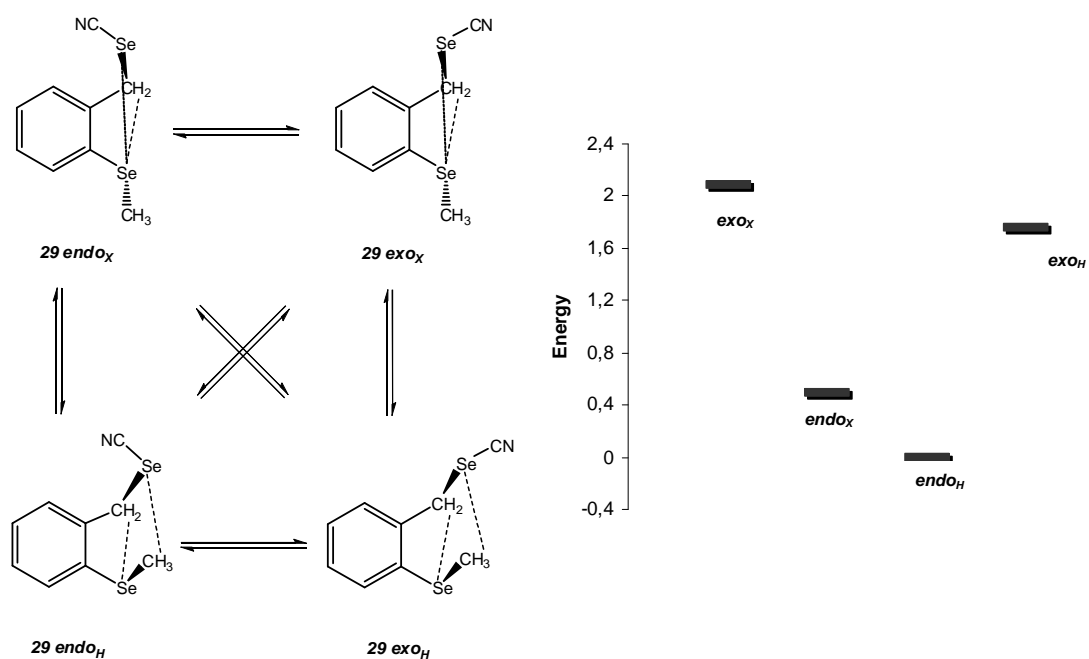


Figure 3.39. Equilibrium diagram for the conformers of compound **29** (left) and energy diagram for the relative energies of the expected conformers. Competing Se...Se (small dotted lines) and Se...H interactions (dashed lines) are depicted for each conformer.

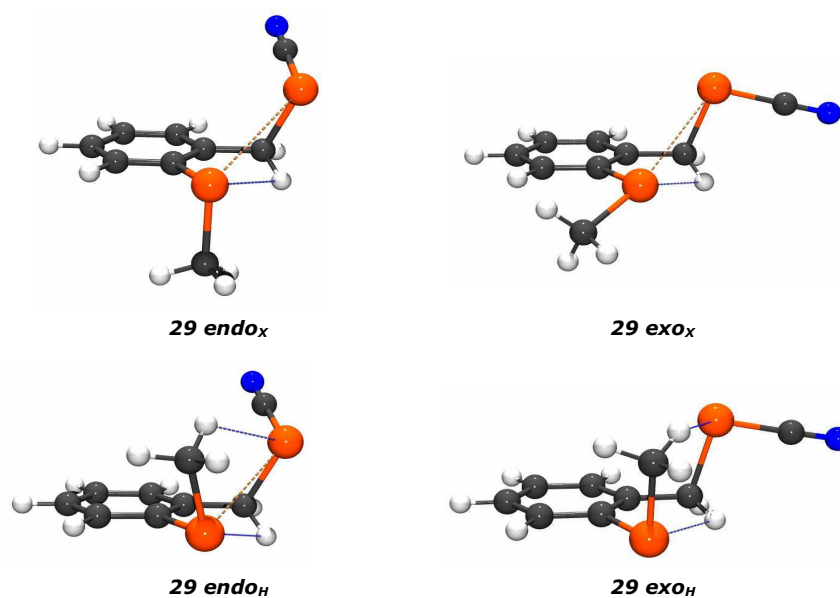


Figure 3.40. The four calculated stable conformers of compound **29**.

It is interesting to observe that although one would expect that the **endo_x** type of the conformer would be the most stable, it only holds true for the case of compound **24**. In the cases of **29** and **33**, the **endo_H** type is marginally more stable, although a stronger Se...Se interaction was experimentally observed. Considering the very small differences (of less than 0.5 kcal/mol), we assume that to be a result of the calculation methods used. Most probably, using a larger basis set or improved functionals would improve the quality of the predictions.

3.3.4.3 Calculations of ⁷⁷Se NMR chemical shifts

As NMR spectroscopy became an increasingly important tool in the study of intermolecular interactions, the *ab initio* calculations of NMR parameters of interacting atoms became much more common. It was driven forward especially because of the interest of understanding the behaviour of ligands interacting with proteins. Since the shielding property is very sensitive to both structure and environment, *ab initio* calculations can likewise be used to decipher the dependence of the shielding on the geometry of the molecule, as well as the intra- and intermolecular interactions present among molecules¹⁶².

Shielding is an extraordinary sensitive probe, and since it is electronic in origin, it can be influenced by factors that can induce a change in the electronic distribution of the molecule. For example, the internal motions which a molecule undergoes during the NMR experiment introduce averaging over the shielding values appropriate to each geometrical configuration sampled during the motion. Likewise, interactions among the molecules themselves can have a significant effect on the shielding property. Not only the experimentally observed shieldings (as chemical shifts), but also theoretical calculated shieldings offer important information referring to the molecule. Owing to its localized nature, shielding offers some advantages over other molecular electronic properties that pertain to the molecule as a whole (like the dipole moment or polarizability) as it offers specificity in location.

A number of calculations of ⁷⁷Se shielding constants and chemical shifts derived from theoretical investigations have been reported. In most of the cases, the performance of calculations for ⁷⁷Se nuclei is used as an important test for newly developed theoretical methods. *Buhl et al.* have performed calculations at the GIAO-SCF, GIAO-MP2¹⁷⁶ and GIAO-CCSD¹⁷⁷ levels of theory. *Magyarfalvi and Pulay*¹⁷⁸ carried out similar investigations with GIAO-SCF and GIAO-MP2 on a very similar set of selenium containing molecules. Both investigations concluded that correlated methods were necessary to give quantitative agreement with experimental values for the ⁷⁷Se chemical shifts. The most popular theoretical method of incorporating electron correlation effects into shielding calculations,

was however until now DFT. In DFT methods, electron exchange and correlation effects are taken into account by semiempirical functionals representing electron density. *Malkin et al.*¹⁷⁹ using their "Loc. 1" and "Loc. 2" approximations, as well as *Schreckenbach et al.*¹⁷⁰ demonstrated that it is possible to obtain results for chemical shifts that are superior to GIAO-SCF. *Wilson*¹⁸⁰ extended his previously developed empirical scheme WAH¹⁸¹ to selenium to obtain particularly accurate results. *Magyarfalvi and Pulay*¹⁶¹ applied a constant level shift to the virtual orbitals, obtaining significant improvement of the DFT results, concluding that the main error of currently used density functional theories with regard to magnetic shieldings is underestimation of the HOMO-LUMO gap, and not the omission of the current-dependent terms from the exchange-correlation functionals. Nevertheless, as it was pointed out by *Van Wüllen*¹⁸², one should always acknowledge that, manipulation of orbital energies leads to a loss of the strict gauge invariance. Lately, encouraging results were obtained by *Keal and Tozer*¹⁸³ using a new generalized gradient approximation functional (KT3)¹⁸⁴ and the LORG method for calculating nuclear shieldings. All these calculations are performed using very large basis sets and in most cases the DFT functionals are not yet available in usual computational chemistry software packages. In our case, considering that the goal was to perform magnetic shielding calculations on relatively large molecules, a benchmarking of the calculation method was necessary.

For benchmarking the calculation methods an admittedly small set of five small molecules (which appear almost always in the before mentioned studies) was optimized at the highest level of theory available, before calculating the nuclear shieldings of the ⁷⁷Se nuclei.

Optimized geometries for the five molecules were obtained at MP2 level of theory, using *Dunning's* correlation consistent triple-zeta basis set (cc-pVTZ)¹⁸⁵. The NMR shielding calculations were performed using the GIAO method at different levels of theory using the TVZP basis sets of *Ahlrichs et al.*¹⁶⁵. The results are presented in Table 3.9. and 3.10.

Table 3.9. ⁷⁷Se isotropic NMR shielding constants, in ppm, calculated at MP2 geometries. The absolute mean deviation $|d|$ is listed in the last entry (^a from lit.¹⁷⁷; ^b from lit.¹⁸⁶; ^c from lit.¹⁸⁷).

Method \ Compound	GIAO-HF-SCF	GIAO-B3LYP	GIAO-B98	GIAO-PBE	GIAO-MP2	GIAO-CCSD ^a	Expt. ^{b,c}
CH₃SeCH₃	1997.3	1754.2	1794.4	1835.6	1982.5	1873.6	1756±64
HSeH	2212.7	2120.4	2139.7	2172.5	2287.2	2207.4	2101±64
SeCO	2325.8	2272.8	2281.5	2293.8	2465.5	2352.6	2348±60
CSe₂	1574.4	1528.0	1545.3	1556.6	1857.1	1596.0	1544±80
CH₃SeH	2090.3	1918.3	1950.4	1987.9	2122.0	2028.0	1911±64
$ d _{\text{CCSD}}$	47.9	92.8	69.3	42.2	131.3		

It is interesting to observe that if one investigates the ^{77}Se NMR shieldings, acceptable results are obtained in Hartree-Fock (HF) calculations in comparison with the calculations done at high-levels of theory, like the couple cluster methods used by *Bühl et al.*¹⁷⁷. The DFT methods used have also interesting results. Although the hybrid functional of *Becke*¹³⁴ and *Lee, Yang and Parr*¹³⁵, known as B3LYP, is among the most popular functional of DFT calculations, it does not perform well when trying to calculate ^{77}Se magnetic shieldings. Significantly better results were obtained using *Becke's* B98 functional¹⁷³, as well as PBE, the hybrid functional of *Perdew, Burke and Ernzerhof*¹⁸⁹ which uses 25% exchange and 75% correlation weighting, as it can be observed from the decreasing values of the absolute mean deviation ($|d|_{\text{CCSD}}$) (see Table 3.9.) in comparison with the CCSD calculations. For the MP2 method, the absolute mean deviation value confirms the overestimation of correlation effects in calculating ^{77}Se shieldings, as already observed by *Bühl et al.*¹⁷⁶

Table 3.10. ^{77}Se chemical shifts, in ppm, calculated at MP2 geometries. The absolute mean deviation $|d|$ is listed in the last entry (^a from lit.¹⁷⁷; ^d From lit.^{112,188}).

Method Compound	GIAO- HF-SCF	GIAO- B3LYP	GIAO- B98	GIAO- PBE	GIAO- MP2	GIAO- CCSD ^a	Expt. ^d
CH₃SeCH₃	0.0	0.0	0.0	0.0	0.0	0.0	0
HSeH	-215.4	-366.2	-345.27	-336.93	-304.7	-333.8	-345
SeCO	-328.5	-518.6	-487.02	-458.23	-483	-479	-447
CSe₂	422.9	226.2	249.14	278.96	125.4	277.6	243
CH₃SeH	-92.96	-164.05	-155.91	-152.36	-139.51	-154.4	-155
$ d $	98.0	23.7	9.5	11.6	41.9	15.7	

If one considers the calculated ^{77}Se chemical shifts (see Table 3.10.), it can be concluded that the DFT methods are performing significantly better than the HF or MP2 methods. The absolute mean deviations from the experimental values are as small as 9.5 ppm in the case of GIAO-B98. This is a very small deviation considering the range of about 700 ppm of the ^{77}Se NMR chemical shifts of this set of molecules.

Comparing our results with the latest results of *Keal and Tozer*¹⁸³, we were surprised to observe that they obtained relatively larger absolute mean deviations ($|d|$) compared with the experimental results, even when using the same functional (as is the case for B3LYP) and a larger basis sets than in our study. The probable explanation is the fact that in our study the geometries were optimized at the MP2 level with smaller basis sets.

After benchmarking the methods for calculating ^{77}Se shieldings and concluding that the GIAO-B98 and GIAO-PBE are seemingly the best performers, we tested the methods on a “test” set of seven Se containing molecules, compounds that were also a part of our experimental NMR chemical shifts analysis.

Table 3.11. ^{77}Se chemical shifts, in ppm, calculated at MP2 geometries. The absolute mean deviation $|d|$ is listed in the last entry.

Compound \ Method	GIAO HF-SCF	GIAO-B3LYP	GIAO-B98	GIAO-PBE	GIAO-MP2	Expt. ^a
CH₃SeCH₃	0	0	0	0	0	0
C₆H₅SeCH₃ (22)	166	193.5	191.5	191.4	237	199
C₆H₅CH₂SeCH₃ (23)	122.2	144.9	142.6	142.6	-	171
C₆H₅SeCCH (31)	161.1	185.2	198.1	199	232	283
C₆H₅CH₂SeCCH (32)	231.7	253.8	259.2	258.9	-	245
C₆H₅SeCN (27)	254.7	231.7	254	253.6	279	318
C₆H₅CH₂SeCN (28)	305.4	300.1	309.1	307.3	-	289
$ d $	49.4	39.3	36.5	36.1	42.7	

The molecular geometries were optimized at the MP2 level of theory, using a combination of basis sets, for the Se and C atoms the cc-pVTZ basis set is preferred, while for the H atoms, a smaller 6-311g(d) basis sets was designated. The NMR shielding calculations were performed using *Ahlrichs's* TVZP basis set¹⁶⁵ with all methods.

Already here we reached the limit of computational power, for some of the compounds, although the geometries could be optimized, the NMR calculations at the MP2 level of theory could not be anymore performed. Once again, the best results were obtained when using the B98 and PBE functionals at the DFT level (see Table 3.11.). The absolute mean deviations from the experimental values were much larger in the case of the “testing” set of molecules in comparison with the “benchmarking” set.

These model studies revealed that a full geometry optimization at the MP2 level of theory for the targeted compounds **24**, **29**, and **33** was not possible. Therefore, we decided to test the performance of the DFT functionals starting from geometries optimized also at the DFT level of theory. Starting with geometries optimized at the DFT level, using the B3LYP functional and the 6-311+G(d) basis set, the NMR shieldings were again calculated using *Ahlrichs's* triple zeta TVZP basis set¹⁶⁵. The B3LYP, B98 and PBE functional were used. Surprisingly enough, the absolute mean deviations ($|d|$) in comparison with the

experimental values are smaller in this case (see Table 3.12.), when compared with the calculations that started from geometries optimized at the MP2 level.

Table 3.12. ^{77}Se chemical shifts, in ppm, calculated at B3LYP geometries. The absolute mean deviation $|d|$ is listed in the last entry.

Compound \ Method	GIAO-B3LYP*	GIAO-B98*	GIAO-PBE*	Expt.
CH₃SeCH₃	0	0	0	0
C₆H₅SeCH₃ (22)	221.8	219.2	217.7	199
C₆H₅CH₂SeCH₃ (23)	164.1	161.1	160.7	171
C₆H₅SeCCH (31)	190.2	204.6	209.0	283
C₆H₅CH₂SeCCH (32)	245.1	250.5	249.8	245
C₆H₅SeCN (27)	243.3	255.2	253.2	318
C₆H₅CH₂SeCN (28)	285.1	294.0	291.3	289
$ d $	33.5	30.3	29.1	

These results are very encouraging, if one considers that these are some of the largest molecules for which the ^{77}Se magnetic shielding constants and chemical shifts have been determined. The combination of DFT level optimized geometries and DFT level GIAO calculations of the nuclear shieldings using several functionals gave some of the best results, in comparison with experimental values.

Our investigations support the already known observation that the most widely-used DFT functional B3LYP, performs relatively poor in comparison with other functionals, even with ones that are already fully implemented in commercially available software packages like Gaussian 03¹⁷².

The geometries for compounds **24**, **29** and **33** were already optimized at various levels for the previously presented conformational analysis. Using the geometries optimized at the B98/6-311+G(d) level of theory, the NMR shielding calculations were performed using Ahlrichs's triple zeta TVZP basis set¹⁶⁵. The chemical shifts were calculated by referencing the shielding values to the shielding value calculated for dimethyl selenide (CH₃SeCH₃) at the same level of theory for both geometry optimization and magnetic shielding calculation (see Table 3.13.).

Table 3.13. Calculated isotropic ^{77}Se nuclear shieldings and chemical shifts for compound **24**, in ppm, at the B98 optimized geometries. The upper line for each conformer refers to the SeCH_3 center and the lower one to the benzylic Se center.

Method Conformer	GIAO-B3LYP		GIAO-B98		GIAO-PBE	
	Shielding	Chem.shift	Shielding	Chem.shift	Shielding	Chem.shift
endo_X	1573.2858	114.9	1612.2263	119.4	1651.2923	122.7
	1493.1304	195.1	1539.2377	192.4	1582.4302	191.5
endo_H	1559.5913	128.6	1602.0998	129.5	1644.4867	129.5
	1467.1299	221.1	1514.6435	217.0	1558.3268	215.6
exo_X	1566.9319	121.3	1605.8635	125.8	1645.3931	128.6
	1551.6643	136.6	1596.5730	135.0	1639.1277	134.8
exo_H	1540.7679	147.5	1583.6350	148.0	1627.2229	146.7
	1523.2156	165.0	1569.5241	162.1	1612.6416	161.3

For all four conformers of **24** (see Table 3.13.), the NMR shielding calculations predict an up-field shift of the chemical shift for the ^{77}Se nuclei, in comparison with the smaller compounds **22** and **23**. The values for the chemical shifts vary significantly between the conformers illustrating the sensitive nature of the NMR shielding property to its environment. The amount of up-field shifts predicted also vary from only a few ppm, up to almost 50 ppm, but interestingly enough it is always an up-field shift predicted regardless of the geometry of the conformer considered. This is in accordance with our experimental results, in which we observed an up-field shift for both ^{77}Se nuclei chemical shifts of **24** in comparison with the corresponding values for the ^{77}Se nuclei from compounds **22** and **23**.

Unexpected, the best agreement between calculated and experimental values (158.9 ppm for the benzylic Se nuclei and 161 ppm for the SeCH_3 group) is observed in the case of the **24 exo_H** conformer, for all three functionals used, with a slightly better performance for the B98 and the PBE functional. For the conformers of **24** we already determined a flat potential energy surface (see Figure 3.35 left). Both observations might suggest that in solution the favored conformer is the one in which the weak $\text{Se}\cdots\text{H}$ have the strongest effect.

Table 3.14. Calculated isotropic ^{77}Se nuclear shieldings and chemical shifts for compound **33**, in ppm, at the B98 optimized geometries. The upper line for each conformer refers to the SeCH_3 center and the lower one to the benzylic Se center.

Method Conformer	GIAO-B3LYP		GIAO-B98		GIAO-PBE	
	Shielding	Chem.shift	Shielding	Chem.shift	Shielding	Chem.shift
endo_X	1579.8613	108.4	1621.1111	110.5	1663.5840	110.4
	1434.7636	253.5	1472.7300	258.9	1515.7199	258.2
endo_H	1573.6711	114.6	1614.8443	116.8	1657.2344	116.7
	1457.3071	230.9	1494.7265	236.9	1537.8187	236.2
exo_X	1560.2110	128.0	1598.1019	133.5	1637.0447	136.9
	1568.9284	119.3	1604.0724	127.5	1643.7183	130.3
exo_H	1536.3942	151.8	1579.4086	152.2	1623.3433	150.6
	1541.0749	147.2	1577.1555	154.5	1617.1030	156.9

In the case of compound **33**, the best agreement between calculated and experimental values was obtained for the two most stable conformers the **endo_{X/H}** type (see Table 3.14.). Encouraging, in this case the best prediction is obtained using the GIAO-B98 and GIAO-PBE methods for the **33 endo_H** conformer, which is also the most stable one of all four conformers. Again, a high-field shift is predicted in comparison with the respective ^{77}Se chemical shift from compounds **32** and **22**. Comparing the calculated values for the ^{77}Se chemical shifts with the experimental ones (157.5 ppm for the SeCH_3 group and 238.3 ppm for the benzylic Se nuclei) one may conclude that also in the case of compound **33**, the most favored conformer in solution is probably the **33 endo_H** conformer. For the cases of **exo_{X/H}** type of conformers, the ^{77}Se chemical shift of the SeCH_3 group is more accurately predicted, but the errors for the second Se atom are very large, with deviations of up to almost 100 ppm. These findings confirm the preference for the **endo_{X/H}** type of conformers.

Table 3.15. illustrates the isotropic nuclear shieldings calculated for the conformers of compound **29**. The same trends as for compound **33** are to be observed here. The values predicted for **endo_{X/H}** type of conformers agree best with the measured chemical shifts of 157.3 ppm for the SeCH_3 group and 283 ppm for the SeCN group. The predicted values of the **exo_{X/H}** type conformer for the Se nuclei of the SeCH_3 group are more accurate, but the large errors in predicting the Se nuclei of the SeCN group make on average the prediction of the **endo_{X/H}** conformers more accurate. In this case, for the most stable conformer **29 endo_H** the predicted NMR chemical shifts are only marginally better than for the **29 endo_X**, the closest in energy conformer.

Table 3.15. Calculated isotropic ^{77}Se nuclear shieldings and chemical shifts for compound **29**, in ppm, at the B98 optimized geometries. The upper line for each conformer refers to the SeCH_3 center and the lower one to the benzylic Se center.

Method Conformer	GIAO-B3LYP		GIAO-B98		GIAO-PBE	
	Shielding	Chem.shift	Shielding	Chem.shift	Shielding	Chem.shift
endo_x	1578.7493	109.5	1620.3064	111.3	1663.0082	111.0
	1402.8878	285.3	1436.7384	294.9	1481.5705	292.4
endo_H	1583.1538	105.1	1624.4776	107.1	1665.9973	108.0
	1420.2273	268.0	1453.7468	277.9	1498.9027	275.1
exo_x	1552.5932	135.6	1590.1497	141.5	1628.6427	145.3
	1559.6834	128.6	1590.3534	141.3	1630.5429	143.4
exo_H	1538.0259	150.2	1580.8058	150.8	1624.7303	149.2
	1535.2192	153.0	1566.5720	165.0	1606.7098	167.3

It is interesting to observe that the solid-state structure of compound **29**, as previously described in Chapter 3.3.3.1.1., looks to be in between the **29 endo_x** and **29 endo_H** conformers. Thus, it confirms our previous observation that although present and relatively strong in solution, as proven by the long range $J_{\text{Se,Se}}$ couplings, the $\text{Se}\cdots\text{Se}$ interactions are weaker than the competing $\text{Se}\cdots\text{H}$ bonding. However, in the solid-state, the $\text{Se}\cdots\text{Se}$ interaction contribution to the stabilization of the structures seems to prevail.

Further investigations would certainly provide more understanding of the $\text{Se}\cdots\text{Se}$ interactions and generally into chalcogen–chalcogen interactions. For the $\text{Se}\cdots\text{Se}$ interaction, the ^{77}Se NMR shielding constants and chemical shifts are promising probes. While better functionals are becoming available and wider used, computational power is increasing, therefore there are good prospects of accurately being able to compute nuclear shieldings, maybe even taking in consideration solvent effect, or in a later stage, computing coupling constants.

4. Outlook

4.1 Syntheses

4.1.1 Selenium containing cycles with larger inner cavities

Synthetically we obtained three interesting isomeric tetraselena-[6.6]cyclophanes, containing aromatic rings as building block, which confirmed the assumption that the introduction of the aromatic rings will open the opportunity for further stabilization based on π - π interactions.

These cyclophanes obtained through a two-component coupling generate columnar structures in all three cases, but their internal cavities proved to be small. Another problem encountered refers to the insolubility of the resulting cyclophanes. Previous synthetic work of Fischer⁹⁷ by-passed this problem by using aromatic rings substituted with long alkylic chains. Positioning the aromatic ring between two alkyne units, while the Se centers are connected through an alkylic chain has the disadvantage that the substituents of the benzene rings, intrude into the cavity.

Therefore, replacing the alkylic chain with a xylene-type fragment could present some advantages in generating columnar structures with larger cavities, either through a two-component coupling reaction and even better through a three-component coupling. For this purpose, an *ortho*- or *meta*-xylene bis-selena fragment would be more suitable than their *para*-xylene isomer. Also by using different substituents on the aromatic ring the solubility of the desired compounds could be improved, without the risk of the substituents blocking the internal cavity (Figure 4.1.). Even more, the properties of the columnar structures thus generated could be controlled. Based on the substituents of the aromatic rings used, the external side of the tubular construction could be made hydrophobic or hydrophilic.

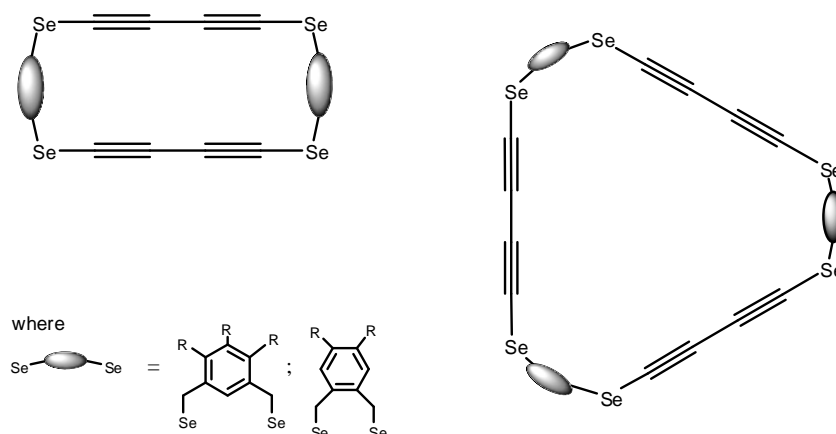
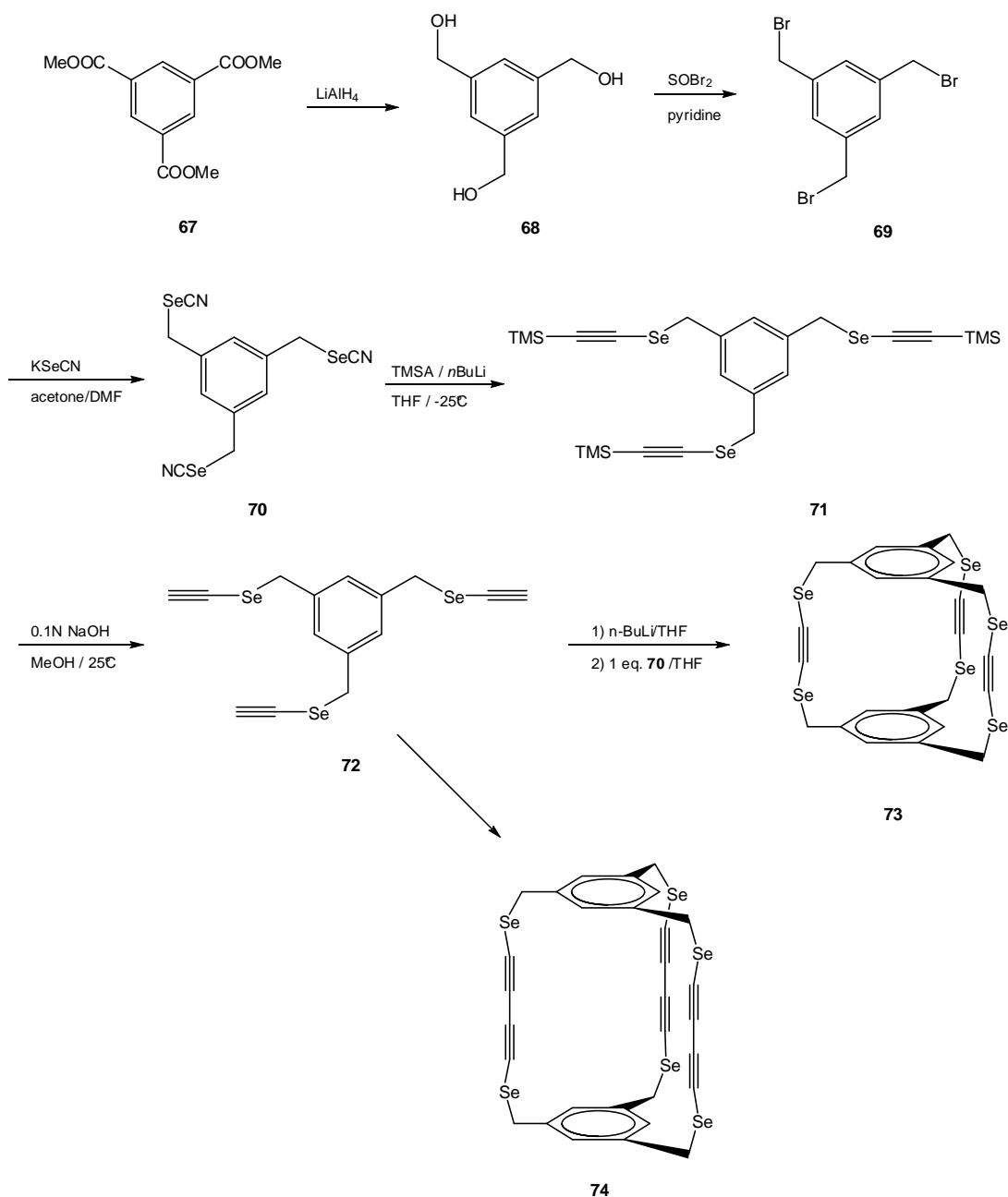


Figure 4.1. Model compounds with larger inner cavities.

4.1.2 Cage molecules

Another interesting synthetic goal would be to generate cage molecules based on diselenium alkyne (as in **73**) or diselenium dialkyne (as in **74**) units, which could be synthesized based on a similar procedure, starting from trimethyl benzene-1,3,5-tricarboxylate (**67**).



Scheme 4.1. Suggested synthetic approach for obtaining the selenium containing cage molecules **73** and **74**.

The bottle-neck of this synthesis could nevertheless lay in purifying the intermediate 1,3,5-tris(selenocyanatomethyl)benzene (**70**) and in the final coupling reactions.

4.2 NMR investigations

^{77}Se chemical shifts and ^{77}Se - ^{77}Se coupling constants are excellent measures to investigate the interactions between divalent selenium atoms. Although the high field shift of the ^{77}Se signal illustrated a trend that could be interpreted in relation with other known data from literature, more insight was gained from investigating the coupling constants. Nevertheless, the coupling mechanisms involved can not be completely assigned to the through-bond or the through-space types. Probably, an interesting option to consider would be to measure the long-range $J_{\text{Se,Se}}$ in a weakly anisotropic liquid solution, that would enable determination of *residual dipolar couplings* (RDCs). These provide information about the direct dipole-dipole interaction between the two Se spins, information that is usually averaged out in isotropic liquids.

T_1 relaxation measurements of the ^{77}Se signal did not provide a very clear picture, therefore it might be useful to investigate the T_1 relaxation time dependence with regard to the strength of the magnetic field. As it was shown by *Wong et al.*¹⁹⁰ the Se longitudinal (spin-lattice) relaxation has a significant *chemical shift anisotropy* (CSA) mechanism part, in addition to the *spin-rotation mechanism* (SR – caused by fast molecular or segmental motion) and the *dipole-dipole interaction* (DD) associated with the nuclear Overhauser effect (NOE)^{111,112}. Building on the understanding of the longitudinal relaxation times of ^{77}Se nuclei, the investigation could be pushed forward to measurements of heteronuclear Overhauser effects between Se and H atoms in the small model compounds already synthesized and to new molecules. These types of experiments would provide information regarding Se-H interactions and the correlation with the long range Se-Se couplings would allow an easier evaluation of the competition between Se···Se and Se-H interactions in the liquid-state. Furthermore, evaluating the Se-H distances would also clarify the conformational preference of the model compounds in liquids, completing thus the picture obtained through the theoretical conformational analysis.

4.3 Theoretical calculations of NMR parameters

Last, but not least, further implementation of new computational chemistry methods which would reduce the computational time would be more than welcomed in our quest for making a more exact comparison between experimentally obtained informations and theoretically calculated ones. An interesting method that is receiving attention lately is the ***linear scaling method*** of *Ochsenfeld et al.*¹⁹¹, with which NMR spectra for molecular

systems with more than a thousand atoms were calculated. Calculating ^{77}Se NMR parameters at the MP2 level of theory with such a method would initially be a good test for the applicability of the method, and would later allow to determine better NMR parameters and thus give the opportunity to interpret better the experimentally obtained results. In the future, theoretical calculations of spin-spin couplings¹⁹² which are now limited to molecules with only a few atoms, would allow a much better understanding of the selenium – selenium interactions and the possible ways in which they can be “manipulated” to obtain new materials with special electronic properties.

5. Preparative procedures

5.1 General considerations

Due to high sensitivity to air and humidity, all reactions were carried out in special treated equipment which was two to three times evacuated by an oil pump, heated up to 150°C and fluted with anhydrous argon. A three-way bubbler filled with paraffin oil served as a device for the pressure balance during reaction under protecting gas. For those reactions that are not sensitive to air or humidity a standard glass tube filled with drying gel was the first choice. The used solvents were dried and degassed under argon atmosphere according to standard methods. These procedures for absorption and degassing of the solvents were done as shortly before use as possible. As reaction vessels, three necked flasks with magnetic stirring were usually used. In the case that a solution containing a metallorganic reagent was added this was done with a syringe through one of the necks which was closed by a thin rubber lid.

Thin layer chromatography: Polygram-DC-micro cards from the company Macherey-Nagel (silica gel: SIL G/UV₂₅₄, 0.20 mm) were the standard application. The detection occurred using UV light at 254 nm and/or dyeing the cards with iodide vapors. The mentioned R_f values are referring to smallest concentration of substances possible; at higher concentration different R_f values can be expected.

Column chromatography: As stationary phase for column chromatographic separations, MN silica gel 60 from the company Macherey-Nagel (0.04-0.063 mm, 230-400 mesh ASTM for column chromatography) was the standard application. Unless otherwise stated, the silica gel was deactivated with 3% (vol.) triethylamine (NEt_3).

Gas chromatography: The GC samples were measured using a HP 59970 CD GC/MS-MSD workstation (separation column: HP-5, 30 m, transport gas: He). The control application with a given starting temperature (ST) of 60° is configured in the following way: 3 min isotherm at the ST, then the temperature was increased for 10°C/min till the end temperature (ET) was reached at 250°C, depending on the sample staying isotherm at ET for some minutes, to give an experimental total time between 32 to 45 minutes.

Nuclear Magnetic Resonance Spectroscopy: The NMR spectra were measured using the following NMR spectrometers:

¹ H-NMR:	250 MHz	Bruker AS 250
	300 MHz	Bruker Avance 300
	500 MHz	Bruker Avance 500
¹³ C-NMR:	75 MHz	Bruker Avance 300
	125 MHz	Bruker Avance 500
⁷⁷ Se-NMR:	95 MHz	Bruker Avance 500

At the ¹H-NMR- and ¹³C-NMR-spectra the prevailing solvents were used as the internal standards. Referencing in the ⁷⁷Se-NMR-spectra was done using the standardized scale δ , in accordance with the IUPAC-reference 2001¹⁹³. ¹³C-NMR spectra were measured using ¹H decoupling. Information regarding the multiplicity of ¹³C-NMR signals was (if necessary) obtained from DEPT-135 experiments. The signals were assigned as exact as possible, the necessary information being extracted from gs-COSY¹⁹⁴, gs-HMQC¹⁹⁵ and gs-HMBC¹⁹⁶ spectra. For complete assignment of the Se signals, standard versions of gs-HMQC and gs-HMBC experiments were modified to afford Se-H correlations, according to gradient selection rules¹⁹⁷. Unless otherwise stated, the NMR measurements were done at room temperature. Long range Se-Se coupling constants were measured from the natural abundance satellites in the ⁷⁷Se NMR spectra when possible, or from a heteronuclear proton decoupled correlation experiment¹⁵³.

Abbreviations:	¹ H-NMR	¹³ C-NMR
	s – singlet	p – primary C atom
	d – doublet	s – secondary C atom
	t – triplet	t – tertiary C atom
	q – quartet	q – quaternary C atom
	dd – doublet of doublets	
	dt – doublet of triplets	
	m – multiplet	
	p – pseudo-...	
	b – broad signal	

UV Spectra: The UV/VIS spectra were recorded on a Hewlett-Packard HP 8452A Diode-Array-Spectrometer. The solvent and the concentrations are stated in the brackets.

IR Spectra: The IR spectra were measured using a Bruker Vector 22-FT-IR-Spectrometer. Solvents or matrix used are presented in brackets. Only the most intensive or characteristic

wavelengths are indicated. The relative intensities are characterized by the following abbreviations:

(vs)	very strong	(s)	strong
(m)	medium	(w)	weak
(b)	broad		

Mass Spectra: The EI and FAB mass spectra were recorded at a JEOL JMS-700 (Jeol, Tokyo, Japan) double-focusing reversed-geometry magnetic sector instrument. Ionization was done by electron impact (70 eV) and for the FAB measurements 2-nitrobenzol served as matrix. On the same device were measured the high-resolution mass spectra (HR-MS). The LIFDI measurements were performed on the same JEOL JMS-700 instrument, admitting toluene from the reservoir inlet to the ion source for tuning and field ionized. The unmodified manufacturer's FD/FI ion source was kept at 80 °C; the emitter potential was 11.0-11.5 kV. Indicated are: ionisation method, mole peak and characteristic fragments. Only peaks with higher relative intensities as the molecular peak and $m/z > 50$ are indicated. The following abbreviations were used: M = mole peak, BP = basis peak.

Melting points: Uncorrected melting points were measured in an opened capillary using a Dr. Tottoli melting point apparatus from Büchi, Swiss Company.

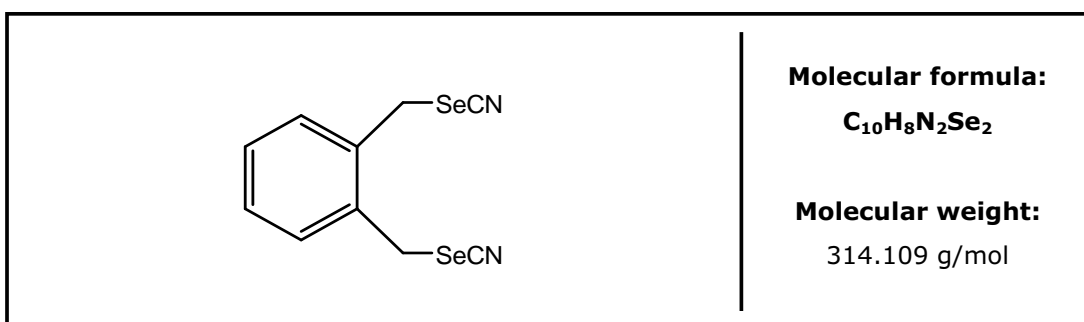
X-ray spectrometry: The X-ray spectrometric investigations were performed by Dr. Frank Rominger on a Bruker Smart CCD system and by Dr. Thomas Oeser on a Bruker Smart Apex system. In all cases a MoK α radiation source was used ($\lambda_1=0.71073$ Å). Diffraction intensities were corrected for Lorentz and polarization effects and an empirical absorption correction was applied using SADABS¹⁹⁸ based on the Laue symmetry of the reciprocal space. Heavy atoms diffractions were solved by direct methods and refined against F2 with a full-matrix least square algorithm. Hydrogen atoms were either isotropically refined or introduced into the models at calculated positions. The structures were solved and refined using the SHELXTL software package¹⁹⁹. For the analysis of the results and depiction of the solid-state structures, WinOrtep²⁰⁰ and Mercury²⁰¹ software packages were used.

5.2 Preparation of tetraselenadiynes cyclophanes

5.2.1 General procedure for preparation of the bis(selenocyanatomethyl)-benzenes

To a stirred solution of dibromoxylene in 200 mL of degassed dry acetone a solution of KSeCN in 200 ml degassed acetone was added dropwise under argon atmosphere at room temperature over a period of 3 h. The reaction mixture was stirred for an additional hour and the resulting KBr was filtered off. The solvent was removed by rotary evaporation and the product was purified by column chromatography on deactivated silica or if the purity of the raw product was determined by NMR spectroscopy to be over 98%, it was used without further purification⁹⁵.

5.2.1.1 1,2-bis(selenocyanatomethyl)-benzene (**15a**)



Materials:

10.56 g	(40.0mmol)	1,2-bis-bromomethylbenzene (14a)
14.4 g	(100 mmol)	potassium selenocyanate (KSeCN)
400 ml		acetone (solvent)

Experimental procedure:

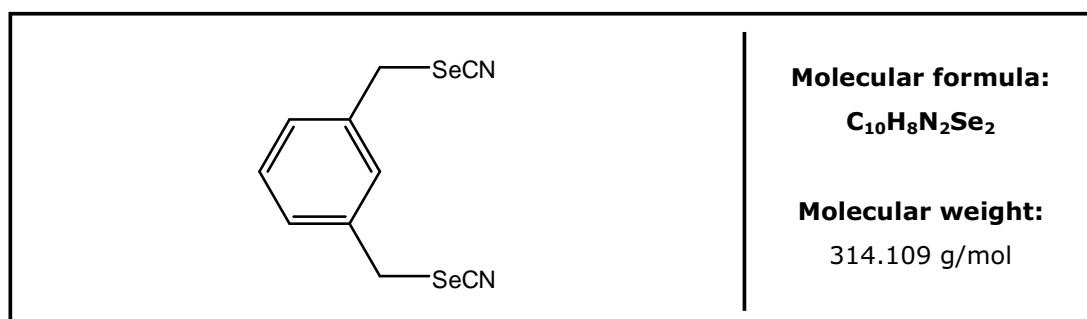
The experimental procedure followed as described in section 5.2.1. Purification by silica-gel column chromatography using a mixture of *n*-hexane / diethyl ether (1:2), resulted in 11.24 g of 1,2-bis(selenacyanatomethyl)-benzene (**15a**).

Yield 11.24 g (35.8 mmols) 89%

Habitus white thin needles

m.p.	106°C
TLC	R _f value 0.34 <i>n</i> -hexane / diethyl ether (1:2)
GC	R _t = 20.19 min
MS	(EI ⁺ ; m/z; %): 314 [M] ⁺ (0.9); 263.9 [C ₈ H ₈ Se ₂] ⁺ (7.8); 209.9 [M-SeCN] ⁺ (52.8); 182.9 [C ₈ H ₈ Se] ⁺ (28.4); 104 [C ₈ H ₈] ⁺ (BP, 100); 78 [C ₆ H ₆] ⁺ (18.2)
¹H-NMR	(500MHz, CD ₂ Cl ₂) δ=4.42 (s, 4H, CH ₂ , ² J _{Se,H} = 15.0 Hz); δ=7.39–7.40 (m, 4H, H _{arom}).
¹³C-NMR	(125MHz, acetone-d ₆): δ=28.9 (2C, s-CH ₂ , ¹ J _{Se,C} =48.5 Hz); δ=101.5 (2C, q-SeCN); δ=130.0 (2C, t-C _{arom}); δ=131.9 (2C, t-C _{arom}); δ=134.5 (2C, q-C _{arom}).
⁷⁷Se-NMR	(95 MHz, acetone-d ₆): δ=302.3.
IR	(KBr, cm ⁻¹): 3442 (vb); 3007 (w); 2148 (s); 2073 (m); 1630 (w); 1491 (m); 1451 (m); 1299 (w); 1210 (w); 1194 (m); 1177 (m); 1068 (m); 1042 (m); 852 (s); 775 (w); 596 (s); 541 (w); 515 (m).
UV	(c = 0.085 mg/ml in CH ₂ Cl ₂): λ = 278 nm; log ε = 3.35; ε = 2216 l/(mol·cm); extinction = 0.06 λ = 248 nm; log ε = 4.09; ε = 12191 l/(mol·cm); extinction = 0.33

5.2.1.2 1,3-bis(selenocyanatomethyl)-benzene (**15b**)



Materials:

5.28 g (20.0 mmol) 1,3-bis-bromomethylbenzene (**14b**)

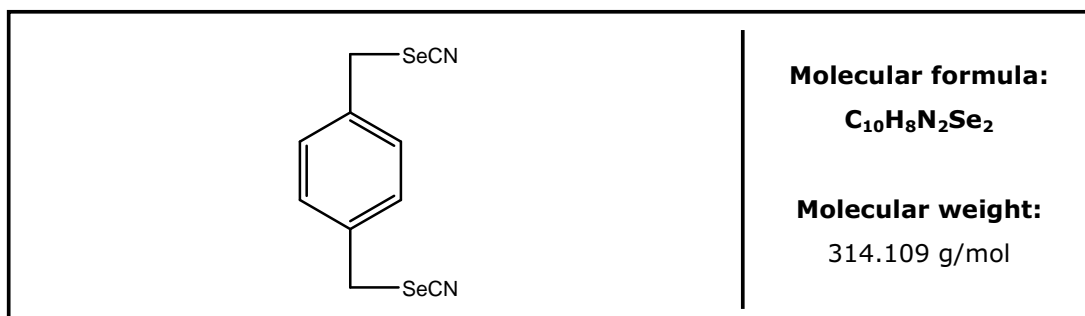
Preparative procedures

8.75 g (60.8 mmol) potassium selenocyanate (KSeCN)
400 ml degassed acetone.

Experimental procedure:

The experimental procedure followed as described in section 5.2.1. Purification by silica-gel column chromatography using a mixture of *n*-hexane / diethyl ether (1:2), resulted in 4.20 g of 1,3-bis(selenocyanatomethyl)-benzene (**15b**).

Yield	4.206 g	(13.4 mmols)	67%
Habitus	white solid		
m.p.	108°C		
TLC	R _f -value	0.32	<i>n</i> -hexane / diethyl ether (1:2)
GC	R _t = 26.15 min		
MS	(EI ⁺ ; m/z; %): 314 [M] ⁺ (0.9); 210 [M-SeCN] ⁺ (37.8); 116 [M-2SeCN] ⁺ (62.2); 104 [M-C ₈ H ₈] ⁺ (BP, 100); 78 [C ₆ H ₆] ⁺ (26.2); 51 [M-C ₄ H ₃] ⁺ (19.2).		
¹H-NMR	(500 MHz, CD ₂ Cl ₂): δ=4.29 (s, 1H, CH ₂ , ² J _{Se,H} = 16.2 Hz); δ=7.35 (s, 1H, H _{arom}); δ=7.37- 7.39 (d, 2H, H _{arom}); δ=7.41 (t, 1H, H _{arom})		
¹³C-NMR	(125 MHz, CD ₂ Cl ₂): δ=32.56 (2C, s-CH ₂ , ¹ J _{Se,C} =48.9 Hz); δ=101.53 (2C, t-CN); δ=129.18 (2C, t-C _{arom}); δ=129.50 (1C, t-C _{arom}); δ=129.78 (1C, t-C _{arom}); δ=137.10 (2 C, q-C _{arom})		
⁷⁷Se-NMR	(95 MHz, CD ₂ Cl ₂): δ=294.6.		
UV	(c = 0.167 mg/ml in CH ₂ Cl ₂): λ = 240 nm; log ε = 4.12; ε = 13083 l/(mol·cm); extinction = 0.5 λ = 246 nm; log ε = 3.96; ε = 9158 l/(mol·cm); extinction = 0.35 λ = 272 nm; log ε = 2.89; ε = 785 l/(mol·cm); extinction = 0.03		
IR	(KBr, cm ⁻¹): 3444 (s); 2151 (s); 1630 (m); 1486 (w); 1444 (m); 1255 (w); 1199 (s); 1160 (w); 1127 (w); 1081 (w); 894 (w); 845 (w); 803 (m); 746 (w); 699 (m); 578 (m); 541 (w); 513 (m).		

5.2.1.3 1,4-bis(selenocyanatomethyl)-benzene (15c)**Materials:**

6.60 g	(25.00 mmol)	1,4-bis-bromomethyl-benzene (14c)
10.80 g	(74.96 mmol)	potassium selenocyanate (KSeCN)
400 ml		degassed acetone.

Experimental procedure:

The experimental procedure followed as described in section 5.2.1. Purification by silica-gel column chromatography using a mixture of *n*-hexane / diethyl ether (1:2), resulted in 7.5 g of 1,4-bis(selenocyanatomethyl)-benzene (**15c**).

Yield 7.47 g (23.78 mmol) 95.1 %

Habitus pale yellow crystals

m.p. 138°C

TLC R_F-value 0.32 dichloromethane

GC R_t = 27.02 min

MS (EI⁺; m/z; %): 316 [M]⁺ (8.3); 210 [M-SeCN]⁺ (74.8); 182 [C₈H₈Se]⁺ (4.2); 104 [C₈H₈]⁺ (BP, 100); 78 [C₆H₆]⁺ (7.2).

¹H-NMR (500 MHz, acetone-d₆): δ=4.44 (s, 4H, CH₂, ²J_{Se,H}= 16.3 Hz); δ=7.46 (s, 4H, H_{arom}).

¹³C-NMR (125 MHz, acetone-d₆): δ=31.81 (2C, s-CH₂); δ=102.21 (2C, q-SeC); δ=129.36 (4C, t-C_{arom}); δ=137.80 (2C, q-C_{arom}).

$^{77}\text{Se-NMR}$ (95 MHz, acetone- d_6): $\delta=307.1$.

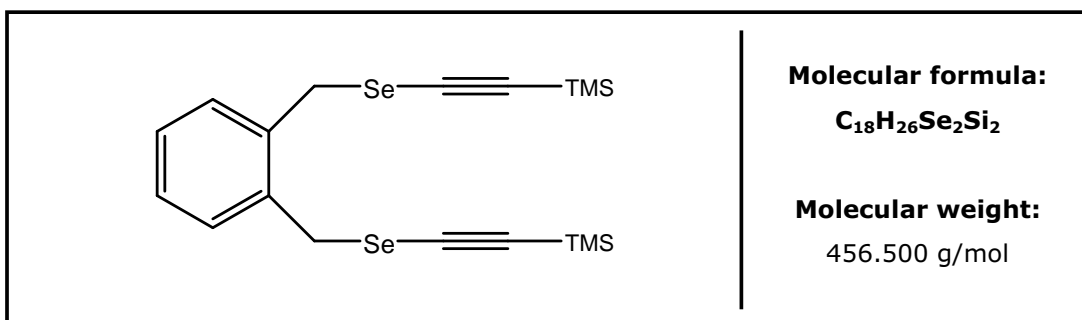
IR (KBr, cm^{-1}): : 3428 (b); 3048 (w); 3013 (w); 2955 (w); 2147 (s); 2073 (s); 1630 (m); 1509 (m); 1425 (m); 1225 (m); 1190 (m); 1130 (w); 1092 (m); 1018 (w); 851 (m); 837 (m); 754 (w); 604 (s); 516 (m).

UV ($c = 0.136 \text{ mg/ml}$ in CH_2Cl_2):
 $\lambda = 283 \text{ nm}$; $\log \epsilon = 3.48$; $\epsilon = 3001 \text{ l}/(\text{mol}\cdot\text{cm})$; extinction = 0.13
 $\lambda = 248 \text{ nm}$; $\log \epsilon = 4.24$; $\epsilon = 17547 \text{ l}/(\text{mol}\cdot\text{cm})$; extinction = 0.76

5.2.2 General procedure for preparation of the bis(trimethylsilyl)-diselenaalkadiynes⁹³

In a four-necked flask, trimethylsilylacetylene (TMSA) was dissolved in dry THF at -35°C . At this temperature a solution of *n*-butyllithium in *n*-hexane was added dropwise over a period of 20 minutes by using a syringe. Then the solution was stirred under the same conditions for two hours. The diselenocyanatoxylylene dissolved in anhydrous THF was added dropwise over a period of 45 minutes at -35°C . After stirring for one hour at this temperature the mixture was allowed to warm up to room temperature. 50 ml of saturated NH_4Cl solution and 100 ml *n*-hexane were added. The aqueous layer was separated and extracted four times with *n*-hexane. After combining the organic layers the mixture was dried over MgSO_4 overnight. The mixture was filtrated, the solvent evaporated and the resulting product was purified by silica-gel column chromatography.

5.2.2.1 1,2-bis(((trimethylsilyl)ethynyl)selenyl)methylbenzene (**16a**)



Materials:

6.3 g (20 mmol) 1,2-bis(selenocyanatomethyl)-benzene (**15a**)

25 ml	(40 mmol)	<i>n</i> -BuLi (solution 1.6 M in <i>n</i> -hexane)
4 g	(40 mmol)	Trimethylsilylacetylene (TMSA)
750 ml		THF

Experimental procedure:

The experimental procedure followed as described in section 5.2.2. Purification by silica-gel column chromatography was carried out using a mixture of light petroleum / diethyl ether (20:1 ratio) affording 5.76 g of 1,2-bis(((trimethylsilyl)ethynyl)selenyl)methyl)-benzene (**16a**) as a dark yellow colored oil.

Habitus dark yellow colored oil

Yield 5.759 g (12.6mmol) 63.1%

GC R_t =28.4 min

TLC R_f -value 0.52 light petroleum / diethyl ether (20:1)

MS (EI+; *m/z*; %): 458 [M]⁺ (<1); 427 [M-2·CH₃]⁺ (1.2); 264 [C₈H₈Se₂]⁺ (2.3); 183 [C₈H₈Se]⁺ (13.6); 143 [C₁₁H₁₁]⁺ (40.9); 128 [C₁₀H₈]⁺ (29.0); 104 [C₈H₈]⁺ (31.2); 97 (28.5) [C₅H₉Si]⁺; 73 [Si(CH₃)₃]⁺ (BP, 100).

¹H-NMR (500 MHz, CDCl₃, ppm): δ =0.16 (s, 18H, Si(CH₃)₃); δ =4.21 (s, 4H, CH₂, ²*J*_{Se,H}= 13.9 Hz); δ =7.23 (m, 2H, H_{arom}); δ =7.26 (m, 2H, H_{arom}).

¹³C-NMR (125 MHz, CD₂Cl₂, ppm): δ =-0.8 (6C, Si(p-CH₃)₃, ¹*J*_{Si,C}= 56.6 Hz); δ =30.3 (2C, s-CH₂, ¹*J*_{Se,C}= 53.4 Hz); δ =86.4 (2C, q-SeC≡); δ =110.1 (2C, q-SiC≡); δ =128.3 (2C, t-C_{arom}); δ =131.4 (2C, t-C_{arom}); δ =136.2 (2C, q-C_{arom}).

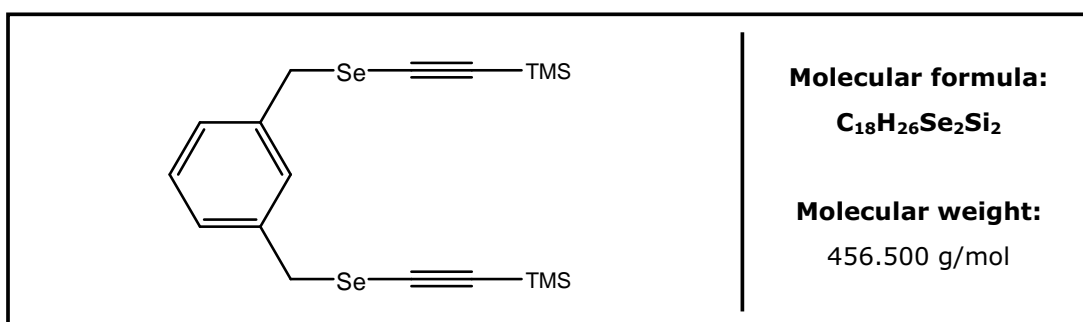
⁷⁷Se-NMR (95 MHz, CD₂Cl₂, ppm): δ =255.0.

IR (film, cm⁻¹): 3112 (w); 3026 (w); 2958 (s); 2897 (m); 2350 (w); 2087 (s); 1491 (w); 1453 (w); 1420 (w); 1262 (m); 1249 (s); 1172 (m); 1066 (w); 1043 (w); 945 (w); 859 (vs); 843 (vs); 760 (vs); 700 (m); 622 (m); 595 (m)

UV (c = 0.121 mg/ml in CH₂Cl₂):
 λ = 304 nm; log ϵ = 2.58; ϵ = 377 l/(mol·cm); extinction = 0.1
 λ = 250 nm; log ϵ = 4.09; ϵ = 12436 l/(mol·cm); extinction = 0.33

HRMS	(EI ⁺):							
m/z	¹² C	¹ H	²⁸ Si	⁸⁰ Se	mmu	Obs.Mass	Calc.Mass	
458	18	26	2	2	-1.8	457.9886	457.9903	

5.2.2.2 1,3-bis(((trimethylsilyl)ethynyl)selenyl)methyl)benzene (**16b**)



Materials:

1.054 g	(3,356 mmol)	1,3-bis-selenocyanatomethyl-benzene (15b)
0.820 g	(8,349 mmol)	trimethylsilylacetylene (TMSA)
5.230 ml	(8,368 mmol)	<i>n</i> -butyllithium (solution 1,6 M in <i>n</i> -hexane)
200 ml		THF

Experimental procedure:

The experimental procedure followed as described in section 5.2.2. Purification by silica-gel column chromatography was carried out using a mixture of *n*-hexane / diethyl ether (12:1 ratio), affording 1.015 g of 1,3-bis(((trimethylsilyl)ethynyl)selenyl)methyl)benzene (**16b**) as a yellow colored oil.

Yield 1.015 g (2.223 mmol) 66.2 %

Habitus yellow colored oil

TLC R_f-value: 0.49 *n*-hexane / diethyl ether (10:1)

GC R_t= 29.00 min

MS (EI⁺; m/z; %): 458 [MP]⁺ (1.1); 281 [M-C₅H₉SeSi]⁺ (1.9); 143 [C₁₁H₁₁]⁺ (40.9); 128 [C₁₀H₈]⁺ (29.0); 104 [C₈H₈]⁺ (31.2); 73 [Si(CH₃)₃]⁺ (BP, 100).

¹H-NMR (500 MHz, CD₂Cl₂): δ=0.15 (s, 18H, Si(CH₃)₃); δ=4.00 (s, 4H, CH₂, ²J_{Se,H}=15.4 Hz); δ=7.20-7.30 (m, 4H, H_{arom}).

¹³C-NMR (125 MHz, CD₂Cl₂): δ=0.01 (6C, p-CH₃); δ=32.97 (2C, s-CH₂); δ=86.61 (2C, q-SeC); δ=109.83 (2C, q-SiC); δ=128.55 (2C, t-C_{arom}); δ=128.99 (1C, t-C_{arom}); δ=129.54 (1C, t-C_{arom}); δ=138.63 (2C, q-C_{arom}).

⁷⁷Se-NMR (95 MHz, CD₂Cl₂): δ=267.6.

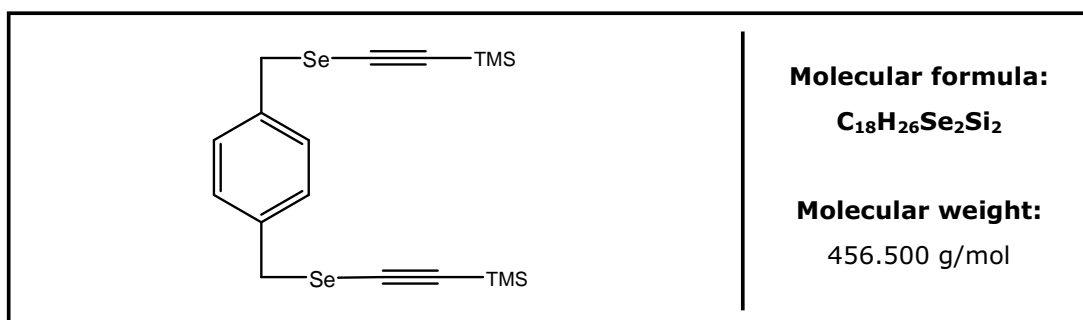
UV (c = 0.167 mg/ml in CH₂Cl₂):
 λ = 284 nm; log ε = 2.87; ε = 734 l/(mol·cm); extinction = 0.27
 λ = 304 nm; log ε = 2.66; ε = 462 l/(mol·cm); extinction = 0.17

IR (film, cm⁻¹): 2958 (s); 2897 (w); 2087 (s), 1605 (w); 1487 (w); 1443 (w); 1410 (w); 1249 (s); 1191 (m); 1079 (w), 862 (s); 793 (m); 761 (s); 699 (m); 622 (w); 579 (w).

HRMS (EI⁺):

m/z	¹² C	¹ H	²⁸ Si	⁸⁰ Se	mmu	Obs.Mass	Calc.Mass
458	18	26	2	21	+1.0	457.9913	457.9903

5.2.2.3 1,4-bis(((trimethylsilyl)ethynyl)selenyl)methyl)benzene (**16c**)



Materials:

5.027	g	(16.00 mmol)	1,4-bis-selenocyanatomethyl-benzene (15c)
3.143	g	(31.99 mmol)	Trimethylsilylacetylene (TMSA)
20.0	ml	(32.00 mmol)	<i>n</i> -butyllithium (solution 1,6 M in <i>n</i> -hexane)
700	ml		THF (solvent)

Experimental procedure:

The experimental procedure followed as described in section **5.2.2**. Purification by silica-gel column chromatography was carried out using a mixture of *n*-hexane / diethyl ether (20:1), affording 3.318 g of 1,4-bis(((trimethylsilyl)ethynyl)selenyl)methyl)benzene (**16c**).

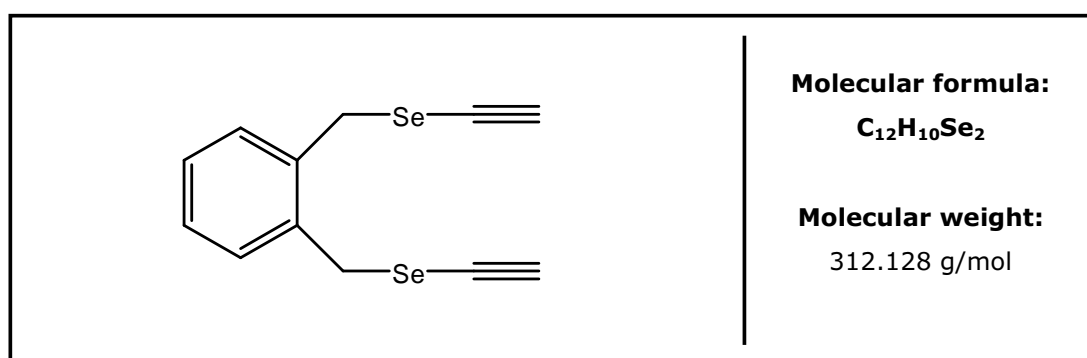
Yield	3.318 g	(7.27 mmol)	45.4 %
Habitus	pale yellow crystals		
m.p.	52-54°C		
TLC	R _f -value:	0.46	<i>n</i> -hexane / diethyl ether (20:1)
GC	R _t =	30.05 min	
MS	(EI ⁺ ; m/z; %): 458 [M] ⁺ (1.1); 442 [M-CH ₃] ⁺ (0.7); 354 [C ₁₃ H ₁₁ Se ₂ Si] ⁺ (6.7); 281 [C ₁₃ H ₁₇ SeSi] ⁺ (12.3); 162 [C ₄ H ₆ SeSi] ⁺ (4.3); 143 [C ₁₁ H ₁₁] ⁺ (10.9); 128 [C ₁₀ H ₈] ⁺ (12.0); 104 [C ₈ H ₈] ⁺ (BP, 100); 73 [Si(CH ₃) ₃] ⁺ (65.0).		
¹H-NMR	(500 MHz, CD ₂ Cl ₂): δ=0.15 (s, 18H, Si(CH ₃) ₃); δ=4.01 (s, 4H, CH ₂ , ² J _{Se,H} =15.4 Hz); δ=7.28 (s, 4H, H _{arom}).		
¹³C-NMR	(125 MHz, CD ₂ Cl ₂): δ=-0.0 (6C, p-CH ₃ , ¹ J _{Si,C} = 56.2 Hz); δ=32.8 (2C, s-CH ₂ , ¹ J _{Se,C} = 52.9 Hz); δ=86.7 (2C, q-SeC); δ=109.8 (2C, q-SiC); δ=129.4 (4C, t-C _{arom}); δ=137.6 (2C, q-C _{arom}).		
⁷⁷Se-NMR	(95 MHz, CD ₂ Cl ₂): δ=269.1		
UV	(c = 0.073 mg/ml in CH ₂ Cl ₂): λ = 246 nm; log ε = 4.31; ε = 20614 l/(mol·cm); extinction = 0.33 λ = 298 nm; log ε = 2.97; ε = 937 l/(mol·cm); extinction = 0.15		
IR	(film, cm ⁻¹): ~3100-3600 (s); 3022 (w); 2957 (m); 2899 (w); 2082 (s); 1636 (w); 1511 (m); 1419 (m); 1253 (s); 1247 (s); 1169 (s); 1122 (w); 1018 (w); 864 (s); 841 (s); 762 (s); 698 (w); 622 (m); 486 (w).		

HRMS	(EI ⁺):						Obs.Mass	Calc.Mass
m/z	¹² C	¹ H	²⁸ Si	⁷⁸ Se	⁸⁰ Se	mmu		
458	18	26	2		2	+2.5	457.9929	457.9903
458	18	26	2	1	1	+1.5	457.9929	457.9903

5.2.3 General procedure for preparation of the diselenaalkadiynes

To a solution of bis(trimethylsilyl)diselenaalkadiynes in 100 ml anhydrous MeOH and 5 ml anhydrous THF, a 0.1N NaOH solution was added dropwise during a period of 15 minutes at room temperature. Then the mixture was stirred for two hours. The reaction was stopped by adding 150 ml ice-water mixture and 150 ml diethyl ether. After separation of the organic layer the aqueous layer was extracted four times with 80 ml of diethyl ether. The combined organic layers were washed three times with saturated NH₄Cl solution and three times with brine. After drying over MgSO₄, the solvent was evaporated and the product purified by silica-gel column chromatography or recrystallized.

5.2.3.1 1,2-bis(ethynylselenenylmethyl)-benzene (**17a**)



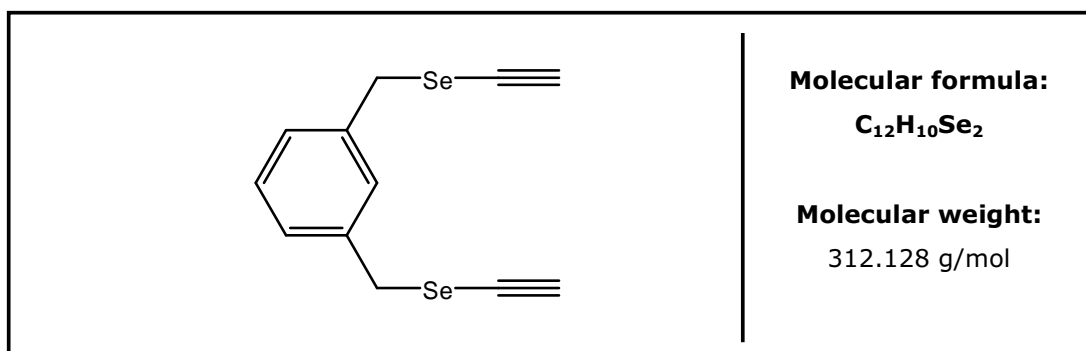
Materials:

4.917 g	(10.77 mmol)	1,2-bis(((trimethylsilyl)ethynylselenenyl)methyl)benzene (16a)
450 ml		MeOH
11 ml		solution 0.1 N NaOH
15 ml		THF (cosolvent)

Experimental procedure:

The experimental procedure followed as described in section 5.2.3. After removal of the solvent through rotary evaporation, the NMR analysis of the raw product showed a purity of more than 99 %. Thus the product was not further purified, but used as obtained for the following reaction step.

Yield	3.028 g	9.701 mmol	90.1 %						
Habitus	dark yellow colored oil								
GC	$R_t = 21.5$ min								
MS	(EI ⁺ ; m/z; %): 313 [M-H] ⁺ (<1); 233 [C ₁₂ H ₉ Se] ⁺ (11.3); 152 [C ₁₂ H ₈] ⁺ (17.9); 128 [C ₁₀ H ₈] ⁺ (100.0); 104 [C ₈ H ₈] ⁺ (63.3); 78 [C ₆ H ₆] ⁺ (32.5).								
¹H-NMR	(500 MHz, CD ₂ Cl ₂): $\delta = 2.93$ (s, 2H, C≡CH); $\delta = 4.21$ (s, 4H, CH ₂ , ² J _{Se,H} = 13.1 Hz); $\delta = 7.25$ (m, 2H, H _{arom}); $\delta = 7.31$ (m, 2H, H _{arom}).								
¹³C-NMR	(125 MHz, CD ₂ Cl ₂): $\delta = 29.9$ (2C, s-CH ₂ , ¹ J _{Se,C} = 51.8 Hz); $\delta = 65.8$ (2C, t-CH); $\delta = 90.4$ (2C, q-SeC, ¹ J _{Se,C} = 37.9 Hz); $\delta = 128.5$ (2C, t-C _{arom}); $\delta = 131.3$ (2C, t-C _{arom}); $\delta = 135.9$ (2C, q-C _{arom}).								
⁷⁷Se-NMR	(95 MHz, CD ₂ Cl ₂): $\delta = 232.1$.								
IR	(KBr, cm ⁻¹): 3277 (s); 3061 (w); 3020 (w); 2954 (w); 2028 (w); 1491 (m); 1452 (m); 1420 (w); 1376 (w); 1300 (w); 1172 (m); 1067 (w); 1042 (w); 948 (w); 875 (w); 834 (w); 762 (m); 681 (m); 592 (m); 436 (w)								
UV	(c = 0.063 mg/ml in CH ₂ Cl ₂): $\lambda = 244$ nm; log $\epsilon = 3.16$; $\epsilon = 1436$ l/(mol·cm); extinction = 0.29								
HRMS	(EI ⁺):								
	m/z	¹² C	¹ H	⁷⁸ Se	⁸⁰ Se	⁸² Se	mmu	Obs.Mass	Calc.Mass
	312	12	9		2		+3.0	312.9065	312.9035
	[M-H]	12	9	1		1	+2.1	312.9065	312.9035

5.2.3.2 1,3-bis(ethynylselenylmethyl)-benzene (17b**)****Materials:**

0.965 g	(2.11 mmol)	1,3-bis(((trimethylsilyl)ethynylselenyl)methyl)benzene (16b)
1.840 ml	(0.18 mmol)	solution 0.1 N NaOH solution
100 ml		MeOH (solvent)
5 ml		THF (cosolvent)

Experimental procedure:

The experimental procedure followed as described in section 5.2.3. Purification by column chromatography on silica gel using *n*-hexane / diethyl ether (6:1) as solvent mixture, affording 1,3-bis(ethynylselenylmethyl)-benzene (**17b**) as a yellow colored oil.

Yield 0.627 g (2.009 mmol) 95.03 %

Habitus yellow colored oil

TLC R_f-value 0.29 *n*-hexane / diethyl ether (6:1)

GC R_t= 21.18 min

MS (EI⁺; m/z; %): 313 [M-H]⁺ (0.4); 233 [C₁₂H₉Se]⁺ (15.1); 153 [C₁₂H₉]⁺ (11.8); 129 [C₁₀H₉]⁺ (49.5); 128 [C₁₀H₈]⁺ (BP, 100); 104 [C₈H₈]⁺ (43.0); 78 [C₆H₆]⁺ (28.0).

¹H-NMR (500 MHz, CD₂Cl₂): δ=2.94 (s, 2H, C≡CH); δ=4.04 (s, 4H, CH₂, J_{Se,H}=14.9Hz); δ=7.20-7.35 (m, 4H, H_{arom}).

$^{13}\text{C-NMR}$ (125 MHz, CD_2Cl_2): $\delta=32.14$ (2C, s- CH_2); $\delta=65.58$ (2C, t-CH, $^1J_{\text{Se,C}}=52.9$ Hz); $\delta=90.02$ (2C, q-SeC, $^1J_{\text{Se,C}}=37.9$ Hz); $\delta=128.16$ (2C, t- C_{arom}); $\delta=128.87$ (1C, t- C_{arom}); $\delta=129.45$ (1C, t- C_{arom}); $\delta=138.18$ (2C, q- C_{arom}).

$^{77}\text{Se-NMR}$ (95 MHz, CD_2Cl_2): $\delta=246.6$.

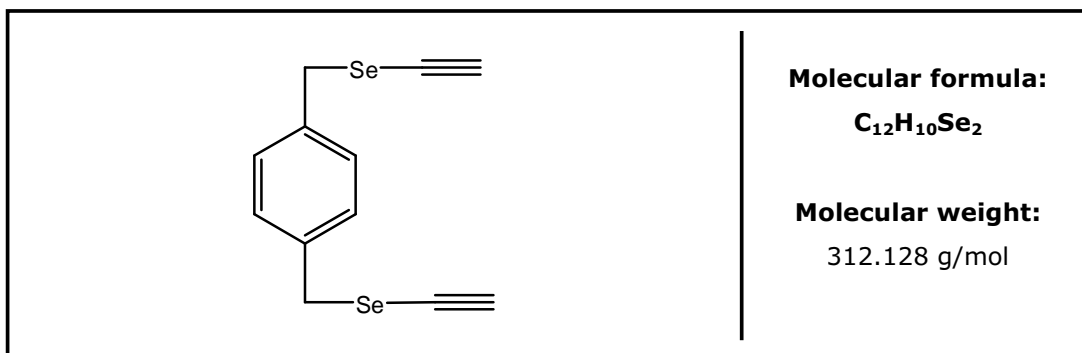
IR (KBr, cm^{-1}): 3277 (s); 3025 (w); 2939 (w); 2028 (m); 1604 (m); 1486 (m); 1443 (m); 1193 (m); 1079 (w); 895 (w); 839 (w); 796 (m); 743 (w); 698 (s); 579 (s); 430 (w).

UV ($c = 0.184$ mg/ml in CH_2Cl_2):
 $\lambda = 274$ nm; $\log \epsilon = 2.90$; $\epsilon = 797$ l/(mol·cm); extinction = 0.47
 $\lambda = 302$ nm; $\log \epsilon = 2.66$; $\epsilon = 458$ l/(mol·cm); extinction = 0.27

HRMS (EI^+):

m/z	^{12}C	^1H	^{80}Se	mmu	Obs.Mass	Calc.Mass
314	12	10	2	+2.6	313.9139	313.9113

5.2.3.3 1,4-bis(ethynylselenylmethyl)-benzene (**17c**)



Materials:

2.981 g	(6.53 mmol)	1,4-bis(((trimethylsilyl)ethynylselenyl)methyl)benzene (16c)
6.537 ml	(0.65 mmol)	0.1 N NaOH solution
300 ml		MeOH (solvent)
15 ml		THF (cosolvent)

Experimental procedure:

The experimental procedure followed as described in section 5.2.3. Purification of the product was carried out by column chromatography using a mixture of *n*-hexane / diethyl ether (6:1), affording 1,4-bis(ethynylselenylmethyl)-benzene (**17c**) as pale yellow crystals.

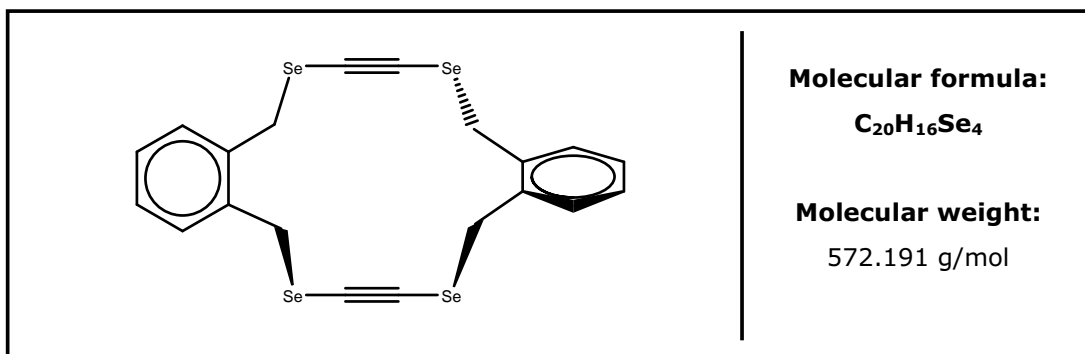
Yield	1.952 g	(6.254 mmol)	95.8 %				
Habitus	pale yellow crystals						
m.p.	78-79°C						
TLC	R _f -value	0.35	<i>n</i> -hexane / diethyl ether (6:1)				
GC	R _t = 22.29 min						
MS	(EI ⁺ ; m/z; %): 314 [M] ⁺ (0.1); 289 [C ₁₀ H ₉ Se ₂] ⁺ (1.3); 209 [C ₁₀ H ₉ Se] ⁺ (12.1); 184 [C ₈ H ₈ Se] ⁺ (1.4); 153 [C ₁₂ H ₉] ⁺ (6.8); 128 [C ₁₀ H ₈] ⁺ (16.4); 104 [C ₈ H ₈] ⁺ (BP, 100); 78 [C ₆ H ₆] ⁺ (21.0).						
¹H-NMR	(500 MHz, CD ₂ Cl ₂): δ=2.93 (s, 2H, C≡CH); δ=4.04 (s, 4H, CH ₂ , ² J _{Se,H} = 14.2 Hz); δ=7.30 (s, 4H, H _{arom}).						
¹³C-NMR	(125 MHz, CD ₂ Cl ₂): δ=32.34 (2C, s-CH ₂); δ=65.93 (2C, t-CH); δ=90.22 (2C, q-SeC); δ=129.45 (4C, t-C _{arom}); δ=137.58 (2C, q-C _{arom}).						
⁷⁷Se-NMR	(95 MHz, CD ₂ Cl ₂): δ=247.8.						
IR	(KBr, cm ⁻¹): ~3100-3600 (s); 3262 (s); 3247 (m); 3052 (w); 2084 (w); 1636 (w); 1510 (w); 1419 (w); 1189 (m); 1089 (w); 861 (w); 843 (m); 834 (w); 756 (w); 702 (m); 694 (m); 607 (m); 586 (m); 545 (w); 481 (w).						
UV	(c = 0.018 mg/ml in CH ₂ Cl ₂): λ = 248 nm; log ε = 4.25; ε = 17853 l/(mol·cm); extinction = 1.03 λ = 292 nm; log ε = 3.02; ε = 1040 l/(mol·cm); extinction = 0.06						
HRMS	(EI ⁺):						
	m/z	¹² C	¹ H	⁸⁰ Se	mmu	Obs.Mass	Calc.Mass
	314	12	10	2	+2.8	313.9141	313.9113

5.2.4 General procedure the preparation of the tetraselena-cyclodiyne

To a solution of diselenaalkadiyne in anhydrous THF in a three neck flask, *n*-butyllithium (1.6 M solution in *n*-hexane) was added dropwise during 15 minutes, while maintaining the temperature below -25°C . The mixture was stirred for one hour at this temperature. To about 500 ml of dry THF in a 2L round bottom three necked flask, cooled to -50°C , the solutions of diselenocyanatoylene and dilithiated diselenaalkadiynes in anhydrous THF were added simultaneously via separate dropping funnels over a time period of 5 - 7 hours. After complete addition the reaction mixture was allowed to warm up to room temperature overnight. The solvent was evaporated to give the raw product which was cleaned by fast silica-gel chromatography with toluene to remove salts and polymers. Further purification was accomplished using silica-gel chromatography with appropriate solvent mixtures.

Note: Melting points (m.p.) for compounds **18 a-c** could not be determined as in all cases, the samples decomposed upon heating in the 60 to 80°C range. Gas chromatography (GC) analysis of compounds **18 a-c** was unsuccessful, decomposition of the samples taking place both on the chromatographic column and in the transfer line to the mass spectrometer detection device.

5.2.4.1 2,5,14,17-tetraselena[6.6]-*ortho*-cyclophan-3,15-diyne (**18a**)



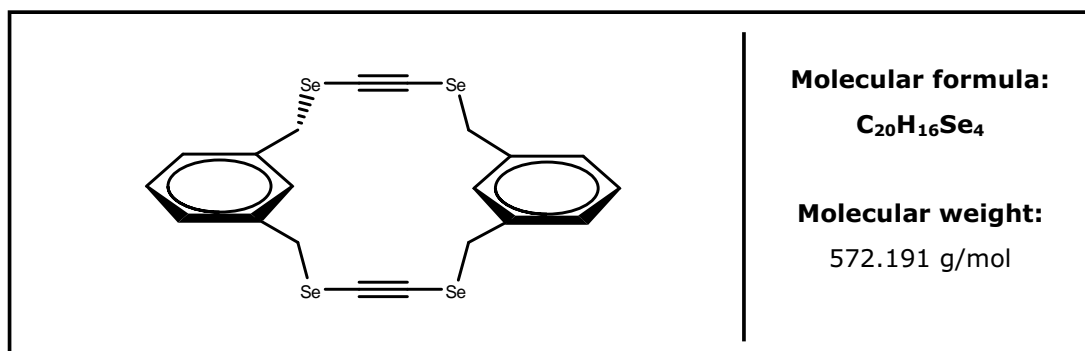
Materials:

2.81 g	(9 mmol)	1,2-bis(ethynylselenenylmethyl)-benzene (17a)
11 ml	(18 mmol)	<i>n</i> -BuLi (solution 1.6 M in <i>n</i> -hexane)
2.83 g	(9 mmol)	1,2-bis(selenocyanatomethyl)-benzene (15a)
1000 ml		THF (solvent)

Experimental procedure:

The experimental procedure was carried out following the description in section 5.2.4. The product was purified using silica-gel column chromatography. First, a *n*-hexane / toluene (3:1) mixture was used as eluent and an enriched fraction was further purified through a second column chromatography using a *n*-hexane / diethyl ether (10:1) mixture. The purified compound (**18a**) was recrystallized from a dichloromethane / *n*-hexane mixture affording thin yellow needle-like crystals.

Yield	0.182g	(0.32 mmol)	3.6%
Habitus	yellow needle-like crystals		
TLC	R _F -value	0.23	<i>n</i> -hexane / toluene (3:1)
¹H-NMR	(500MHz, CDCl ₃): δ=4.47 (s, 8H, CH ₂ , ² J _{Se,H} = 7.9 Hz); δ=7.22 (bs, 8H, H _{arom}).		
¹³C-NMR	(125 MHz, CDCl ₃): δ=33.05 (4C, s-CH ₂); δ=85.92 (4C, q-SeC≡CSe); δ=128.41 (4C, t-C _{arom}); δ=130.87 (4C, t-C _{arom}); δ=135.46 (4C, q-C _{arom}).		
⁷⁷Se-NMR	(95 MHz, CDCl ₃): δ=235.04.		
IR	(KBr, cm ⁻¹): 3100-3600(s); 1772(w); 1636(m); 1559(w); 1507(w); 1490(w); 1452(w); 1419(w); 1384(w); 1249(w); 1174(w); 1162(w); 1105(w); 845(w); 759(m); 617(w); 536(w); 458(w); 443 (w); 436 (w); 416 (w).		
UV	(c = 0.068 mg/ml in CH ₂ Cl ₂): λ = 238 nm; log ε = 4.76; ε = 57200 l/(mol·cm); extinction = 0.68		
MS	(LIFDI, ion mode: FD+, toluene):		
	m/z	Obs. Mass	Calc.Mass %
	574	573.60	573.79 100
	572	571.59	571.79 92

5.2.4.2 2,5,14,17-tetraselena[6,6]-meta-cyclophan-3,15-diyne (18b)**Materials:**

0.568 g	(1.820 mmol)	1,3-bis-(ethynylselenylmethyl)-benzene (17b)
2.250 ml	(3.600 mmol)	<i>n</i> -butyllithium (solution 1,6 M in <i>n</i> -hexane)
0.565 g	(1.799 mmol)	1,3-bis-(selenocyanatomethyl)-benzene (15b)
1000 ml		THF

Experimental procedure:

The experimental procedure was followed as described in section 5.2.4., with an addition period of 7 hours. The product was purified using silica-gel column chromatography, firstly with a mixture of *n*-hexane/toluene (4:1) and then an enriched fraction was further purified with a mixture of *n*-hexane/toluene (1:2). Finally, the clean product was obtained from a further enriched fraction using chromatography on silica-gel with a mixture of *n*-hexane / diethyl ether (5:1), obtaining **18b** as thin colourless needles.

Yield 0.076 g (0.133 mmol) 7.4%

Habitus thin colourless needles

TLC R_f-value 0.22 *n*-hexane / diethyl ether (5:1)

¹H-NMR (500 MHz, CD₂Cl₂): δ=3.93 (s, 8H, CH₂, ²J_{Se,H}=17.4 Hz); δ=7.18 (dd, 4H, J=7.5, 1.3 Hz, H_{arom}); δ=7.19 (dt, 2H, J=1.3, 0.9 Hz, H_{arom}); δ=7.29 (td, 2H, J=7.5Hz; 0.9 Hz, H_{arom}).

¹³C-NMR (125 MHz, CD₂Cl₂): δ=33.92 (4C, s-CH₂); δ=85.66 (4C, q-SeC); δ=128.31 (2C, t-C_{arom}); δ=128.92 (1C, t-C_{arom}); δ=130.73 (1C, t-C_{arom}); δ=138.37 (2C, q-C_{arom}).

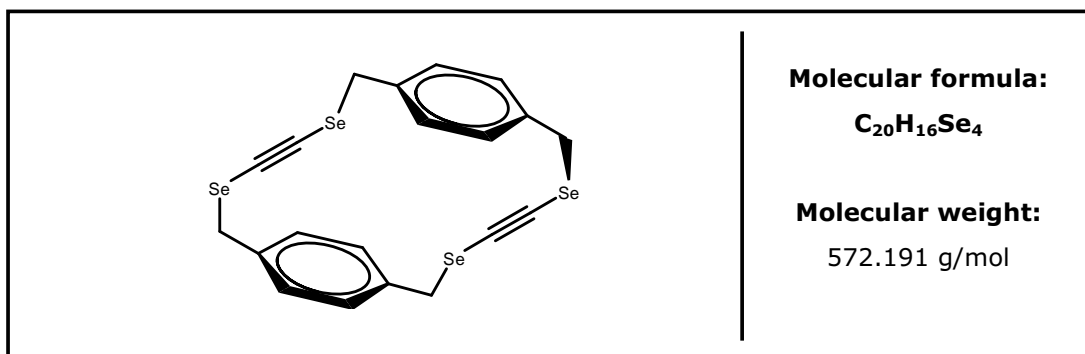
⁷⁷Se-NMR (95 MHz, CD₂Cl₂): δ =288.52.

IR (CH₂Cl₂, cm⁻¹): 3679(s); 3600(m); 2930(s); 2852(w); 2371(w); 2335(m); 1702(w); 1605(s); 1487(w); 1464(w); 1442(w); 1187(m); 894(w); 838(w); 798(m); 778(m); 669(w); 618 (m).

MS (LIFDI, ion mode: FD⁺, toluene):

m/z	Obs. Mass	Calc. Mass	%
574	573.62	573.79	100
572	571.62	571.79	92

5.2.4.3 2,5,14,17-tetraselena[6,6]-*para*-cyclophan-3,15-diyne (**18c**)



Materials:

0.780 g	(2.499 mmol)	1,4-bis(ethynylselenylmethyl)-benzene (17c)
3.125 ml	(5.000 mmol)	<i>n</i> -butyllithium (solution 1,6 M in <i>n</i> -hexane)
0.785g	(2.499 mmol)	1,4-bis(selenocyanatomethyl)-benzene (15c)
800 ml		THF

Experimental procedure:

The experimental procedure was followed as described in section 5.2.4., with an addition period of 5 hours. The product was purified using silica-gel column chromatography, using with a mixture of *n*-hexane / diethyl ether (5:1). After rotary evaporation of solvents the product was recrystallised from a mixture of *n*-hexane and dichloromethane, resulting in 0.045g of **18c** as thin colourless crystals.

Yield	0.045g	(0.08 mmol)	1.8%
Habitus	thin colourless crystals		
TLC	R _f -value	0.22	<i>n</i> -hexane /diethyl ether (5:1)
¹H-NMR	(500 MHz, CD ₂ Cl ₂): δ=3.89 (s, 8H, CH ₂ , ² J _{Se,H} = 20.3 Hz); δ=7.15 (s, 8H, H _{arom}).		
¹³C-NMR	(75 MHz, CD ₂ Cl ₂): δ=33.32 (4C, s-CH ₂); δ=84.37 (4C, q-SeC); δ=129.20 (8C, t-C _{arom}); δ=138.31 (4C, q-C _{arom}).		
⁷⁷Se-NMR	(95 MHz, CD ₂ Cl ₂): δ=299.81.		
IR	(CHCl ₃ , cm ⁻¹): 3582(w); 2957(s); 2927(vs); 2856 (s); 2676 (w); 2241 (w); 1712(w); 1650(m); 1604(w); 1557(w); 1538(w); 1509(w); 1457(m); 1366(w); 1261(m); 1182(w); 1082(m); 1017(m); 810(m); 594(w).		
MS	(LIFDI, ion mode: FD ⁺ , toluene):		
	m/z	Obs. Mass	Calc.Mass %
	574	573.67	573.79 100
	572	571.67	571.79 92

5.3 Experimental procedures for synthesis of small model compounds

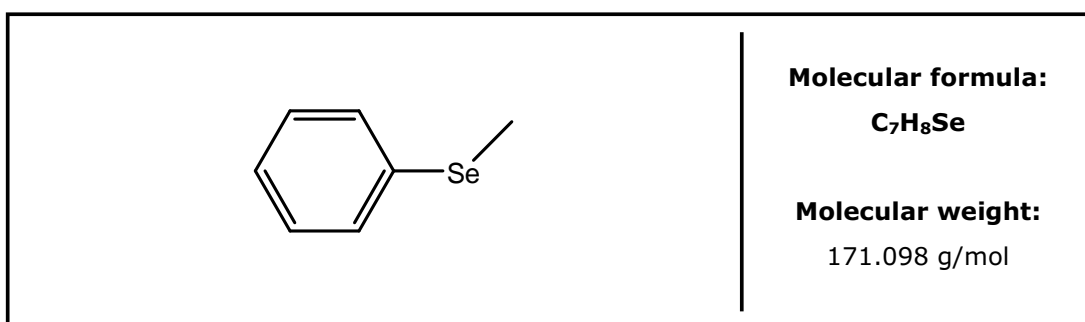
5.3.1 General preparation procedure for synthesis of lithium methyl selenide (MeSeLi)

MeSeLi was prepared using a slightly modified procedure of *Tiecco et al.*¹¹⁹. To a stirred solution of powder gray selenium (3.2 g, 40 mmols) in 50 ml of THF cooled at - 25°C was added dropwise methyllithium (commercial solution 1.6M in ether - 30 ml, 45 mmol) using a syringe, under argon atmosphere. After complete addition of the MeLi solution, under continuous stirring the reaction mixture was allowed to warm to room temperature for 2 h. When reaching room temperature, full consumption of powder selenium could be observed

and a white suspension of MeSeLi was obtained. MeSeLi obtained using this procedure was used in several syntheses described in the following sections.

5.3.2 Model compounds containing one selenium center

5.3.2.1 Phenyl methyl selenide (**22**)



Materials:

1.57 g	(10 mmol)	phenyl bromide (35)
4.26 g	(30 mmol)	methyl iodide
3.03 g	(30 mmol)	lithium methyl selenide (as THF/DE solution)
25 ml		dimethylformamide (DMF)

Experimental procedure¹¹⁹:

To a freshly prepared solution of lithium methyl selenide in THF and diethyl ether (DE) (see section 5.3.1.), was added dropwise and under stirring phenyl bromide dissolved in dry DMF was added dropwise under stirring. After 4 hours of stirring at room temperature, the THF and DE were distilled off. When only DMF was left as solvent, the reaction flask was fitted with a reflux condenser and the reaction mixture was refluxed for 90 hours. Afterwards, MeI was added dropwise under stirring and the reaction was allowed to cool down to room temperature. After cooling, it was poured into cold distilled water. After extraction with diethyl ether, the organic layers were washed with water and brine and dried over Na₂SO₄. Following rotary evaporation of the solvent the raw product was purified through silica-gel column chromatography, using a mixture of light petroleum and diethyl ether, affording compound **22** as dark yellow colored oil.

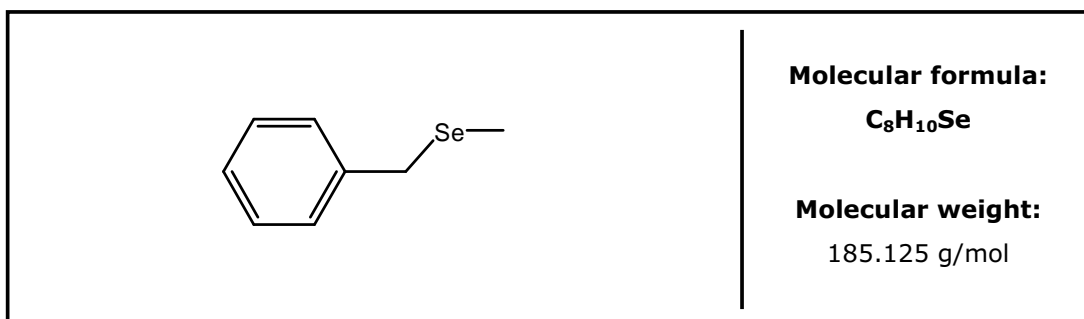
Yield 0.867 g (5.07 mmol) 50.7 %

Habitus yellow colored oil

Preparative procedures

TLC	R _f -value	0.51	petrol ether (45-60) / diethyl ether	(9:1)			
GC	R _t =	10.69 min					
MS	(EI ⁺ ; m/z; %):	172 [M] ⁺ (96.8); 157 [M-CH ₃] ⁺ (BP, 100); 91 [C ₇ H ₇] ⁺ (64.9); 77 [C ₆ H ₅] ⁺ (69.6); 65 [C ₅ H ₅] ⁺ (16.9).					
¹H-NMR	(500 MHz, CD ₂ Cl ₂):	δ=2.30 (s, 3H, CH ₃ , ² J _{Se,H} = 11.0 Hz); δ=7.20 (tt, 1H, J= 7.3, 1.3 Hz, H _{arom}); δ=7.27 (td, 2H, J= 7.3, 1.3 Hz, H _{arom}); δ=7.42 (dd, 2H, J= 7.3, 1.3 Hz, H _{arom}).					
¹³C-NMR	(125 MHz, CD ₂ Cl ₂):	δ=7.22 (3C, p-CH ₃ , ¹ J _{Se,C} =63.4 Hz); δ=126.3 (1C, t-C _{arom}); δ=129.4 (1C, t-C _{arom}); δ=130.5 (1C, t-C _{arom} , ² J _{Se,C} =11.5 Hz); ¹ J _{Se,C} =63.4 Hz); δ=132.4 (1C, q-C _{arom} Se, ¹ J _{Se,C} =104.5 Hz).					
⁷⁷Se-NMR	(95 MHz, CD ₂ Cl ₂):	δ=199.8.					
IR	(film, cm ⁻¹):	3774 (w); 3057 (w); 2999 (w); 2927 (m); 2252 (w); 1579 (m); 1478 (s); 1437 (m); 1299 (w); 1273 (w); 1074 (m); 1023 (m); 999 (w); 904 (m); 734 (vs); 690 (s); 670 (m); 536 (w); 520 (w); 513(w).					
HRMS	(EI ⁺):						
	m/z	¹² C	¹ H	⁸⁰ Se	mmu	Obs.Mass	Calc.Mass
	172	7	8	1	+0.9	171.9800	171.9791

5.3.2.2 Benzyl methyl selenide (23)



Materials:

1.748 g (20.5 mmol) benzyl bromide
124

2.071 g (20.5 mmol) lithium methyl selenide – (as a THF / DE solution)
50 ml THF

Experimental procedure¹¹⁹:

To a freshly prepared (see section 5.3.1.) solution of lithium methyl selenide in THF, was added dropwise using a syringe a solution of benzyl bromide in THF. The colouring of the reaction turned from pale yellow to a darker orange during the addition. After the complete addition of the benzyl bromide the reaction was stirred for 2 hours at room temperature and finally refluxed for about 30 minutes. Alkylating agent, methyl iodide, was added dropwise and the reaction mixture was allowed to cool down to room temperature. The reaction mixture was hydrolyzed with deionized water and the organic phase separated, washed with water, saturated solution of sodium bicarbonate and brine, and then dried over sodium sulfate. Rotary evaporation of the solvent afforded the raw product as dark yellow colored oil. After purification through silica-gel column chromatography using a *n*-hexane / dichloromethane (1:1) mixture, benzyl methyl selenide (**23**) was obtained as yellow colored oil.

Yield 2.304 g (12.4 mmol) 60.5 %

Habitus yellow colored oil

TLC R_F-value 0.183 *n*-hexane / dichloromethane (1:1)

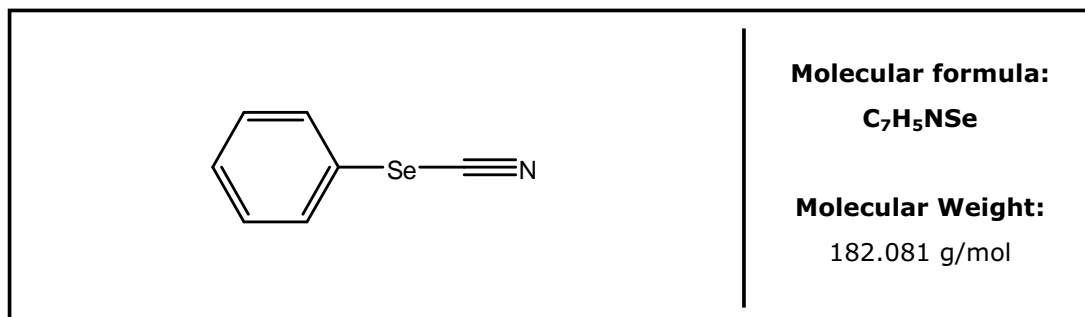
GC R_t= 12.57 min

MS (EI⁺; m/z; %): 186 [M]⁺ (11.6); 169 [M-CH₃]⁺ (1,3); 91 [C₇H₇]⁺ (BP, 100); 65 [C₅H₅]⁺ (19.5).

¹H-NMR: (500 MHz, CD₂Cl₂): δ=1.92 (s, 3H, CH₃, ²J_{Se,H}= 10.5 Hz); δ=3.76 (s, 2H, CH₂, ²J_{Se,H}= 13.2 Hz); δ=7.23 (tt, 1H, H_{arom}, J= 6.8, 1.7 Hz); δ=7.27-7.34 (m, 4H, H_{arom}).

¹³C-NMR (125 MHz, CD₂Cl₂): δ=4.2 (1C, p-CH₃, ¹J_{Se,C}=64.2 Hz); δ=28.3 (2C, s-CH₂, ¹J_{Se,C}=58.3 Hz); δ=126.6 (1C, t-C_{arom}); δ=128.4 (2C, t-C_{arom}); δ=128.7 (2C, t-C_{arom}); δ=139.2 (1C, q-C_{arom}).

⁷⁷Se-NMR (95 MHz, CD₂Cl₂): δ=172.0.

5.3.2.3 Phenyl selenocyanate (27)**Materials:**

6.18 g	(32.3 mmol)	phenyl selenyl chloride (37)
4.5 ml	(35 mmol)	trimethylsilyl cyanate (TMSCN)
200ml		tetrahydrofuran (THF)

Experimental procedure¹²²:

A solution of phenyl selenyl chloride (**37**) in dry THF was added dropwise over a period of 15 minutes to a solution of TMSCN in dry THF under stirring, at room temperature in an inert gas atmosphere. After the addition of **37** was completed, the reaction mixture was stirred for further 45 minutes. The solvent, as well as the unreacted TMSCN were removed by rotary evaporation, resulting in a colorless oil residue. GC-MS analysis showed a purity of the raw product of over 99.5%. For ulterior use compound **27** was not further purified.

Yield 5.69 g (31 mmol) 96 %

Habitus colorless oil (solid at -20°C)

GC R_t = 10.75 min

MS (EI⁺; m/z; %): 183 [M]⁺ (BP, 100); 156 [M-CN]⁺ (31,3); 103 [SeCN]⁺ (94.7); 77 [C₆H₅]⁺ (81.5); 65 [C₅H₅]⁺ (4.3); 51 [C₄H₃]⁺ (27.4).

¹H-NMR (500 MHz, CD₂Cl₂): δ=7.39-7.47 (m, 3H, H_{arom}); δ=7.65 (ddd, 2H, H_{arom}, J= 8.9, 2.0, 0.8 Hz).

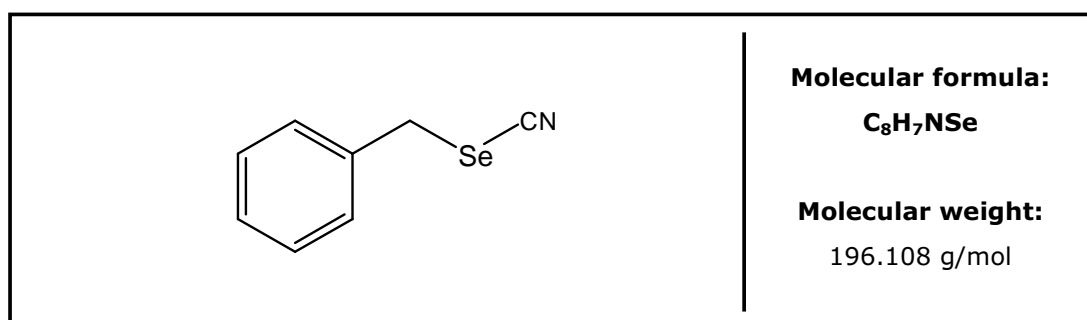
¹³C-NMR (125 MHz, CD₂Cl₂): δ=101.8 (1C, q-SeCN); δ=122.4 (1C, q-SeC_{arom}); δ=130.1 (1C, t-C_{arom}); δ=130.7 (2C, t-C_{arom}); δ=133.1 (2C, t-C_{arom}, ²J_{Se,C}= 12.7 Hz).

$^{77}\text{Se-NMR}$ (95 MHz, CD_2Cl_2): $\delta=317.3$.

IR (film, cm^{-1}): 3063 (w); 2153 (m); 1577 (m); 1478 (s); 1441 (s); 1356 (w); 1324(w); 1067 (m); 1019 (m); 999 (m); 738 (s); 686 (s); 667 (m); 613 (w); 586 (w); 553 (w); 547 (w); 539 (w); 534 (w); 522 (w); 517 (m); 511 (m); 504 (w).

UV (c = 0.168 mg/ml in CH_2Cl_2):
 $\lambda = 272 \text{ nm}$; $\log \epsilon = 2.77$; $\epsilon = 587 \text{ l}/(\text{mol}\cdot\text{cm})$; extinction = 0.06
 $\lambda = 264 \text{ nm}$; $\log \epsilon = 2.89$; $\epsilon = 783 \text{ l}/(\text{mol}\cdot\text{cm})$; extinction = 0.08
 $\lambda = 238 \text{ nm}$; $\log \epsilon = 3.63$; $\epsilon = 4305 \text{ l}/(\text{mol}\cdot\text{cm})$; extinction = 0.44

5.3.2.4 Benzyl selenocyanate (**28**)



Materials:

3.42 g	(20 mmol)	benzyl bromide (35)
6.00 g	(40 mmol)	potassium selenocyanate
50 ml		dimethylformamide

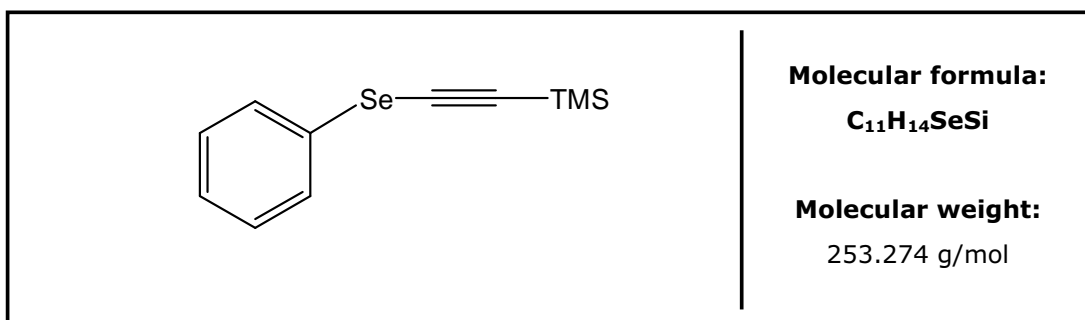
Experimental procedure¹²³:

A solution of benzyl bromide in dry DMF was added dropwise by using a syringe into a solution of KSeCN in dry distilled DMF. A two-necked round bottom flask fitted with a magnetic stirrer, a rubber lid and a reflux condenser connected to an argon line was used as a reaction vessel. The reaction mixture was heated at 80°C under continuous stirring for a period of 8 hours, then it was cooled to room temperature. The reaction mixture was then hydrolyzed and the organic compounds were extracted with diethyl ether. The ethereal fractions were combined, washed with water and dried over magnesium sulfate. After rotary evaporation of the solvent an orange solid was obtained as raw material. Further

recrystallization from methanol afforded the purified product as white solid, crystallized in a needle-like form.

Yield	3.724 g	(18.9 mmol)	76.3 %
Habitus	white needles		
m.p.	70°C		
GC	R _t = 15.31 min		
MS	(EI ⁺ ; m/z; %): 197 [M] ⁺ (3.6); 169 [C ₇ H ₇ Se] ⁺ (1,3); 91 [C ₇ H ₇] ⁺ (BP, 100); 65 [C ₅ H ₅] ⁺ (74.3).		
¹H-NMR	(500 MHz, CD ₂ Cl ₂): δ=4.29 (s, 2H, CH ₂ , ² J _{Se,H} = 15.8 Hz); δ=7.31-7.36 (m, 1H, H _{arom}); δ=7.36-7.39 (m, 5H, H _{arom}).		
¹³C-NMR	(125 MHz, CD ₂ Cl ₂): δ=33.2 (2C, s-CH ₂); δ=102.0 (1C, q-CN); δ=128.9 (1C, t-C _{arom}); δ=129.34 (2C, t-C _{arom}); δ=129.36 (2C, t-C _{arom}); δ=136.4 (1C, q-C _{arom}).		
⁷⁷Se-NMR	(95 MHz, CD ₂ Cl ₂): δ=288.9		
IR	(KBr, cm ⁻¹): 3441(bs); 3083(w); 3069(w); 3027(m); 3002(m); 2147(vs); 1952(w); 1883(w); 1810(w); 1492(s); 1455(s); 1425(m); 1219(m); 1193(s); 1178(m); 1070(m); 1028(w); 763(s); 696(s); 592(s); 551(m); 518(m).		
UV	(c = 0.19 mg/ml in CH ₂ Cl ₂): λ = 274 nm; log ε = 2.73; ε = 539 l/(mol·cm); extinction = 0.52		

5.3.2.5 Phenyl-2-(trimethylsilyl)-ethynyl selenide (**38**)



Materials:

4.55 g	(25 mmol)	phenyl selenocyanate (27)
2.65 g	(27.5 mmol)	trimethylsilylacetylene (TMSA)
17.2 ml	(27.5 mmol)	<i>n</i> -butyl lithium (as a 1.6 M solution in <i>n</i> -hexane)
400 ml		dry THF (solvent)
450 ml		light petroleum ether

Experimental procedure⁹³:

To a solution of TMSA in 250 ml of dry THF a solution of *n*-butyl lithium in *n*-hexane was added slowly at -25°C in such a way that the temperature does not exceed -25°C. After complete addition of *n*-BuLi the pale yellow solution was stirred for 2 hours at -30°C. The solution of **27** in ca. 100 ml of dry THF was slowly added to the reaction flask, without letting the temperature exceed -20°C. After the addition was completed, the reaction mixture was allowed to stir for 2 hours at a temperature under -10°C. At the end of the reaction time, ca. 100 ml of a saturated NH₄Cl aqueous solution was added to the reaction mixture. After transferring the reaction mixture into a separation funnel, the organic phases were extracted with light petroleum ether (3 times ca. 125 ml). The organic phases were collected together, washed with water and brine and dried overnight on MgSO₄. After removal of the solvent by rotary evaporation, the raw product was purified through column chromatography on deactivated silica-gel using a solvent mixture of light petroleum ether / dichloromethane (10:1) to afford compound **38** as yellow colored oil.

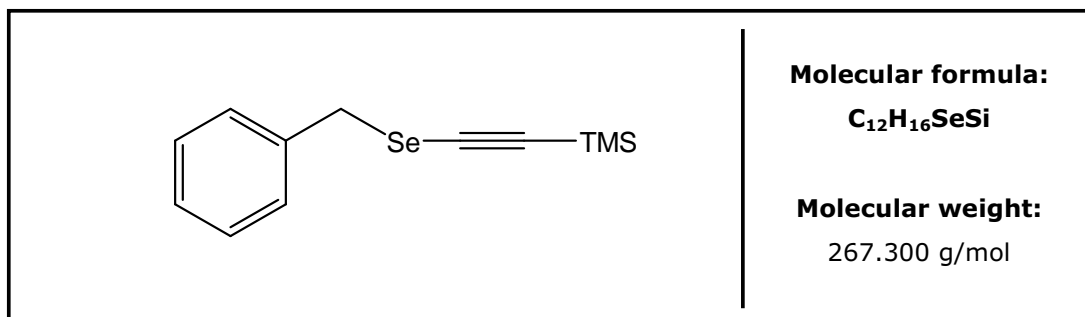
Yield 4.31 g (17 mmol) 68 %

Habitus yellow colored oil

TLC R_F-value 0.48 light petroleum ether / dichloromethane (5:1)

GC	$R_t = 16.54$ min																
MS	(EI ⁺ ; m/z; %): 254 [M] ⁺ (41.3); 239 [M-CH ₃] ⁺ (61.2); 209 [M-3CH ₃] ⁺ (4); 159 [M-C ₅ H ₁₉ Si] ⁺ (86.9); 97 [C ₅ H ₉ Si] ⁺ (6); 73 [C ₃ H ₉ Si] ⁺ (BP, 100).																
¹H-NMR	(500 MHz, CD ₂ Cl ₂); $\delta=0.23$ (s, 9H, Si(CH ₃) ₃); $\delta=7.27$ (tt, $J = 7.4, 1.2$ Hz, 1H, H _{arom}); $\delta=7.33$ (td, $J = 7.4, 1.2$ Hz, 2H, H _{arom}); $\delta=7.52$ (dt, $J = 7.4, 1.2$ Hz, 2H, H _{arom}).																
¹³C-NMR	(125 MHz, CD ₂ Cl ₂); $\delta=-0.05$ (p-Si(CH ₃) ₃); $^1J_{Si,C}=56.7$ Hz); $\delta=84.4$ (q-SeCC); $\delta=112.0$ (q-SiCC); $\delta=127.5$ (t-C _{arom}); $\delta=128.7$ (q-C _{arom} Se); $\delta=129.1$ (t-C _{arom} , 2C, $^2J_{Se,C}=14.5$ Hz); $\delta=129.9$ (t-C _{arom} , 2C).																
⁷⁷Se-NMR	(95 MHz, CD ₂ Cl ₂) $\delta=283.8$.																
IR	(film, cm ⁻¹): 3060 (w); 2959 (m); 2091 (s); 1578 (m); 1477 (s); 1440 (m); 1409 (w); 1325 (w); 1250 (s); 1067 (w); 1021 (m); 999 (w); 860 (vs); 761 (s); 733 (s); 687 (m); 667 (w); 623 (w); 513 (w).																
UV	(c = 0.047 mg/ml in CH ₂ Cl ₂): $\lambda = 304$ nm; log $\epsilon = 4.68$; $\epsilon = 47979$ l/(mol·cm); extinction = 0.41 $\lambda = 278$ nm; log $\epsilon = 4.99$; $\epsilon = 97128$ l/(mol·cm); extinction = 0.83																
HRMS	(EI ⁺): <table><thead><tr><th>m/z</th><th>¹²C</th><th>¹H</th><th>Si</th><th>⁸⁰Se</th><th>mmu</th><th>Obs.Mass</th><th>Calc.Mass</th></tr></thead><tbody><tr><td>254</td><td>11</td><td>14</td><td>1</td><td>1</td><td>+3.2</td><td>254.0062</td><td>254.0030</td></tr></tbody></table>	m/z	¹² C	¹ H	Si	⁸⁰ Se	mmu	Obs.Mass	Calc.Mass	254	11	14	1	1	+3.2	254.0062	254.0030
m/z	¹² C	¹ H	Si	⁸⁰ Se	mmu	Obs.Mass	Calc.Mass										
254	11	14	1	1	+3.2	254.0062	254.0030										

5.3.2.6 Benzyl-2-(trimethylsilyl)-ethynyl selenide (**39**)



Materials:

1.96 g	(10 mmol)	benzylselenocynante (28)
1.03 g	(10.5 mmol)	trimethylsilylacetylene (TMSA)
6.6 ml	(10.5 mmol)	<i>n</i> -butyl lithium (as a 1.6 M solution in <i>n</i> -hexane)
250 ml		THF (solvent)
375 ml		light petroleum ether

Experimental procedure⁹³:

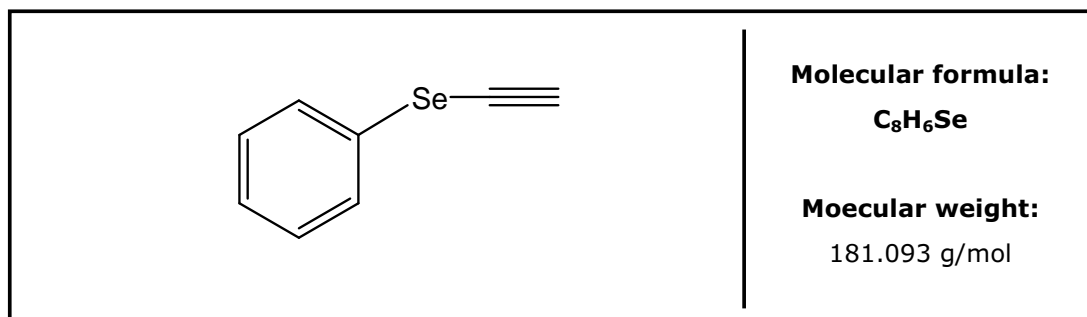
To a solution of TMSA in 250 ml of dry THF a solution of *n*-butyl lithium in *n*-hexane was added slowly at -25°C in such a way that the temperature does not exceed -25°C. After complete addition of *n*-BuLi the pale yellow solution was stirred for 2 hours at -25°C. The solution of **28** in ca. 100 ml dry THF was slowly added to the reaction flask, without letting the temperature exceed -20°C. After the addition was completed, the reaction mixture was allowed to stir for 2 hours at a temperature under -10°C. At the end of the reaction time, ca. 75 ml of a saturated NH₄Cl aqueous solution was added to the reaction mixture. After transferring the reaction mixture into a separation funnel, the organic phases were extracted with light petroleum ether (3 times 125 ml). The organic phases were collected together, washed with water and brine and dried overnight on MgSO₄. After removal of the solvent by rotary evaporation, the raw product was purified through column chromatography on deactivated silica-gel using a solvent mixture of light petroleum ether / dichloromethane (2:1) to afford compound **39** as pale yellow colored oil.

Yield 1.5 g (5.6 mmol) 56 %

Habitus pale yellow colored oil

TLC R_f-value 0.53 light petroleum ether / dichloromethane (2:1)

GC	$R_t = 18.44$ min																
MS	(EI ⁺ ; m/z; %): 268 [MP] ⁺ (2); 253 [M-CH ₃] ⁺ (1); 194 [M-C ₃ H ₉ Si] ⁺ (1); 171 [C ₇ H ₇ Se] ⁺ (2); 162 [C ₄ H ₆ SeSi] ⁺ (4); 147 [C ₃ H ₃ SeSi] ⁺ (2); 91 [C ₇ H ₇] ⁺ (BP, 100); 73 [C ₃ H ₉ Si] ⁺ (54.2); 65 [C ₅ H ₅] ⁺ (14.5).																
¹H-NMR	(500 MHz, CD ₂ Cl ₂); $\delta=0.18$ (s, 9H, Si(CH ₃) ₃); $\delta=4.02$ (s, ² J _{Se,H} =15.7 Hz, 2H, CH ₂ Se); $\delta=7.28$ (tt, J= 8.4, 1.2 Hz, 1H, H _{arom}); $\delta=7.32-7.35$ (m, 4H, H _{arom}).																
¹³C-NMR	(125 MHz, CD ₂ Cl ₂); $\delta=-0.1$ (p-Si(CH ₃) ₃ , ¹ J _{Si,C} =52.9 Hz); $\delta=33.1$ (p-CH ₂ , ¹ J _{Se,C} =56.3 Hz); $\delta=86.8$ (q-SeC); $\delta=109.8$ (q-CSi); $\delta=127.9$ (t-C _{arom}); $\delta=128.8$ (t-C _{arom} , 2C); $\delta=129.3$ (t-C _{arom} , 2C); $\delta=138.3$ (q-C _{arom} CH ₂).																
⁷⁷Se-NMR	(95 MHz, CD ₂ Cl ₂): $\delta=269.3$.																
IR	(film, cm ⁻¹): 3063 (w); 3029 (m); 2958 (s); 2897 (m); 2088 (vs); 1495 (s); 1454 (m); 1408 (w); 1262 (m); 1249 (vs); 1218 (w); 1186 (m); 1067(m); 1029 (w); 862 (bs); 760 (vs); 695 (vs); 622 (m); 594 (m); 551 (w).																
UV	(c = 0.133 mg/ml in CH ₂ Cl ₂): $\lambda = 240$ nm; log $\epsilon = 4.01$; $\epsilon = 10277$ l/(mol·cm); extinction = 0.51 $\lambda = 274$ nm; log $\epsilon = 2.74$; $\epsilon = 544$ l/(mol·cm); extinction = 0.27 $\lambda = 296$ nm; log $\epsilon = 2.53$; $\epsilon = 343$ l/(mol·cm); extinction = 0.17 $\lambda = 274$ nm; log $\epsilon = 2.08$; $\epsilon = 121$ l/(mol·cm); extinction = 0.06																
HRMS	(EI ⁺): <table><thead><tr><th>m/z</th><th>¹²C</th><th>¹H</th><th>Si</th><th>⁸⁰Se</th><th>mmu</th><th>Obs.Mass</th><th>Calc.Mass</th></tr></thead><tbody><tr><td>268</td><td>12</td><td>16</td><td>1</td><td>1</td><td>-2.0</td><td>268.0166</td><td>268.0187</td></tr></tbody></table>	m/z	¹² C	¹ H	Si	⁸⁰ Se	mmu	Obs.Mass	Calc.Mass	268	12	16	1	1	-2.0	268.0166	268.0187
m/z	¹² C	¹ H	Si	⁸⁰ Se	mmu	Obs.Mass	Calc.Mass										
268	12	16	1	1	-2.0	268.0166	268.0187										

5.3.2.7 Phenyl ethynyl selenide (31)**Materials:**

0.345 g	(1.4 mmol)	phenyl-2-(trimethylsilyl)-ethynyl selenide (38)
1.5 ml	(1.5 mmol)	0.1 N aqueous solution NaOH
20 ml		methanol

Experimental procedure:

The experimental procedure followed as described previously in section 5.2.3. After removal of the solvent through rotary evaporation compound **31** was obtained as a brown colored oil. GC-MS analysis showed a purity of more than 99.5 %, therefore it was not further purified.

Yield 0.050 g (0.27 mmol) 20 %

Habitus brown colored oil

GC R_t = 11.8 min

MS (EI⁺; m/z; %): 182 [M]⁺ (58); 157 [M-C₂H]⁺ (6.9); 103 [C₂Se]⁺ (BP, 100); 77 [C₆H₅]⁺ (21.6); 51 [C₄H₃]⁺ (22.4).

¹H-NMR (500 MHz, CD₂Cl₂): δ=3.24 (s, 1H, CH); δ=7.27 (tt, J = 7.3, 1.1 Hz, 1H, H_{arom}); δ=7.34 (td, J = 7.3, 1.2 Hz, 2H, H_{arom}); δ=7.57 (dt, J = 7.3, 1.1 Hz, 2H, H_{arom}).

¹³C-NMR (125 MHz, CD₂Cl₂): δ=64.6 (1C, t-CH); δ=91.9 (1C, q-SeC, ¹J_{Se,C}=33.6 Hz); δ=127.76 (q-C_{arom}Se); δ=127.78 (t-C_{arom}); δ=127.7 (t-C_{arom}, 2C, ³J_{Se,C}=14.2 Hz); δ=129.9 (t-C_{arom}, 2C).

⁷⁷Se-NMR (95 MHz, CD₂Cl₂): δ =269.1.

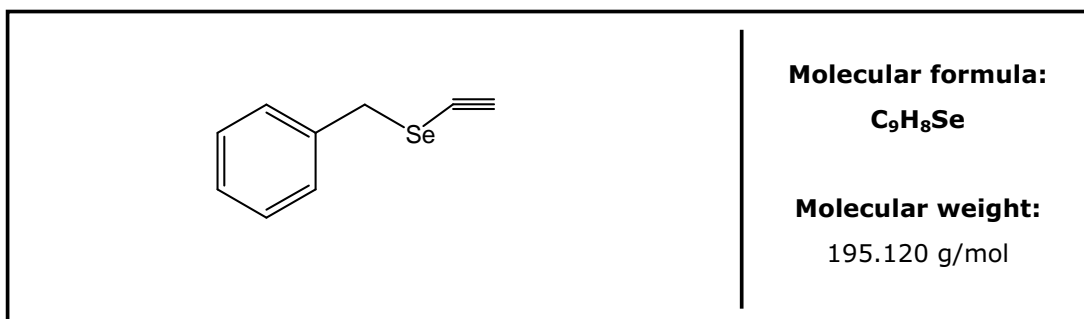
IR (film, cm⁻¹): 3288 (m); 3057 (m); 2920 (w); 2254 (w); 1685 (w); 1577 (m); 1476 (s); 1439 (m); 1301 (w); 1177 (w); 1068 (w); 1021 (m); 999 (m); 953 (s); 806 (w); 736 (vs); 712 (s); 688 (vs); 577 (m); 525 (w); 513 (w).

UV (c = 0.082 mg/ml in CH₂Cl₂):
 λ = 254 nm; log ϵ = 3.62; ϵ = 4194 l/(mol·cm); extinction = 0.19
 λ = 284 nm; log ϵ = 3.49; ϵ = 3090 l/(mol·cm); extinction = 0.14
 λ = 330 nm; log ϵ = 3.30; ϵ = 1987 l/(mol·cm); extinction = 0.09

HRMS (EI⁺):

m/z	¹² C	¹ H	⁸⁰ Se	mmu	Obs.Mass	Calc.Mass
182	8	6	1	+1.2	181.9647	181.9635

5.3.2.8 Benzyl ethynyl selenide (**32**)



Materials:

1.5 g	(5.6 mmol)	benzyl-2-(trimethylsilyl)-ethynyl selenide (39)
5.6 ml	(0.56 mmol)	0.1 N NaOH solution
40 ml		methanol (solvent)

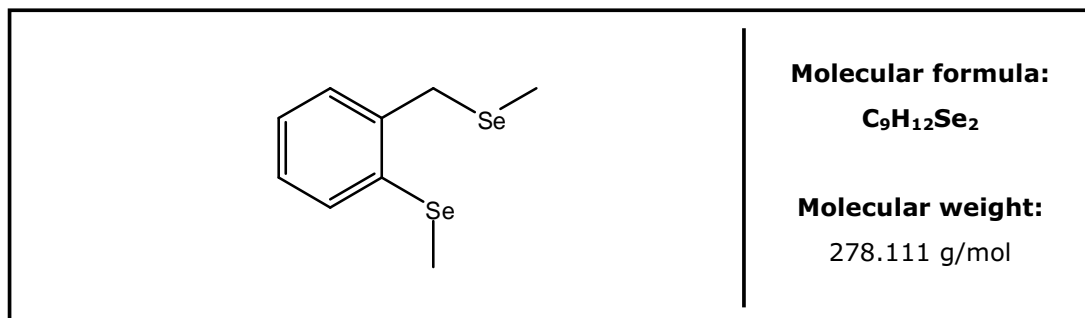
Experimental procedure:

The experimental procedure followed as described previously in section 5.3.2. After removal of the solvent through rotary evaporation compound **32** was obtained as yellow colored oil. GC-MS analysis showed a purity of more than 99 %, therefore it was not further purified.

Yield	0.584 g	(2.9 mmol)	53 %				
Habitus	light yellow colored oil						
GC	R _t = 13.71 min						
MS	(EI ⁺ ; m/z; %): 196 [M] ⁺ (5); 169 [C ₇ H ₇ Se] ⁺ (1); 105 [C ₂ HSe] ⁺ (5.4); 91 [C ₇ H ₇] ⁺ (BP, 100); 65 [C ₅ H ₅] ⁺ (14.5).						
¹H-NMR	(500 MHz, CD ₂ Cl ₂): δ=2.93 (s, 1H, CH); δ=4.05 (s, ² J _{Se,H} =14.8 Hz, 2H, CH ₂ Se); δ=7.27 (tt, J = 6.5, 1.9 Hz, 1H, H _{arom}); δ=7.30–7.36 (m, 4H, H _{arom}).						
¹³C-NMR	(125 MHz, CD ₂ Cl ₂): δ=32.7 (2C, ¹ J _{Se,C} =52.4 Hz, s-CH ₂); δ=66.0 (2C, t-CH); δ=90.0 (2C, ¹ J _{Se,C} =38,4 Hz, q-SeC); δ=127.9 (t-C _{arom}); δ=128.9 (t-C _{arom} , 2C); δ=129.2 (t-C _{arom} , 2C); δ=138.1 (q-C _{arom} CH ₂).						
⁷⁷Se-NMR	(95 MHz, CD ₂ Cl ₂): δ=245.3.						
IR	(film, cm ⁻¹): 3279(vs); 3084(w); 3062(w); 3028(m); 2936(w); 2029(m); 1949(w); 1877(w); 1805(w); 1601(w); 1494(vs); 1454(s); 1418(s); 1218(m); 1188(m); 1067(m); 1029(m); 913(w); 842(w); 802(w); 759(s); 696(vs); 595 (s); 552(m).						
UV	(c = 0.145 mg/ml in CH ₂ Cl ₂): λ = 242 nm; log ε = 3.83; ε = 6759 l/(mol·cm); extinction = 0.5 λ = 266 nm; log ε = 2.67; ε = 473 l/(mol·cm); extinction = 0.35 λ = 294 nm; log ε = 2.39; ε = 243 l/(mol·cm); extinction = 0.18						
HRMS	(EI ⁺):						
	m/z	¹² C	¹ H	⁸⁰ Se	mmu	Obs.Mass	Calc.Mass
	196	9	8	1	+1.8	195.9809	195.9791

5.3.3 Model compounds with two selenium centers

5.3.3.1 2-(methylselenyl) benzyl-methyl-selenide (**24**)



Materials:

2.5 g	(10 mmol)	2-bromo-benzyl bromide (40 a)
4.04 g	(40 mmol)	lithium methyl selenide (as THF solution)
2.5 ml	(40 mmol)	methyl iodide

Experimental procedure¹¹⁹:

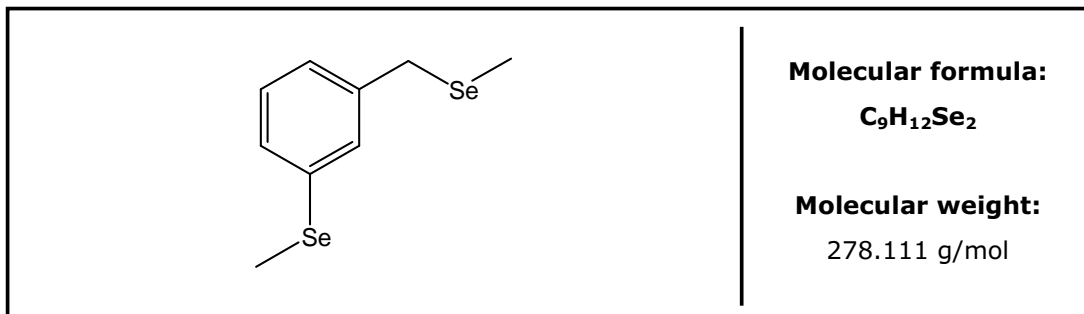
A solution of 2-bromo benzylbromide (**40 a**) in freshly distilled DMF was added dropwise via syringe under stirring to a solution of lithium methyl selenide in THF (see section 5.3.1.1.). The reaction flask, a four-necked round bottom flask, was immersed into a silicon bath and the THF and DE were distilled off. Then the flask was fitted with a reflux condenser, and the reaction mixture was kept under reflux for 50 hours at 135°C. After refluxing, the alkylating agent methyl iodide was added under stirring and the reaction mixture was allowed to cool down to room temperature. The reaction mixture was quenched by dropping it into 50 mL of deionized water and extracted with diethyl ether (3 times ca. 50 ml). The combined organic layers were washed with water and brine and dried over anhydrous $MgSO_4$ overnight, then the solvent was removed by rotary evaporation to afford a brown redish oil. After purification through silica-gel column chromatography using a solvent mixture of petrol ether / diethyl ether (20:1 to 10:1), compound **24** was obtained as yellow colored oil.

Yield 0.713 g (2.5 mmol) 25 %

Habitus yellow colored oil

TLC R_f -value 0.41 light petrol ether / diethyl ether (10:1)

GC	$R_t = 18.98$ min																																				
MS	(EI ⁺ ; m/z; %): 280 [M] ⁺ (42.5); 265 [M-CH ₃] ⁺ (62.1); 250 [M-2CH ₃] ⁺ (40.6); 185 [M-SeCH ₃] ⁺ (37.4); 169 (53.9) [C ₇ H ₇ Se] ⁺ ; 105 (BP) [C ₈ H ₉] ⁺ ; 91 (43.8) [C ₇ H ₇] ⁺ ; 78 (11.5) [C ₆ H ₅] ⁺ .																																				
¹H-NMR	(500 MHz, CD ₂ Cl ₂): $\delta=1.94$ (s, 3H, CH ₂ SeCH ₃ , $^2J_{Se,H}=10.6$ Hz); $\delta=2.32$ (s, 3H, CH ₃ , $^2J_{Se,H}=11.8$ Hz); $\delta=3.87$ (s, 2H, CH ₂ , $^2J_{Se,H}=12.6$ Hz); $\delta=7.11-7.19$ (m, 3H, H _{arom} / at low temperature it separated in 3 signals: $\delta=7.25$ - dt, $J=7.8$, 7.5, 1.5 Hz, 1H; $\delta=7.16$ - dt, $J=7.8$, 7.6, 1.2 Hz, 1H; $\delta=7.09$ - dd, $J = 7.5$, 1.2 Hz, 1H); $\delta=7.41$ (dd, $J = 7.6$, 1.5 Hz 1H, H _{arom})																																				
¹³C-NMR	(125MHz, CD ₂ Cl ₂): $\delta=4.6$ (p-CH ₂ SeCH ₃ , $^1J_{Se,C}=64.6$ Hz); $\delta=7.6$ (p-SeCH ₃ , $^1J_{Se,C}=65.1$ Hz); $\delta=28,9$ (s-CH ₂ Se, $^1J_{Se,C}=57.9$ Hz, $^3J_{Se,C}=13.0$ Hz); $\delta=126.2$ (t-C _{arom}); $\delta=127.8$ (t-C _{arom}); $\delta=129.8$ (t-C _{arom}); $\delta=131.4$ (t-C _{arom}); $\delta=133.4$ (q-C _{arom} , C-Se); $\delta=140.2$ (q-C _{arom} , C-CH ₂).																																				
⁷⁷Se-NMR	(95 MHz, CD ₂ Cl ₂): $\delta=158.8$ (SeCH ₃ , $^4J_{Se,Se}=37.8$ Hz); $\delta=161,2$ (CH ₂ SeCH ₃ , $^4J_{Se,Se}=37.8$ Hz).																																				
IR	(film, cm ⁻¹): 3055(w); 3001(m); 2923(s); 2072(w); 1948(w); 1917(w); 1692 (w); 1636(m); 1583(m); 1566(w); 1463(s); 1438(s); 1424(s); 1270(m); 1031(m); 904(m); 754(vs); 727(m); 614(w).																																				
HRMS	(EI ⁺):																																				
	<table border="0"> <thead> <tr> <th>m/z</th> <th>¹²C</th> <th>¹H</th> <th>⁷⁸Se</th> <th>⁸⁰Se</th> <th>⁸²Se</th> <th>mmu</th> <th>Obs.Mass</th> <th>Calc.Mass</th> </tr> </thead> <tbody> <tr> <td>280</td> <td>9</td> <td>12</td> <td></td> <td>2</td> <td></td> <td>+1.7</td> <td>279.9287</td> <td>279.9269</td> </tr> <tr> <td>280</td> <td>9</td> <td>12</td> <td>1</td> <td></td> <td>1</td> <td>+0.8</td> <td>279.9287</td> <td>279.9269</td> </tr> <tr> <td>278</td> <td>9</td> <td>12</td> <td>1</td> <td>1</td> <td></td> <td>+1.8</td> <td>277.9295</td> <td>277.9277</td> </tr> </tbody> </table>	m/z	¹² C	¹ H	⁷⁸ Se	⁸⁰ Se	⁸² Se	mmu	Obs.Mass	Calc.Mass	280	9	12		2		+1.7	279.9287	279.9269	280	9	12	1		1	+0.8	279.9287	279.9269	278	9	12	1	1		+1.8	277.9295	277.9277
m/z	¹² C	¹ H	⁷⁸ Se	⁸⁰ Se	⁸² Se	mmu	Obs.Mass	Calc.Mass																													
280	9	12		2		+1.7	279.9287	279.9269																													
280	9	12	1		1	+0.8	279.9287	279.9269																													
278	9	12	1	1		+1.8	277.9295	277.9277																													

5.3.3.2 3-(methylselenyl) benzyl-methyl-selenide (25)**Materials:**

5 g	(20 mmol)	3-bromobenzyl bromide (40 b)
10.1 g	(100 mmol)	lithium methyl selenide (as THF/DE solution)
6.25 ml	(100 mmol)	methyl iodide

Experimental procedure¹¹⁹:

The experimental procedure follows the description from section 5.3.1.10. The reaction mixture was refluxed in DMF at 135°C for 66 hours. Purification of compound **25** was achieved by using a silica-gel column chromatography, with a light petroleum ether / diethyl ether (10:1 ratio) mixture as eluent.

Yield	0.742 g	(2.6 mmol)	13.3 %
Habitus	yellow colored oil		
TLC	R _f -value	0.22	light petroleum ether (30/40) / diethyl ether (10:1)
GC	R _t = 19.05 min		
MS	(EI ⁺ ; m/z; %): 280 [M] ⁺ (24.2); 265 [M-CH ₃] ⁺ (0.5); 249 [M-2CH ₃] ⁺ (0.9); 185 [M-SeCH ₃] ⁺ (BP, 100); 170 [C ₇ H ₇ Se] ⁺ (31.3); 104 [C ₈ H ₉] ⁺ (32.5); 95 [CH ₃ Se] ⁺ (7); 91 [C ₇ H ₇] ⁺ (8.9); 78 [C ₆ H ₅] ⁺ (5.9).		
¹H-NMR	(500 MHz, CD ₂ Cl ₂): δ=1.91 (s, 3H, CH ₃ , ² J _{Se,H} =10.6 Hz); δ=2.34 (s, 3H, CH ₃ , ² J _{Se,H} =11.2 Hz); δ=3.69 (s, 2H, CH ₂ , ² J _{Se,H} =13.3 Hz); δ=7.094 (dt, J= 7.6, 1.3 Hz, 1H, H _{arom}); δ=7.18 (t, J= 7.6, 1H, H _{arom}); δ=7.25 (dt, J= 7.6, 1.3 Hz, 1H, H _{arom}); δ=7.32 (t, J = 1.3 Hz, 1H, H _{arom}).		

¹³C-NMR (125MHz, CD₂Cl₂): δ=4.4 (p-CH₂SeCH₃); δ=7.1 (p-SeCH₃); δ=28,3 (s-CH₂Se); δ=126.9 (t-C_{arom}); δ=128.5 (t-C_{arom}); δ=129.3 (t-C_{arom}); δ=130.6 (t-C_{arom}); δ=132.4 (q-C_{arom}, C-CH₂); δ=140.9 (q-C_{arom}, C-Se).

⁷⁷Se-NMR (95 MHz, CD₂Cl₂): δ=173.5 (SeCH₃); δ=201.1 (CH₂SeCH₃).

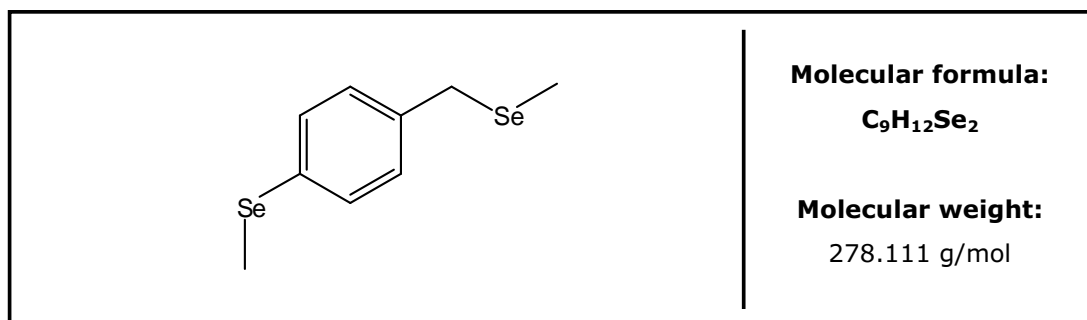
IR (film, cm⁻¹): 3049 (w); 3000 (m); 2923 (s); 2253 (w); 1687 (w); 1598 (s); 1568 (s); 1474 (s); 1423 (s); 1272 (m); 1216 (w); 1185 (w); 1074 (m); 996 (w); 903 (m); 853 (w); 782 (s); 696 (vs); 668 (w); 564 (w); 520 (w).

UV (c = 0.137 mg/ml in CH₂Cl₂):
 λ = 248 nm; log ε = 3.94; ε = 8788 l/(mol·cm); extinction = 0.43
 λ = 268 nm; log ε = 3.83; ε = 6745 l/(mol·cm); extinction = 0.33

HRMS (EI⁺):

m/z	¹² C	¹ H	⁷⁸ Se	⁸⁰ Se	⁸² Se	mmu	Obs.Mass	Calc.Mass
280	9	12		2		-0.5	279.9265	279.9269
280	9	12	1		1	-1.5	279.9265	279.9269
278	9	12	1	1		-0.5	277.9272	277.9277

5.3.3.3 4-(methylselenyl) benzyl-methyl-selenide (26)



Materials:

2.45 g	(10 mmol)	4-bromo-benzyl bromide (40 c)
4.04 g	(40 mmol)	lithium methyl selenide (as THF solution)
2.5 ml	(40 mmol)	methyl iodide

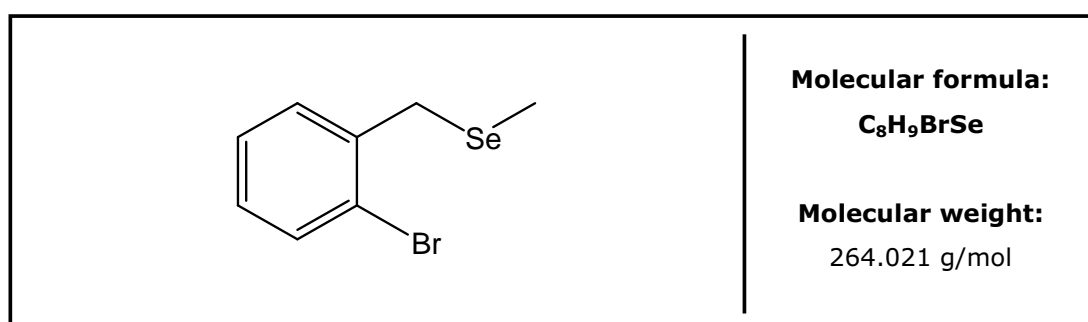
Experimental procedure¹¹⁹:

The experimental procedure follows the description from section 5.3.1.10. The reaction mixture was refluxed in DMF at 125°C for 60 hours. Purification of compound **26** was achieved by using a silica-gel column chromatography, with a light petroleum ether / diethyl ether (100:1 ratio) solvent mixture.

Yield	0.58 g	(2.1 mmol)	21 %
Habitus	yellow colored oil		
TLC	R _f -value	0.23	light petroleum ether (30/40) / diethyl ether (100:1)
GC	R _t = 19.33 min		
MS	(EI ⁺ ; m/z; %): 280 [M] ⁺ (14.5); 265 [M-CH ₃] ⁺ (1.1); 249 [M-2CH ₃] ⁺ (0.6); 185 [M-SeCH ₃] ⁺ (BP,100); 170 [C ₇ H ₇ Se] ⁺ (61.6); 104 [C ₈ H ₉] ⁺ (12) ; 95 [CH ₃ Se] ⁺ (3.7); 91 [C ₇ H ₇] ⁺ (4.8); 78 [C ₆ H ₅] ⁺ (15).		
¹H-NMR	(500 MHz, CD ₂ Cl ₂): δ=1.89 (s, 3H, CH ₃ , ² J _{Se,H} =10.6 Hz); δ=2.33 (s, 3H, CH ₃ , ² J _{Se,H} =11.1 Hz); δ=3.69 (s, 2H, CH ₂ , ² J _{Se,H} =14.4 Hz); δ=7.16 (m, J= 8.4, 2.1, 0.9 Hz, 2H, H _{arom}); δ=7.33 (m, J= 8.4, 2.1 Hz, 2H, H _{arom}).		
¹³C-NMR	(125MHz, CD ₂ Cl ₂): δ=4.3 (p-CH ₂ SeCH ₃ , ¹ J _{Se,C} =64.3 Hz); δ=7.3 (p-SeCH ₃ , ¹ J _{Se,C} =64.9 Hz); δ=28.1 (s-CH ₂ Se, ¹ J _{Se,C} =58.4 Hz); δ=129.8 (t-C _{arom}); δ=130.3 (q-C _{arom} , C-CH ₂); δ=130.6 (t-C _{arom} , ² J _{Se,C} =11.5 Hz); δ=137.9 (q-C _{arom} , C-Se).		
⁷⁷Se-NMR	(95 MHz, CD ₂ Cl ₂): δ=174.5 (SeCH ₃); δ=197.3 (CH ₂ SeCH ₃).		
IR	(film, cm ⁻¹): 3047 (w); 2999 (m); 2922 (s); 2818 (w); 2226 (w); 1593 (w); 1489 (s); 1423 (m); 1398 (m); 1272 (m); 1185 (w); 1094 (w); 1070 (m); 905 (m); 826 (m); 717 (w); 622 (w); 600 (w); 537 (w); 514 (w).		
UV	(c = 0.083 mg/ml in CH ₂ Cl ₂): λ = 276 nm; log ε = 4.01; ε = 10157 l/(mol·cm); extinction = 0.3 λ = 258 nm; log ε = 3.96; ε = 9141 l/(mol·cm); extinction = 0.27		

HRMS	(EI ⁺):								
	m/z	¹² C	¹ H	⁷⁸ Se	⁸⁰ Se	⁸² Se	mmu	Obs.Mass	Calc.Mass
	280	9	12			2		-1.6	279.9254
280	9	12	1			1	-2.5	279.9254	279.9269

5.3.3.4 2-bromobenzyl methyl selenide (**41**)



Materials:

10.0 g	(40 mmol)	2-bromobenzyl bromide (40 a)
6.05 g	(60 mmol)	lithium methyl selenide (as THF/DE solution)
2.5 ml	(40 mmol)	methyl iodide

Experimental procedure¹¹⁹:

Lithium methyl selenide was prepared according to the procedure described in section 5.3.1. The subsequent synthesis follows the procedure described in section 5.3.2.2. Refluxing period was 4 hours and stirring at room temperature took place for a period of 12 hours. The product was purified by silica-gel column chromatography using a solvent mixture of *n*-hexane / dichloromethane (20:1).

Yield 4.17 g (15.8 mmol) 39.5 %

Habitus yellow colored oil

TLC R_F-value 0.34 *n*-hexane / dichloromethane (20:1)

GC R_t = 16.7 min

MS (EI⁺; m/z; %): 264 [M]⁺ (18.8); 169 [C₇H₆Br]⁺ (BP, 100); 91 [C₇H₆]⁺ (40.7); 63 [C₅H₃]⁺ (22.3).

¹H-NMR (500 MHz, CD₂Cl₂): δ=1.97 (s, 3H, CH₃, ²J_{Se,H}= 10.8 Hz); δ=3.85 (s, 2H, CH₂, ²J_{Se,H}= 13.1 Hz), δ=7.09 (ddd, 1H, J= 7.9, 7.0, 2.1 Hz; H_{arom}), δ=7.25 (p-dt, 1H, J= 7.6, 7.0, 1.0 Hz; H_{arom}); δ=7.28 (dd, 1H, J= 7.6, 2.1 Hz; H_{arom}); δ=7.54 (dd, 1H, J= 7.90, 0.91 Hz, H_{arom}).

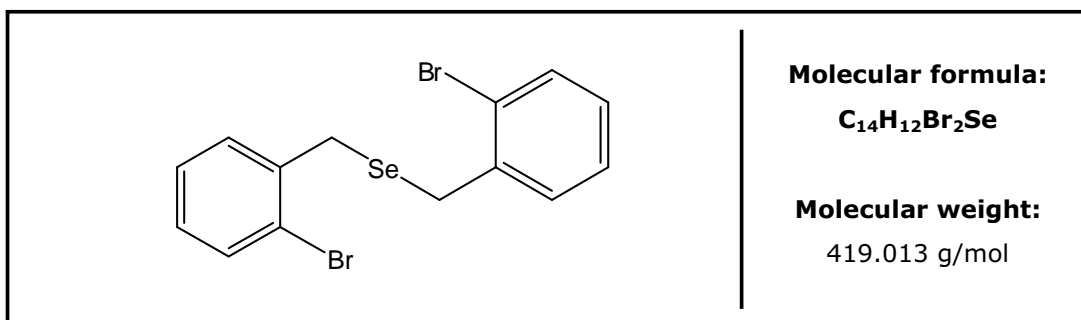
¹³C-NMR (125 MHz, CD₂Cl₂): δ= 4.5 (3C, s-CH₃) δ=28.7 (2C, s-CH₂, ¹J_{Se,C}= 61.8 Hz); δ=124.5 (1C, q-C_{arom}); δ=127.8 (1C, t-C_{arom}); δ=128.6 (1C, t-C_{arom}); δ=130.9 (1C, q-C_{arom}CH₂); δ=133.4 (1C, t-C_{arom}); δ=139.5 (1C, q-C_{arom}Se).

⁷⁷Se-NMR (95 MHz, CD₂Cl₂): δ=166.9.

IR (film, cm⁻¹): 3055 (m); 2996 (m); 2922 (m); 2818 (w); 1565 (m); 1472 (s); 1465(m); 1439 (s); 1422 (s); 1275 (m); 1187 (m); 1096 (m); 1043 (w); 1023 (s); 943 (m); 919 (m); 817 (w); 754 (vs); 723 (m); 658 (m); 615 (w); 568 (w).

UV (c = 0.086 mg/ml in CH₂Cl₂):
λ = 274 nm; log ε = 3.04; ε = 1105 l/(mol·cm); extinction = 0.36

5.3.3.5 Bis-(2-bromobenzyl) selenide (**42**)



Materials:

10.0 g	(40 mmol)	2-bromobenzyl bromide (40 a)
6.05 g	(60 mmol)	lithium methyl selenide (as THF/DE solution)
2.5 ml	(40 mmol)	methyl iodide

Experimental procedure:

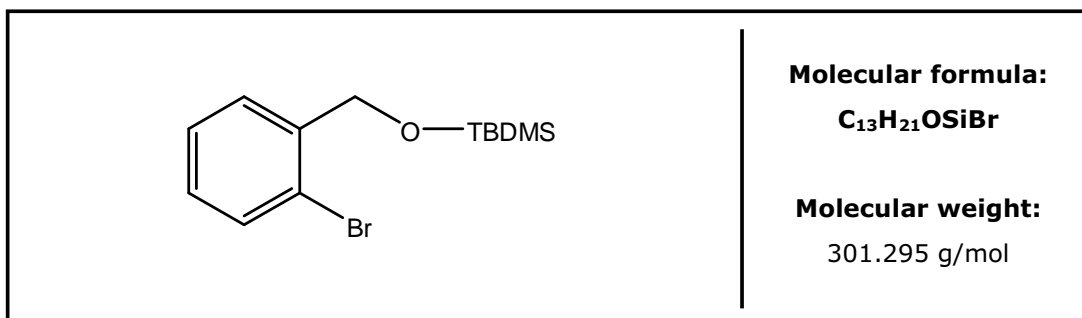
The compound **42** was obtained as a by-product at the synthesis of 2-bromobenzyl methyl selenide (**41**). The experimental procedure is described in section 5.3.3.4. Purification by

column chromatography on silica-gel using a solvent mixture of *n*-hexane / dichloromethane (20:1) afforded pure **42**.

Yield	1.812 g	(4.3 mmol)	10.7 %						
Habitus	light yellow crystals								
TLC	R _F -value	0.17	<i>n</i> -hexane / dichloromethane (20:1)						
GC	R _t = 29.7 min								
MS	(EI ⁺ ; m/z; %): 420 [M] ⁺ (11.8); 169 [C ₇ H ₆ Br] ⁺ (BP, 100); 91 [C ₇ H ₆] ⁺ (30.7); 63 [C ₅ H ₃] ⁺ (12.3).								
¹H-NMR	(500 MHz, CD ₂ Cl ₂): δ=3.94 (s, 4H, CH ₂ , ² J _{Se,H} = 11.4 Hz), δ=7.09 (dt, 2H, J= 7.9, 7.7, 1.9 Hz, H _{arom}), δ=7.24 (dt, 2H, J= 7.7, 7.6, 1.2 Hz, H _{arom}); δ=7.30 (dd, 2H, J= 7.6, 1.9 Hz, H _{arom}); δ=7.54 (dd, 2H, J= 7.9, 1.2 Hz, H _{arom}).								
¹³C-NMR	(125 MHz, CD ₂ Cl ₂): δ=28.6 (2C, s-CH ₂ , ¹ J _{Se,C} = 62.9 Hz); δ=124.6 (2C, q-C _{arom}); δ=127.9 (2C, t-C _{arom}); δ=128.8 (2C, t-C _{arom}); δ=131.0 (2C, q-C _{arom} CH ₂); δ=133.4 (2C, t-C _{arom}); δ=139.2 (2C, q-C _{arom} Se).								
⁷⁷Se-NMR	(95 MHz, CD ₂ Cl ₂): δ=314.3.								
IR	(KBr, cm ⁻¹): 3442(bs); 3079(w); 3066(w); 3050(w); 2985(w); 2943(m); 1648(w); 1565(w); 1475(m); 1465(m); 1439(s); 1418(m); 1264(w); 1188(w); 1182(m); 1137(w); 1043(m); 1026(s); 1021(s); 946(w); 838(m); 763(vs); 753(vs); 723(s); 658(m); 609(w); 573(m); 481(m).								
UV	(c = 0.026 mg/ml in CH ₂ Cl ₂): λ = 270 nm; log ε = 4.00; ε = 9944 l/(mol·cm); extinction = 0.062								
HRMS	(EI ⁺):								
	m/z	¹² C	¹ H	⁸¹ Br	⁷⁸ Se	mmu	Obs.Mass	Calc.Mass	
	420	14	12	2	1	+1.6	419.8454	419.8451	
	m/z	¹² C	¹ H	⁷⁹ Br	⁸¹ Br	⁸⁰ Se	mmu	Obs.Mass	Calc.Mass
	420	14	12	1	1	1	+0.4	419.8454	419.8451

m/z	¹² C	¹ H	⁷⁹ Br	⁸² Se	mmu	Obs.Mass	Calc.Mass
420	14	12	2	1	-1.9	419.8454	419.8451

5.3.3.6 2-bromobenzyl-*t*-butyldimethylsilyl ether (**44**)



Materials:

5.79 g	(31.0 mmol)	2-bromobenzyl alcohol (43)
5.58 g	(37.0 mmol)	<i>t</i> -butyldimethylchloro silane (TBDMS-Cl)
5.20 g	(76.4 mmol)	imidazole
ca. 60 ml		dimethylformamide (solvent)

Experimental procedure¹²⁸:

To a solution of 2-bromobenzyl alcohol (**43**) and imidazole in 50 ml of dry DMF in a 250 ml Schlenk-flask was added a solution of TBDMS-Cl in 10 ml dry DMF using a syringe. The reaction mixture was stirred for the next 20 h at room temperature. After that time the reaction was quenched by 100 ml deionized water and stirred for further 1.5 h. Afterwards the work up was carried out by extracting the reaction mixture with diethyl ether (4 times ca. 70 ml). The combined organic layers were washed with water, brine and then dried over MgSO₄. The solvent was evaporated to afford a brown oil as raw product. The product was isolated by purification using column chromatography on silica gel, eluting with a petroleum ether / dichloromethane (10:1 ratio) solvent mixture.

Yield 8.580 g (28.5 mmol) 92%

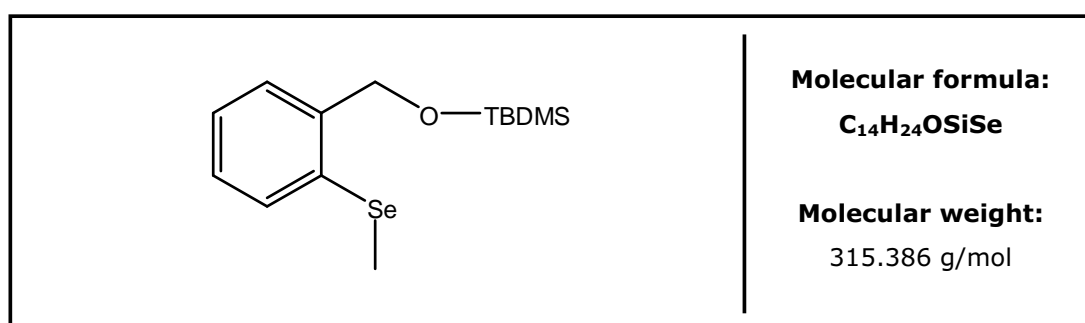
Habitus colourless, clear oil

TLC R_f-value 0.45 petroleum ether (30/40) / dichloromethane (10:1)

GC R_t = 18.50 min

MS	(EI ⁺ ; m/z; %): 301 [M] ⁺ (~1); 243 [M-C ₄ H ₉] ⁺ (BP, 100); 213 [M-C ₆ H ₁₅] ⁺ (27.2); 169 [M-C ₆ H ₁₅ OSi] ⁺ (46.9); 105 [C ₇ H ₆ O] ⁺ (5.2); 90 [C ₇ H ₆] ⁺ (3.5).
¹H-NMR	(500 MHz, CDCl ₃): δ=0.14 (s, 6H, Si(CH ₃) ₂); δ=0.97 (s, 9H, SiC(CH ₃) ₃); δ=4.74 (s, CH ₂); δ=7.12 (td, 1H, J= 7.8, 0.5 Hz, H _{arom}); δ=7.33 (td, 1H, J= 7.8, 0.6 Hz, H _{arom}); δ=7.49 (dd, 1H, J= 7.9, 0.5 Hz, H _{arom}); δ=7.56 (dd, 1H, J= 7.8, 0.6 Hz, H _{arom}).
¹³C-NMR	(125 MHz, CDCl ₃): δ=-5.3 (2C, p-Si(CH ₃) ₂); δ=18.4 (q-SiC(CH ₃) ₃); δ=25.9 (3C, p-SiC(CH ₃) ₃); δ=64.6 (s-CH ₂); δ=121.0 (q-C _{ar} Br); δ=127.3 (t-C _{arom}); δ=127.5 (t-C _{arom}); δ=128.1 (t-C _{arom}); δ=132.0 (t-C _{arom}); δ=140.3 (q-C _{ar} CH ₂).
IR	(KBr, cm ⁻¹): 3500-3150 (bs); 2955 (s); 2930 (s); 2885 (m); 2857 (s); 1700 (m); 1592(w); 1571 (w); 1471 (m); 1442 (m); 1430 (w); 1421 (w); 1291 (s); 1255 (m); 1201(m); 1130 (m); 1098 (m); 1044 (m); 1027 (m); 1006 (w); 940 (w); 837 (s); 778 (s); 749 (s); 671 (m).
UV	(c = 0.136 mg/ml in CH ₂ Cl ₂): λ = 306 nm; log ε = 2.59; ε = 390 l/(mol·cm); extinction = 0.11 λ = 282 nm; log ε = 2.78; ε = 602 l/(mol·cm); extinction = 0.17 λ = 256 nm; log ε = 3.24; ε = 1735 l/(mol·cm); extinction = 0.49 λ = 244 nm; log ε = 3.35; ε = 2231 l/(mol·cm); extinction = 0.63

5.3.3.7 2-(methylselenyl)-benzyl-*t*-butyldimethylsilyl ether (**45**)



Materials:

6.03 g	(20.0 mmol)	2-bromobenzyl- <i>t</i> -butyldimethylsilyl ether (44)
6.06 g	(60.0 mmol)	lithium methyl selenide (as a THF / DE solution)
3.8 ml	(60.0 mmol)	methyl iodide
ca. 100 ml		tetrahydrofuran (solvent)

ca. 100 ml dimethylformamide (solvent)

Experimental procedure¹¹⁹:

To a solution of 6.03 g (20 mmol) of 44 in 100 ml of dry DMF was added 6.06 (20 mmol) of lithium methyl selenide as a THF/diethyl ether solution, prepared as described in section 5.3.1.1. The reaction mixture was heated up to 70°C in order to remove the THF and diethyl ether by distillation. Subsequently the reaction solution was heated at 80 - 90°C under vigorous stirring for further 60 h. After cooling down to room temperature, MeI was added and stirred for 45 min, then the reaction was quenched with ca. 200 ml water and stirred for 1.5 h. After extraction with diethyl ether (4 times 100ml) the combined organic layers were washed with water, saturated NaHCO₃ solution and brine, then dried over MgSO₄. After removal of the solvent, the raw product was obtained as orange oil. The pure product was isolated by column chromatography on silica gel, eluting with petroleum ether (30/40) / diethyl ether (10:1 ratio) solvent mixture.

Yield	2.98 g	(9.4 mmol)	47%
Habitus	dark yellow colored oil		
TLC	R _f -value	0.62	petroleum ether (30/40) / diethyl ether (10:1)
GC	R _t = 20.1 min		
MS	(EI ⁺ ; m/z; %): 316 [M] ⁺ (>1); 259 [M-C ₄ H ₉] ⁺ (BP, 100); 185 [M-C ₆ H ₁₅ SiO] ⁺ (50.7); 169 [M-C ₇ H ₁₈ SiO] ⁺ (12.0); 91 [M-C ₇ H ₁₈ SiOSe] ⁺ (27.2); 105 [C ₇ H ₅ O] ⁺ (49.3).		
¹H-NMR	(500 MHz, CDCl ₃): δ=0.12 (s, 6H, Si(CH ₃) ₂); δ=0.95 (s, 9H, SiC(CH ₃) ₃); δ=2.31 (s, 3H, SeCH ₃); δ=4.77 (s, 2H, CH ₂); δ=7.20 (td, 1H, J= 7.4, 1.3 Hz, H _{arom}); δ=7.23 (td, 1H, J= 7.4, 0.5 Hz, H _{arom}); δ=7.37 (dd, 1H, J= 7.4, 1.3 Hz, H _{arom}); δ=7.45 (td, 1H, J= 7.4, 0.5 Hz, H _{arom}).		
¹³C-NMR	(125 MHz, CDCl ₃): δ=-5.3 (2C, p-Si(CH ₃) ₂); δ=6.9 (p-SeCH ₃); δ=18.4 (q-SiC(CH ₃) ₃); δ=26.0 (3C, p-SiC(CH ₃) ₃); δ=64.6 (s-CH ₂); δ=126.1 (t-C _{arom}); δ=126.6 (t-C _{arom}); δ=127.6 (t-C _{arom}); δ=129.6 (t-C _{arom}); δ=130.4 (q-C _{arom} -SeCH ₃); δ=141.2 (q-C _{arom} CH ₂).		
⁷⁷Se-NMR	(95 MHz, CD ₂ Cl ₂): δ=154.5.		

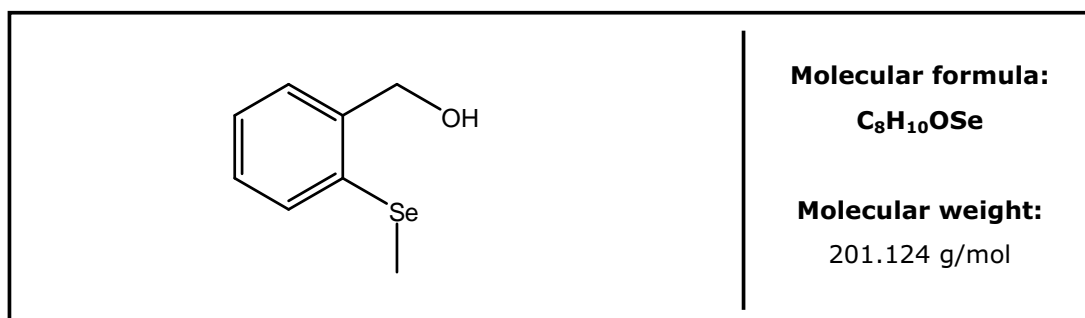
IR (film, cm^{-1}): 3059 (w); 2954 (s); 2929 (s); 2885 (m); 2856 (s); 1528(w); 1467 (m); 1448 (m); 1431 (w); 1255 (s); 1201(m); 1123 (m); 1093 (s); 1051 (m); 1034 (m); 1006 (w); 839 (s); 815 (m); 777 (s); 745 (m); 672 (m).

UV ($c = 0.136 \text{ mg/ml}$ in CH_2Cl_2):
 $\lambda = 282 \text{ nm}$; $\log \epsilon = 3.63$; $\epsilon = 4281 \text{ l}/(\text{mol}\cdot\text{cm})$; extinction = 0.21
 $\lambda = 248 \text{ nm}$; $\log \epsilon = 3.67$; $\epsilon = 4689 \text{ l}/(\text{mol}\cdot\text{cm})$; extinction = 0.23

HRMS (EI+):

m/z	^{12}C	^1H	^{16}O	^{28}Si	^{80}Se	mmu	Obs.Mass	Calc.Mass
316	14	24	1	1	1	-0.1	316.0760	316.0762

5.3.3.8 2-(methylselenyl)-benzyl alcohol (**46**)



Materials:

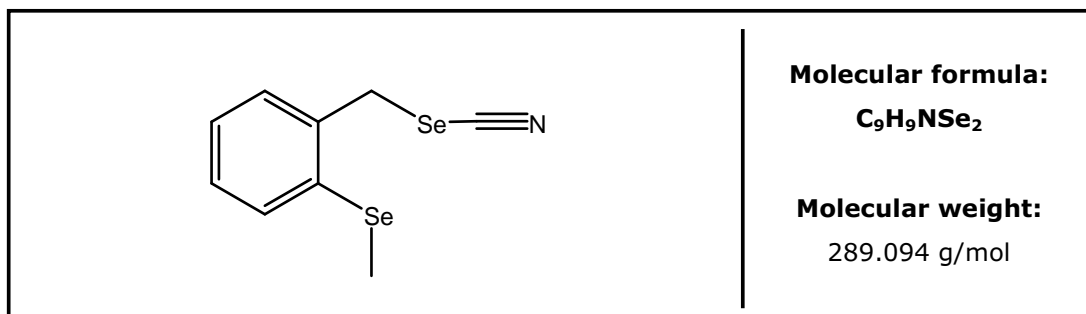
5.670 g	(18 mmol)	2-(methylselenyl)-benzyl- <i>tert</i> -butyldimethylsilyl ether (45)
103 ml		concentrated acetic acid
34 ml		tetrahydrofuran
34 ml		water

Experimental procedure¹²⁸:

To a solution consisting of acetic acid, THF and water was added compound **45**. The slightly pale mixture was stirred for 20 h at room temperature. After extraction with diethyl ether (4 times 100 ml), the combined organic layers were washed with a large quantity of water, then saturated NaHCO_3 solution and brine. The organic layers were dried over MgSO_4 and then the solvent was removed by rotary evaporation. The final product was purified by column chromatography on deactivated silica gel, eluting with a petroleum ether (30/40) / dichloromethane (1:1 ratio) solvent mixture.

Preparative procedures

Yield	3.356 g	(16.7 mmol)	93 %
Habitus	light yellow colored oil	(crystals at -25°C)	
TLC	R _f -value	0.05	petroleum ether (30/40) / dichloromethane (1:1)
GC	R _t = 16.25 min		
MS	(EI+; m/z; %): 202 [M] ⁺ (61.0); 187 [M-CH ₃] ⁺ (36.6); 157 [M-C ₂ H ₅ O] ⁺ (28.0); 105 [C ₇ H ₅ O] ⁺ (95.1); 77 [C ₆ H ₅] ⁺ (BP, 100).		
¹H-NMR	(500 MHz, CDCl ₃): δ=2.19 (s, 1H, OH); δ=2.33 (s, 3H, SeCH ₃ ² J _{Se,H} =11.6 Hz); δ=4.75 (s, 2H, CH ₂); δ=7.21-7.26 (m, 2H, H _{arom}); δ=7.35-7.39 (m, 1H, H _{arom}); δ=7.41-7.45 (m, 1H, H _{arom}).		
¹³C-NMR	(125 MHz, CDCl ₃): δ=7.4 (p-SeCH ₃); δ=65.1 (s-CH ₂); δ=126.5 (t-C _{arom}); δ=128.1 (t-C _{arom}); δ=128.4 (t-C _{arom}); δ=130.7 (t-C _{arom}); δ=131.5 (q-C _{arom} SeCH ₃); δ=140.9 (q-C _{arom} CH ₂).		
⁷⁷Se-NMR	(95 MHz, CD ₂ Cl ₂): δ=155.1.		
IR	(film, cm ⁻¹): 3348(bs); 3057(m); 3007(w); 2927(m); 2874(w); 1587(w); 1568(w); 1464(m); 1442(s); 1428(s); 1271(w); 1197(m); 1060(m); 1028(s); 908(m); 749(vs); 661(w); 603(m); 533(w); 516(w).		

5.3.3.9 2-(methylselenyl)-benzyl selenocyanate (29)**Materials:**

1.410 g	(7.0 mmol)	2-(methylselenyl)-benzyl alcohol (46)
4.180 g	(29.0 mmol)	potassium selenocyanate
0.75 ml	(14.6 mmol)	bromine
3.777g	(7.2 mmol)	triphenylphosphine (PPh ₃)
ca. 250 ml		dichloro methane
ca. 200 ml		tetrahydrofuran

Experimental procedure¹²⁹:

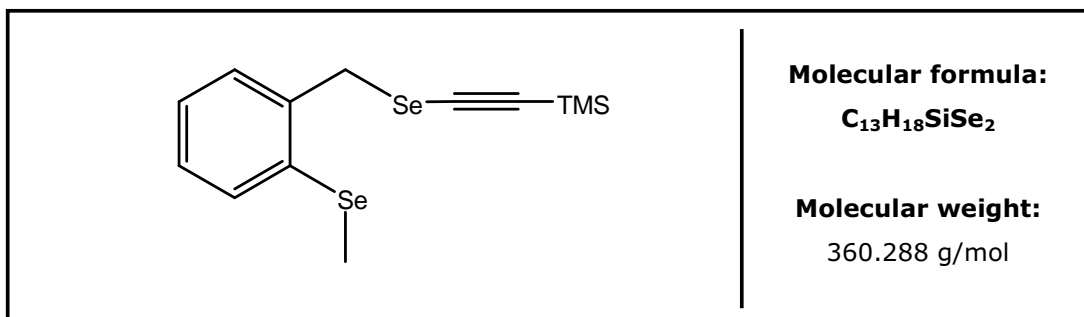
To synthesize selenocyanogen¹³¹, KSeCN was dissolved in ca. 200 ml of THF and placed into a 500 ml three-necked flask. After cooling to -15°C bromine was added by using a syringe through a rubber lid. An orange colouring appeared which changed to a strong yellow colour at the end of the addition process. The mixture was cooled to -75°C, stirred for 45 min and filtrated over a glass frit (under vacuum) to a 1000 ml three-necked flask already cooled down to -75°C. The PPh₃ dissolved in 200 ml anhydrous CH₂Cl₂, was added dropwise using a cooled dropping funnel, taking care that the reaction mixture did not warm up over a temperature of -65°C. The colour changed while adding to a dark orange. Then the alcohol **46** dissolved in 50 ml of dichloromethane was slowly added by syringe in a controlled manner so that the reaction temperature would not exceed -70°C. Following complete addition of the alcohol, the reaction mixture was cooled to -75°C and stirred overnight. Allowed to warm up to room temperature the reaction mixture was filtered and the solvent evaporated. The product was purified by column chromatography on deactivated silica-gel, with a mixture of petroleum ether (30/40) / dichloromethane (1:1 ratio) as eluent.

Yield 0.534 g (1.85 mmol) 26%

Habitus pale yellow crystals

Preparative procedures

TLC	R _f -value	0.26	petroleum ether (30/40) / dichloro methane	(1:1)					
GC	R _t =	21.15 min							
MS	(EI ⁺ ; m/z; %):	291 [M] ⁺ (3.7); 185 [M-SeCN] ⁺ (45.7); 169 [M-CH ₃ SeCN] ⁺ (23.0); 105 [SeCN] ⁺ (BP, 100); 91 [C ₇ H ₇] ⁺ (48.1).							
¹H-NMR	(500 MHz, CD ₂ Cl ₂):	δ=2.37 (s, 3H, SeCH ₃ , ² J _{Se,H} =11.4 Hz); δ=4.39 (s, 2H, CH ₂ , ² J _{Se,H} =15.2 Hz); δ=7.25 (td, J= 7.4, 1.6, 1H, H _{arom}); δ=7.27 (td, J= 7.4, 2.0, 1H, H _{arom}); δ=7.35 (dd, J= 7.4, 2.0, 1H, H _{arom}) δ=7.52 (dd, J=7.4, 1.6, 1H, H _{arom}).							
¹³C-NMR	(125 MHz, CD ₂ Cl ₂):	δ=9.0 (p-SeCH ₃); δ=34.4 (s-CH ₂); δ=102.6 (q-SeCN); δ=127.5 (t-C _{arom}); δ=129.8 (t-C _{arom}); δ=130.1 (t-C _{arom}); δ=132.8 (t-C _{arom}); δ=133.5 (q-C _{arom} SeCH ₃); δ=137.7 (q-C _{arom} CH ₂).							
⁷⁷Se-NMR	(95 MHz, CD ₂ Cl ₂):	δ=157.3 (SeCH ₃ , ⁴ J _{Se,Se} =58.8 Hz); δ=282.9 (SeCN, ⁴ J _{Se,Se} =58.8 Hz).							
IR	(KBr, cm ⁻¹):	3424 (bm); 3060(w); 2992(w); 2925(m); 2153(s); 1627(w); 1558(w); 1473(m); 1462(s); 1440(m); 1420(s); 1269(w); 1209(m); 1187 (m); 1055(w); 1029(s); 916(m); 840(w); 765(s); 725(m); 657(m); 597(s); 564(w); 523(w).							
UV	(c = 0.136 mg/ml in CH ₂ Cl ₂):	λ = 272 nm; log ε = 3.45; ε = 2846 l/(mol·cm); extinction = 1.33 λ = 292 nm; log ε = 3.26; ε = 1819 l/(mol·cm); extinction = 0.85 λ = 300 nm; log ε = 3.19; ε = 1541 l/(mol·cm); extinction = 0.72							
HRMS	(EI ⁺)								
	m/z	¹² C	¹ H	¹⁴ N	⁷⁸ Se	⁸⁰ Se	mmu	Obs.Mass	Calc.Mass
	291	9	9	1	1	1	+0.5	290.9080	290.9065
	291	9	9	1		2	+1.5	290.9080	290.9065

5.3.3.10 2-(methylselenyl)-benzyl-2-(trimethylsilyl)-ethynyl selenide (47)**Materials:**

0.613 g	(2.12 mmol)	2-(methylselenyl)-benzyl selenocyanate (29)
0.212 g	(2.16 mmol)	trimethylsilyl acetylene (as DE solution)
1.35 ml	(2.16 mmol)	<i>n</i> -butyllithium
ca. 300 ml		tetrahydrofuran (solvent)

Experimental procedure⁹³:

To a solution of TMSA (0.212 g, 2.16 mmol) in 200 ml dry THF, cooled at -25°C, *n*-BuLi was added dropwise through a rubber lid by using a syringe within a period of 10 min, then stirred for 2 h at -40°C. 2-(methylselenyl)-benzyl selenocyanate (**29**) dissolved in ca. 100 ml of dry THF was added dropwise through a cooled dropping funnel during a period of 1.5 h at -30°C and stirred for an additional hour. The pale yellow colored reaction mixture was allowed to warm up to room temperature and mixed with ca. 60 ml of saturated NH₄Cl-solution. As a result a white precipitation appeared. After adding 80 ml of light petroleum ether, the layers were separated. The aqueous layer was further extracted three times with ca. 50 ml of light petroleum ether. The combined organic layers were washed with brine and dried over MgSO₄. The solvents were removed through rotary evaporation and the resulting residue was purified by silica-gel column chromatography using a mixture of petroleum ether (30/40) / diethyl ether (10:1) as eluent.

Yield 0.259 g (7.19 mmol) 34%

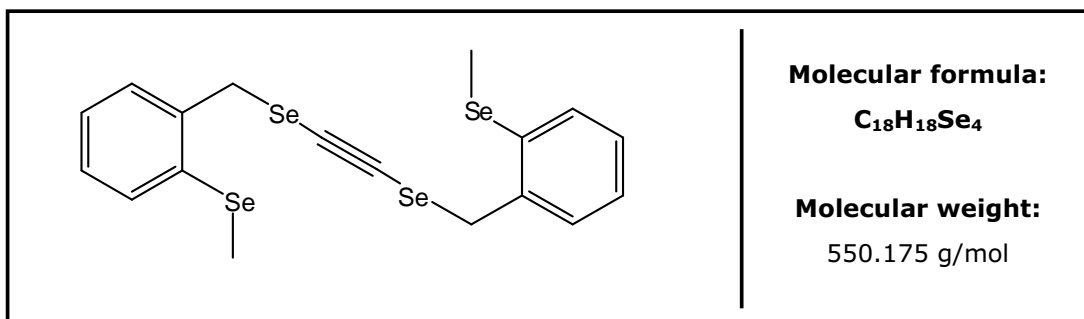
Habitus colourless oil

TLC R_f-value 0.56 petroleum ether (30/40) / diethyl ether (10:1)

GC R_t = 22.80 min

- MS** (EI⁺; m/z; %): 362 [M]⁺ (6.9); 347 [M-CH₃]⁺ (4.9); 185 [M-SeC₅H₉Si]⁺ (64.2); 169 [M-SeC₆H₁₂Si]⁺ (21.0); 105 [SeC₂H₂]⁺ (BP, 100).
- ¹H-NMR** (500 MHz, CDCl₃): δ=0.21 (s, 9H, Si(CH₃)₃); δ=2.40 (s, 3H, SeCH₃, ²J_{Se,H}=11.6 Hz); δ=4.22 (s, 2H, CH₂, ²J_{Se,H}=15.8 Hz); δ=7.22–7.30 (m, 2H, H_{arom}); δ=7.33 (dd, J= 7.1, 1.7 Hz, 1H, H_{arom}); δ=7.52 (dd, J= 7.6, 1.1 Hz, 1H, H_{arom}).
- ¹³C-NMR** (125 MHz, CDCl₃): δ=-0.3 (3C, p-Si(CH₃)₃); δ=7.9 (p-SeCH₃); δ=33.6 (s-CH₂); δ=86.5 (q-SeCC); δ=109.5 (q-SiCC); δ=126.3 (t-C_{arom}); δ=128.4 (t-C_{arom}); δ=130.1 (t-C_{arom}); δ=131.5 (t-C_{arom}); δ=133.0 (q-C_{ar}SeCH₃); δ=138.5 (q-C_{ar}CH₂).
- ⁷⁷Se-NMR** (95 MHz, CDCl₃): δ=157.2 (SeCH₃); δ=260.7 (SeC≡CTMS).

5.3.3.11 1,6-bis(2'-methylselenylbenzene)-2,5-diselena-3-hexyne (48)

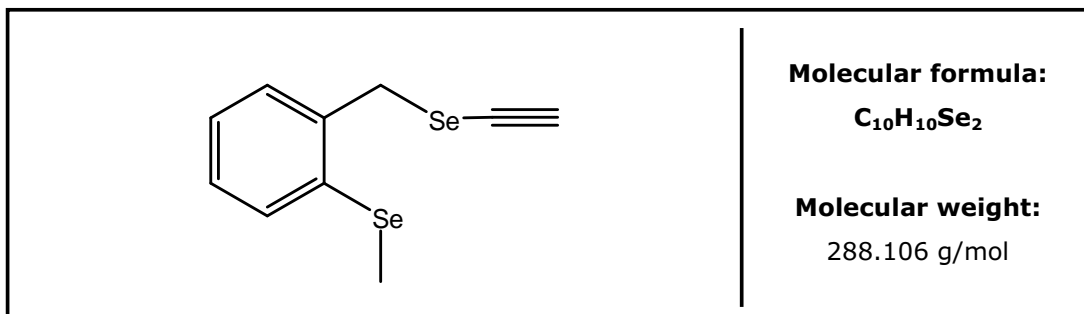


Materials:	see section 5.3.3.10.
0.613 g	(2.12 mmol) 2-(methylselenyl)-benzyl selenocyanate
0.212 g	(2.16 mmol) trimethylsilyl acetylene
1.35 ml	(2.16 mmol) <i>n</i> -butyllithium
ca. 300 ml	tetrahydrofuran (solvent)

Experimental procedure:

Compound **48** was obtained as a secondary product at the synthesis of compound **47**, the experimental procedure being previously described in section 5.3.3.10. Compound **48** was purified through silica-gel column chromatography, resulting in small white needles.

Yield	0.082 g	(0.15 mmol)	14%						
Habitus	white thin needles								
TLC	R _F -value	0.21	petroleum ether (30/40) / diethyl ether (10:1)						
GC	R _t = 29.86 min								
MS	(EI ⁺ ; m/z; %): 550.9 [M] ⁺ (0.9); 534.9 [M-CH ₃] ⁺ (11.2); 366.9 [C ₁₀ H ₉ Se ₃] ⁺ (14.9); 265.0 [C ₈ H ₉ Se ₂] ⁺ (73.6); 249.9 [C ₇ H ₆ Se ₂] ⁺ (4.3); 185.0 [C ₈ H ₉ Se] ⁺ (91); 105.0 [C ₂ HSe] ⁺ (BP, 100); 91.1 [C ₇ H ₇] ⁺ (38.9).								
¹H-NMR	(500 MHz, CD ₂ Cl ₂): δ=2.34 (s, 3H, SeCH ₃ , ² J _{Se,H} =11.6 Hz); δ=4.10 (s, 2H, CH ₂ , ² J _{Se,H} =15.6 Hz); δ=7.12 (dd, J= 7.5, 1.8 Hz, 1H, H _{arom}); δ=7.16 (ddd, J= 7.5, 7.4, 1.3 Hz, 1H, H _{arom}); δ=7.19 (ddd, J= 7.6, 7.4, 1.8 Hz, 1H, H _{arom}); δ=7.45 (dd, J = 7.6, 1.3 Hz, 1H, H _{arom}).								
¹³C-NMR	(125MHz, CD ₂ Cl ₂): δ=7.8 (p-SeCH ₃); δ=34.6 (s-CH ₂); δ=84.6 (q-C≡C); δ=126.3 (t-C _{arom}); δ=128.2 (t-C _{arom}); δ=130.0 (t-C _{arom}); δ=131.3 (t-C _{arom}); δ=132.9 (q-C _{arom} SeCH ₃); δ=138.3 (q-C _{arom} CH ₂).								
⁷⁷Se-NMR	(95 MHz, CDCl ₃): δ=159.8 (SeCH ₃); δ=273.3 (SeC≡C).								
IR	(film, cm ⁻¹): 3054 (w); 3003 (w); 2925 (m); 2850 (w); 1688 (w); 1667 (w); 1584 (w); 1463 (m); 1439 (m); 1424 (m); 1268 (w); 1203 (w); 1179 (w); 1055 (w); 1030 (m); 952 (w); 907 (w); 840 (w); 753 (s); 726 (m); 710 (w); 659 (w); 512 (m).								
UV	(c = 0.047 mg/ml in CH ₂ Cl ₂): λ = 304 nm; log ε = 4.68; ε = 47979 l/(mol·cm); extinction = 0.41 λ = 278 nm; log ε = 4.99; ε = 97128 l/(mol·cm); extinction = 0.83								
HRMS	(EI ⁺).								
	m/z	¹² C	¹ H	⁷⁸ Se	⁸⁰ Se	⁸² Se	mmu	Obs.Mass	Calc.Mass
	551	18	18	1		3	+1.8	551.8095	551.8077
	551	18	18	2	1	1	+0.8	551.8095	551.8077

5.3.3.12 2-(methylselenyl)-benzyl ethynyl selenide (33)**Materials:**

0.18 g	(0.5 mmol)	2-(methylselenyl)-benzyl 2-(trimethylsilyl)-ethynyl selenide (47)
0.5 ml	(0.05 mmol)	0.1N NaOH solution
50 ml		methanol (solvent)
10 ml		tetrahydrofuran (solvent)

Experimental procedure:

To a solution of compound **47** in 50 ml methanol and 10 ml THF was added the 0.1N NaOH solution dropwise over a period of 5 minutes. The reaction mixture was stirred for 2 h at room temperature. Then the mixture was poured into 100 ml of ice/water mixture, and 100 ml of diethyl ether was added. The layers were separated and the aqueous layer was extracted 3 times with diethyl ether. The combined organic layers were washed with NH₄Cl solution and brine and dried over MgSO₄ for 1 h. After rotary evaporation, the product was purified by silica-gel column chromatography, eluting with a mixture of petroleum ether (30/40) / diethyl ether (20:1).

Yield 0.109 g (0.38 mmol) 76%

Habitus colourless oil

TLC R_f-value 0.41 petroleum ether (30/40) / diethyl ether (20:1)

GC R_t = 19.71 min

MS (EI⁺; m/z; %): 290 [M]⁺ (4.9); 185 [M-SeC₂H]⁺ (45.5); 169 [M-SeC₃H₄]⁺ (22.4); 105 [SeC₂H₂]⁺ (BP, 100).

¹H-NMR (500 MHz, CD₂Cl₂): δ=2.35 (s, 3H, SeCH₃, ²J_{Se,H}=11.6 Hz); δ=2.93 (s, C≡CH); δ=4.19 (s, 2H, CH₂, ²J_{Se,H}=14.9 Hz); δ=7.19 (td, J = 7.4, 1.4, 1H, H_{arom}); δ=7.22 (td, J = 7.4, 1.8, 1H, H_{arom}); δ=7.29 (dd, J = 7.1, 1.8, 1H, H_{arom}) δ=7.47 (dd, J = 7.4, 1.4, 1H, H_{arom}).

¹³C-NMR (125 MHz, CD₂Cl₂): δ=8.3 (p-SeCH₃); δ=33.6 (s-CH₂, ¹J_{Se,C}=51.6 Hz); δ=66.1 (t-CH); δ=90.1 (q-SeCCH); δ=126.7 (t-C_{arom}); δ=128.8 (t-C_{arom}); δ=130.1 (t-C_{arom}); δ=131.9 (t-C_{arom}); δ=133.4 (q-C_{ar}-SeCH₃); δ=138.7 (q-C_{ar}CH₂).

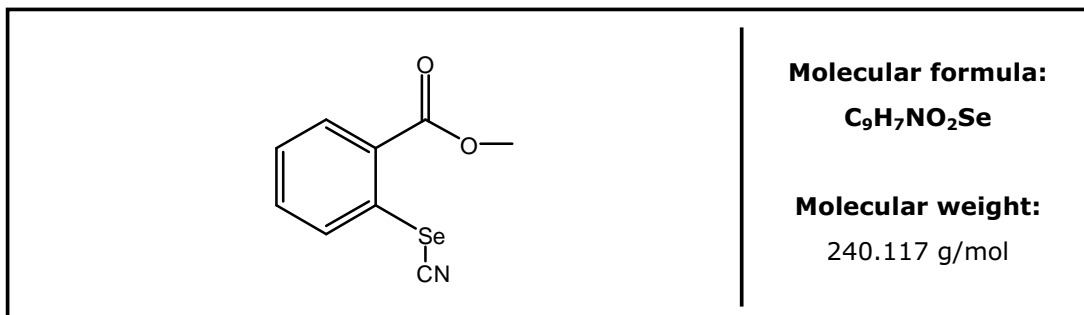
⁷⁷Se-NMR (95 MHz, CD₂Cl₂): δ=157.5 (SeCH₃, ⁴J_{Se,Se}=40.9 Hz); δ=238.3 (SeC≡CH, ⁴J_{Se,Se}=40.9 Hz).

IR (film, cm⁻¹): 3277 (s); 3161 (w); 3055 (w); 3002 (w); 2926 (w); 2882 (w); 2615 (w); 2028 (w); 1912 (m); 1563 (w); 1463 (m); 1440 (m); 1423 (m); 1269 (m); 1208 (m); 1184 (s); 1096 (m); 1054 (m); 1031 (s); 909 (m); 840 (m); 812 (m); 755 (vs); 726 (s); 678 (m); 660 (m); 597 (m); 567 (m); 536 (m); 513 (w).

UV (c = 0.13 mg/ml in CH₂Cl₂):
 λ = 302 nm; log ε = 3.62; ε = 4209 l/(mol·cm); extinction = 0.19
 λ = 272 nm; log ε = 3.25; ε = 1772 l/(mol·cm); extinction = 0.08

HRMS (EI⁺):

m/z	¹² C	¹ H	⁷⁸ Se	⁸⁰ Se	⁸² Se	mmu	Obs.Mass	Calc.Mass
290	10	10		2		+1.3	289.9126	289.9113
290	10	10	1		1	+0.3	289.9126	289.9113
288	10	10	1	1		+1.2	287.9132	287.9121

5.3.3.13 Methyl 2-selenocyanatobenzoate (50)**Materials:**

39.45 g	(261 mmol)	methylantranilate (49)
21.61 g	(313 mmol)	sodium nitrite (as aqueous 3M solution)
36.76 g	(255 mmol)	potassium selenocyanate (KSeCN)
150 ml		HCl 6N solution
ca. 60 g		sodium acetate

Experimental procedure¹³²:

Methyl anthranilate (**49**) was suspended in 6N HCl at -20°C and the solution of NaNO₂ was added dropwise, in such a way that the temperature of the reaction mixture was kept below -10°C. After stirring for 1 hour, saturated aqueous CH₃COONa was added dropwise until the pH of the reaction solution reached a value around 5.7-6.2. Then the mixture was filtered and poured into aqueous solution of KSeCN all at once. The resulting precipitate was collected and washed with a small amount of water. Recrystallization from methanol afforded yellow crystals, which were dried under vacuum to remove all traces of solvent.

Yield 37.1 g (154 mmol) 61 %

Habitus redish yellow crystals

GC R_t = 19.07 min

MS (EI⁺; m/z; %): 241 [M]⁺ (83.2); 210 [M-CH₃O]⁺ (100); 182 [C₇H₄NSe]⁺, (64.7); 156 [C₆H₄Se]⁺, (28.9); 104 [C₇H₄O]⁺ (11.5); 92 [CHSe]⁺ (8.6); 76 [C₆H₄]⁺ (32.5).

¹H-NMR (500 MHz, CD₂Cl₂): δ= 3.99 (s, 3H, CH₃); δ=7.44 (dt, *J*= 7.7, 7.4, 0.8, 1H, H_{arom}); δ=7.44 (ddd, *J*= 8.1, 7.4, 1.5, 1H, H_{arom}); δ=8.06 (dd, *J*= 8.1, 0.8, 1H, H_{arom}); δ=8.12 (dd, *J*= 7.7, 1.5, 1H, H_{arom}).

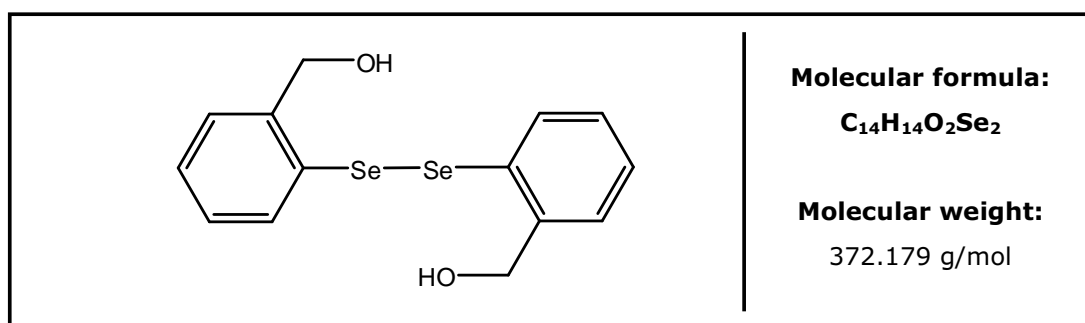
¹³C-NMR (125 MHz, CD₂Cl₂): δ=3.7 (1C, p-CH₃); δ= 105.8 (1C, q-SeCN); δ=126.7 (1C, q-C_{arom}); δ=128.1 (1C, t-C_{arom}); δ=130.3 (1C, t-C_{arom}); δ=131.4 (1C, q-C_{arom}); δ=131.8 (1C, t-C_{arom}); δ=135.0 (1C, t-C_{arom}); δ=168.7 (1C, q-C=O).

⁷⁷Se-NMR (95 MHz, CD₂Cl₂): δ=391.1.

IR (KBr, cm⁻¹): 3442 (b); 2953 (w); 2918 (m); 2850 (w); 2148 (w); 1725 (w); 1686 (vs); 1586 (m); 1568 (w); 1467 (m); 1437 (s); 1312 (vs); 1291 (vs); 1267 (m); 1194 (m); 1144 (m); 1113 (m); 1052 (m); 1029 (m); 804 (w); 738 (vs); 681 (w).

UV (c = 0.075 mg/ml in CH₂Cl₂):
 λ = 308 nm; log ε = 3.46 ; ε = 2880 l/(mol·cm); extinction = 0.09
 λ = 250 nm; log ε = 3.85 ; ε = 7040 l/(mol·cm); extinction = 0.22

5.3.3.14 2,2'- diselenobis(benzyl alcohol) (**51**)



Materials:

22.68 g	(94.0 mmol)	methyl 2-selenocyanatobenzoate (50)
5.33 g	(140,0 mmol)	lithium aluminium hydride
ca. 40 ml		6N HCl solution
600 ml		diethyl ether (solvent)

Experimental procedure¹³²:

To a suspension of LiAlH₄ in dry diethyl ether was added slowly under argon atmosphere an ethereal solution of methyl 2-selenocyanatobenzoate (**50**) was added slowly to the mixture under stirring. After addition was complete, the reaction mixture was refluxed for 2.5 hours. After cooling down, an excess of 6N HCl solution was carefully added until all solid residue formed during the reflux was dissolved. Through a needle, air was bubbled into the reaction mixture under stirring overnight. After extraction with diethyl ether, the organic layers were washed with water and brine, then dried over Na₂SO₄. Removal of solvent through rotary evaporation and further recrystallization from dichloromethane and light petroleum yielded 2,2'-diselenonobis(benzyl alcohol) (**51**) as a yellow solid.

Yield	15.81 g	(42.5 mmol)	45 %
Habitus	yellow solid		
m.p.	94°C		
GC	R _t = 25.05 min		
MS	(FAB ⁺ ; m/z; %): 374 [M] ⁺ (21.4); 357 [M-OH] ⁺ (12.1); 339 [M-2·OH] ⁺ (3.6); 154 [C ₆ H ₄ Se] ⁺ (BP, 100).		
¹H-NMR	(300 MHz, CDCl ₃): δ=1.79 (s, 2H, OH) , δ=4.72 (s, 2H, CH ₂); δ=7.19 (td, 2H, J= 7.6, 7.5, 1.4 Hz, H _{arom}); δ=7.30 (dt, 2H, J= 7.6, 7.5, 1.0 Hz, H _{arom}); δ=7.39 (dd, 2H, J= 7.6, 1.4 Hz, H _{arom}); δ=7.68 (dd, 2H, J= 7.5, 1.0 Hz, H _{arom}).		
¹³C-NMR	(75 MHz, CDCl ₃): δ=65.3 (2C, s-CH ₂); δ=128.4 (2C, t-C _{arom}); δ=128.8 (2C, t-C _{arom}); δ=128.9 (2C, t-C _{arom}); δ=130.6 (2C, q-C _{arom} CH ₂); δ=134.9 (2C, t-C _{arom}); δ=142.1 (2C, q-C _{arom} Se).		
⁷⁷Se-NMR	(95 MHz, CD ₂ Cl ₂): δ=431.4.		
IR	(KBr, cm ⁻¹): 3313 (bs); 3056 (w); 2965 (w); 2891 (w); 2848 (m); 1523 (w); 1566 (m); 1488 (m); 1469 (m); 1458 (m); 1441 (s); 1369 (w); 1262 (m); 1192 (m); 1192 (m); 1153 (w); 1113 (m); 1054 (vs); 1044 (vs); 1024 (vs); 990 (w); 798 (m); 740 (s).		

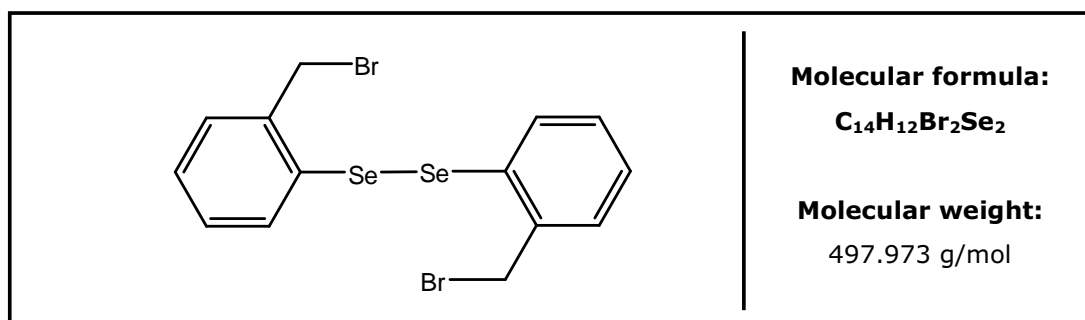
UV (c = 0.121 mg/ml in CH₂Cl₂):
 $\lambda = 326 \text{ nm}$; $\log \epsilon = 2.96$; $\epsilon = 922 \text{ l}/(\text{mol}\cdot\text{cm})$; extinction = 0.03
 $\lambda = 246 \text{ nm}$; $\log \epsilon = 4.14$; $\epsilon = 13835 \text{ l}/(\text{mol}\cdot\text{cm})$; extinction = 0.45

HRMS (EI⁺):

m/z	¹² C	¹ H	O	⁸⁰ Se	mmu	Obs.Mass	Calc.Mass
374	14	14	2	2	+0.1	373.9325	373.9327

m/z	¹² C	¹ H	O	⁷⁸ Se	⁸² Se	mmu	Obs.Mass	Calc.Mass
374	14	14	2	1	1	-0.9	373.9325	373.9327

5.3.3.15 2,2'-diselenobis(benzyl bromide) (**52**)



Materials:

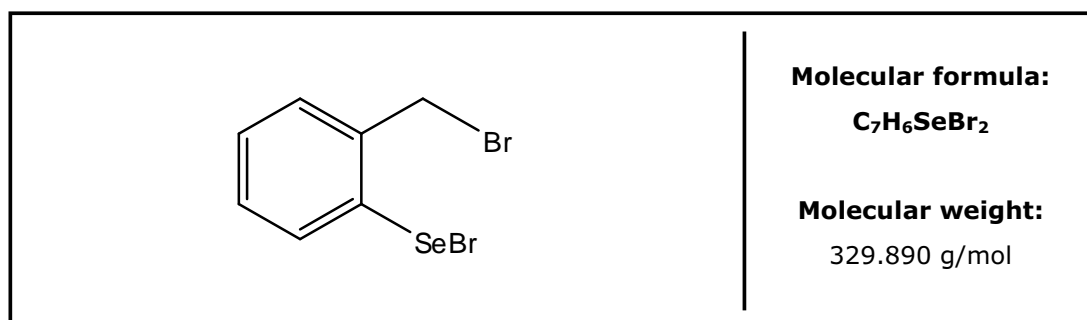
18.285 g	(49.1 mmol)	2,2'-diselenobis(benzyl alcohol) (51)
11.659 g	(147.4 mmol)	pyridine
24.512 g	(117.9 mmol)	thionyl bromide
150 ml		6N HCl solution
450 ml		dichloromethane (solvent)

Experimental procedure³:

To a solution of 2,2'-diselenobis(benzyl alcohol) (**51**) in dichloromethane was added 11.66 g of pyridine and cooled to -10°C. Thionyl bromide was slowly added dropwise to the solution under vigorous stirring. The reaction mixture was allowed to warm up to room temperature and stirred for 4 hours at room temperature. An excess amount of 6N HCl solution was added and after extracting with dichloromethane, the raw product, obtained after evaporation of the solvents, was purified by silica-gel column chromatography to afford compound **52** as a yellow solid.

Yield 22.57 g (45.3 mmol) 92 %

Habitus	yellow solid																
m.p.	76.5°C																
GC	R _t = 25.7 min																
MS	(FAB ⁺ - matrix NBA; m/z; %): 497.7 [M] ⁺ (52.7); 418.8 [M-Br] ⁺ (25.1); 339.9 [M-2·Br] ⁺ (9.6); 154 [C ₆ H ₄ Se] ⁺ (BP, 100).																
¹H-NMR	(500 MHz, CD ₂ Cl ₂): δ=4.62 (s, 2H, CH ₂); δ=7.23 (dt, 2H, J= 7.6, 7.5, 1.4 Hz, H _{arom}); δ=7.29 (dt, 2H, J= 7.6, 7.5, 1.1 Hz, H _{arom}); δ=7.38 (dd, 2H, J= 7.5, 1.4 Hz, H _{arom}); δ=7.75 (dd, 2H, J= 7.6, 1.1 Hz, H _{arom}).																
¹³C-NMR	(125 MHz, CD ₂ Cl ₂): δ=34.4 (2C, s-CH ₂); δ=129.4 (2C, t-C _{arom}); δ=130.0 (2C, t-C _{arom}); δ=130.4 (2C, t-C _{arom}); δ=132.8 (2C, q-C _{arom} CH ₂); δ=135.6 (2C, t-C _{arom}); δ=139.6 (2C, q-C _{arom} Se).																
⁷⁷Se-NMR	(95 MHz, CD ₂ Cl ₂): δ=432.5.																
IR	(KBr, cm ⁻¹): 3440(bs); 3047(w); 3023(w); 1948(w); 1916(w); 1628(m); 1580(w); 1563(w); 1465(m); 1441(m); 1274(w); 1222(s); 1200(m); 1137(w); 1049(m); 1026(w); 816(m); 755(vs); 722(m); 654(w); 601(s); 559(m); 485(w).																
UV	(c = 0.063 mg/ml in CH ₂ Cl ₂): λ = 332 nm; log ε = 3.16; ε = 1457 l/(mol·cm); extinction = 0.29 λ = 296 nm; log ε = 3.67; ε = 4724 l/(mol·cm); extinction = 0.94 λ = 254 nm; log ε = 4.30; ε = 20101 l/(mol·cm); extinction = 0.4																
HRMS	(FAB ⁺): <table><thead><tr><th>m/z</th><th>¹²C</th><th>¹H</th><th>⁸¹Br</th><th>⁸⁰Se</th><th>mmu</th><th>Obs.Mass</th><th>Calc.Mass</th></tr></thead><tbody><tr><td>498</td><td>14</td><td>12</td><td>2</td><td>2</td><td>+2.2</td><td>497.7636</td><td>497.7660</td></tr></tbody></table>	m/z	¹² C	¹ H	⁸¹ Br	⁸⁰ Se	mmu	Obs.Mass	Calc.Mass	498	14	12	2	2	+2.2	497.7636	497.7660
m/z	¹² C	¹ H	⁸¹ Br	⁸⁰ Se	mmu	Obs.Mass	Calc.Mass										
498	14	12	2	2	+2.2	497.7636	497.7660										

5.3.3.16 2-(bromoselenyl)-benzyl bromide (55)**Materials:**

1.0 g	(2.0 mmol)	2,2'- diselenobis(benzyl bromide) (52)
0.11 ml	(2.1 mmol)	bromine
100 ml		dichloromethane (solvent)

Experimental:

To a solution of compound **52** dissolved in 100 ml dichloromethane in a Schlenk flask, bromine was added dropwise from a syringe through a septum. The solution started to change its colour to a dark brown. After addition of bromine was completed the reaction mixture was stirred for 1 h at room temperature. The solvent and the unreacted bromine were removed through evaporation under medium vacuum conditions in anhydrous argon atmosphere and compound **55** was obtained as a dark brown wax-like solid. The raw product was kept for a short time under argon and used, without any further purification, for synthesizing 2-(cyanoselenyl)-benzyl bromide (**56**).

Yield 0.320 g raw product (49%)

Habitus dark brown amorphous solid

¹H-NMR (300 MHz, CDCl₃): δ=4.58 (s, 2H, CH₂); δ=7.06 (m, H_{arom}, 2H); δ=7.22 (m, H_{arom}, 1H); δ=7.33 (m, H_{arom}, 1H).

¹³C-NMR (125 MHz, CDCl₃): δ=36.9 (s-CH₂), δ=125.7 (t-C_{arom}); δ=126.38 (t-C_{arom}); δ=126.39 (t-C_{arom}); δ=127.3 (t-C_{arom}); δ=137.4 (q-C_{arom}SeBr); δ=143.0 (q-C_{arom}CH₂).

⁷⁷Se-NMR (75 MHz, CDCl₃): δ=787.4

Preparative procedures

IR (film, cm^{-1}): 3600–3100 (bs); 3058 (m); 1622 (bm); 1584 (m); 1373 (w); 1222 (s); 1199 (m); 1058 (m); 755 (s); 723 (m); 666 (w); 605 (w); 564 (s); 520 (m); 502 (m).

UV ($c = 0.095 \text{ mg/ml}$ in CH_2Cl_2):
 $\lambda = 460 \text{ nm}$; $\log \epsilon = 2.96$; $\epsilon = 914 \text{ l}/(\text{mol}\cdot\text{cm})$; extinction = 0.14
 $\lambda = 386 \text{ nm}$; $\log \epsilon = 3.29$; $\epsilon = 1958 \text{ l}/(\text{mol}\cdot\text{cm})$; extinction = 0.30
 $\lambda = 302 \text{ nm}$; $\log \epsilon = 4.12$; $\epsilon = 13053 \text{ l}/(\text{mol}\cdot\text{cm})$; extinction = 0.20
 $\lambda = 266 \text{ nm}$; $\log \epsilon = 4.58$; $\epsilon = 37853 \text{ l}/(\text{mol}\cdot\text{cm})$; extinction = 0.58
 $\lambda = 250 \text{ nm}$; $\log \epsilon = 4.70$; $\epsilon = 50253 \text{ l}/(\text{mol}\cdot\text{cm})$; extinction = 0.77

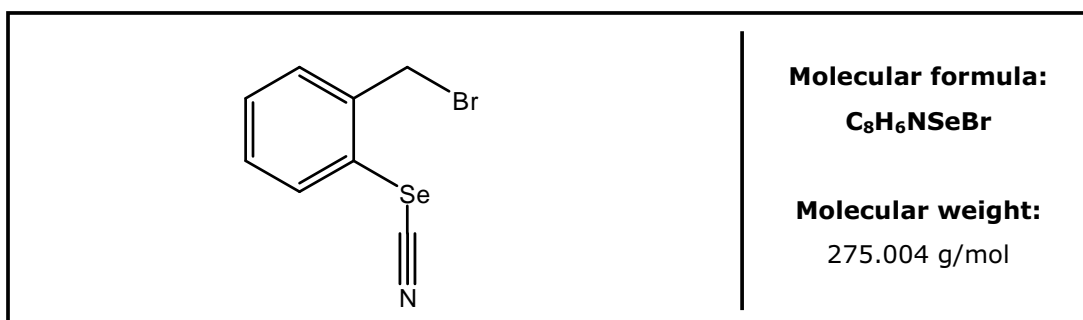
HRMS (EI^+):

m/z	^{12}C	^1H	^{81}Br	^{78}Se	mmu	Obs.Mass	Calc.Mass
330	7	6	2	1	+0.0	329.7968	329.7981

m/z	^{12}C	^1H	^{79}Br	^{81}Br	^{80}Se	mmu	Obs.Mass	Calc.Mass
330	7	6	1	1	1	-1.3	329.7968	329.7981

m/z	^{12}C	^1H	^{79}Br	^{82}Se	mmu	Obs.Mass	Calc.Mass
330	7	6	2	1	-3.5	329.7968	329.7981

5.3.3.17 2-(cyanoselenenyl)-benzyl bromide (**56**)



Materials:

1.19 g	(2.4 mmol)	2,2'- diselenobis(benzyl bromide) (52)
0.12 ml	(2.4 mmol)	bromine
100 ml		dichloromethane (solvent)
0.96 ml	(7.2 mmol)	trimethylsilylcyanide (TMSCN)
100 ml		tetrahydrofuran (solvent)

Experimental procedure:

Compound **56** was synthesized in a one-pot reaction from compound **52**, having as an intermediate compound **55**, following the procedure from section 5.3.1.25. The solid dark brown colored raw product containing **55** was dissolved into 100 ml of dry THF under argon atmosphere. Afterwards TMSCN was added carefully and stirred for 2h. The colour of the reaction mixture changed from dark redish to light orange. The solvent was evaporated and the raw material purified by silica-gel column chromatography, eluting with a mixture of petroleum ether (30/40) / dichloromethane (2:1), obtaining pure compound **56** as a viscous oil, that slowly solidifies at room temperature.

Yield	1.255 g	(4.5 mmol)	95 %
Habitus	light yellow solid		
TLC	R _F -value	0.17	petroleum ether (30/40) / dichloromethane (2 : 1)
GC	R _t =	19.15 min	
MS	(EI ⁺ ; m/z; %): 275 [M] ⁺ (13.6); 196 [M-Br] ⁺ (54.3); 169 [M-BrCN] ⁺ (BP, 100); 89 [C ₇ H ₅] ⁺ (48.6).		
¹H-NMR	(500 MHz, CD ₂ Cl ₂): δ=4.65 (s, 2H, CH ₂); δ=7.37 (dt, J = 7.6, 1.5 Hz, 1H, H _{arom}); δ=7.43 (dt, J = 7.5, 1.1 Hz, 1H, H _{arom}); δ=7.49 (dd, J = 7.5, 1.5 Hz, 1H, H _{arom}); δ=7.86 (dd, J = 7.6, 1.1 Hz, 1H, H _{arom}).		
¹³C-NMR	(125 MHz, CD ₂ Cl ₂): δ=33.6 (s-CH ₂); δ=101.4 (q-SeCN); δ=124.9 (q-C _{arom}); δ=130.9 (t-C _{arom}); δ=131.0 (t-C _{arom}); δ=131.4 (t-C _{arom}); δ=135.8 (t-C _{arom}); δ=139.8 (q-C _{arom}).		
⁷⁷Se-NMR	(95 MHz, CD ₂ Cl ₂): δ=276.3.		
IR	(KBr, cm ⁻¹): 3426(b); 3070(w); 3024(m); 2964(w); 2153(s); 1567(m); 1464(s); 1443(s); 1428(s); 1278(w); 1223(s); 1196(m); 1027(m); 819(m); 759(s); 717(s); 652(m); 602(s); 567(m); 520(m); 484(w); 439(m).		
UV	(c = 0.196 mg/ml in CH ₂ Cl ₂): λ = 246 nm; log ε = 3.80; ε = 6314 l/(mol·cm); extinction = 0.45 λ = 274 nm; log ε = 3.32; ε = 2105 l/(mol·cm); extinction = 0.15		

HRMS	(EI ⁺):								
	m/z	¹² C	¹ H	¹⁴ N	⁷⁹ Br	⁸⁰ Se	mmu	Obs.Mass	Calc.Mass
	275	8	6	1	1	1	+0.0	290.8849	290.8849

5.3.3.18 2-(cyanoselenyl)-benzyl selenocyanate (57)**Materials:**

0.55 g	(2 mmol)	2-methylselenyl-benzyl bromide (56)
0.36 g	(2.5 mmol)	potassium selenocyanate (KSeCN)
ca. 50 ml		acetone (solvent)

Experimental procedure:

To a solution of KSeCN in 35 ml of dry degassed acetone was added a solution of **56** in 15 ml of acetone by using a syringe. The reaction mixture was heated to 60°C under reflux and stirred for 4 hours. The solvent was removed through rotary evaporation. The brown solid obtained as a raw material, was dissolved in dichloromethane. A white precipitate appeared and it was removed through filtration under vacuum. Dichloromethane was removed by rotary evaporation, yielding a viscous oil as raw material. The GC/MS analysis showed the desired product as 50% of the raw material, in a mixture with an unknown product (1:1 ratio) with a molecular peak corresponding to 3*H*-1,2-benzodiselenole (**58**). Several attempts of purifying compound **57** through silica-gel column chromatography or recrystallization failed. NMR spectroscopic analysis were done using some enriched fractions from silica-gel column chromatography.

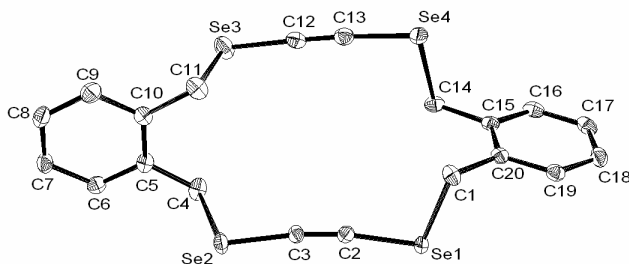
Yield 0.270 g (0.9 mmol) 45% (yield from the GC analysis).

GC R_t = 22.95 min

MS	(EI ⁺ ; m/z; %): 300 [M] ⁺ (2.2); 247 [M-C ₂ N ₂] ⁺ (11.1); 196 [M-SeCN] ⁺ (35.8); 169 [M-SeC ₂ N ₂] ⁺ (BP, 100); 116 [SeC ₃ H] ⁺ (27.2); 89 [M-Se ₂ C ₂ N ₂] ⁺ (60.5).
¹H-NMR	(500 MHz, CD ₂ Cl ₂): δ=4.48 (s, 2H, CH ₂ , ² J _{Se,H} =17.4 Hz); δ=7.37–7.43 (m, 1H, H _{arom}); δ=7.51–7.53 (m, 2H, H _{arom}); δ=7.89 (d, J = 7.8 Hz, 1H, H _{arom}).
¹³C-NMR	(125 MHz, CDCl ₃): δ=32.7 (s-CH ₂ , ¹ J _{Se,C} =49.4Hz); δ=100.56 (q-SeCN); δ=100.61 (q-SeCN); δ=122.8 (q-C _{arom}); δ=130.8 (t-C _{arom}); δ=131.5 (t-C _{arom}); δ=131.7 (t-C _{arom}); δ=137.3 (t-C _{arom}); δ=138.8 (q-C _{arom}).
⁷⁷Se-NMR	(95 MHz, CDCl ₃): δ=267.9 (⁴ J _{Se,Se} =34 Hz, SeCN); δ=309.0 (⁴ J _{Se,Se} =34 Hz, SeCN).

6. X-ray structures

6.1 2,5,14,17-Tetraselena[6.6]-*ortho*-cyclophan-3,15-diyne (**18 a**)



Crystal data and structure refinement

Operator	F. Rominger
Identification code	al12
Empirical formula	C ₂₀ H ₁₆ Se ₄
Formula weight	572.17
Temperature	100(2) K
Wavelength	0.71073 Å
Crystal system	monoclinic
Space group	C2/c
Z	8
Unit cell dimensions	a = 24.293(2) Å α = 90 deg. b = 5.2235(5) Å β = 92.753(2) deg. c = 30.239(3) Å γ = 90 deg.
Volume	3832.6(7) Å ³
Density (calculated)	1.98 g/cm ³
Absorption coefficient	7.66 mm ⁻¹
Crystal shape	polyhedron
Crystal size	0.20 x 0.08 x 0.05 mm ³
Crystal colour	colorless
Theta range for data collection	1.7 to 28.3 deg.
Index ranges	-32 ≤ h ≤ 32, -6 ≤ k ≤ 6, -40 ≤ l ≤ 40
Reflections collected	19112
Independent reflections	4744 (R(int) = 0.0384)
Observed reflections	3821 (I > 2σ(I))
Absorption correction	Semi-empirical from equivalents
Max. and min. transmission	0.70 and 0.31
Refinement method	Full-matrix least-squares on F ²
Data/restraints/parameters	4744 / 0 / 217
Goodness-of-fit on F ²	1.01
Final R indices (I > 2σ(I))	R1 = 0.029, wR2 = 0.058
Largest diff. peak and hole	0.55 and -0.41 eÅ ⁻³

Atomic coordinates and equivalent isotropic displacement parameters (\AA^2) for 18a

U_{eq} is defined as one third of the trace of the orthogonalized U_{ij} tensor

Atom	x	y	z	U_{eq}
Se1	0.5149(1)	1.0104(1)	0.4444(1)	0.0172(1)
Se2	0.5177(1)	0.5534(1)	0.3072(1)	0.0216(1)
Se3	0.7192(1)	0.4538(1)	0.3257(1)	0.0300(1)
Se4	0.7227(1)	1.0473(1)	0.4487(1)	0.0222(1)
C1	0.5782(1)	1.2550(5)	0.4484(1)	0.0195(6)
C2	0.5256(1)	0.8478(5)	0.3923(1)	0.0168(5)
C3	0.5266(1)	0.7091(5)	0.3606(1)	0.0167(5)
C4	0.5774(1)	0.2919(5)	0.3097(1)	0.0229(6)
C5	0.6015(1)	0.2773(5)	0.2651(1)	0.0188(6)
C6	0.5813(1)	0.0966(5)	0.2348(1)	0.0204(6)
C7	0.6009(1)	0.0820(5)	0.1924(1)	0.0222(6)
C8	0.6415(1)	0.2483(5)	0.1803(1)	0.0239(6)
C9	0.6624(1)	0.4284(5)	0.2103(1)	0.0242(6)
C10	0.6427(1)	0.4471(5)	0.2524(1)	0.0192(5)
C11	0.6671(1)	0.6398(5)	0.2845(1)	0.0253(6)
C12	0.7233(1)	0.6841(5)	0.3711(1)	0.0229(6)
C13	0.7248(1)	0.8313(5)	0.4014(1)	0.0218(6)
C14	0.6623(1)	0.8766(5)	0.4797(1)	0.0196(6)
C15	0.6393(1)	1.0699(5)	0.5107(1)	0.0162(5)
C16	0.6572(1)	1.0722(5)	0.5548(1)	0.0202(6)
C17	0.6377(1)	1.2517(5)	0.5841(1)	0.0220(6)
C18	0.6000(1)	1.4332(5)	0.5691(1)	0.0223(6)
C19	0.5817(1)	1.4332(5)	0.5250(1)	0.0185(5)
C20	0.6005(1)	1.2540(5)	0.4952(1)	0.0164(5)

Hydrogen coordinates and isotropic displacement parameters (\AA^2) for 18a

Atom	x	y	z	U_{eq}
H1A	0.6070	1.2011	0.4282	0.023
H1B	0.5656	1.4291	0.4398	0.023
H4A	0.6062	0.3402	0.3324	0.028
H4B	0.5622	0.1232	0.3178	0.028
H6	0.5535	-0.0193	0.2432	0.024
H7	0.5864	-0.0416	0.1719	0.027
H8	0.6552	0.2394	0.1515	0.029
H9	0.6907	0.5411	0.2017	0.029
H11A	0.6376	0.7214	0.3012	0.030
H11B	0.6867	0.7748	0.2686	0.030
H14A	0.6331	0.8178	0.4580	0.024
H14B	0.6767	0.7263	0.4965	0.024
H16	0.6834	0.9486	0.5653	0.024
H17	0.6503	1.2497	0.6143	0.026
H18	0.5867	1.5574	0.5889	0.027
H19	0.5557	1.5584	0.5148	0.022

Anisotropic displacement parameters (\AA^2) for 18a

The anisotropic displacement factor exponent form: $-2 \pi^2 (h^2 a^{*2} U_{11} + \dots + 2 h k a^* b^* U_{12})$

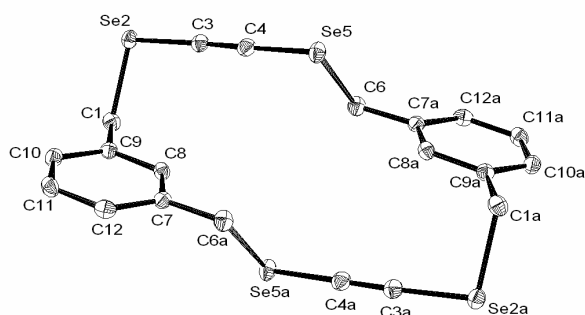
Atom	U_{11}	U_{22}	U_{33}	U_{23}	U_{13}	U_{12}
Se1	0.0190(1)	0.0188(1)	0.0139(1)	-0.0035(1)	0.0019(1)	-0.0004(1)

Se2	0.0266(2)	0.0238(1)	0.0142(1)	-0.0052(1)	-0.0022(1)	0.0020(1)
Se3	0.0281(2)	0.0271(2)	0.0337(2)	-0.0101(1)	-0.0086(1)	0.0078(1)
Se4	0.0202(2)	0.0226(1)	0.0241(2)	-0.0029(1)	0.0054(1)	-0.0053(1)
C1	0.0245(15)	0.0165(12)	0.0173(14)	0.0018(10)	-0.0024(11)	-0.0038(11)
C2	0.0164(13)	0.0187(13)	0.0151(13)	0.0015(10)	0.0003(10)	0.0029(10)
C3	0.0189(14)	0.0179(12)	0.0134(13)	0.0006(10)	0.0020(11)	-0.0034(10)
C4	0.0314(16)	0.0171(13)	0.0204(15)	0.0014(11)	0.0031(12)	0.0044(11)
C5	0.0237(15)	0.0157(12)	0.0171(14)	0.0019(10)	0.0009(11)	0.0043(10)
C6	0.0197(14)	0.0190(13)	0.0224(15)	0.0010(11)	0.0023(11)	0.0009(10)
C7	0.0240(15)	0.0230(14)	0.0195(14)	-0.0069(11)	0.0004(11)	0.0032(11)
C8	0.0267(16)	0.0284(15)	0.0169(14)	-0.0003(12)	0.0042(12)	0.0042(12)
C9	0.0257(15)	0.0240(14)	0.0231(15)	0.0035(12)	0.0045(12)	-0.0017(12)
C10	0.0203(14)	0.0158(12)	0.0213(14)	0.0003(11)	-0.0017(11)	0.0024(10)
C11	0.0281(16)	0.0190(13)	0.0285(16)	0.0012(12)	-0.0044(13)	0.0001(12)
C12	0.0162(14)	0.0259(14)	0.0264(16)	0.0000(12)	-0.0018(12)	-0.0008(11)
C13	0.0176(14)	0.0252(14)	0.0225(15)	0.0016(12)	-0.0001(12)	0.0011(11)
C14	0.0181(14)	0.0169(12)	0.0241(15)	0.0043(11)	0.0030(11)	-0.0021(10)
C15	0.0141(13)	0.0171(12)	0.0174(13)	0.0029(10)	0.0008(10)	-0.0035(10)
C16	0.0174(14)	0.0191(13)	0.0238(15)	0.0072(11)	-0.0023(11)	-0.0036(10)
C17	0.0231(15)	0.0273(14)	0.0152(14)	0.0052(11)	-0.0037(12)	-0.0096(12)
C18	0.0268(15)	0.0207(13)	0.0199(14)	-0.0044(11)	0.0042(12)	-0.0080(11)
C19	0.0167(13)	0.0159(12)	0.0228(14)	0.0004(11)	0.0002(11)	-0.0016(10)
C20	0.0172(13)	0.0159(12)	0.0164(13)	0.0023(10)	0.0021(11)	-0.0048(10)

Bond lengths (Å) and angles (deg) for 18a

Se1-C2	1.818(3)	C20-C1-Se1	107.41(17)
Se1-C1	1.997(3)	C3-C2-Se1	168.7(2)
Se2-C3	1.813(3)	C2-C3-Se2	167.1(2)
Se2-C4	1.990(3)	C5-C4-Se2	108.34(18)
Se3-C12	1.825(3)	C6-C5-C10	118.9(3)
Se3-C11	1.986(3)	C6-C5-C4	119.2(2)
Se4-C13	1.825(3)	C10-C5-C4	121.9(2)
Se4-C14	1.990(3)	C5-C6-C7	121.3(3)
C1-C20	1.492(4)	C8-C7-C6	119.4(3)
C2-C3	1.203(4)	C7-C8-C9	120.1(3)
C4-C5	1.500(4)	C8-C9-C10	121.1(3)
C5-C6	1.388(4)	C9-C10-C5	119.2(2)
C5-C10	1.405(4)	C9-C10-C11	120.0(3)
C6-C7	1.391(4)	C5-C10-C11	120.8(3)
C7-C8	1.377(4)	C10-C11-Se3	107.26(18)
C8-C9	1.385(4)	C13-C12-Se3	178.2(3)
C9-C10	1.387(4)	C12-C13-Se4	176.2(3)
C10-C11	1.500(4)	C15-C14-Se4	107.28(16)
C12-C13	1.195(4)	C16-C15-C20	119.3(2)
C14-C15	1.503(4)	C16-C15-C14	119.8(2)
C15-C16	1.385(4)	C20-C15-C14	120.9(2)
C15-C20	1.410(4)	C15-C16-C17	121.3(3)
C16-C17	1.387(4)	C18-C17-C16	119.8(3)
C17-C18	1.380(4)	C17-C18-C19	119.6(3)
C18-C19	1.386(4)	C18-C19-C20	121.5(3)
C19-C20	1.392(4)	C19-C20-C15	118.6(2)
C2-Se1-C1	102.08(12)	C19-C20-C1	119.7(2)
C3-Se2-C4	102.59(12)	C15-C20-C1	121.7(2)
C12-Se3-C11	99.15(12)		
C13-Se4-C14	98.12(12)		

6.2 2,5,14,17-tetraselena[6,6]-meta-cyclophan-3,15-diyne (18 b)



Crystal data and structure refinement.

Operator	T. Oeser	
Identification code	al15	
Empirical formula	$C_{20}H_{16}Se_4$	
Formula weight	572.17	
Temperature	100(2) K	
Wavelength	0.71073 Å	
Crystal system	monoclinic	
Space group	$P2_1/n$	
Z	2	
Unit cell dimensions	$a = 8.057(1)$ Å	$\alpha = 90.0$ deg.
	$b = 4.7364(6)$ Å	$\beta = 98.151(2)$ deg.
	$c = 24.438(3)$ Å	$\gamma = 90.0$ deg.
Volume	$923.2(2)$ Å ³	
Density (calculated)	2.06 g/cm ³	
Absorption coefficient	7.95 mm ⁻¹	
Crystal shape	needles	
Crystal size	0.32 x 0.06 x 0.03 mm ³	
Crystal colour	colourless	
Theta range for data collection	1.7 to 28.3 deg.	
Index ranges	$-10 \leq h \leq 10$, $-6 \leq k \leq 6$, $-32 \leq l \leq 32$	
Reflections collected	8715	
Independent reflections	2306 ($R(\text{int}) = 0.0407$)	
Observed reflections	1963 ($I > 2\sigma(I)$)	
Absorption correction	Semi-empirical from equivalents	
Max. and min. transmission	0.80 and 0.19	
Refinement method	Full-matrix least-squares on F^2	
Data/restraints/parameters	2306 / 0 / 141	
Goodness-of-fit on F^2	1.05	
Final R indices ($I > 2\sigma(I)$)	$R1 = 0.026$, $wR2 = 0.056$	
Largest diff. peak and hole	0.83 and -0.43 eÅ ⁻³	

Atomic coordinates and equivalent isotropic displacement parameters (Å²) for 18b

U_{eq} is defined as one third of the trace of the orthogonalized U_{ij} tensor

Atom	x	y	z	U_{eq}
Se2	0.5964(1)	0.4018(1)	0.3318(1)	0.0171(1)
Se5	0.7133(1)	-0.2000(1)	0.4937(1)	0.0184(1)

C1	0.8218(3)	0.5834(5)	0.3379(1)	0.0180(5)
C3	0.6327(3)	0.1893(5)	0.3947(1)	0.0164(5)
C4	0.6634(3)	0.0434(5)	0.4354(1)	0.0183(5)
C6	0.7780(4)	0.0851(5)	0.5522(1)	0.0186(5)
C7	1.1579(3)	0.0573(5)	0.3943(1)	0.0150(5)
C8	1.0292(3)	0.2560(5)	0.3909(1)	0.0147(5)
C9	0.9623(3)	0.3764(5)	0.3405(1)	0.0153(5)
C10	1.0274(3)	0.2981(5)	0.2926(1)	0.0177(5)
C11	1.1568(3)	0.1043(5)	0.2957(1)	0.0181(5)
C12	1.2228(3)	-0.0161(6)	0.3461(1)	0.0174(5)

Hydrogen coordinates and isotropic displacement parameters (\AA^2) for **18b**

Atom	x	y	z	U_{eq}
H1A	0.830(4)	0.705(6)	0.3716(12)	0.025(8)
H1B	0.818(4)	0.695(6)	0.3074(12)	0.019(7)
H6A	0.677(4)	0.185(6)	0.5544(11)	0.012(7)
H6B	0.857(4)	0.188(6)	0.5401(11)	0.012(7)
H8	0.990(3)	0.301(5)	0.4231(10)	0.004(6)
H10	0.988(4)	0.385(6)	0.2591(12)	0.018(7)
H11	1.199(4)	0.048(6)	0.2634(13)	0.027(8)
H12	1.312(3)	-0.149(6)	0.3502(11)	0.016(7)

Anisotropic displacement parameters (\AA^2) for **18b**

The anisotropic displacement factor exponent takes the form: $-2 \pi^2 (h^2 a^{*2} U_{11} + \dots + 2 h k a^* b^* U_{12})$

Atom	U_{11}	U_{22}	U_{33}	U_{23}	U_{13}	U_{12}
Se2	0.0183(2)	0.0179(1)	0.0146(1)	0.0020(1)	0.0013(1)	0.0024(1)
Se5	0.0256(2)	0.0150(1)	0.0143(1)	0.0010(1)	0.0015(1)	0.0003(1)
C1	0.0209(15)	0.0145(12)	0.0192(13)	0.0005(10)	0.0051(11)	-0.0007(10)
C3	0.0175(13)	0.0164(12)	0.0155(12)	-0.0036(10)	0.0027(10)	0.0001(10)
C4	0.0178(14)	0.0201(14)	0.0167(12)	-0.0024(9)	0.0015(10)	-0.0005(10)
C6	0.0231(15)	0.0149(12)	0.0177(12)	0.0003(10)	0.0028(11)	-0.0002(11)
C7	0.0166(13)	0.0123(12)	0.0157(12)	0.0009(9)	0.0006(10)	-0.0025(9)
C8	0.0179(13)	0.0132(12)	0.0137(11)	-0.0016(9)	0.0046(10)	-0.0007(9)
C9	0.0180(13)	0.0121(11)	0.0156(12)	-0.0009(9)	0.0021(10)	-0.0031(10)
C10	0.0207(14)	0.0170(12)	0.0148(12)	0.0011(10)	0.0008(10)	-0.0019(11)
C11	0.0204(14)	0.0191(12)	0.0164(12)	-0.0034(10)	0.0082(10)	-0.0009(11)
C12	0.0152(13)	0.0151(11)	0.0222(13)	-0.0012(10)	0.0032(10)	0.0009(11)

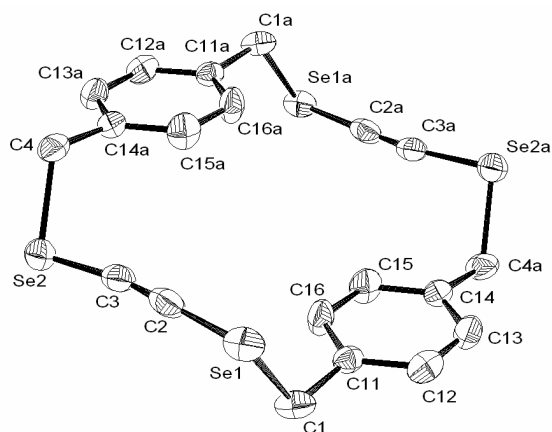
Bond lengths (\AA) and angles (deg) for **18b**

Se2-C3	1.826(2)	C7-C6#1	1.499(3)
Se2-C1	1.997(3)	C8-C9	1.396(3)
Se5-C4	1.833(3)	C8-H8	0.91(2)
Se5-C6	1.981(3)	C9-C10	1.399(3)
C1-C9	1.492(4)	C10-C11	1.383(4)
C1-H1A	1.00(3)	C10-H10	0.93(3)
C1-H1B	0.91(3)	C11-C12	1.392(4)
C3-C4	1.206(4)	C11-H11	0.94(3)
C6-C7#1	1.499(3)	C12-H12	0.95(3)
C6-H6A	0.95(3)	C3-Se2-C1	98.02(11)
C6-H6B	0.89(3)	C4-Se5-C6	97.95(11)
C7-C8	1.394(4)	C9-C1-Se2	113.36(17)
C7-C12	1.398(3)	C9-C1-H1A	112.6(18)

Se2-C1-H1A	105.0(17)	C7-C8-C9	121.2(2)
C9-C1-H1B	111.0(18)	C7-C8-H8	117.0(16)
Se2-C1-H1B	105.2(19)	C9-C8-H8	121.8(16)
H1A-C1-H1B	109(2)	C8-C9-C10	119.1(2)
C4-C3-Se2	176.8(2)	C8-C9-C1	120.1(2)
C3-C4-Se5	175.7(2)	C10-C9-C1	120.7(2)
C7#1-C6-Se5	110.27(16)	C11-C10-C9	120.0(2)
C7#1-C6-H6A	111.5(16)	C11-C10-H10	119.9(17)
Se5-C6-H6A	103.9(16)	C9-C10-H10	120.0(17)
C7#1-C6-H6B	111.2(18)	C10-C11-C12	120.7(2)
Se5-C6-H6B	105.2(17)	C10-C11-H11	120.0(19)
H6A-C6-H6B	114(2)	C12-C11-H11	119.3(19)
C8-C7-C12	118.9(2)	C11-C12-C7	120.1(2)
C8-C7-C6#1	121.1(2)	C11-C12-H12	123.7(17)
C12-C7-C6#1	120.0(2)	C7-C12-H12	116.2(17)

Symmetry transformations used to generate equivalent atoms: #1 -x+2,-y,-z+1

6.3 2,5,14,17-tetraselena[6,6]-*para*-cyclophan-3,15-diyne (18 c)



Crystal data and structure refinement

Operator	F. Rominger	
Identification code	al17	
Empirical formula	C ₂₀ H ₁₆ Se ₄	
Formula weight	572.17	
Temperature	200(2) K	
Wavelength	0.71073 Å	
Crystal system	monoclinic	
Space group	P2 ₁ /c	
Z	2	
Unit cell dimensions	a = 10.7377(5) Å	α = 90 deg.
	b = 9.2932(4) Å	β = 107.836(1) deg.
	c = 10.0453(5) Å	γ = 90 deg.
Volume	954.22(8) Å ³	

Density (calculated)	1.99 g/cm ³
Absorption coefficient	7.69 mm ⁻¹
Crystal shape	polyhedron
Crystal size	0.20 x 0.11 x 0.01 mm ³
Crystal colour	colorless
Theta range for data collection	3.0 to 24.1 deg.
Index ranges	-12 ≤ h ≤ 12, -10 ≤ k ≤ 10, -11 ≤ l ≤ 11
Reflections collected	6786
Independent reflections	1512 (R(int) = 0.0785)
Observed reflections	1105 (I > 2σ(I))
Absorption correction	Semi-empirical from equivalents
Max. and min. transmission	0.96 and 0.31
Refinement method	Full-matrix least-squares on F ²
Data/restraints/parameters	1512 / 0 / 109
Goodness-of-fit on F ²	1.10
Final R indices (I > 2σ(I))	R1 = 0.052, wR2 = 0.093
Largest diff. peak and hole	0.89 and -0.54 eÅ ⁻³

Atomic coordinates and equivalent isotropic displacement parameters (Å²) for 18c

U_{eq} is defined as one third of the trace of the orthogonalized U_{ij} tensor

Atom	x	y	z	U _{eq}
Se1	0.1623(1)	-0.2459(1)	0.5986(1)	0.0394(3)
Se2	0.0861(1)	0.1097(1)	0.2292(1)	0.0412(3)
C1	0.2723(8)	-0.3790(9)	0.5278(9)	0.037(2)
C2	0.1444(8)	-0.1056(10)	0.4659(9)	0.039(2)
C3	0.1286(8)	-0.0147(10)	0.3795(9)	0.035(2)
C11	0.4168(8)	-0.3456(8)	0.5751(8)	0.0287(19)
C12	0.5024(8)	-0.4244(9)	0.6809(8)	0.037(2)
C13	0.6344(9)	-0.4009(9)	0.7150(9)	0.041(2)
C14	0.6862(8)	-0.3006(9)	0.6464(8)	0.0309(19)
C15	0.5998(8)	-0.2195(9)	0.5422(9)	0.042(2)
C16	0.4666(8)	-0.2417(9)	0.5076(9)	0.040(2)
C4	0.1687(7)	0.2872(9)	0.3238(9)	0.041(2)

Hydrogen coordinates and isotropic displacement parameters (Å²) for 18c

Atom	x	y	z	U _{eq}
H1A	0.2599	-0.4779	0.5582	0.045
H1B	0.2406	-0.3776	0.4244	0.045
H12	0.4697	-0.4950	0.7299	0.044
H13	0.6919	-0.4556	0.7883	0.050
H15	0.6327	-0.1480	0.4942	0.050
H16	0.4087	-0.1848	0.4366	0.048
H4A	0.1267	0.3702	0.2654	0.049
H4B	0.1491	0.2950	0.4136	0.049

Anisotropic displacement parameters (Å²) for 18c

The anisotropic displacement factor exponent takes the form: -2 π² (h² a² U₁₁ + ... + 2 h k a^{*} b^{*} U₁₂)

Atom	U ₁₁	U ₂₂	U ₃₃	U ₂₃	U ₁₃	U ₁₂
Se1	0.0376(5)	0.0409(5)	0.0440(5)	-0.0092(5)	0.0187(4)	-0.0063(4)
Se2	0.0338(5)	0.0391(5)	0.0458(5)	-0.0073(5)	0.0049(4)	0.0044(4)
C1	0.042(5)	0.029(5)	0.047(5)	-0.010(4)	0.022(4)	-0.006(4)

X-ray structures

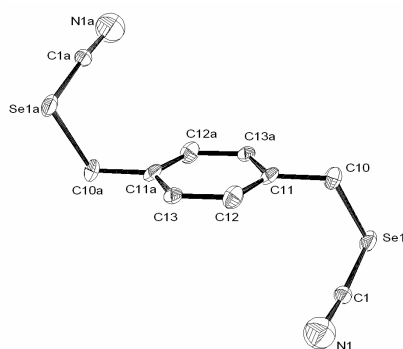
C2	0.025(5)	0.043(6)	0.046(6)	-0.017(5)	0.005(4)	-0.006(4)
C3	0.028(5)	0.033(5)	0.043(5)	-0.014(4)	0.009(4)	-0.002(4)
C11	0.037(5)	0.024(4)	0.027(4)	0.000(4)	0.012(4)	-0.002(4)
C12	0.047(6)	0.031(5)	0.039(5)	0.002(4)	0.023(5)	0.003(4)
C13	0.048(6)	0.034(5)	0.037(5)	0.006(4)	0.006(4)	0.010(4)
C14	0.033(5)	0.027(5)	0.033(5)	-0.002(4)	0.009(4)	0.002(4)
C15	0.040(5)	0.038(5)	0.050(6)	0.017(4)	0.016(4)	-0.010(4)
C16	0.029(5)	0.038(5)	0.048(5)	0.019(5)	0.004(4)	-0.002(4)
C4	0.033(5)	0.029(5)	0.058(6)	-0.009(4)	0.009(4)	0.005(4)

Bond lengths (Å) and angles (deg) for 18c

Se1-C2	1.833(10)	C3-Se2-C4	99.7(4)
Se1-C1	1.987(8)	C11-C1-Se1	115.2(5)
Se2-C3	1.844(10)	C3-C2-Se1	177.9(8)
Se2-C4	1.973(8)	C2-C3-Se2	171.8(7)
C1-C11	1.509(11)	C16-C11-C12	118.8(8)
C2-C3	1.186(11)	C16-C11-C1	120.4(7)
C11-C16	1.379(11)	C12-C11-C1	120.7(7)
C11-C12	1.383(11)	C13-C12-C11	120.1(8)
C12-C13	1.370(12)	C12-C13-C14	122.0(8)
C13-C14	1.373(11)	C13-C14-C15	117.8(8)
C14-C15	1.390(11)	C13-C14-C4#1	120.8(8)
C14-C4#1	1.500(11)	C15-C14-C4#1	121.2(7)
C15-C16	1.380(11)	C16-C15-C14	120.6(7)
C4-C14#1	1.500(11)	C11-C16-C15	120.6(8)
C2-Se1-C1	97.1(4)	C14#1-C4-Se2	116.9(5)

Symmetry transformations used to generate equivalent atoms: #1 -x+1,-y,-z+1

6.4 1,4-bis(selenocyanatomethyl)-benzene (15c)



Crystal data and structure refinement.

Operator	F. Rominger
Identification code	al18
Empirical formula	C ₁₀ H ₈ N ₂ Se ₂
Formula weight	314.10
Temperature	200(2) K

Wavelength	0.71073 Å	
Crystal system	monoclinic	
Space group	P2 ₁ /c	
Z	4	
Unit cell dimensions	a = 22.2635(9) Å	α = 90 deg.
	b = 5.9933(3) Å	β = 98.896(1) deg.
	c = 8.3679(4) Å	γ = 90 deg.
Volume	1103.11(9) Å ³	
Density (calculated)	1.89 g/cm ³	
Absorption coefficient	6.66 mm ⁻¹	
Crystal shape	needles	
Crystal size	2.00 x 0.04 x 0.02 mm ³	
Crystal colour	colorless	
Theta range for data collection	0.9 to 27.5 deg.	
Index ranges	-28 ≤ h ≤ 28, -7 ≤ k ≤ 7, -10 ≤ l ≤ 10	
Reflections collected	9528	
Independent reflections	2488 (R(int) = 0.0694)	
Observed reflections	1835 (I > 2σ(I))	
Absorption correction	Semi-empirical from equivalents	
Max. and min. transmission	0.88 and 0.03	
Refinement method	Full-matrix least-squares on F ²	
Data/restraints/parameters	2488 / 0 / 108	
Goodness-of-fit on F ²	1.30	
Final R indices (I > 2σ(I))	R1 = 0.108, wR2 = 0.257	
Largest diff. peak and hole	3.37 and -1.36 eÅ ⁻³	

Atomic coordinates and equivalent isotropic displacement parameters (Å²) for 15c

U_{eq} is defined as one third of the trace of the orthogonalized U_{ij} tensor

Atom	x	y	z	U _{eq}
Se11	0.3133(1)	0.5719(3)	0.9206(2)	0.0255(5)
C11	0.3173(6)	0.282(2)	0.9189(17)	0.018(3)
N11	0.3255(9)	0.074(3)	0.918(2)	0.055(5)
C101	0.3844(7)	0.618(3)	0.809(2)	0.034(4)
C111	0.4442(6)	0.557(3)	0.907(2)	0.026(3)
C121	0.4703(7)	0.353(3)	0.8867(19)	0.026(3)
C131	0.5258(6)	0.292(3)	0.9772(18)	0.020(3)
Se12	0.1852(1)	0.5963(3)	0.5801(2)	0.0274(5)
C12	0.1794(10)	0.272(4)	0.575(3)	0.054(5)
N12	0.1814(8)	0.096(3)	0.572(2)	0.042(4)
C102	0.1145(7)	0.629(3)	0.4032(19)	0.029(3)
C112	0.0548(7)	0.564(3)	0.4549(18)	0.023(3)
C122	0.0299(7)	0.354(3)	0.4104(18)	0.025(3)
C132	0.0251(7)	0.290(3)	0.4570(17)	0.020(3)

Hydrogen coordinates and isotropic displacement parameters (Å²) for 15c

Atom	x	y	z	U _{eq}
H10A	0.3788	0.5274	0.7087	0.041
H10B	0.3857	0.7764	0.7773	0.041
H121	0.4500	0.2512	0.8095	0.031
H131	0.5434	0.1513	0.9611	0.024
H10A2	0.1120	0.7867	0.3664	0.035
H10B2	0.1214	0.5356	0.3103	0.035
H122	0.0505	0.2553	0.3485	0.030

X-ray structures

H132-0.0419 0.1471 0.4283 0.024

Anisotropic displacement parameters (\AA^2) for 15cThe anisotropic displacement factor exponent takes the form: $-2 \pi^2 (h^2 a^2 U_{11} + \dots + 2 h k a^* b^* U_{12})$

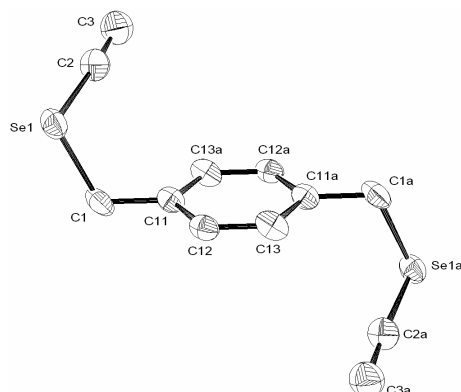
Atom	U_{11}	U_{22}	U_{33}	U_{23}	U_{13}	U_{12}
Se11	0.0130(7)	0.0278(9)	0.0352(10)	0.0003(7)	0.0027(6)	0.0021(6)
C101	0.014(7)	0.039(9)	0.050(11)	0.013(8)	0.008(7)	0.008(6)
C111	0.012(6)	0.035(9)	0.031(8)	0.008(7)	0.007(6)	-0.004(6)
C121	0.020(7)	0.033(8)	0.024(8)	-0.005(6)	0.001(6)	-0.003(6)
C131	0.016(6)	0.026(7)	0.019(7)	0.005(6)	0.008(5)	-0.001(5)
Se12	0.0234(8)	0.0232(8)	0.0359(10)	0.0000(7)	0.0052(7)	0.0007(6)
C102	0.023(8)	0.045(10)	0.020(8)	0.004(7)	0.007(6)	0.001(7)
C112	0.019(7)	0.027(8)	0.021(7)	0.008(6)	-0.003(5)	0.000(6)
C122	0.029(8)	0.029(8)	0.017(7)	-0.013(6)	0.005(6)	-0.001(6)
C132	0.023(7)	0.024(7)	0.014(6)	0.001(5)	0.001(5)	0.001(6)

Bond lengths (\AA) and angles (deg) for 15c

Se11-C11	1.737(14)	C11-Se11-C101	95.1(7)
Se11-C101	1.977(16)	N11-C11-Se11	174.6(14)
C11-N11	1.26(2)	C111-C101-Se11	114.7(12)
C101-C111	1.49(2)	C121-C111-C131#1	119.2(14)
C111-C121	1.38(2)	C121-C111-C101	120.2(15)
C111-C131#1	1.41(2)	C131#1-C111-C101	120.6(15)
C121-C131	1.39(2)	C111-C121-C131	121.3(15)
C131-C111#1	1.41(2)	C121-C131-C111#1	119.5(14)
Se12-C12	1.95(2)	C12-Se12-C102	92.4(9)
Se12-C102	1.997(16)	N12-C12-Se12	174(2)
C12-N12	1.05(3)	C112-C102-Se12	112.9(10)
C102-C112	1.51(2)	C132#2-C112-C122	120.7(14)
C112-C132#2	1.38(2)	C132#2-C112-C102	120.2(14)
C112-C122	1.40(2)	C122-C112-C102	119.1(14)
C122-C132	1.40(2)	C132-C122-C112	120.1(14)
C132-C112#2	1.38(2)	C112#2-C132-C122	119.2(14)

Symmetry transformations used to generate equivalent atoms: #1 -x+1,-y+1,-z+2
#2 -x,-y+1,-z+1

6.5 1,4-bis(ethynylselenylmethyl)-benzene (**17c**)



Crystal data and structure refinement

Operator	F. Rominger	
Identification code	al16	
Empirical formula	$C_{12}H_{10}Se_2$	
Formula weight	312.12	
Temperature	200(2) K	
Wavelength	0.71073 Å	
Crystal system	orthorhombic	
Space group	Pbca	
Z	4	
Unit cell dimensions	a = 5.9208(3) Å	$\alpha = 90$ deg.
	b = 8.5285(4) Å	$\beta = 90$ deg.
	c = 22.4766(9) Å	$\gamma = 90$ deg.
Volume	1134.97(9) Å ³	
Density (calculated)	1.83 g/cm ³	
Absorption coefficient	6.47 mm ⁻¹	
Crystal shape	polyhedron	
Crystal size	0.20 x 0.18 x 0.06 mm ³	
Crystal colour	colorless	
Theta range for data collection	1.8 to 27.5 deg.	
Index ranges	-7 ≤ h ≤ 7, -11 ≤ k ≤ 11, -29 ≤ l ≤ 29	
Reflections collected	10337	
Independent reflections	1300 (R(int) = 0.3352)	
Observed reflections	951 (I > 2σ(I))	
Absorption correction	Semi-empirical from equivalents	
Max. and min. transmission	0.70 and 0.36	
Refinement method	Full-matrix least-squares on F ²	
Data/restraints/parameters	1300 / 0 / 64	
Goodness-of-fit on F ²	1.14	
Final R indices (I > 2σ(I))	R1 = 0.088, wR2 = 0.190	
Largest diff. peak and hole	2.10 and -1.20 eÅ ⁻³	

Atomic coordinates and equivalent isotropic displacement parameters (\AA^2) for 17c

U_{eq} is defined as one third of the trace of the orthogonalized U_{ij} tensor

Atom	x	y	z	U_{eq}
Se1	0.2186(2)	0.8870(1)	0.1689(1)	0.0369(4)
C1	0.099(2)	0.7853(12)	0.0961(5)	0.041(2)
C2	-0.0179(18)	1.0204(14)	0.1832(5)	0.040(3)
C3	-0.168(2)	1.1041(17)	0.1955(6)	0.054(3)
C11	0.0471(15)	0.8956(11)	0.0469(4)	0.0301(19)
C12	0.2122(16)	0.9311(12)	0.0041(4)	0.032(2)
C13	0.1631(17)	1.0330(12)	-0.0413(5)	0.036(2)

Hydrogen coordinates and isotropic displacement parameters (\AA^2) for 17c

Atom	x	y	z	U_{eq}
H1A	0.2110	0.7078	0.0818	0.049
H1B	-0.0404	0.7274	0.1065	0.049
H3	-0.2895	1.1719	0.2055	0.064
H12	0.3577	0.8846	0.0066	0.039
H13	0.2767	1.0556	-0.0699	0.043

Anisotropic displacement parameters (\AA^2) for 17c

The anisotropic displacement factor exponent takes the form: $-2 \pi^2 (h^2 a^{*2} U_{11} + \dots + 2 h k a^* b^* U_{12})$

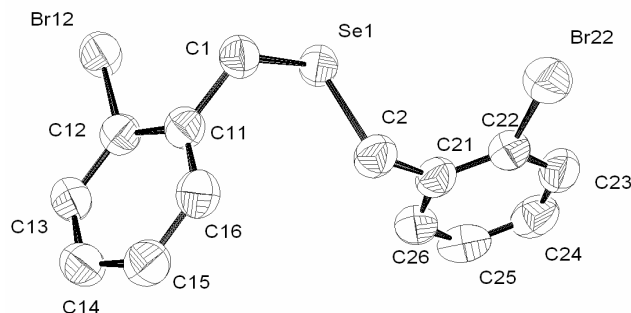
Atom	U_{11}	U_{22}	U_{33}	U_{23}	U_{13}	U_{12}
Se1	0.0354(6)	0.0318(6)	0.0436(7)	0.0032(4)	-0.0061(4)	0.0058(4)
C1	0.046(6)	0.023(5)	0.054(6)	0.000(4)	-0.006(5)	0.008(4)
C2	0.028(5)	0.047(7)	0.046(6)	0.000(5)	-0.007(4)	0.003(5)
C3	0.050(7)	0.055(8)	0.056(7)	-0.001(6)	-0.005(6)	0.007(7)
C11	0.026(4)	0.026(5)	0.038(5)	-0.002(4)	-0.002(3)	-0.003(4)
C12	0.026(4)	0.030(5)	0.040(5)	-0.007(4)	-0.007(4)	0.004(4)
C13	0.024(4)	0.031(5)	0.053(6)	-0.003(4)	0.003(4)	-0.002(4)

Bond lengths (\AA) and angles (deg) for 17c

Se1-C2	1.832(11)	C2-Se1-C1	98.2(5)
Se1-C1	1.982(11)	C11-C1-Se1	114.3(7)
C1-C11	1.484(14)	C3-C2-Se1	176.4(11)
C2-C3	1.173(17)	C13#1-C11-C12	117.7(9)
C11-C13#1	1.392(13)	C13#1-C11-C1	122.0(9)
C11-C12	1.405(14)	C12-C11-C1	120.2(9)
C12-C13	1.370(15)	C13-C12-C11	119.9(9)
C13-C11#1	1.392(13)	C12-C13-C11#1	122.3(10)

Symmetry transformations used to generate equivalent atoms: #1 -x,-y+2,-z

6.6 Bis-(2-bromobenzyl) selenide (42)



Crystal data and structure refinement

Operator	T. Oeser	
Identification code	al13	
Empirical formula	$C_{14}H_{12}Br_2Se$	
Formula weight	419.02	
Temperature	200(2) K	
Wavelength	0.71073 Å	
Crystal system	triclinic	
Space group	P-1	
Z	2	
Unit cell dimensions	a = 6.9710(3) Å	$\alpha = 78.534(1)$ deg.
	b = 7.6909(3) Å	$\beta = 80.586(1)$ deg.
	c = 13.5259(6) Å	$\gamma = 80.280(1)$ deg.
Volume	694.12(5) Å ³	
Density (calculated)	2.01 g/cm ³	
Absorption coefficient	8.44 mm ⁻¹	
Crystal shape	blocks	
Crystal size	0.20 x 0.14 x 0.04 mm ³	
Theta range for data collection	1.5 to 27.5 deg.	
Index ranges	-9 ≤ h ≤ 9, -9 ≤ k ≤ 9, -17 ≤ l ≤ 17	
Reflections collected	7216	
Independent reflections	3141 (R(int) = 0.0290)	
Observed reflections	2521 (I > 2σ(I))	
Absorption correction	Semi-empirical from equivalents	
Max. and min. transmission	0.73 and 0.28	
Refinement method	Full-matrix least-squares on F ²	
Data/restraints/parameters	3141 / 0 / 154	
Goodness-of-fit on F ²	1.04	
Final R indices (I > 2σ(I))	R1 = 0.059, wR2 = 0.134	
Largest diff. peak and hole	1.42 and -0.51 eÅ ⁻³	

Atomic coordinates and equivalent isotropic displacement parameters (\AA^2) for 42

U_{eq} is defined as one third of the trace of the orthogonalized U_{ij} tensor

Atom	x	y	z	U_{eq}
Se1	0.2543(1)	0.8461(1)	0.7223(1)	0.0550(2)
Br12	0.7682(1)	0.8079(1)	0.5584(1)	0.0654(2)
Br22	-0.3048(1)	0.8225(1)	0.8619(1)	0.0786(2)
C1	0.3276(7)	0.7213(6)	0.6048(3)	0.0532(9)
C2	0.1436(8)	0.6473(6)	0.8176(4)	0.0604(11)
C11	0.4849(6)	0.5645(6)	0.6214(3)	0.0508(9)
C12	0.6855(7)	0.5792(6)	0.6047(3)	0.0511(9)
C13	0.8286(7)	0.4319(6)	0.6203(4)	0.0556(10)
C14	0.7746(8)	0.2612(7)	0.6533(4)	0.0609(11)
C15	0.5753(8)	0.2418(7)	0.6708(4)	0.0610(11)
C16	0.4339(7)	0.3908(7)	0.6546(4)	0.0572(10)
C21	0.0777(7)	0.6992(6)	0.9205(4)	0.0560(10)
C22	-0.1092(7)	0.7779(7)	0.9506(4)	0.0597(11)
C23	-0.1640(9)	0.8259(7)	1.0470(4)	0.0705(14)
C24	-0.0272(10)	0.7928(8)	1.1134(4)	0.0741(15)
C25	0.1646(10)	0.7125(7)	1.0851(4)	0.0754(15)
C26	0.2138(8)	0.6685(7)	0.9907(4)	0.0651(12)

Hydrogen coordinates and isotropic displacement parameters (\AA^2) for 42

Atom	x	y	z	U_{eq}
H1A	0.2098	0.6794	0.5906	0.064
H1B	0.3735	0.8071	0.5442	0.064
H2A	0.0306	0.6181	0.7913	0.072
H2B	0.2441	0.5396	0.8234	0.072
H13	0.9634	0.4471	0.6085	0.067
H14	0.8719	0.1593	0.6638	0.073
H15	0.5368	0.1262	0.6938	0.073
H16	0.2992	0.3753	0.6662	0.069
H23	-0.2939	0.8805	1.0663	0.085
H24	-0.0629	0.8248	1.1789	0.089
H25	0.2589	0.6890	1.1312	0.090
H26	0.3444	0.6153	0.9715	0.078

Anisotropic displacement parameters (\AA^2) for 42

The anisotropic displacement factor exponent takes the form: $-2 \pi^2 (h^2 a^{*2} U_{11} + \dots + 2 h k a^* b^* U_{12})$

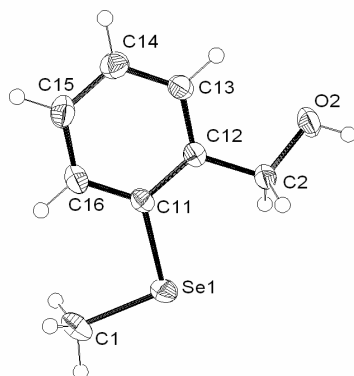
Atom	U_{11}	U_{22}	U_{33}	U_{23}	U_{13}	U_{12}
Se1	0.0539(3)	0.0496(3)	0.0581(3)	-0.0090(2)	0.0016(2)	-0.0071(2)
Br12	0.0574(3)	0.0543(3)	0.0814(4)	-0.0103(2)	0.0012(2)	-0.0113(2)
Br22	0.0645(3)	0.0809(4)	0.0830(4)	0.0060(3)	-0.0139(3)	-0.0099(3)
C1	0.050(2)	0.059(2)	0.049(2)	-0.0113(19)	-0.0065(18)	-0.0024(18)
C2	0.069(3)	0.050(2)	0.059(3)	-0.009(2)	0.002(2)	-0.012(2)
C11	0.053(2)	0.054(2)	0.046(2)	-0.0110(18)	-0.0068(17)	-0.0052(18)
C12	0.055(2)	0.049(2)	0.051(2)	-0.0109(18)	-0.0050(18)	-0.0088(18)
C13	0.052(2)	0.058(2)	0.057(2)	-0.015(2)	-0.0075(19)	-0.0016(19)
C14	0.066(3)	0.056(3)	0.059(3)	-0.012(2)	-0.011(2)	0.003(2)
C15	0.069(3)	0.056(3)	0.058(3)	-0.012(2)	-0.005(2)	-0.011(2)

C16	0.053(2)	0.063(3)	0.058(3)	-0.015(2)	-0.0055(19)	-0.012(2)
C21	0.061(3)	0.049(2)	0.056(2)	-0.0065(19)	0.001(2)	-0.0131(19)
C22	0.057(2)	0.055(2)	0.062(3)	-0.001(2)	-0.005(2)	-0.0088(19)
C23	0.073(3)	0.055(3)	0.073(3)	-0.010(2)	0.015(3)	-0.008(2)
C24	0.105(4)	0.061(3)	0.055(3)	-0.011(2)	0.001(3)	-0.018(3)
C25	0.105(4)	0.059(3)	0.064(3)	0.003(2)	-0.024(3)	-0.020(3)
C26	0.067(3)	0.051(2)	0.072(3)	-0.003(2)	-0.004(2)	-0.008(2)

Bond lengths (Å) and angles (deg) for 42

Se1-C2	1.970(5)	C21-C2-H2B	109.7
Se1-C1	1.971(4)	Se1-C2-H2B	109.7
Br12-C12	1.899(4)	H2A-C2-H2B	108.2
Br22-C22	1.906(5)	C12-C11-C16	116.7(4)
C1-C11	1.494(6)	C12-C11-C1	123.4(4)
C1-H1A	0.9900	C16-C11-C1	119.8(4)
C1-H1B	0.9900	C13-C12-C11	122.4(4)
C2-C21	1.503(7)	C13-C12-Br12	117.9(4)
C2-H2A	0.9900	C11-C12-Br12	119.7(3)
C2-H2B	0.9900	C12-C13-C14	119.9(4)
C11-C12	1.399(6)	C12-C13-H13	120.1
C11-C16	1.408(7)	C14-C13-H13	120.1
C12-C13	1.384(6)	C13-C14-C15	119.2(4)
C13-C14	1.394(7)	C13-C14-H14	120.4
C13-H13	0.9500	C15-C14-H14	120.4
C14-C15	1.399(7)	C16-C15-C14	120.2(5)
C14-H14	0.9500	C16-C15-H15	119.9
C15-C16	1.386(7)	C14-C15-H15	119.9
C15-H15	0.9500	C15-C16-C11	121.7(4)
C16-H16	0.9500	C15-C16-H16	119.2
C21-C22	1.374(7)	C11-C16-H16	119.2
C21-C26	1.410(7)	C22-C21-C26	117.2(5)
C22-C23	1.401(8)	C22-C21-C2	123.7(5)
C23-C24	1.373(9)	C26-C21-C2	119.1(5)
C23-H23	0.9500	C21-C22-C23	121.8(5)
C24-C25	1.401(9)	C21-C22-Br22	120.5(4)
C24-H24	0.9500	C23-C22-Br22	117.7(4)
C25-C26	1.360(8)	C24-C23-C22	119.1(5)
C25-H25	0.9500	C24-C23-H23	120.5
C26-H26	0.9500	C22-C23-H23	120.5
C2-Se1-C1	96.4(2)	C23-C24-C25	120.5(5)
C11-C1-Se1	113.0(3)	C23-C24-H24	119.7
C11-C1-H1A	109.0	C25-C24-H24	119.7
Se1-C1-H1A	109.0	C26-C25-C24	119.0(6)
C11-C1-H1B	109.0	C26-C25-H25	120.5
Se1-C1-H1B	109.0	C24-C25-H25	120.5
H1A-C1-H1B	107.8	C25-C26-C21	122.3(5)
C21-C2-Se1	110.0(3)	C25-C26-H26	118.9
C21-C2-H2A	109.7	C21-C26-H26	118.9
Se1-C2-H2A	109.7		

6.7 2-(methylselenenyl)-benzyl alcohol (46)



Crystal data and structure refinement

Operator	F. Rominger	
Identification code	al20	
Empirical formula	C ₈ H ₁₀ OSe	
Formula weight	201.12	
Temperature	200(2) K	
Wavelength	0.71073 Å	
Crystal system	monoclinic	
Space group	P2 ₁ /n	
Z	4	
Unit cell dimensions	a = 13.1179(2) Å	α = 90 deg.
	b = 4.7578(1) Å	β = 99.294(1) deg.
	c = 13.2194(3) Å	γ = 90 deg.
Volume	814.22(3) Å ³	
Density (calculated)	1.64 g/cm ³	
Absorption coefficient	4.54 mm ⁻¹	
Crystal shape	polyhedron	
Crystal size	0.45 x 0.18 x 0.18 mm ³	
Crystal colour	colorless	
Theta range for data collection	2.0 to 27.4 deg.	
Index ranges	-16 ≤ h ≤ 16, -6 ≤ k ≤ 6, -17 ≤ l ≤ 17	
Reflections collected	7591	
Independent reflections	1822 (R(int) = 0.0545)	
Observed reflections	1538 (I > 2σ(I))	
Absorption correction	Semi-empirical from equivalents	
Refinement method	Full-matrix least-squares on F ²	
Data/restraints/parameters	1822 / 0 / 95	
Goodness-of-fit on F ²	1.04	
Final R indices (I > 2σ(I))	R1 = 0.029, wR2 = 0.065	
Largest diff. peak and hole	0.59 and -0.53 eÅ ⁻³	

Atomic coordinates and equivalent isotropic displacement parameters (Å²) for 46

U_{eq} is defined as one third of the trace of the orthogonalized U_{ij} tensor

Atom	x	y	z	U _{eq}
Se1	0.6876(1)	0.1359(1)	0.8599(1)	0.0345(1)
C1	0.7322(2)	-0.0719(6)	0.9864(2)	0.0400(7)

C2	0.5477(2)	0.2477(5)	0.6520(2)	0.0284(5)
O2	0.4927(2)	0.2523(4)	0.5497(1)	0.0368(4)
C11	0.5535(2)	-0.0286(5)	0.8166(2)	0.0236(5)
C12	0.4998(2)	0.0455(5)	0.7196(2)	0.0221(5)
C13	0.4026(2)	-0.0697(5)	0.6867(2)	0.0274(5)
C14	0.3591(2)	-0.2605(6)	0.7473(2)	0.0333(6)
C15	0.4128(2)	-0.3348(6)	0.8424(2)	0.0366(6)
C16	0.5091(2)	-0.2184(5)	0.8777(2)	0.0317(6)

Hydrogen coordinates and isotropic displacement parameters (\AA^2) for 46

Atom	x	y	z	U_{eq}
H1A	0.6848	-0.0334	1.0350	0.060
H1B	0.8022	-0.0131	1.0164	0.060
H1C	0.7319	-0.2737	0.9715	0.060
H2A	0.5483	0.4391	0.6815	0.034
H2B	0.6202	0.1917	0.6508	0.034
H2C	0.5147	0.1236	0.5155	0.05(2)
H2D	0.5060	0.4020	0.5208	0.05(2)
H13	0.3652	-0.0172	0.6218	0.033
H14	0.2931	-0.3392	0.7235	0.040
H15	0.3837	-0.4661	0.8837	0.044
H16	0.5450	-0.2678	0.9436	0.038

Anisotropic displacement parameters (\AA^2) for 46.

The anisotropic displacement factor exponent takes the form: $-2 \pi^2 (h^2 a^{*2} U_{11} + \dots + 2 h k a^* b^* U_{12})$

Atom	U_{11}	U_{22}	U_{33}	U_{23}	U_{13}	U_{12}
Se1	0.0302(2)	0.0348(2)	0.0344(2)	0.0046(1)	-0.0073(1)	-0.0027(1)
C1	0.0375(15)	0.0499(16)	0.0285(13)	0.0013(12)	-0.0069(11)	0.0067(12)
C2	0.0357(14)	0.0241(11)	0.0235(12)	0.0038(10)	-0.0009(10)	-0.0024(10)
O2	0.0531(12)	0.0325(10)	0.0220(9)	0.0056(8)	-0.0023(8)	-0.0029(9)
C11	0.0252(12)	0.0234(11)	0.0213(11)	-0.0008(9)	0.0012(9)	0.0037(9)
C12	0.0263(12)	0.0190(10)	0.0209(11)	-0.0015(8)	0.0038(9)	0.0039(9)
C13	0.0291(13)	0.0262(12)	0.0252(12)	-0.0004(9)	-0.0007(10)	0.0007(10)
C14	0.0271(13)	0.0356(13)	0.0373(15)	0.0011(11)	0.0052(11)	-0.0025(11)
C15	0.0403(16)	0.0382(15)	0.0335(14)	0.0086(12)	0.0125(12)	-0.0020(12)
C16	0.0352(15)	0.0357(13)	0.0238(12)	0.0067(10)	0.0032(11)	0.0036(11)

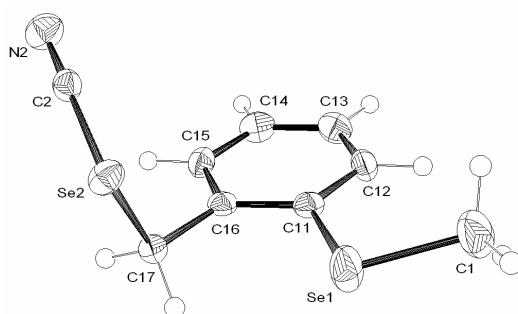
Bond lengths (\AA) and angles (deg) for 46

Se1-C11	1.926(2)	C11-C12	1.405(3)
Se1-C1	1.950(3)	C12-C13	1.392(3)
C1-H1A	0.9800	C13-C14	1.392(4)
C1-H1B	0.9800	C13-H13	0.9500
C1-H1C	0.9800	C14-C15	1.384(4)
C2-O2	1.427(3)	C14-H14	0.9500
C2-C12	1.517(3)	C15-C16	1.389(4)
C2-H2A	0.9900	C15-H15	0.9500
C2-H2B	0.9900	C16-H16	0.9500
O2-H2C	0.8400	C11-Se1-C1	100.47(11)
O2-H2D	0.8400	Se1-C1-H1A	109.5
C11-C16	1.399(4)	Se1-C1-H1B	109.5

X-ray structures

H1A-C1-H1B	109.5	C13-C12-C11	119.1(2)
Se1-C1-H1C	109.5	C13-C12-C2	120.7(2)
H1A-C1-H1C	109.5	C11-C12-C2	120.2(2)
H1B-C1-H1C	109.5	C14-C13-C12	121.1(2)
O2-C2-C12	112.0(2)	C14-C13-H13	119.5
O2-C2-H2A	109.2	C12-C13-H13	119.5
C12-C2-H2A	109.2	C15-C14-C13	119.6(2)
O2-C2-H2B	109.2	C15-C14-H14	120.2
C12-C2-H2B	109.2	C13-C14-H14	120.2
H2A-C2-H2B	107.9	C14-C15-C16	120.4(2)
C2-O2-H2C	109.5	C14-C15-H15	119.8
C2-O2-H2D	109.5	C16-C15-H15	119.8
C16-C11-C12	119.7(2)	C15-C16-C11	120.2(2)
C16-C11-Se1	122.41(18)	C15-C16-H16	119.9
C12-C11-Se1	117.92(17)	C11-C16-H16	119.9

6.8 2-(methylselenyl)-benzyl selenocyanate (29)



Crystal data and structure refinement

Operator	F. Rominger	
Identification code	al8	
Empirical formula	C ₉ H ₉ NSe ₂	
Formula weight	289.09	
Temperature	200(2) K	
Wavelength	0.71073 Å	
Crystal system	monoclinic	
Space group	P2 ₁ /c	
Z	4	
Unit cell dimensions	a = 8.8538(1) Å	α = 90 deg.
	b = 16.6622(4) Å	β = 113.004(1) deg.
	c = 7.2143(2) Å	γ = 90 deg.
Volume	979.65(4) Å ³	
Density (calculated)	1.96 g/cm ³	
Absorption coefficient	7.49 mm ⁻¹	
Crystal shape	polyhedron	
Crystal size	0.26 x 0.14 x 0.04 mm ³	
Theta range for data collection	2.4 to 27.5 deg.	
Index ranges	-11 ≤ h ≤ 11, -21 ≤ k ≤ 21, -9 ≤ l ≤ 9	
Reflections collected	10108	
Independent reflections	2259 (R(int) = 0.0602)	
Observed reflections	1723 (I > 2σ(I))	

Absorption correction	Semi-empirical from equivalents
Max. and min. transmission	0.75 and 0.25
Refinement method	Full-matrix least-squares on F ²
Data/restraints/parameters	2259 / 0 / 110
Goodness-of-fit on F ²	1.02
Final R indices (I > 2σ(I))	R1 = 0.031, wR2 = 0.065
Largest diff. peak and hole	0.75 and -0.84 eÅ ⁻³

Atomic coordinates and equivalent isotropic displacement parameters (Å²) for 29

U_{eq} is defined as one third of the trace of the orthogonalized U_{ij} tensor

Atom	x	y	z	U _{eq}
Se1	1.1915(1)	0.0546(1)	0.9520(1)	0.0398(1)
Se2	0.7551(1)	0.1195(1)	0.7661(1)	0.0264(1)
C1	1.4096(5)	0.0930(3)	1.1030(6)	0.0519(12)
C2	0.6676(4)	0.1991(2)	0.5770(5)	0.0231(7)
N2	0.6127(4)	0.2492(2)	0.4618(4)	0.0335(7)
C11	1.1386(4)	0.1062(2)	0.6981(5)	0.0227(7)
C12	1.2551(4)	0.1478(2)	0.6490(5)	0.0269(7)
C13	1.2100(4)	0.1849(2)	0.4637(5)	0.0318(8)
C14	1.0509(4)	0.1808(2)	0.3250(5)	0.0313(8)
C15	0.9346(4)	0.1398(2)	0.3709(5)	0.0253(7)
C16	0.9760(4)	0.1011(2)	0.5560(5)	0.0209(7)
C17	0.8462(4)	0.0562(2)	0.5988(5)	0.0229(7)

Hydrogen coordinates and isotropic displacement parameters (Å²) for 29

Atom	x	y	z	U _{eq}
H1A	1.4831	0.0741	1.0401	0.078
H1B	1.4478	0.0728	1.2413	0.078
H1C	1.4092	0.1518	1.1046	0.078
H12	1.3656	0.1506	0.7433	0.032
H13	1.2897	0.2135	0.4320	0.038
H14	1.0211	0.2062	0.1977	0.038
H15	0.8245	0.1378	0.2750	0.030
H17A	0.8936	0.0056	0.6696	0.027
H17B	0.7560	0.0420	0.4696	0.027

Anisotropic displacement parameters (Å²) for 29

The anisotropic displacement factor exponent takes the form: $-2\pi^2 (h^2 a^{*2} U_{11} + \dots + 2hk a^* b^* U_{12})$

Atom	U ₁₁	U ₂₂	U ₃₃	U ₂₃	U ₁₃	U ₁₂
Se1	0.0290(2)	0.0501(3)	0.0299(2)	0.0162(2)	0.0003(2)	-0.0079(2)
Se2	0.0276(2)	0.0274(2)	0.0265(2)	0.0052(1)	0.0132(2)	0.0057(2)
C1	0.042(2)	0.050(3)	0.040(2)	0.0114(19)	-0.010(2)	-0.014(2)
C2	0.0200(17)	0.0248(18)	0.0260(17)	-0.0019(14)	0.0106(14)	-0.0013(14)
N2	0.0360(18)	0.0334(17)	0.0343(17)	0.0039(14)	0.0174(15)	0.0053(14)
C11	0.0252(18)	0.0177(16)	0.0258(16)	-0.0019(13)	0.0106(14)	0.0016(13)
C12	0.0198(17)	0.0279(18)	0.0311(18)	-0.0044(14)	0.0078(15)	-0.0045(14)
C13	0.035(2)	0.0291(19)	0.034(2)	0.0001(15)	0.0162(17)	-0.0041(16)
C14	0.041(2)	0.0296(19)	0.0269(18)	0.0039(15)	0.0166(17)	0.0031(17)
C15	0.0208(17)	0.0284(18)	0.0236(16)	-0.0001(14)	0.0053(14)	0.0029(14)

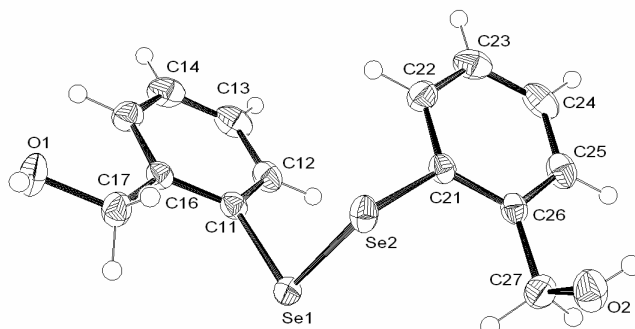
X-ray structures

C16	0.0242(17)	0.0157(16)	0.0238(16)	-0.0033(12)	0.0104(14)	0.0014(13)
C17	0.0208(17)	0.0209(16)	0.0262(16)	-0.0017(13)	0.0084(14)	0.0002(13)

Bond lengths (Å) and angles (deg) for 29

Se1-C11	1.909(3)	C2-Se2-C17	94.86(13)
Se1-C1	1.919(4)	N2-C2-Se2	178.9(3)
Se2-C2	1.842(3)	C12-C11-C16	119.5(3)
Se2-C17	1.995(3)	C12-C11-Se1	122.5(3)
C2-N2	1.144(4)	C16-C11-Se1	118.0(2)
C11-C12	1.398(5)	C13-C12-C11	120.2(3)
C11-C16	1.406(5)	C14-C13-C12	120.5(3)
C12-C13	1.383(5)	C13-C14-C15	119.9(3)
C13-C14	1.374(5)	C14-C15-C16	121.1(3)
C14-C15	1.380(5)	C15-C16-C11	118.7(3)
C15-C16	1.397(4)	C15-C16-C17	119.4(3)
C16-C17	1.501(4)	C11-C16-C17	121.9(3)
C11-Se1-C1	102.08(16)	C16-C17-Se2	112.6(2)

6.9 2,2'- diselenobis(benzyl alcohol) (51)



Crystal data and structure refinement

Operator	F. Rominger	
Identification code	al2	
Empirical formula	C ₁₄ H ₁₄ O ₂ Se ₂	
Formula weight	372.17	
Temperature	200(2) K	
Wavelength	0.71073 Å	
Crystal system	triclinic	
Space group	P $\bar{1}$	
Z	2	
Unit cell dimensions	a = 8.4461(2) Å	α = 72.904(1) deg.
	b = 8.9003(3) Å	β = 78.950(1) deg.
	c = 9.7427(3) Å	γ = 76.978(1) deg.
Volume	675.81(3) Å ³	
Density (calculated)	1.83 g/cm ³	
Absorption coefficient	5.46 mm ⁻¹	
Crystal shape	polyhedron	

Crystal size	0.24 x 0.16 x 0.10 mm ³
Theta range for data collection	2.2 to 27.5 deg.
Index ranges	-10 ≤ h ≤ 10, -11 ≤ k ≤ 11, -12 ≤ l ≤ 12
Reflections collected	6951
Independent reflections	3051 (R(int) = 0.0291)
Observed reflections	2667 (I > 2σ(I))
Absorption correction	Semi-empirical from equivalents
Max. and min. transmission	0.61 and 0.35
Refinement method	Full-matrix least-squares on F ²
Data/restraints/parameters	3051 / 0 / 171
Goodness-of-fit on F ²	1.09
Final R indices (I > 2σ(I))	R1 = 0.026, wR2 = 0.069
Largest diff. peak and hole	0.60 and -0.52 eÅ ⁻³

Atomic coordinates and equivalent isotropic displacement parameters (Å²) for 51.

U_{eq} is defined as one third of the trace of the orthogonalized U_{ij} tensor

Atom	x	y	z	U _{eq}
Se1	0.3297(1)	0.8337(1)	0.4287(1)	0.0264(1)
Se2	0.0975(1)	0.9716(1)	0.3166(1)	0.0266(1)
O1	0.0427(3)	0.4895(2)	0.7814(2)	0.0342(4)
O2	0.1712(3)	1.3434(2)	0.0417(2)	0.0379(5)
H2	0.149(5)	1.374(5)	-0.033(4)	0.059(13)
C11	0.3137(3)	0.6194(3)	0.4352(2)	0.0234(5)
C12	0.4015(3)	0.5537(3)	0.3245(3)	0.0300(6)
C13	0.3932(3)	0.4003(3)	0.3251(3)	0.0375(7)
C14	0.2973(3)	0.3125(3)	0.4361(3)	0.0357(6)
C15	0.2078(3)	0.3768(3)	0.5477(3)	0.0293(5)
C16	0.2153(3)	0.5299(3)	0.5500(2)	0.0224(5)
C17	0.1211(3)	0.6030(3)	0.6692(3)	0.0299(5)
C21	0.1801(3)	0.9551(3)	0.1218(2)	0.0228(5)
C22	0.1505(3)	0.8264(3)	0.0839(3)	0.0289(5)
C23	0.2023(3)	0.8097(3)	-0.0559(3)	0.0361(6)
C24	0.2818(3)	0.9230(4)	-0.1574(3)	0.0367(7)
C25	0.3128(3)	1.0502(3)	-0.1191(3)	0.0312(6)
C26	0.2637(3)	1.0691(3)	0.0212(2)	0.0235(5)
C27	0.3022(3)	1.2092(3)	0.0571(3)	0.0310(6)
H1	-0.022(4)	0.540(4)	0.819(3)	0.036(9)

Hydrogen coordinates and isotropic displacement parameters (Å²) for 51.

Atom	x	y	z	U _{eq}
H2	0.149(5)	1.374(5)	-0.033(4)	0.059(13)
H12	0.4678	0.6146	0.2479	0.036
H13	0.4535	0.3557	0.2491	0.045
H14	0.2921	0.2069	0.4366	0.043
H15	0.1410	0.3151	0.6230	0.035
H17A	0.1969	0.6431	0.7101	0.036
H17B	0.0375	0.6950	0.6288	0.036
H22	0.0948	0.7494	0.1537	0.035
H23	0.1832	0.7210	-0.0816	0.043
H24	0.3152	0.9134	-0.2537	0.044
H25	0.3687	1.1265	-0.1897	0.037
H27A	0.3269	1.1758	0.1582	0.037

X-ray structures

H27B	0.4015	1.2415	-0.0072	0.037
H1	-0.022(4)	0.540(4)	0.819(3)	0.036(9)

Anisotropic displacement parameters (\AA^2) for 51

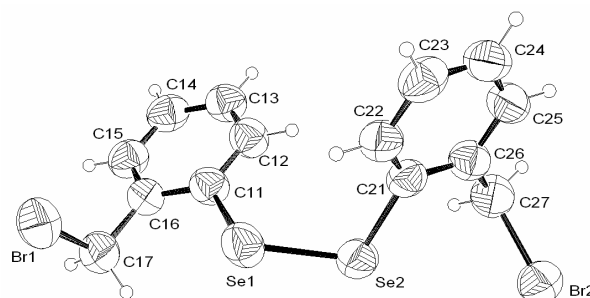
The anisotropic displacement factor exponent takes the form: $-2 \pi^2 (h^2 a^2 U_{11} + \dots + 2 h k a^* b^* U_{12})$

Atom	U_{11}	U_{22}	U_{33}	U_{23}	U_{13}	U_{12}
Se1	0.0338(2)	0.0243(1)	0.0224(1)	-0.0049(1)	-0.0042(1)	-0.0094(1)
Se2	0.0321(2)	0.0217(1)	0.0214(1)	-0.0049(1)	0.0015(1)	-0.0008(1)
O1	0.0405(11)	0.0269(10)	0.0270(10)	-0.0019(8)	0.0078(8)	-0.0066(9)
O2	0.0521(13)	0.0267(10)	0.0314(11)	-0.0082(8)	-0.0067(9)	0.0019(9)
C11	0.0276(12)	0.0205(11)	0.0225(11)	-0.0060(9)	-0.0080(9)	-0.0008(10)
C12	0.0303(13)	0.0370(14)	0.0228(12)	-0.0105(10)	-0.0015(10)	-0.0042(11)
C13	0.0395(15)	0.0384(16)	0.0397(15)	-0.0246(13)	-0.0110(12)	0.0066(13)
C14	0.0417(15)	0.0255(13)	0.0458(16)	-0.0185(12)	-0.0137(13)	0.0011(12)
C15	0.0335(13)	0.0212(12)	0.0340(13)	-0.0064(10)	-0.0079(11)	-0.0045(10)
C16	0.0249(11)	0.0212(11)	0.0209(11)	-0.0057(9)	-0.0060(9)	-0.0012(9)
C17	0.0386(14)	0.0267(13)	0.0242(12)	-0.0081(10)	0.0024(10)	-0.0090(11)
C21	0.0246(12)	0.0214(12)	0.0209(11)	-0.0050(9)	-0.0041(9)	-0.0008(9)
C22	0.0304(13)	0.0254(13)	0.0310(13)	-0.0062(10)	-0.0043(10)	-0.0068(10)
C23	0.0377(15)	0.0376(15)	0.0407(15)	-0.0213(13)	-0.0103(12)	-0.0031(12)
C24	0.0349(14)	0.0494(17)	0.0261(13)	-0.0188(12)	-0.0065(11)	0.0055(13)
C25	0.0271(13)	0.0381(15)	0.0237(12)	-0.0052(11)	-0.0015(10)	-0.0018(11)
C26	0.0209(11)	0.0237(12)	0.0227(11)	-0.0033(9)	-0.0042(9)	-0.0001(9)
C27	0.0310(13)	0.0280(14)	0.0326(14)	-0.0048(11)	-0.0036(11)	-0.0076(11)

Bond lengths (\AA) and angles (deg) for 51

Se1-C11	1.924(2)	C12-C11-Se1	118.61(19)
Se1-Se2	2.3441(3)	C16-C11-Se1	121.07(17)
Se2-C21	1.929(2)	C13-C12-C11	120.4(2)
O1-C17	1.424(3)	C14-C13-C12	119.7(2)
O2-C27	1.427(3)	C13-C14-C15	120.7(2)
C11-C12	1.387(3)	C16-C15-C14	120.6(3)
C11-C16	1.413(3)	C15-C16-C11	118.3(2)
C12-C13	1.381(4)	C15-C16-C17	122.1(2)
C13-C14	1.375(4)	C11-C16-C17	119.6(2)
C14-C15	1.392(4)	O1-C17-C16	111.1(2)
C15-C16	1.385(3)	C22-C21-C26	121.0(2)
C16-C17	1.504(3)	C22-C21-Se2	117.09(18)
C21-C22	1.387(3)	C26-C21-Se2	121.91(17)
C21-C26	1.400(3)	C21-C22-C23	120.1(2)
C22-C23	1.389(4)	C24-C23-C22	119.7(3)
C23-C24	1.382(4)	C25-C24-C23	120.1(2)
C24-C25	1.381(4)	C24-C25-C26	121.5(3)
C25-C26	1.399(3)	C25-C26-C21	117.6(2)
C26-C27	1.505(4)	C25-C26-C27	119.2(2)
C11-Se1-Se2	98.92(7)	C21-C26-C27	123.3(2)
C21-Se2-Se1	99.06(7)	O2-C27-C26	113.0(2)
C12-C11-C16	120.3(2)		

6.10 2,2'- diselenobis(benzyl bromide) (52)



Crystal data and structure refinement

Operator	T.Oeser	
Identification code	al10	
Empirical formula	$C_{14}H_{12}Br_2Se_2$	
Formula weight	497.98	
Temperature	296(2) K	
Wavelength	0.71073 Å	
Crystal system	monoclinic	
Space group	C2/c	
Z	8	
Unit cell dimensions	a = 11.409(1) Å	$\alpha = 90.0$ deg.
	b = 11.359(1) Å	$\beta = 101.861(2)$ deg.
	c = 24.176(2) Å	$\gamma = 90.0$ deg.
Volume	3066.2(5) Å ³	
Density (calculated)	2.16 g/cm ³	
Absorption coefficient	10.02 mm ⁻¹	
Crystal shape	irregular	
Crystal size	0.13 x 0.11 x 0.04 mm ³	
Theta range for data collection	2.8 to 22.0 deg.	
Index ranges	-12 ≤ h ≤ 12, -11 ≤ k ≤ 11, -25 ≤ l ≤ 25	
Reflections collected	9097	
Independent reflections	1866 (R(int) = 0.0273)	
Observed reflections	1468 (I > 2σ(I))	
Absorption correction	Semi-empirical from equivalents	
Max. and min. transmission	0.69 and 0.36	
Refinement method	Full-matrix least-squares on F ²	
Data/restraints/parameters	1866 / 0 / 163	
Goodness-of-fit on F ²	1.08	
Final R indices (I > 2σ(I))	R1 = 0.065, wR2 = 0.148	
Largest diff. peak and hole	1.24 and -0.33 eÅ ⁻³	

Atomic coordinates and equivalent isotropic displacement parameters (Å²) for 52

U_{eq} is defined as one third of the trace of the orthogonalized U_{ij} tensor

Atom	x	y	z	U_{eq}
Se1	0.6998(1)	0.0999(1)	0.7924(1)	0.1099(5)
Se2	0.6617(1)	0.1613(1)	0.6993(1)	0.1057(4)
Br1	0.7616(1)	0.0670(1)	0.9534(1)	0.1188(5)
Br2	0.5963(1)	0.2043(1)	0.5455(1)	0.1223(5)

X-ray structures

C11	0.8099(8)	0.2206(7)	0.8291(4)	0.090(2)
C12	0.8937(8)	0.2664(8)	0.8023(4)	0.097(2)
C13	0.9695(8)	0.3530(8)	0.8284(4)	0.099(3)
C14	0.9626(9)	0.3915(9)	0.8799(5)	0.104(3)
C15	0.8788(9)	0.3463(8)	0.9068(4)	0.100(3)
C16	0.8015(7)	0.2602(8)	0.8828(4)	0.089(2)
C17	0.7079(8)	0.2141(9)	0.9123(4)	0.103(3)
C21	0.7901(7)	0.0875(8)	0.6697(4)	0.088(2)
C22	0.8493(8)	-0.0075(9)	0.6958(4)	0.101(3)
C23	0.9377(9)	-0.0602(9)	0.6714(5)	0.109(3)
C24	0.9647(9)	-0.0162(10)	0.6229(5)	0.111(3)
C25	0.9032(8)	0.0800(10)	0.5972(5)	0.105(3)
C26	0.8150(8)	0.1343(8)	0.6197(4)	0.093(2)
C27	0.7544(9)	0.2408(9)	0.5913(5)	0.114(3)

Hydrogen coordinates and isotropic displacement parameters (\AA^2) for 52

Atom	x	y	z	U_{eq}
H12	0.8994	0.2393	0.7666	0.117
H13	1.0261	0.3851	0.8100	0.119
H14	1.0152	0.4493	0.8974	0.124
H15	0.8742	0.3749	0.9424	0.120
H17A	0.6346	0.1994	0.8848	0.123
H17B	0.6910	0.2728	0.9388	0.123
H22	0.8317	-0.0370	0.7290	0.122
H23	0.9785	-0.1260	0.6884	0.131
H24	1.0243	-0.0511	0.6073	0.133
H25	0.9214	0.1092	0.5640	0.126
H27A	0.8039	0.2750	0.5673	0.137
H27B	0.7458	0.2987	0.6197	0.137

Anisotropic displacement parameters (\AA^2) for 52

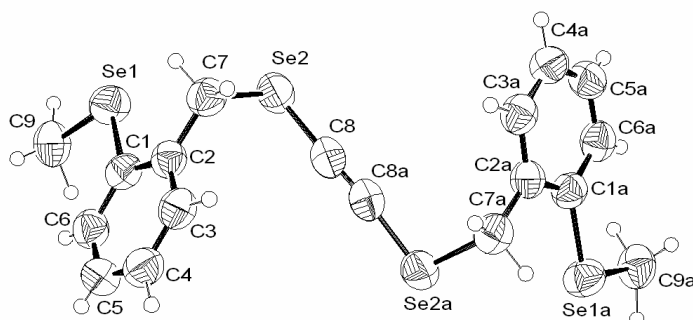
The anisotropic displacement factor exponent takes the form: $-2 \pi^2 (h^2 a^{*2} U_{11} + \dots + 2 h k a^* b^* U_{12})$

Atom	U_{11}	U_{22}	U_{33}	U_{23}	U_{13}	U_{12}
Se1	0.1124(8)	0.1183(8)	0.1053(8)	-0.0172(6)	0.0369(6)	-0.0331(6)
Se2	0.0887(7)	0.1256(8)	0.1013(7)	-0.0178(5)	0.0163(5)	0.0132(5)
Br1	0.1366(9)	0.1138(8)	0.1111(8)	0.0098(6)	0.0372(7)	-0.0073(6)
Br2	0.1030(8)	0.1458(10)	0.1139(8)	0.0126(7)	0.0126(6)	0.0091(6)
C11	0.085(5)	0.090(5)	0.097(6)	-0.008(5)	0.023(5)	-0.014(4)
C12	0.098(6)	0.097(6)	0.099(6)	-0.005(5)	0.027(5)	-0.008(5)
C13	0.090(6)	0.093(6)	0.115(7)	0.008(5)	0.023(5)	-0.015(5)
C14	0.090(6)	0.099(6)	0.115(7)	-0.020(6)	0.006(5)	-0.008(5)
C15	0.096(6)	0.099(6)	0.100(6)	-0.014(5)	0.010(5)	0.003(5)
C16	0.083(5)	0.099(6)	0.085(5)	0.001(5)	0.020(4)	0.003(5)
C17	0.103(7)	0.112(7)	0.095(6)	-0.003(5)	0.025(5)	0.007(5)
C21	0.075(5)	0.097(6)	0.089(6)	-0.017(5)	0.008(4)	-0.004(4)
C22	0.090(6)	0.114(7)	0.098(6)	-0.005(5)	0.015(5)	0.017(5)
C23	0.102(6)	0.096(6)	0.118(8)	-0.012(6)	-0.004(6)	0.018(5)
C24	0.084(6)	0.123(8)	0.125(9)	-0.032(7)	0.022(6)	0.000(6)
C25	0.088(6)	0.124(8)	0.108(7)	-0.021(6)	0.031(5)	-0.009(6)
C26	0.090(6)	0.091(5)	0.100(6)	-0.002(5)	0.020(5)	-0.004(4)
C27	0.111(7)	0.115(7)	0.115(7)	0.000(6)	0.025(6)	-0.005(6)

Bond lengths (Å) and angles (deg) for 52

Se1-C11	1.947(8)	C14-C13-H13	119.7
Se1-Se2	2.3096(16)	C12-C13-H13	119.7
Se2-C21	1.947(8)	C13-C14-C15	120.2(9)
Br1-C17	1.975(9)	C13-C14-H14	119.9
Br2-C27	1.957(10)	C15-C14-H14	119.9
C11-C12	1.364(12)	C14-C15-C16	121.5(9)
C11-C16	1.395(13)	C14-C15-H15	119.3
C12-C13	1.374(13)	C16-C15-H15	119.3
C12-H12	0.9300	C15-C16-C11	117.7(8)
C13-C14	1.338(14)	C15-C16-C17	120.7(8)
C13-H13	0.9300	C11-C16-C17	121.6(8)
C14-C15	1.363(14)	C16-C17-Br1	111.0(6)
C14-H14	0.9300	C16-C17-H17A	109.4
C15-C16	1.365(12)	Br1-C17-H17A	109.4
C15-H15	0.9300	C16-C17-H17B	109.4
C16-C17	1.496(12)	Br1-C17-H17B	109.4
C17-H17A	0.9700	H17A-C17-H17B	108.0
C17-H17B	0.9700	C22-C21-C26	122.1(8)
C21-C22	1.357(13)	C22-C21-Se2	120.8(7)
C21-C26	1.403(13)	C26-C21-Se2	117.0(7)
C22-C23	1.403(13)	C21-C22-C23	118.5(10)
C22-H22	0.9300	C21-C22-H22	120.8
C23-C24	1.367(15)	C23-C22-H22	120.8
C23-H23	0.9300	C24-C23-C22	120.8(10)
C24-C25	1.376(15)	C24-C23-H23	119.6
C24-H24	0.9300	C22-C23-H23	119.6
C25-C26	1.383(13)	C23-C24-C25	119.6(9)
C25-H25	0.9300	C23-C24-H24	120.2
C26-C27	1.489(13)	C25-C24-H24	120.2
C27-H27A	0.9700	C24-C25-C26	121.4(10)
C27-H27B	0.9700	C24-C25-H25	119.3
		C26-C25-H25	119.3
C11-Se1-Se2	101.9(3)	C25-C26-C21	117.5(9)
C21-Se2-Se1	102.9(3)	C25-C26-C27	119.2(9)
C12-C11-C16	120.6(8)	C21-C26-C27	123.3(8)
C12-C11-Se1	120.0(7)	C26-C27-Br2	112.1(7)
C16-C11-Se1	119.4(6)	C26-C27-H27A	109.2
C11-C12-C13	119.4(9)	Br2-C27-H27A	109.2
C11-C12-H12	120.3	C26-C27-H27B	109.2
C13-C12-H12	120.3	Br2-C27-H27B	109.2
C14-C13-C12	120.6(9)	H27A-C27-H27B	107.9

6.11 1,6-bis-(2'-methylselenenylbenzene)-2,5-diselena-3-hexyne (48)



Crystal data and structure refinement

Operator	T.Oeser	
Identification code	al14	
Empirical formula	$C_{18}H_{18}Se_4$	
Formula weight	550.16	
Temperature	200(2) K	
Wavelength	0.71073 Å	
Crystal system	monoclinic	
Space group	C2/c	
Z	4	
Unit cell dimensions	$a = 15.856(2)$ Å	$\alpha = 90$ deg.
	$b = 5.2497(7)$ Å	$\beta = 101.456(3)$ deg.
	$c = 22.816(3)$ Å	$\gamma = 90$ deg.
Volume	$1861.4(4)$ Å ³	
Density (calculated)	1.96 g/cm ³	
Absorption coefficient	7.88 mm ⁻¹	
Crystal shape	polyhedron	
Crystal size	$0.35 \times 0.06 \times 0.04$ mm ³	
Crystal colour	colorless	
Theta range for data collection	1.8 to 26.1 deg.	
Index ranges	$-19 \leq h \leq 19, -6 \leq k \leq 6, -28 \leq l \leq 28$	
Reflections collected	7851	
Independent reflections	1846 (R(int) = 0.0422)	
Observed reflections	1486 ($I > 2\sigma(I)$)	
Absorption correction	Semi-empirical from equivalents	
Max. and min. transmission	0.74 and 0.17	
Refinement method	Full-matrix least-squares on F^2	
Data/restraints/parameters	1846 / 0 / 101	
Goodness-of-fit on F^2	1.04	
Final R indices ($I > 2\sigma(I)$)	R1 = 0.033, wR2 = 0.074	
Largest diff. peak and hole	0.72 and -0.45 eÅ ⁻³	

Atomic coordinates and equivalent isotropic displacement parameters (\AA^2) for 48.

U_{eq} is defined as one third of the trace of the orthogonalized U_{ij} tensor

Atom	x	y	z	U_{eq}
Se1	0.4034(1)	0.3005(1)	0.4620(1)	0.0474(2)
Se2	0.5402(1)	0.1295(1)	0.3574(1)	0.0452(2)
C1	0.3316(2)	0.1384(7)	0.3948(2)	0.0317(8)
C2	0.3695(2)	-0.0517(7)	0.3657(2)	0.0297(8)
C3	0.3173(3)	-0.1821(7)	0.3193(2)	0.0356(9)
C4	0.2316(3)	-0.1247(8)	0.3016(2)	0.0428(10)
C5	0.1964(2)	0.0685(8)	0.3299(2)	0.0423(10)
C6	0.2459(3)	0.1987(8)	0.3765(2)	0.0394(9)
C7	0.4621(2)	-0.1204(7)	0.3832(2)	0.0388(9)
C8	0.5081(2)	0.0971(8)	0.2769(2)	0.0402(9)
C9	0.3250(3)	0.5466(8)	0.4843(2)	0.0529(12)

Hydrogen coordinates and isotropic displacement parameters (\AA^2) for 48

Atom	x	y	z	U_{eq}
H3	0.3415	-0.3140	0.2993	0.043
H4	0.1967	-0.2176	0.2701	0.051
H5	0.1375	0.1117	0.3171	0.051
H6	0.2211	0.3304	0.3960	0.047
H7A	0.4712	-0.2885	0.3658	0.047
H7B	0.4773	-0.1372	0.4273	0.047
H9A	0.3031	0.6578	0.4501	0.079
H9B	0.3552	0.6494	0.5178	0.079
H9C	0.2768	0.4576	0.4962	0.079

Anisotropic displacement parameters (\AA^2) for 48.

The anisotropic displacement factor exponent takes the form: $-2\pi^2(h^2 a^2 U_{11} + \dots + 2hk a^* b^* U_{12})$

Atom	U_{11}	U_{22}	U_{33}	U_{23}	U_{13}	U_{12}	U_{12}
Se1	0.0515(3)	0.0484(3)	0.0399(3)	-0.0125(2)	0.0032(2)	0.0039(2)	
Se2	0.0339(2)	0.0557(3)	0.0476(3)	-0.0108(2)	0.0118(2)	-0.0019(2)	
C1	0.038(2)	0.0318(19)	0.0256(19)	0.0031(15)	0.0063(15)	-0.0024(16)	
C2	0.0330(19)	0.0270(18)	0.0305(19)	0.0063(15)	0.0092(15)	-0.0016(15)	
C3	0.049(2)	0.0291(19)	0.031(2)	0.0026(16)	0.0137(18)	-0.0013(17)	
C4	0.044(2)	0.049(2)	0.034(2)	0.0010(18)	0.0025(18)	-0.0069(19)	
C5	0.030(2)	0.054(3)	0.042(2)	0.006(2)	0.0062(18)	-0.0017(18)	
C6	0.040(2)	0.042(2)	0.039(2)	0.0034(18)	0.0152(18)	0.0072(18)	
C7	0.045(2)	0.037(2)	0.035(2)	0.0046(17)	0.0096(18)	0.0066(18)	
C8	0.031(2)	0.044(2)	0.050(2)	0.0006(17)	0.019(2)	0.0035(17)	
C9	0.072(3)	0.043(2)	0.050(3)	-0.012(2)	0.027(2)	-0.001(2)	

Bond lengths (\AA) and angles (deg) for 48

Se1-C1	1.918(4)	Se2-C7	1.973(4)
Se1-C9	1.930(4)	C1-C6	1.377(5)
Se2-C8	1.814(4)	C1-C2	1.399(5)

X-ray structures

C2-C3	1.388(5)	C2-C1-Se1	116.9(3)
C2-C7	1.488(5)	C3-C2-C1	117.8(3)
C3-C4	1.372(5)	C3-C2-C7	119.5(3)
C4-C5	1.378(6)	C1-C2-C7	122.7(3)
C5-C6	1.371(6)	C4-C3-C2	121.4(4)
C8-C8#1	1.202(8)	C3-C4-C5	119.6(4)
C1-Se1-C9	101.34(18)	C6-C5-C4	120.5(4)
C8-Se2-C7	99.99(17)	C5-C6-C1	119.9(4)
C6-C1-C2	120.8(3)	C2-C7-Se2	113.8(3)
C6-C1-Se1	122.3(3)	C8#1-C8-Se2	173.3(3)

Symmetry transformations used to generate equivalent atoms: #1 -x+1,y,-z+1/2

7. Literature

- [1] a) Werz, D. B., Staeb, T. H., Benisch, C., Rausch, B. J., Rominger, F. and Gleiter, R. *Org. Lett.* **2002**, *4*, 339-342; b) Gleiter, R., Werz, D. B. and Rausch, B. J. *Chem. Eur. J.* **2003**, *9*, 2676-2683; c) Gleiter, R. and Werz, D. B. *Chem. Lett.* **2005**, *34*, 126-131.
- [2] a) Bleiholder, C., Gleiter, R., Werz, D. B. and Koeppel, H. *Inorg. Chem.* **2007**, *46*, 2249-2260; b) Bleiholder, C., Werz, D. B., Koeppel, H. and Gleiter, R. *J. Am. Chem. Soc.* **2006**, *128*, 2666-2674.
- [3] Iwaoka, M., Katsuda, T., Komatsu, H. and Tomoda, S. *J. Org. Chem.* **2005**, *70*, 321-327.
- [4] Steed, J. W. and Atwood, J. L. *Supramolecular Chemistry: A Concise Introduction*; J. Wiley and Sons, Chichester, **2000**.
- [5] a) Zacharias, N. and Dougherty, D. A. *Trends Pharmacol. Sci.* **2002**, *23*, 281-287; b) Ma, J. C. and Dougherty, D. A. *Chem. Rev.* **1997**, *97*, 1303-1324.
- [6] Yamada, S. *Org. Biomol. Chem.* **2007**, *5*, 2903-2912.
- [7] Steiner, T. *Angew. Chem., Int. Ed.* **2002**, *41*, 48-76.
- [8] Desiraju, G. R. and Steiner, T. *The Weak Hydrogen Bond: In Structural Chemistry and Biology*; Oxford University Press, Oxford, **1999**.
- [9] Philp, D. and Stoddart, J. F. *Angew. Chem., Int. Ed.* **1996**, *35*, 1155-1196.
- [10] Stryer, L. In *Biochemistry*; 3rd ed.; W. H. Freeman, New York, **1988**, p 852.
- [11] Klug, A. *Angew. Chem., Int. Ed.* **1983**, *22*, 565-582.
- [12] Bent, H. A. *Chem. Rev.* **1968**, *68*, 587-648.
- [13] Eisenberg, B. *Acc. Chem. Res.* **1998**, *31*, 117-123.
- [14] Borgnia, M., Nielsen, S., Engel, A. and Agre, P. *Annu. Rev. Biochem.* **1999**, *68*, 425-458.
- [15] a) Sigler, P. B., Xu, Z., Rye, H. S., Burston, S. G., Fenton, W. A. and Horwich, A. L. *Annu. Rev. Biochem.* **1998**, *67*, 581-608; b) Voges, D., Zwickl, P. and Baumeister, W. *Annu. Rev. Biochem.* **1999**, *68*, 1015-1068.
- [16] a) Demus, D., Goodby, J., Gray, G. W., Spiess, H.-W. and Vill, V., Eds.; *Handbook of Liquid Crystals*, Wiley-VCH, Weinheim, **1998**; b) Hamley, I. W. *Angew. Chem., Int. Ed.* **2003**, *42*, 1692-1712; c) Kato, T., Mizoshita, N. and Kishimoto, K. *Angew. Chem., Int. Ed.* **2006**, *45*, 38-68.
- [17] a) Katz, M. J., Kaluarachi, H., Batchelor, R. J., Bokov, A. A., Ye, Z.-G. and Leznoff, D. B. *Angew. Chem., Int. Ed.* **2007**, *46*, 8804-8807; b) Sanyal, S. and Ghosh, A. *Appl. Opt.* **2000**, *39*, 2321-2325; c) Kinnstatter, K., Ojima, M. and Yonezawa, S. *Appl. Opt.* **1990**, *29*, 4408; d) Yeh, P. *Appl. Opt.* **1982**, *21*, 3806-3808.
- [18] a) Burrington, J. D., George, H. F., Byfleet, W. D., Baker, M. R., Hurley, S., Sumiejski, J. L. and Ineman, J. M. (The Lubrizol Corporation, USA), **2006**, *Solid additive composition and method thereof*. US Patent: WO/2006/105025 b) Wolfe, D. L. (Dow Chemical Co., USA), **1984**, *Anti-misting additive for hydrocarbon fluids*. European Patent: EP0110003.
- [19] Hirsch, A. *Angew. Chem., Int. Ed.* **2002**, *41*, 1853-1859.

- [20] a) Haddon, R. C., Ed., [Special Issue] "Carbon Nanotubes", *Acc. Chem. Res.*, **2002**, *35*, 997-1113; b) Dresselhaus, M. S., Dresselhaus, G. and Avouris, P., Eds.; *Carbon Nanotubes: Synthesis, Structure, Properties, and Applications; Topics in Applied Physics*, Vol. 80, Springer, Berlin / Heidelberg, **2001**; c) Jorio, A., Dresselhaus, G. and Dresselhaus, M. S., Eds.; *Carbon Nanotubes: Advanced Topics in the Synthesis, Structure, Properties and Applications Topics in Applied Physics*, Vol. 111, Springer, Berlin / Heidelberg, **2008**.
- [21] a) Meyer, J. C., Geim, A. K., Katsnelson, M. I., Novoselov, K. S., Booth, T. J. and Roth, S. *Nature* **2007**, *446*, 60-63; b) Geim, A. K. and Novoselov, K. S. *Nat. Mater.* **2007**, *6*, 183-191.
- [22] Ciuparu, D., Klie, R. F., Zhu, Y. and Pfefferle, L. *J. Phys. Chem. B* **2004**, *108*, 3967-3969.
- [23] Xiaobao, Y., Yi, D. and Jun, N. *Phys. Rev. B: Condens. Matter Mater. Phys.* **2008**, *77*, 041402.
- [24] Hill, D. J., Mio, M. J., Prince, R. B., Hughes, T. S. and Moore, J. S. *Chem. Rev.* **2001**, *101*, 3893-4012.
- [25] Han, S., Anderson, D. R., Bond, A. D., Chu, H. V., Disch, R. L., Holmes, D., Schulman, J. M., Teat, S. J., Vollhardt, K. P. C. and Whitener, G. D. *Angew. Chem., Int. Ed.* **2002**, *41*, 3227-3230.
- [26] Basis sets were partly obtained from the Extensible Computational Chemistry Environment Basis Set Database, Version 02/25/04, as developed and distributed by the Molecular Science Computing Facility, Environmental and Molecular Sciences Laboratory which is part of the Pacific Northwest Laboratory, P.O. Box 999, Richland, WA 99352, U.S.A., and funded by the U.S. Department of Energy. The Pacific Northwest Laboratory is a multiprogram laboratory operated by Battelle Memorial Institute for the U.S. Department of Energy under contract DE-AC06-76RLO 1830.
- [27] Itojima, Y., Ogawa, Y., Tsuno, K., Handa, N. and Yanagawa, H. *Biochemistry* **1992**, *31*, 4757-4765.
- [28] Imae, T., Takahashi, Y. and Muramatsu, H. *J. Am. Chem. Soc.* **1992**, *114*, 3414-3419.
- [29] Nakashima, N., Asakuma, S. and Kunitake, T. *J. Am. Chem. Soc.* **1985**, *107*, 509-510.
- [30] Srisiri, W., Sisson, T. M., O'Brien, D. F., McGrath, K. M., Han, Y. and Gruner, S. M. *J. Am. Chem. Soc.* **1997**, *119*, 4866-4873.
- [31] a) Fuhrhop, J. H., Schnieder, P., Boekema, E. and Helfrich, W. *J. Am. Chem. Soc.* **1988**, *110*, 2861-2867; b) Frankel, D. A. and O'Brien, D. F. *J. Am. Chem. Soc.* **1994**, *116*, 10057-10069.
- [32] Schnur, J. M. *Science* **1993**, *262*, 1669-1676.
- [33] Percec, V., Ahn, C. H., Ungar, G., Yearley, D. J. P., Moller, M. and Sheiko, S. S. *Nature* **1998**, *391*, 161-164.
- [34] De Santis, P., Morosetti, S. and Rizzo, R. *Macromolecules* **1974**, *7*, 52-58.
- [35] Berl, V., Huc, I., Khoury, R. G., Krische, M. J. and Lehn, J.-M. *Nature* **2000**, *407*, 720-723.
- [36] Zhu, J., Parra, R. D., Zeng, H., Skrzypczak-Jankun, E., Zeng, X. C. and Gong, B. *J. Am. Chem. Soc.* **2000**, *122*, 4219-4220.

- [37] a) Prest, P.-J., Prince, R. B. and Moore, J. S. *J. Am. Chem. Soc.* **1999**, *121*, 5933-5939; b) Mio, M. J., Prince, R. B., Moore, J. S., Kuebel, C. and Martin, D. C. *J. Am. Chem. Soc.* **2000**, *122*, 6134-6135; c) Kuebel, C., Mio, M. J., Moore, J. S. and Martin, D. C. *J. Am. Chem. Soc.* **2002**, *124*, 8605-8610.
- [38] Doyle, D. A., Cabral, J. M., Pfuetzner, R. A., Kuo, A., Gulbis, J. M., Cohen, S. L., Chait, B. T. and MacKinnon, R. *Science* **1998**, *280*, 69-77.
- [39] Schafmeister, C. E., Miercke, L. J. W. and Stroud, R. M. *Science* **1993**, *262*, 734-738.
- [40] Wyman, T. B., Nicol, F., Zelphati, O., Scaria, P. V., Plank, C. and Szoka, F. C., Jr. *Biochemistry* **1997**, *36*, 3008-3017.
- [41] Ghadiri, M. R., Granja, J. R., Milligan, R. A., McRee, D. E. and Khazanovich, N. *Nature* **1993**, *366*, 324-327.
- [42] Bong, D. T., Clark, T. D., Granja, J. R. and Ghadiri, M. R. *Angew. Chem., Int. Ed.* **2001**, *40*, 988-1011.
- [43] Horne, W. S., Stout, C. D. and Ghadiri, M. R. *J. Am. Chem. Soc.* **2003**, *125*, 9372-9376.
- [44] Seebach, D., Matthews, J. L., Meden, A., Wessels, T., Baerlocher, C. and McCusker, L. B. *Helv. Chim. Acta* **1997**, *80*, 173-182.
- [45] Ranganathan, D. *Acc. Chem. Res.* **2001**, *34*, 919-930.
- [46] Fujimura, F., Fukuda, M., Sugiyama, J., Morita, T. and Kimura, S. *Org. Biomol. Chem.* **2006**, *4*, 1896-1901.
- [47] Cramer, F. *Angew. Chem.* **1952**, *64*, 136.
- [48] Muller, N. *Acc. Chem. Res.* **1990**, *23*, 23-28.
- [49] Harata, K. *J. Inclusion Phenom.* **1992**, *13*, 77-86.
- [50] Ashton, P. R., Cantrill, S. J., Gattuso, G., Menzer, S., Nepogodiev, S. A., Shipway, A. N., Stoddart, J. F. and Williams, D. J. *Chem. Eur. J.* **1997**, *3*, 1299-1314.
- [51] Saenger, W. In *Inclusion Compounds*; Atwood, J. L., Davies, J. E., MacNicol, D. D., Eds.; Academic Press, London, **1984**; Vol. 2, 231-259.
- [52] Harada, A., Li, J. and Kamachi, M. *Nature* **1993**, *364*, 516-518.
- [53] Liu, Y., You, C.-C., Zhang, H.-Y., Kang, S.-Z., Zhu, C.-F. and Wang, C. *Nano Lett.* **2001**, *1*, 613-616.
- [54] Kim, E., Paliwal, S. and Wilcox, C. S. *J. Am. Chem. Soc.* **1998**, *120*, 11192-11193.
- [55] Janiak, C. *Dalton* **2000**, 3885-3896.
- [56] Hunter, C. A. and Sanders, J. K. M. *J. Am. Chem. Soc.* **1990**, *112*, 5525-5534.
- [57] a) Venkataraman, D., Lee, S., Zhang, J. and Moore, J. S. *Nature* **1994**, *371*, 591-593; b) Höger, S. and Meckenstock, A.-D. *Chem. Eur. J.* **1999**, *5*, 1686-1691; c) Grave, C. and Schluter, A. D. *Eur. J. Org. Chem.* **2002**, 3075-3098.
- [58] Zhao, D. and Moore, J. S. *Chem. Commun.* **2003**, 807-818.
- [59] Block, M. A. B., Kaiser, C., Khan, A. and Hecht, S. *Top. Curr. Chem.* **2005**, *245*, 89-150.
- [60] Höger, S., Morrison Donald, L. and Enkelmann, V. *J. Am. Chem. Soc.* **2002**, *124*, 6734-6736.
- [61] Pedireddi, V. R., Reddy, D. S., Goud, B. S., Craig, D. C., Rae, A. D. and Desiraju, G. R. *J. Chem. Soc., Perkin Trans. 2* **1994**, 2353-2360.

- [62] Williams, J. M., Ferraro, J. R. and Thorn, R. J. *Organic superconductors (including fullerenes). Synthesis structure, properties and theory*; Prentice-Hall Englewood Cliffs, NJ (United States), **1992**.
- [63] Price, S. L., Stone, A. J., Lucas, J., Rowland, R. S. and Thornley, A. E. *J. Am. Chem. Soc.* **1994**, *116*, 4910-4918.
- [64] Morita, Y., Miyazaki, E., Toyoda, J. and Nakasuji, K. *Bull. Chem. Soc. Jpn.* **2003**, *76*, 205-206.
- [65] Novoa, J. J., Whangbo, M. H. and Williams, J. M. In *Organic Superconductivity*; Kresin, V. Z., Little, W. A., Eds.; Plenum Press New York, **1990**, 231-242.
- [66] Werz, D. B., Gleiter, R. and Rominger, F. *J. Org. Chem.* **2004**, *69*, 2945-2952.
- [67] Mundt, O., Becker, G., Baumgarten, J., Riffel, H. and Simon, A. *Z. Anorg. Allg. Chem.* **2006**, *632*, 1687-1709.
- [68] Epp, O., Ladenstein, R. and Wendel, A. *Eur. J. Biochem.* **1983**, *133*, 51-69.
- [69] Shchedrina, V. A., Novoselov, S. V., Malinoski, M. Y. and Gladyshev, V. N. *Proc. Natl. Acad. Sci. U. S. A.* **2007**, *104*, 13919-13924.
- [70] Goldstein, B. M., Kennedy, S. D. and Hennen, W. J. *J. Am. Chem. Soc.* **1990**, *112*, 8265-8268.
- [71] Burling, F. T. and Goldstein, B. M. *J. Am. Chem. Soc.* **1992**, *114*, 2313-2320.
- [72] Wirth, T. *Molecules* **1998**, *3*, 164-166; Iwaoka, M. and Tomoda, S. *J. Am. Chem. Soc.* **1994**, *116*, 2557-2561.
- [73] a) Back, T. G. *Organoselenium Chemistry: A Practical Approach*; Oxford University Press, Oxford, **1999**; b) Wirth, T., Ed.; *Organoselenium Chemistry: Modern Developments in Organic Synthesis Top. Curr. Chem.*, Vol. 208, Springer Berlin/Heidelberg, **2000**.
- [74] Nishibayashi, Y. and Uemura, S. *Top. Curr. Chem.* **2000**, *208*, 236-255.
- [75] Iwaoka, M. and Tomoda, S. *J. Chem. Soc., Chem. Commun.* **1992**, 1165-1167.
- [76] a) Fragale, G., Neuburger, M. and Wirth, T. *Chem. Commun.* **1998**, 1867-1868; b) Fragale, G. and Wirth, T. *Eur. J. Org. Chem.* **1998**, 1361-1369.
- [77] a) Desiraju, G. R. *Crystal Engineering: The Design of Organic Solids*; Elsevier, Amsterdam, **1989**; b) Desiraju, G. R. *Curr. Sci.* **2001**, *81*, 1038-1042.
- [78] a) Wudl, F., Smith, G. M. and Hufnagel, E. J. *Chem. Commun.* **1970**, 1453-1454; b) Narita, M. and Pittman, C. U., Jr. *Synthesis* **1976**, 489-514.
- [79] Ferraris, J., Cowan, D. O., Walatka, V. and Perlstein, J. H. *J. Am. Chem. Soc.* **1973**, *95*, 948-949.
- [80] Jerome, D., Mazaud, A., Ribault, M. and Bechgaard, K. *J. Phys. Lett.* **1980**, *41*, 95-98.
- [81] Novoa, J. J., Rovira, M. C., Rovira, C., Veciana, J. and Tarres, J. *Adv. Mater.* **1995**, *7*, 233-237.
- [82] Kobayashi, H., Cui, H. and Kobayashi, A. *Chem. Rev.* **2004**, *104*, 5265-5288.
- [83] Vargas-Baca, I. and Chivers, T. *Phosphorus, Sulfur Silicon Relat. Elem.* **2000**, *164*, 207-227.
- [84] Berger, S., Braun, S. and Kalinowski, H. O. *NMR Spectroscopy of the Non-Metallic Elements*, **1997**.
- [85] Werz, D. B. *Ph.D. Thesis*, University of Heidelberg, **2003**.
- [86] Bleihoder, C. *Diplomarbeit*, University of Heidelberg, **2004**.
- [87] Fromm, E. and Siebert, E. *Chem. Ber.* **1922**, *55*, 1014-1030.
- [88] Brandsma, L. *Recueil des Travaux Chimiques des Pays-Bas* **1964**, *83*, 307-314.

- [89] a) Gleiter, R. and Hopf, H., Eds.; *Modern Cyclophane Chemistry*, Wiley-VCH, Weinheim, Germany, **2004**; b) Diederich, F. *Cyclophanes (Monographs in Supramolecular Chemistry)*, **1991**; c) Voegtle, F., Ed.; *Comprehensive Supramolecular Chemistry, Volume 2: Molecular Recognition: Receptors for Molecular Guests*, **1996**.
- [90] Voegtle, F., Pawlitzki, G. and Hahn, U. In *Modern Cyclophane Chemistry*; Gleiter, R., Hopf, H., Eds.; Wiley-VCH, Weinheim, Germany, **2004**, p 41-80.
- [91] a) Mitchell, R. H. *Can. J. Chem.* **1980**, *58*, 1398-1406; b) Bushnell, G. W. and Mitchell, R. H. *Can. J. Chem.* **1982**, *60*, 362-367.
- [92] Higuchi, H. and Misumi, S. *Tetrahedron Lett.* **1982**, *23*, 5571-5574.
- [93] Brandsma, L. *Preparative Acetylene Chemistry*; 2nd ed.; Elsevier, Amsterdam, **1988**.
- [94] a) Benisch, C. *Ph.D Thesis*, University of Heidelberg, **2000**; b) Benisch, C., Bethke, S., Gleiter, R., Oeser, T., Pritzkow, H. and Rominger, F. *Eur. J. Org. Chem.* **2000**, 2479-2488.
- [95] Hojjatie, M., Muralidharan, S. and Freiser, H. *Tetrahedron* **1989**, *45*, 1611-1622.
- [96] Eaborn, C., Eastmond, R. and Walton, D. R. M. *J. Chem. Soc. B* **1971**, 127-130.
- [97] Werz, D. B., Fischer, F. R., Kornmayer, S. C., Rominger, F. and Gleiter, R. *J. Org. Chem.* **2008** in print.
- [98] McWhinnie, S. L. W., Brooks, A. B. and Abrahams, I. *Acta Cryst.* **1998**, *C54*, 126-128.
- [99] Werz, D. B., Gleiter, R. and Rominger, F. *J. Org. Chem.* **2002**, *67*, 4290-4297.
- [100] Bondi, A. *J. Phys. Chem.* **1964**, *68*, 441-451.
- [101] a) Franklin, R. E. *Acta Cryst.* **1951**, *4*, 253-261; b) Freise, E. J. *Nature* **1962**, *193*, 671-672; c) Camerman, A. and Trotter, J. *Acta Crystallogr.* **1965**, *18*, 636-643.
- [102] Allen, F. H. *Acta Crystallogr.* **2002**, *B58*, 380-388.
- [103] Rosenfield, R. E., Jr., Parthasarathy, R. and Dunitz, J. D. *J. Am. Chem. Soc.* **1977**, *99*, 4860-4862.
- [104] Guru Row, T. N. and Parthasarathy, R. *J. Am. Chem. Soc.* **1981**, *103*, 477-479.
- [105] Berman, H., Henrick, K. and Nakamura, H. *Nat. Struct. Mol. Biol.* **2003**, *10*, 980-980.
- [106] Chakrabarti, P. *Biochemistry* **1989**, *28*, 6081-6085.
- [107] Ramasubbu, N. and Parthasarathy, R. *Phosphorus, Sulfur Silicon Relat. Elem.* **1987**, *31*, 221-229.
- [108] Fukui, K., Yonezawa, T. and Shingu, H. *J. Chem. Phys.* **1952**, *20*, 722-725.
- [109] Nyburg, S. C. and Faerman, C. H. *Acta Crystallogr.* **1985**, *B41*, 274-279.
- [110] McFarlane, W., Rycroft, D. S. and Turner, C. J. *Bull. Soc. Chim. Belg.* **1977**, *86*, 457-463.
- [111] Duddeck, H. *Prog. Nucl. Magn. Reson. Spectrosc.* **1995**, *27*, 1-323.
- [112] Duddeck, H. *Annu. Rep. NMR Spectrosc.* **2004**, *52*, 105-166.
- [113] Iwaoka, M., Komatsu, H., Katsuda, T. and Tomoda, S. *J. Am. Chem. Soc.* **2002**, *124*, 1902-1909.
- [114] Landrum, G. A. and Hoffmann, R. *Angew. Chem., Int. Ed.* **1998**, *37*, 1887-1890.
- [115] Buerger, H. B. and Dunitz, J. D. *J. Am. Chem. Soc.* **1987**, *109*, 2924-2926.

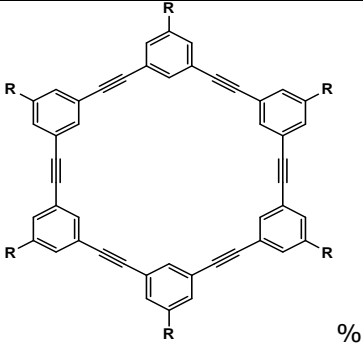
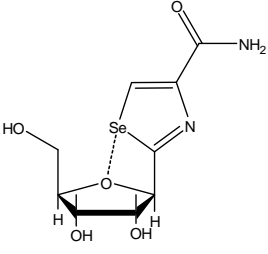
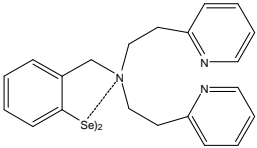
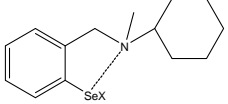
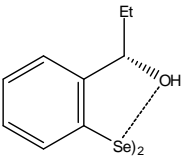
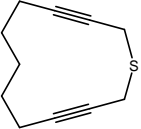
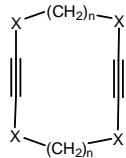
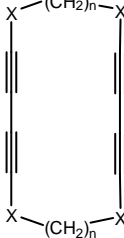
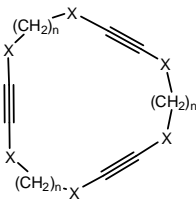
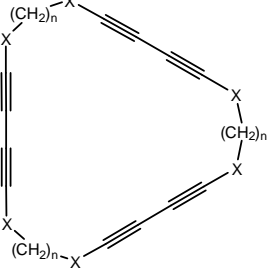
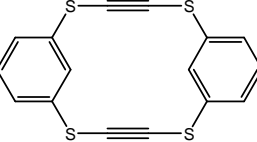
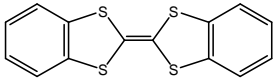
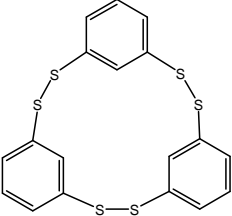
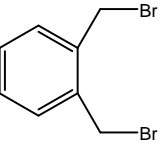
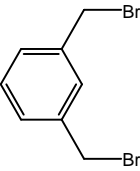
- [116] a) Masunov, A. E. and Zorkii, P. M. *Zh. Strukt. Khim.* **1992**, *33*, 105-118; b) Minkin, V. I., Minyaev, R. M., Milov, A. A. and Gribanova, T. N. *Russ. Chem. Bull.* **2001**, *50*, 2028-2045.
- [117] a) Angyan, J. G., Csizmadia, I. G., Daudel, R. and Poirier, R. A. *Chem. Phys. Lett.* **1986**, *131*, 247-251; b) Angyan, J. G., Poirier, R. A., Kucsman, A. and Csizmadia, I. G. *J. Am. Chem. Soc.* **1987**, *109*, 2237-2245.
- [118] Gleiter, R. and Gygax, R. *Top. Curr. Chem.* **1976**, *63*, 49-88.
- [119] Tiecco, M., Testaferri, L., Tingoli, M., Chianelli, D. and Montanucci, M. *J. Org. Chem.* **1983**, *48*, 4289-4296.
- [120] Gulliver, D. J., Hope, E. G., Levason, W., Murray, S. G., Potter, D. M. and Marshall, G. L. *J. Chem. Soc., Perkin Trans. 2* **1984**, 429-434.
- [121] Tiecco, M., Testaferri, L., Tingoli, M., Chianelli, D. and Montanucci, M. *Synth. Commun.* **1983**, *13*, 617-620.
- [122] Tomoda, S., Takeuchi, Y. and Nomura, Y. *Chem. Lett.* **1981**, 1069-1070.
- [123] Krief, A., Delmotte, C. and Dumont, W. *Tetrahedron* **1997**, *53*, 12147-12158.
- [124] Kocienski, P. J. *Protecting Groups*; Georg Thieme, Stuttgart, **1994**.
- [125] Friesen, R. W., Sturino, C. F., Daljeet, A. K. and Kolaczewska, A. *J. Org. Chem.* **1991**, *56*, 1944-1947.
- [126] Newton, R. F., Reynolds, D. P., Finch, M. A. W., Kelly, D. R. and Roberts, S. M. *Tetrahedron Lett.* **1979**, 3981-3982.
- [127] Nicolaou, K. C. and Webber, S. E. *Synthesis* **1986**, 453-461.
- [128] Corey, E. J. and Venkateswarlu, A. *J. Am. Chem. Soc.* **1972**, *94*, 6190-6191.
- [129] Tamura, Y., Adachi, M., Kawasaki, T. and Kita, Y. *Tetrahedron Lett.* **1979**, 2251-2252.
- [130] Horner, L., Oediger, H. and Hoffmann, H. *Justus Liebigs Ann. Chem.* **1959**, 626, 26-34.
- [131] a) Agenas, L. B. *Acta Chem. Scand.* **1963**, *17*, 268-270; b) Meinke, P. T., Krafft, G. A. and Guram, A. *J. Org. Chem.* **1988**, *53*, 3632-3634.
- [132] Iwaoka, M. and Tomoda, S. *Phosphorus, Sulfur Silicon Relat. Elem.* **1992**, *67*, 125-130.
- [133] Dunitz, J. D. and Gavezzotti, A. *Helv. Chim. Acta* **2002**, *85*, 3949-3964.
- [134] Becke, A. D. *J. Chem. Phys.* **1993**, *98*, 5648-5652.
- [135] Lee, C., Yang, W. and Parr, R. G. *Phys. Rev. B: Condens. Matter Mater. Phys.* **1988**, *37*, 785-789.
- [136] Iwaoka, M. and Tomoda, S. *J. Am. Chem. Soc.* **1994**, *116*, 4463-4464.
- [137] Iwaoka, M., Komatsu, H., Katsuda, T. and Tomoda, S. *J. Am. Chem. Soc.* **2004**, *126*, 5309-5317.
- [138] Iwaoka, M. and Tomoda, S. *Phosphorus, Sulfur Silicon Relat. Elem.* **2005**, *180*, 755-766.
- [139] a) Beraldin, M. T., Vauthier, E. and Fliszar, S. *Can. J. Chem.* **1982**, *60*, 106-110; b) Jaccard, G., Carrupt, P. A. and Lauterwein, J. *Magn. Reson. Chem.* **1988**, *26*, 239-244.
- [140] Tripathi, S. K., Patel, U., Roy, D., Sunoj, R. B., Singh, H. B., Wolmershauser, G. and Butcher, R. J. *J. Org. Chem.* **2005**, *70*, 9237-9247.
- [141] McFarlane, W. and Wood, R. J. *J. Chem. Soc., Dalton Trans.* **1972**, 1397-1402.
- [142] Nakanishi, W., Hayashi, S. and Toyota, S. *J. Org. Chem.* **1998**, *63*, 8790-8800.
- [143] Luca, S., Heise, H. and Baldus, M. *Acc. Chem. Res.* **2003**, *36*, 858-865.

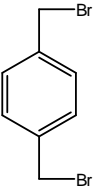
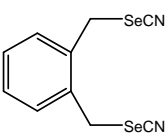
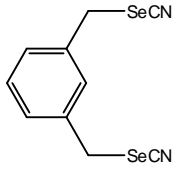
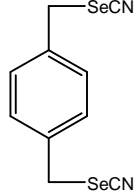
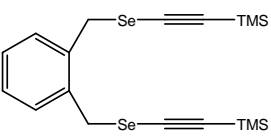
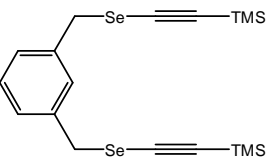
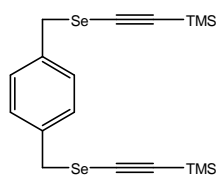
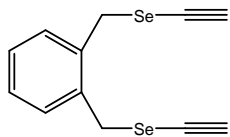
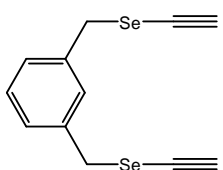
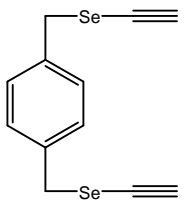
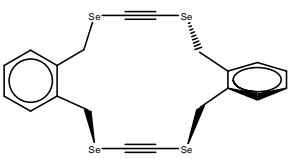
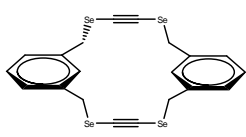
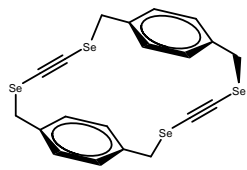
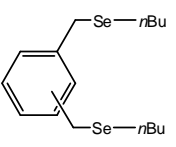
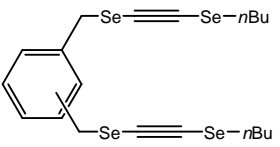
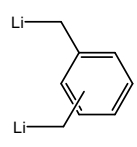
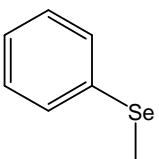
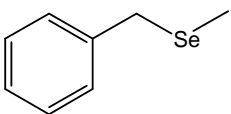
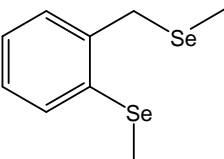
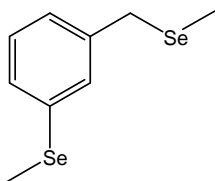
- [144] a) Wu, R., Hernandez, G., Odom, J. D., Dunlap, R. B. and Silks, L. A. *Chem. Commun.* **1996**, 1125-1126; b) Michalczyk, R., Schmidt, J. G., Moody, E., Li, Z., Wu, R., Dunlap, R. B., Odom, J. D. and Silks, L. A., III *Angew. Chem., Int. Ed.* **2000**, *39*, 3067-3070.
- [145] Heckmann, G. and Wolmershauser, G. *Chem. Ber.* **1993**, *126*, 1071-1076.
- [146] Levitt, M. H. *Spin Dynamics: basics of nuclear magnetic resonance*; John Wiley & Sons, Ltd, Chichester, England, **2001**.
- [147] Iwaoka, M., Komatsu, H. and Tomoda, S. *Chem. Lett.* **1998**, 969-970.
- [148] Iwaoka, M. and Tomoda, S. *J. Am. Chem. Soc.* **1996**, *118*, 8077-8084.
- [149] Tonkikh, N., Duddeck, H., Petrova, M., Neilands, O. and Strakovs, A. *Eur. J. Org. Chem.* **1999**, *1999*, 1585-1588.
- [150] a) Johannsen, I. and Eggert, H. *J. Am. Chem. Soc.* **1984**, *106*, 1240-1243; b) Johannsen, I., Henriksen, L. and Eggert, H. *J. Org. Chem.* **1986**, *51*, 1657-1663; c) Malon, M., Imakubo, T. and Koshino, H. *Magn. Reson. Chem.* **2008**, *46*, 150-155.
- [151] a) Pekonen, P., Hiltunen, Y., Laitinen, R. S. and Pakkanen, T. A. *Inorg. Chem.* **1990**, *29*, 2770-2773; b) Laitinen, R. S. and Pakkanen, T. A. *Inorg. Chem.* **1987**, *26*, 2598-2603.
- [152] a) Nakanishi, W., Hayashi, S. and Uehara, T. *J. Phys. Chem. A* **1999**, *103*, 9906-9912; b) Nakanishi, W., Hayashi, S. and Toyota, S. *Chem. Commun.* **1996**, 371-372; c) Nakanishi, W., Hayashi, S. and Yamaguchi, H. *Chem. Lett.* **1996**, 947-948.
- [153] a) Aue, W. P., Bartholdi, E. and Ernst, R. R. *J. Chem. Phys.* **1976**, *64*, 2229-2246; b) Nagayama, K., Kumar, A., Wuethrich, K. and Ernst, R. R. *J. Magn. Reson.* **1980**, *40*, 321-334.
- [154] Helgaker, T., Jaszunski, M. and Ruud, K. *Chem. Rev.* **1999**, *99*, 293-352.
- [155] London, F. *Journal de Physique et le Radium* **1937**, *8*, 397-409.
- [156] Kutzelnigg, W. *Isr. J. Chem.* **1980**, *19*, 193-200.
- [157] Hansen, A. E. and Bouman, T. D. *J. Chem. Phys.* **1985**, *82*, 5035-5047.
- [158] Keith, T. A. and Bader, R. F. W. *Chem. Phys. Lett.* **1992**, *194*, 1-8.
- [159] Keith, T. A. and Bader, R. F. W. *Chem. Phys. Lett.* **1993**, *210*, 223-231.
- [160] Wolinski, K., Hinton, J. F. and Pulay, P. *J. Am. Chem. Soc.* **1990**, *112*, 8251-8260.
- [161] Magyarfalvi, G. and Pulay, P. *J. Chem. Phys.* **2003**, *119*, 1350-1357.
- [162] de Dios, A. C. *Prog. Nucl. Magn. Reson. Spectrosc.* **1996**, *29*, 229-278.
- [163] Jameson, C. J. *Annu. Rev. Phys. Chem.* **1996**, *47*, 135-169.
- [164] Schindler, M. and Kutzelnigg, W. *J. Chem. Phys.* **1982**, *76*, 1919-1933.
- [165] Schaefer, A., Huber, C. and Ahlrichs, R. *J. Chem. Phys.* **1994**, *100*, 5829-5835.
- [166] a) Dunning, T. H., Jr. *J. Chem. Phys.* **1989**, *90*, 1007-1023; b) Dunning, T. H., Jr., Thom, H. and Peterson, K. A. In *Encyclopedia of Computational Chemistry*; Schleyer, P. v. R., Ed.; Wiley, New York, **1998**; Vol. 1, 88-115.
- [167] Cramer, C. J. *Essentials of Computational Chemistry. Theories and Models*; John Wiley & Sons Ltd., Chichester, England, **2002**.
- [168] Kaupp, M., Bühl, M. and Malkin, V. G., Eds.; *Calculations of NMR and EPR Parameters. Theory and Applications*, Wiley-VCH, Weinheim, **2004**.
- [169] Yates, J. R., Pickard, C. J., Payne, M. C. and Mauri, F. *J. Chem. Phys.* **2003**, *118*, 5746-5753.

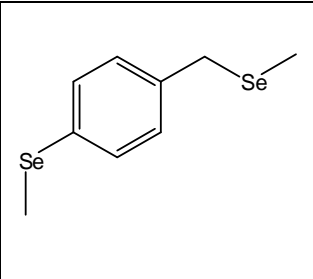
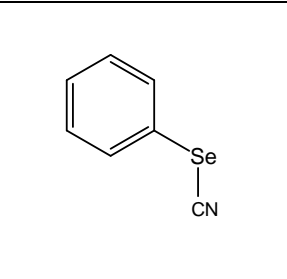
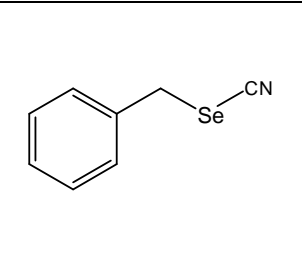
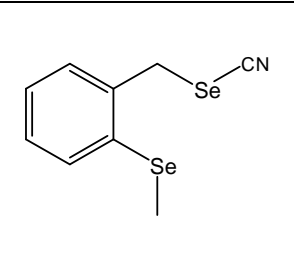
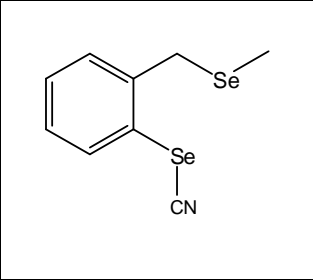
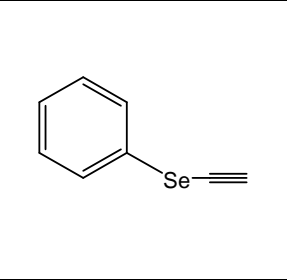
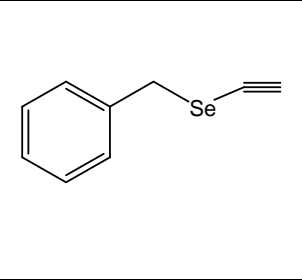
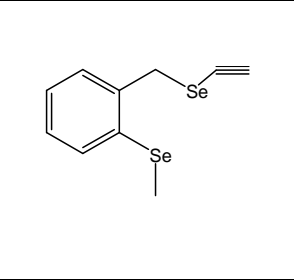
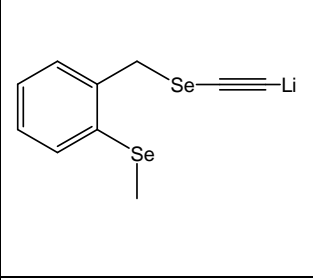
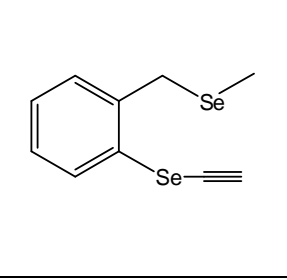
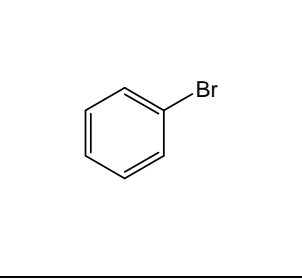
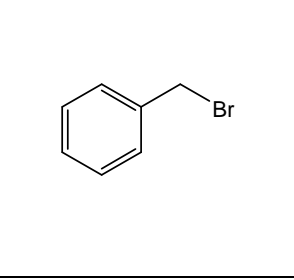
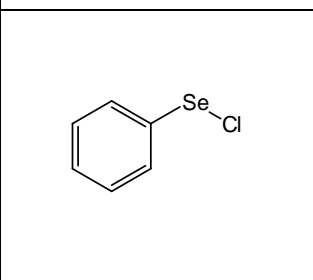
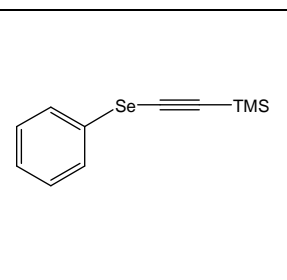
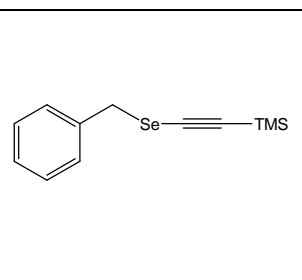
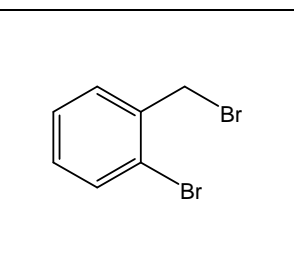
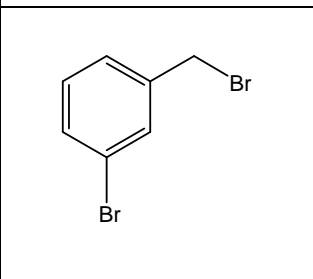
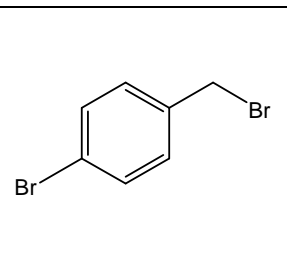
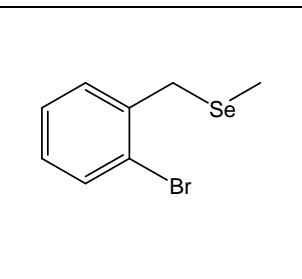
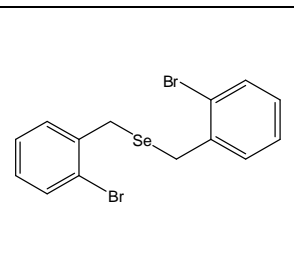
- [170] Schreckenbach, G., Ruiz-Morales, Y. and Ziegler, T. *J. Chem. Phys.* **1996**, *104*, 8605-8612.
- [171] a) Krishnan, R., Binkley, J. S., Seeger, R. and Pople, J. A. *J. Chem. Phys.* **1980**, *72*, 650-654; b) McLean, A. D. and Chandler, G. S. *J. Chem. Phys.* **1980**, *72*, 5639-5648; c) Curtiss, L. A., McGrath, M. P., Blaudeau, J.-P., Davis, N. E., Binning, r. C., Jr. and Radom, L. *J. Chem. Phys.* **1995**, *103*, 6104-6113; d) Clark, T., Chandrasekhar, J., Spitznagel, G. W. and Schleyer, P. v. R. *J. Comput. Chem.* **1983**, *4*, 294-301.
- [172] Pople, J. A. *et al.* Gaussian 03, Gaussian, Inc., Wallingford, CT, **2004**.
- [173] Schmider, H. L. and Becke, A. D. *J. Chem. Phys.* **1998**, *108*, 9624-9631.
- [174] Becke, A. D. *J. Chem. Phys.* **1997**, *107*, 8554-8560.
- [175] Moller, C. and Plesset, M. S. *Phys. Rev.* **1934**, *46*, 618-622.
- [176] Buehl, M., Thiel, W., Fleischer, U. and Kutzelnigg, W. *J. Phys. Chem.* **1995**, *99*, 4000-4007.
- [177] Buehl, M., Gauss, J. and Stanton, J. F. *Chem. Phys. Lett.* **1995**, *241*, 248-252.
- [178] Magyarfalvi, G. and Pulay, P. *Chem. Phys. Lett.* **1994**, *225*, 280-284.
- [179] Malkin, V. G., Malkina, O. L., Casida, M. E. and Salahub, D. R. *J. Am. Chem. Soc.* **1994**, *116*, 5898-5908.
- [180] Wilson, P. J. *Mol. Phys.* **2001**, *99*, 363-367.
- [181] Wilson, P. J., Amos, R. D. and Handy, N. C. *Chem. Phys. Lett.* **1999**, *312*, 475-484.
- [182] van Wuelen, C. *J. Chem. Phys.* **1995**, *102*, 2806-2811.
- [183] Keal, T. W. and Tozer, D. J. *Mol. Phys.* **2005**, *103*, 1007-1011.
- [184] Keal, T. W. and Tozer, D. J. *J. Chem. Phys.* **2004**, *121*, 5654-5660.
- [185] Kendall, R. A., Dunning, T. H., Jr. and Harrison, R. J. *J. Chem. Phys.* **1992**, *96*, 6796-6806.
- [186] Jameson, C. J. In *Nuclear Magnetic Resonance* **1997**; *26*, 46-87.
- [187] Jameson, C. J. and De Dios, A. C. *Nuclear Magnetic Resonance* **1999**, *28*, 42-76.
- [188] Duddeck, H., Bradenahl, R., Stefaniak, L., Jazwinski, J. and Kamienski, B. *Magn. Reson. Chem.* **2001**, *39*, 709-713.
- [189] a) Perdew, J. P., Burke, K. and Ernzerhof, M. *Phys. Rev. Lett.* **1996**, *77*, 3865-3868; b) Perdew, J. P., Burke, K. and Ernzerhof, M. *Phys. Rev. Lett.* **1997**, *78*, 1396.
- [190] Wong, T. C., Ang, T. T., Guziec, F. S. and Moustakins, C. A. *J. Magn. Reson.* **1984**, *57*, 463-470.
- [191] Ochsenfeld, C., Kussmann, J. and Koziol, F. *Angew. Chem., Int. Ed.* **2004**, *43*, 4485-4489.
- [192] Vaara, J., Jokisaari, J., Wasylshen, R. E. and Bryce, D. L. *Prog. Nucl. Magn. Reson. Spectrosc.* **2002**, *41*, 233-304.
- [193] Harris, R. K., Becker, E. D., Cabral De Menezes, S. M., Goodfellow, R. and Granger, P. *Pure Appl. Chem.* **2001**, *73*, 1795-1818.
- [194] Hurd, R. E. *J. Magn. Reson.* **1990**, *87*, 422-428.
- [195] Willker, W., Leibfritz, D., Kerssebaum, R. and Bermel, W. *Magn. Reson. Chem.* **1993**, *31*, 287-292.
- [196] Ruiz-Cabello, J., Vuister, G. W., Moonen, C. T. W., Van Gelderen, P., Cohen, J. S. and Van Zijl, P. C. M. *J. Magn. Reson.* **1992**, *100*, 282-302.

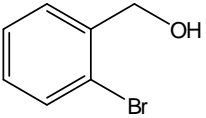
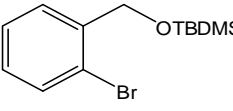
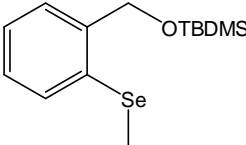
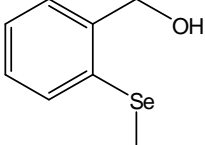
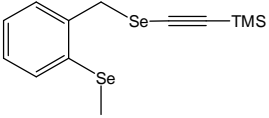
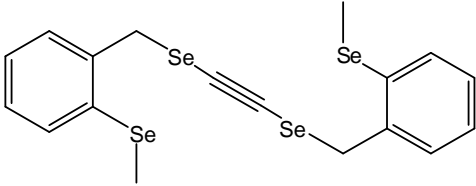
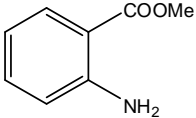
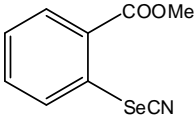
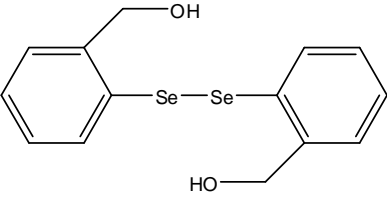
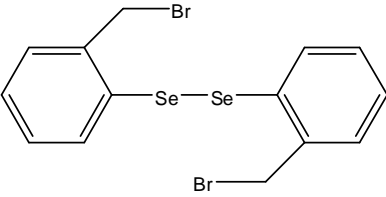
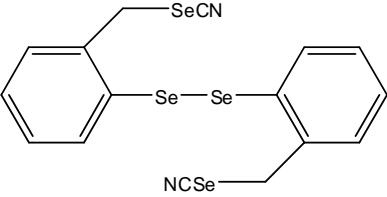
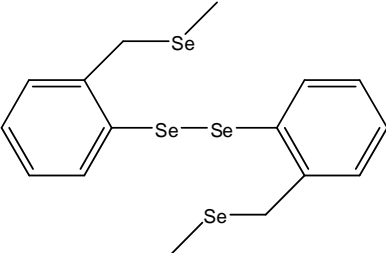
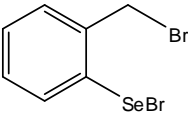
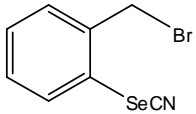
- [197] Parella, T. *Magn. Reson. Chem.* **1998**, *36*, 467-495; Canet, D. *Prog. Nucl. Magn. Reson. Spectrosc.* **1997**, *30*, 101-135.
- [198] Sheldrick, G. M., SABADS V2.03, Bruker Analytical X-ray Division, Madison, Wisconsin, **2001**.
- [199] Sheldrick, G. M., SHELXTL V6.12, Bruker Analytical X-ray Division, Madison, Wisconsin, **2001**.
- [200] Farrugia, L. J. *J. Appl. Crystallogr.* **1997**, *30*, 565.
- [201] Macrae, C. F., Edgington, P. R., McCabe, P., Pidcock, E., Shields, G. P., Taylor, R., Towler, M. and van de Streek, J. *J. Appl. Crystallogr.* **2006**, *39*, 453-457.

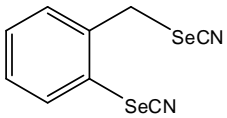
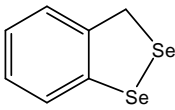
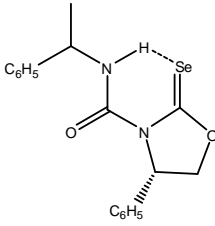
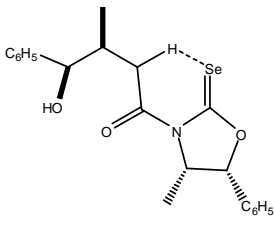
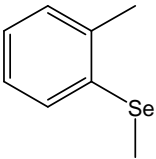
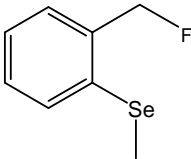
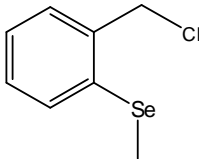
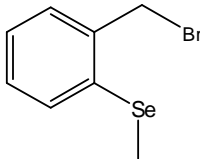
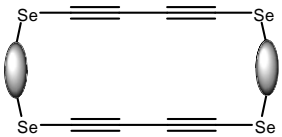
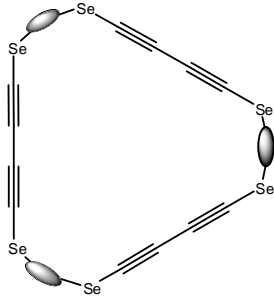
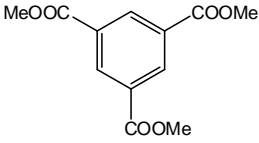
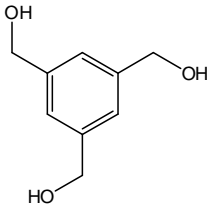
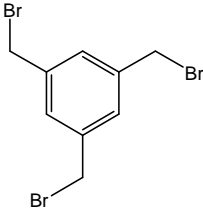
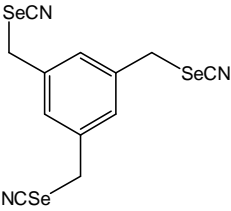
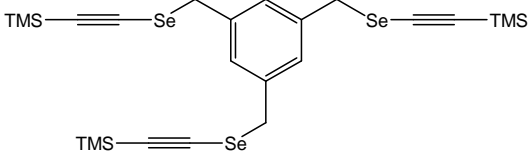
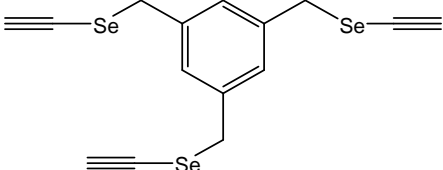
Appendix: Index of Compounds

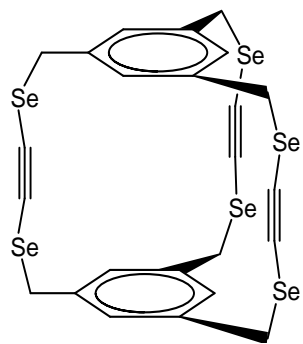
 <p style="text-align: center;">1 a-f %</p>	 <p style="text-align: center;">2</p>	 <p style="text-align: center;">3</p>	
 <p style="text-align: center;">4</p>	 <p style="text-align: center;">5</p>	 <p style="text-align: center;">6</p>	 <p style="text-align: center;">7</p>
 <p style="text-align: center;">8</p>	 <p style="text-align: center;">9</p>	 <p style="text-align: center;">10</p>	 <p style="text-align: center;">11</p>
 <p style="text-align: center;">12</p>	 <p style="text-align: center;">13</p>	 <p style="text-align: center;">14 a</p>	 <p style="text-align: center;">14 b</p>

			
14 c	15 a	15 b	15 c
			
16 a	16 b	16 c	17 a
			
17 b	17 c	18 a	18 b
			
18 c	19 a-c	20 a-c	21 a-c
			
22	23	24	25

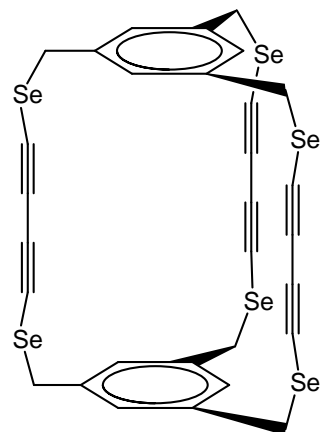
			
26	27	28	29
			
30	31	32	33
			
33a	34	35	36
			
37	38	39	40 a
			
40 b	40 c	41	42

			
<p style="text-align: center;">43</p>	<p style="text-align: center;">44</p>	<p style="text-align: center;">45</p>	<p style="text-align: center;">46</p>
			
<p style="text-align: center;">47</p>	<p style="text-align: center;">48</p>		<p style="text-align: center;">49</p>
			
<p style="text-align: center;">50</p>		<p style="text-align: center;">51</p>	
			
<p style="text-align: center;">52</p>		<p style="text-align: center;">53</p>	
			
<p style="text-align: center;">54</p>		<p style="text-align: center;">55</p>	<p style="text-align: center;">56</p>

			
57	58	59	60
			
61	62	63	64
			
65		66	
			
67	68	69	70
			
71		72	



73



74

Acknowledgements

THANK YOU !!!

It is hard to put into words my gratitude to my Ph.D. supervisor Prof. Dr. Rolf Gleiter. Without his continuous support, understanding, tactful guidance and endless patience this thesis would not have been possible. I would like to thank him for giving me the opportunity to undertake this research project and also for passing on some of his impressive knowledge to me. It has been a great experience that I will always remember with deep appreciation.

I wish to express my sincere gratitude to Prof. Stefan Berger for opening the doors of NMR spectroscopy for me. His honesty, straightforward approach to problems and his art of imparting knowledge and skills have been instructive and inspirational to me.

I want to express my deepest gratitude to my first mentor, the late Prof. Dr. Eng. Mircea Banciu for the confidence he always showed in my abilities. Not only did his constant encouragement and guidance help me develop my independent thinking and research skills, but also, above all, meeting and knowing him has made me a better person.

I would like to show my appreciation to Prof. Dr. Eurico Cabrita for introducing me to the subtleties of NMR spectroscopy and for our discussions, his valuable ideas and useful tips and tricks for this fascinating field. I would like to thank Dr. Manolo Angulo for showing me the wonders a patient shimming could do on a NMR spectra.

I want to thank my colleagues in the Organic Chemistry Institute for making the working atmosphere so enjoyable. Dr. Björn Hellbach, Dr. Tobi Stüb, Dr. Silke Stüb (Gath) and Dr. Johannes Büber made my first months in Heidelberg a lot easier. To Stefan Wetzel I am grateful for his computer troubleshooting skills and even more for our enjoyable long discussions. My great appreciation goes to Olivia Körner, Stefan Kornmayer, Dr. Birgit Esser and "our Azubis" (Mike, Teresa and Martin) for their unfailing support and for the good times outside the labs. I want to thank also Dr. Arkasish Bandyopadhyay for encouraging me in the last months during my struggles with the manuscript.

Special thanks to Dr. Martin Baier for his support and friendship and the good times in the "Chef-Labor". I will not forget the "important" expressions he taught me in German. Nor the guided tours in Heidelberg's Altstadt which made my stay here more pleasant and surely longer than originally planned.

I also thank my "Forschungspraktikanten" Ingo Braun, Robert Michling, Matthias Reinmuth and Wolfgang Woievode for their interest and enthusiasm during their research placements. Alex Flatow's help in ordering chemicals and laboratory equipment repairs and maintenance made the completion of this Ph.D. thesis much easier.

Petra Krämer deserves special thanks. Beside the many IR and UV measurements of even the tiniest amounts of substances and her help in organizing the NMR measurement of hundreds of NMR samples, I am grateful to her for always being there when I needed

to complain and for all her kind advice. Despite not always listening to it all, I very much appreciated it and learnt a lot from it. Thank you very much!!

I am deeply indebted to Christiane Eckert for never answering "No" to my annoying and repetitive questions: "Hello Christiane, do you have a bit of time? Do you know...?" Without her help my battle with the never-ending bureaucracy would have been lost long ago.

I wish to thank Bianka Flock, Angelika Seith, Norbert Nieth and Dr. Jürgen H. Gross for mass spectra, Tanja Coelho, Margaret Fischer, Christian Henke, Dr. Jürgen Graf and Dr. Jullien Furrer for NMR spectra and for helping me with my "special" ^{77}Se -NMR measurements. I thank Marcus Richter, Frank Dallmann, Dr. Thomas Oeser and Dr. Frank Rominger for supplying the X-Ray structures of the smallest crystals possible, with a special thanks to Dr. Rominger for always answering my questions about crystal structure analysis.

I am grateful for Dr. Bodo Martin's competent administration of the Graduate College 850 cluster. I thank Dr. Christian Bleiholder and Dr. Peter Bischof for their help with everything related to Linux, Gaussian, GaussView, Molden and all the other computational chemistry hurdles.

I am thankful to Benny and Christoph for their useful suggestions and comments during the preparation of this manuscript, and to Julia and Thomas for making sure that I did not bend too many rules of the English language.

I would like to acknowledge that without my gymnasium chemistry teacher Gabriela Borza I might have never have had the pleasure and curiosity of looking into what happens in the "fascinating world of molecules".

I would like to thank all of my friends for helping and supporting me unconditionally on this long and sometimes difficult journey. You know who you are and wherever you may be (Romania, Germany, France, Portugal, Spain, USA, UK, India, or just cruising around the world), I thank you for the great times we spent together. The memories and stories from those times would fill a book thicker than this one and would definitely make for very interesting reading.

And no...I haven't finished yet. None of this would have been accomplished without the help of C.I. Her affection, understanding and encouragement provided me with a lot of motivation and made the last period of time a wonderful experience.

Last, but most importantly, I wish to thank my mother, Mihaela-Rodica. Her life experience, having to start over again several times, and never giving up no matter how tough it got, has made her an inspirational role model for me. I thank her from the bottom of my heart for everything she had done for me.

Erklärungen gemäß § 8 (3) b) und c) der Promotionsordnung:

- a) ich erkläre hiermit, dass ich die vorgelegte Dissertation selbst verfasst und mich keiner anderen als der von mir ausdrücklich bezeichneten Quellen und Hilfe bedient habe,
- b) ich erkläre hiermit, dass ich an keiner anderen Stelle ein Prüfungsverfahren beantragt bzw. die Dissertation in dieser oder anderer Form bereits anderweitig als Prüfungsarbeit verwendet oder einer anderen Fakultät als Dissertation vorgelegt habe.

Heidelberg, im September 2008

